

Biologically Active Metal Ions and Complexes: Reactivity and Interactions

Zdeněk Chval

Faculty of Health and Social Studies, University of South Bohemia, České Budějovice

Habilitation thesis

Field: Biophysics
Faculty of Science
University of South Bohemia
České Budějovice

2017

Table of contents

1. Introduction	4
2. Results	
2.1. Bonding and non-bonding interactions of Pt(II)-complexes	5
2.2. Hydrolysis reactions of piano-stool Ru(II)-complexes	11
2.3. Mg ²⁺ ions in the RNA environment	14
3. Future perspectives	15
4. Summary	16
5. References	16
Appendix	19

Papers included in the thesis:

P1) Z.Chval and M.Šíp: Force Field for Platinum Binding to Adenine and Guanine Taking into Account Flexibility of Nucleic Acids Bases. *Journal of Physical Chemistry B* **1998**, 102, 1659-1661

P2) Z.Chval and M.Šíp: Pentacoordinated Transition States of Cisplatin Hydrolysis- ab initio study. *Journal of Molecular Structure: THEOCHEM* **2000**, 532, 59-68

P3) Z. Chval and M. Šíp: Transition States of Cisplatin Binding to Guanine and Adenine: ab initio Reactivity Study. *Collection of Czechoslovak Chemical Communications* **2003**, 68, 1105-1117

P4) Z. Chval, M. Šíp, J.V. Burda: The trans effect in square-planar platinum(II) complexes - A density functional study. *Journal of Computational Chemistry* **2008**, 29, 2370-2381

P5) T. Zimmermann, Z. Chval, J.V. Burda: Cisplatin Interaction with Cysteine and Methionine in Aqueous Solution: Computational DFT/PCM Study. *Journal of Physical Chemistry B* **2009**, 113, 3139-3150

P6) Z. Chval, Z. Futera, and J.V. Burda: Comparison of hydration reactions for “piano-stool” RAPTA-B and [Ru(η^6 -arene)(en)Cl]⁺ complexes; DFT computational study. *Journal of Chemical Physics* **2011**, 134, 2, 024520

- P7) Z. Chval, D. Chvalová, and F. Leclerc: Modeling the RNA 2' OH Activation: Possible Roles of Metal Ion and Nucleobase as Catalysts in Self-Cleaving Ribozymes. *Journal of Physical Chemistry B* **2011**, 115, 10943-10956
- P8) I. Romancová, Z. Chval, M. Předota: Influence of the Environment on the Specificity of the Mg(II) Binding to Uracil. *Journal of Physical Chemistry A* **2012**, 116, 1786–1793
- P9) Z. Chval, M. Kabeláč, J.V. Burda: Mechanism of the cis-[Pt(1R,2R-DACH)(H₂O)₂]²⁺ Intrastrand Binding to the Double-Stranded (pGpG)·(CpC) Dinucleotide in Aqueous Solution: A Computational DFT Study. *Inorganic Chemistry* **2013**, 52, 5801-5813
- P10) J.V. Burda, Z. Futera, Z. Chval: Exploration of various electronic properties along the reaction coordinate for hydration of Pt(II) and Ru(II) complexes: the CCSD, MPx, and DFT computational study. *Journal of Molecular Modeling*, **2013**, 19, 5245-5255
- P11) O. Kroutil, M. Předota, Z. Chval: Pt···H Non-Classical Interaction in Water Dissolved Pt(II)-Complexes: Coaction of Electronic Effects with Solvent-Assisted Stabilization. *Inorganic Chemistry* **2016**, 55, 3252–3264
- P12) T. Zábojníková, R. Cajzl, J. Kljun, Z. Chval, I. Turel, J. V. Burda: Interactions of the Piano-stool [Ruthenium(II)(6-arene)(quinolone)Cl]⁺ complexes with water; DFT computational study. *Journal of Computational Chemistry* **2016**, 37, 1766-1780

1. Introduction

Metal cations play a crucial role in many important biochemical and biophysical processes. They stabilize structure mainly of negatively charged biomolecules and/or their groups. Moreover, they are essential for the catalytic activity of many proteins and ribozymes. The importance of metal cations for a proper function of nucleic acids can be demonstrated by a simple statistics: although metal ions such as Na^+ and Mg^{2+} are hardly detectable by X-ray or spectroscopic methods more than half of the entries in the Protein Data Bank (PDB, www.pdb.org) contains metal atoms.¹

Anticancer drugs containing heavy metal cations do not occur naturally in the living organisms but they represent another type of metal cation complexes important in cellular processes. Coordination of these complexes to the DNA chain can cause substantial changes that influence functionality of the genetic code preventing its replication or transcription. They can also block several other important molecular mechanisms, e.g. irreversible platinum adducts with the cysteine side-chain irreversibly inhibit thioredoxin, glutaredoxin, and the thioredoxin reductase enzyme, and hereby decrease the ability of the cell to resist oxidative stress.² Beside well established platinum drugs (e.g. cisplatin and carboplatin) other transition metal complexes have been also intensively explored.

The thesis is written as the comments of twelve fully theoretical papers in which we studied the systems of interest by static quantum mechanical (QM) and quantum mechanical molecular dynamical (QMMD) calculations. Theoretical calculations have reached experimental accuracy thanks to the increasing computer power and the development of new more reliable and effective methods. Moreover, they have been proved to be extremely powerful in the interpretation of (experimental) results linking structural to functional information. The methods used were mostly based on density functional theory (DFT).

Seven papers (**P1-P5**, **P9**, **P11**) are focused on reactions which occur after the administration of Pt(II) complexes: their reactions with water (aquation/hydrolysis reactions), DNA and proteins or their active parts. Three papers (**P6**, **P10**, **P12**) are describing hydrolysis reactions of ‘piano-stool’ Ru(II) complexes. Finally, two papers (**P7**, **P8**) are dealing with two possible chemical changes promoted by the presence of the Mg^{2+} ions in the RNA environment: the self-cleavage activity of ribozymes and the tautomer equilibrium shift of uracil.

2. Results

2.1. Bonding and non-bonding interactions of Pt(II)-complexes

Pt(II) complexes are diamagnetic square-planar structures. The most studied representative is cisplatin which was already synthesized by Peyron in 1845 and its structure was deduced by Werner in 1893. Chemical reactivity of the square-planar Pt(II) complexes is driven by the trans effect which was introduced by Chernyaev in the twenties of the last century. The stability of the ligand is strongly influenced by the ligand in the trans position.³⁻⁸ Trans effect is a kinetic phenomenon whose origin lies in reactant destabilization and/or the transition state (TS) stabilization. The reactant destabilization is manifested itself by the Pt- trans ligand bond elongation and it is sometimes called the trans influence.⁹ The trans effect depends on the nature of the coordinating atom and its hardness.⁶

In **P4** we have explained the trans effect in terms of well-known concepts of σ -donation and π -back-donation and quantified the strength of these effects by electron occupations of the NBO valence orbitals on the Pt(II) atom in the plane of the complex (orbitals 6s, 5d(xy), 5d(x²-y²)) and in the perpendicular plane to the plane of the complex (orbital 5d(xz)), respectively. The stabilization of the pentacoordinated TS depends strongly on the electron density in the latter plane since it is the plane from which the nucleophilic attack of the entering ligand takes place. Thus, in the TS structure this plane has to accommodate both the leaving and the entering groups.

Trans influence is mainly a consequence of σ -donation while π -back-donation leads to the TS stabilization. It results in different reaction mechanisms (Figure 1): ligands with a strong σ -donation ability promote the dissociative interchange mechanism with a tricoordinated T-shaped TS structure while for ligands with strong π -back-donation the pentacoordinated structure is stabilized forming a stable minimum (intermediate) on the reaction coordinate and the reaction follows a two-step associative mechanism. This intermediate could not be described in previous theoretical studies³ relying on the Hartree-Fock method since electron correlation is needed for the stabilization of this minimum. For the other ligands, the substitution proceeds by a one-step associative interchange mechanism via pentacoordinated TS with similar structure as for cisplatin hydrolysis (see below).

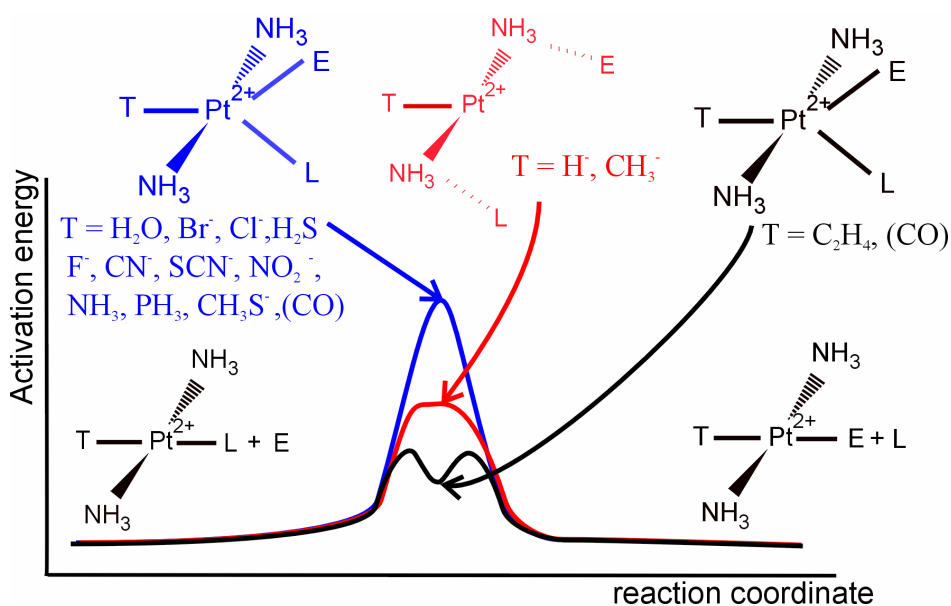


Figure 1: Dependence of the energy profiles of substitution reactions on the nature of the ligand T in the trans position. (leaving ligand = L; entering ligand = E)

The discovery of the antitumor activity of cisplatin by Rosenberg more than 40 years ago¹⁰ started the extended research of chemical and biological properties of platinum compounds. Cisplatin is a very efficient drug against ovarian, bladder, head, neck as well as non-small lung and cervical cancers.¹¹ Being applied intravenously cisplatin is relatively stable in the blood plasma and it is hydrolyzed in the cytoplasm due to the drop of concentration of the Cl⁻ ions. Both steps of hydrolysis were described in **P2** as a nucleophilic attack of the entering water ligand. As ammine groups have weak σ -donation and π -back-donation abilities both hydrolytic reactions proceed by the one-step mechanism via pentacoordinated TS structures with the shape of the distorted trigonal bipyramid. Such a shape had been predicted in previous studies^{3,12} but in **P2** the TS structures were fully optimized in a mathematically rigorous way for the first time. A substantial elongation of the bonds from the central platinum atom towards the leaving and entering ligands compared to bond lengths of these ligands in square-planar complexes was shown. Both hydrolysis steps were endergonic reactions (Figure 2).

A number of DFT functionals in combination with different basis sets was also tested. The best results were obtained with the B3P86 functional. Substantial improvement of the geometry of cisplatin and its derivatives could be achieved by the inclusion of the polarization f functions on the platinum atom.

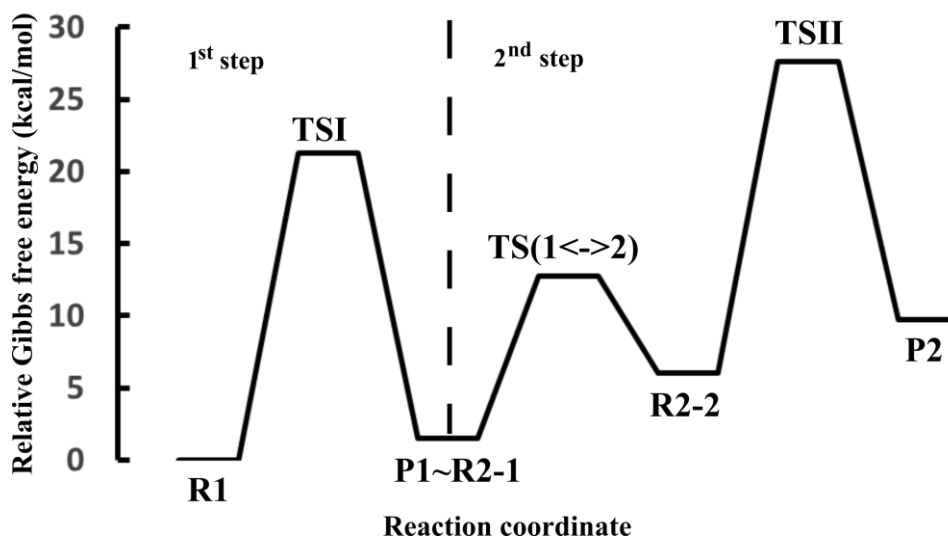


Figure 2: Gibbs free energy profile for two steps of cisplatin hydrolysis in water calculated at the BLYP/SCIPCM/LANL2DZ*/6-31G**/B3P86/ LANL2DZ/6-31G* level. The designation of the structures is taken from **P2**.

A hydrolyzed positively charged drug then attacks DNA. The binding of the Pt(II) drugs to DNA is believed to be responsible for their antitumor activity. At first cisplatin always binds the N7 atom of guanine. In the second step, it binds predominantly to adjacent guanine and adenine to form 1,2-GG and 1,2-GA crosslinks, respectively. The formation of these adducts leads to the destacking of the two bases, a roll of 25–50 degrees between the two bases involved in cross-linking and a global bend of the helix axis towards the major groove by about 20–40 degrees.^{13–15} The molecular structure of this complex was solved by X-ray diffraction in the Dickerson group for the first time.¹⁶ The phosphodiester backbone conformations of various conformers of the cisplatin adduct with d(GpG) were discussed in the study of Marzilli et al.¹⁷ They combined several experimental methods (¹H and ³¹P NMR, CD spectroscopy) with molecular mechanical (MM) and molecular dynamical (MD) calculations.

Modified structure of DNA is recognized by many proteins including NER (nucleotide excision repair), MMR (mismatch repair system) or HMG (high-mobility group) domain proteins.¹⁸ A ternary complex of DNA oligomer with cisplatin and HMG1 protein was solved from the crystal structure by Ohndorf et al.¹⁹ The key interaction for the recognition process was the stacking of the phenylalanine side chain of the HMG1 protein between the two destacked guanine bases which formed a crosslink with cisplatin. The binding of the protein to the platinated DNA can be too stable and thus the protein may block the DNA chain and hinder important processes as transcription or replication that may lead to apoptosis.

Despite the fast progress in a computational power still only relatively small systems can be explored by DFT methods. Therefore, DNA is usually represented by a single nucleobase (guanine, adenine in case of Pt(II) complexes) in reactivity studies. **P3** was the first study in which all relevant structures along the possible reaction pathways were fully optimized. Structures of TSs were similar to those for cisplatin hydrolysis and we have shown a kinetic preference of cisplatin binding to N7 atom of guanine compared to adenine. The O6 and NH₂ groups of guanine and adenine, respectively, had stabilizing role in the structures as H-bond acceptors. For guanine we also evaluated activation energies for the Pt-O6 bond formation. Similar systems were deeply analyzed in many subsequent studies.²⁰⁻²³

P3 and the above cited studies described reasonably the chemistry of the binding but did not consider the conformation of the structures in a real DNA environment. For example when binding of cisplatin to two guanine bases was studied the final diadduct with the head-to-tail conformation of the two bound guanine rings was the most stable. However, the less stable diadduct with the head-to-head conformation was closer to guanines' conformation in DNA.²⁴ Mantri et al. used the single stranded AGA trinucleotide as a substrate for the cisplatin binding.²⁵ They showed that a strong preference for AG adducts over GA adducts is caused by the TS stabilization by the H-bond between the ammine ligand of cisplatin and the 5'-phosphate group of the trinucleotide. The formation of this H-bond was not feasible in the GA adduct.

The use of cisplatin in the treatment of various tumors has several limitations such as severe side effects and the possibility of intrinsic and acquired resistance. The search for new less toxic and more efficient drugs resulted in the discovery of second- and, later, third-generation drugs, such as carboplatin, oxaliplatin, satraplatin (Pt(IV) complex labeled as JM216) or dinuclear and trinuclear derivatives (BBR 3464). Chemistry of currently used drugs²⁶ is limited since only sufficiently stable compounds do not react too early in the blood stream but are activated after entering the cell. In the second-generation drugs two chloride ligands were displaced by bidentate groups (e.g. by cyclobutanedicarboxylate in carboplatin) bound by the oxygen atoms to the Pt(II) central atom. The mechanism of hydrolysis of these groups is still not well understood and it is not clear in which form these drugs react with DNA.^{27,28} The non-leaving groups are always bound by the nitrogen atom to the Pt(II)-atom and they differ by the nature of the attached carbohydrate residue. In the third-generation drug oxaliplatin two ammine ligands were replaced by the bidentate cyclohexane-1R,2R-diamine (DACH) ligand. Oxaliplatin forms similar intrastrand adducts with 1,2- d(GpG) bases of the DNA oligomer as cisplatin²⁹ but different nature of the non-leaving group may change interactions with the proteins affecting cellular uptake of the drug and the repair of

DNA-drug lesions.³⁰

In **P9** we described the binding of the fully hydrolyzed oxaliplatin with the double stranded pGpG sequence that represented the smallest possible model which ensured relative positions of the two reactive guanine rings close to real DNA. Aim of this study was to see the influence of the DNA backbone's rigidity and non-covalent interactions on the energetics of the binding of the Pt(II) complex (platination) and the specificity of the oxaliplatin binding. All structures were fully optimized to observe the changes of the DNA structure, the base pairing strengths and charge distribution not only for the final 1,2-GG diadduct but mainly for the TS structures that are not experimentally observable.

The formation of the diadduct could proceed in two steps via the formation of either 3'- or 5'-monoadducts. The monoadduct formation was the rate determining step for the whole reaction. The formation of the 5'G monoadduct was kinetically strongly preferred. TS in the 3'G direction had more diffusive character from the steric reasons that resulted in a higher activation barrier. The binding in the 3'G direction was competitive with the 5'G binding only when the DACH ligand adjoined the sugar-phosphate backbone which however completely changed the direction of the 5'-phosphate group disrupting the helical structure of DNA. In agreement with experiments³¹ the DNA conformation changed from the standard B-form toward the A-form during the platination (Figure 3).

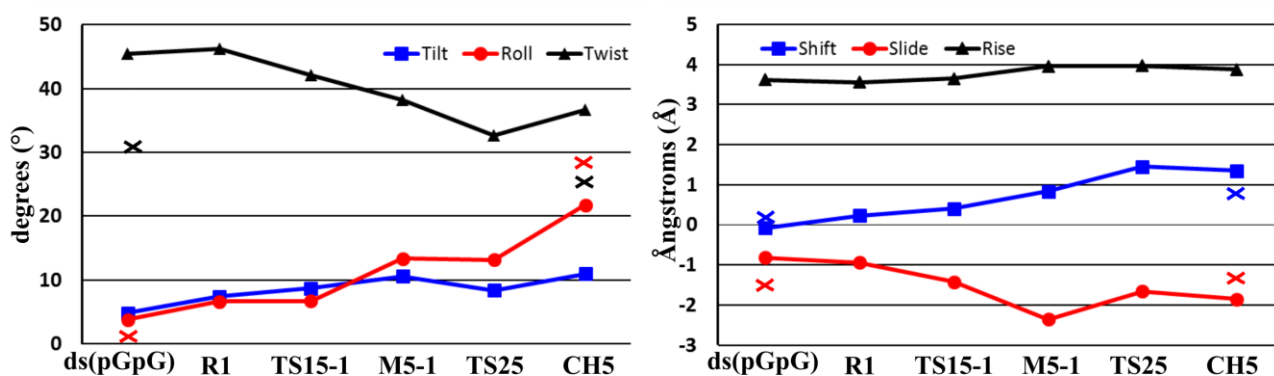


Figure 3: Changes of the DNA parameters during the Pt-DACH binding to the ds(pGpG) dinucleotide. Values from NMR experiments³² are shown by crosses on the left and right parts of the graphs for pure DNA and the DNA-oxaliplatin adduct, respectively. The designation of the structures is taken from **P9**.

Deformation energy of the ds(pGpG) dinucleotide was linearly dependent on the angle between the planes of two guanine rings. Thus, destacking of the two purine bases can be considered as

energetically the most expensive part of the DNA conformational change connected with the platination and the changes of the sugar-phosphate backbone conformation should be less demanding.

The total strength of H-bond interactions in two platinated G-C base pairs was not changed. As it was already suggested³³ in both base pairs the H-bond from O6 oxygen was weakened since this atom was involved in interactions with the drug but in the same time the other two H-bonds became stronger.

Charge transfer proceeded in three steps. The first step corresponded to the H-bond formation between the drug and the ds(pGpG) dinucleotide and changed to some extent the charges of all parts of the system. The other two steps were connected with dative bond formations between Pt(II) complex and the two guanines keeping rest of the DNA system almost unaffected.

The complex of cisplatin with GpG dinucleotide was examined by Carloni et al.³⁴ who also considered certain hydration aspects of cisplatin (cf. below) using Car-Parrinello MD simulations. Reactivity studies of the drug-DNA systems can be also described by combined QM/MM simulations in which the reactive part of the system is described quantum mechanically and the rest of the system is described by classical molecular mechanics.³⁵⁻³⁷ However, in most previous theoretical studies the conformational changes caused by the Pt-DNA adduct formation were described by classical MM and MD simulations.³⁸⁻⁴⁰ The reliability of these studies depends strongly on the quality of the force fields used and the force fields for metal complexes are still under development.^{41,42} We contributed to this field of research in **P1** showing that the base plane puckering should not be neglected in MM and MD calculations. When this deformation was incorporated as a correction into the value of the out-of-plane bending constant of the Pt-N7 bond it led to the decrease of this parameter by about 40 % increasing the flexibility of platinated DNA in MD simulations.

The side effects of cisplatin include nephrotoxicity, nausea and vomiting. They can be treated by extensive hydration and administration of serotonin receptor antagonists⁴³ or by a combination of a 5-hydroxytryptamine receptor antagonist, a neurokinin-1 antagonist, and dexamethasone,⁴⁴ but other side effects like ototoxicity and peripheral neuropathy still remain. A non-specific binding to proteins is probably responsible for the side effects of Pt(II) drugs.⁴⁵ In **P5** we calculated reaction Gibbs free energies for interactions of hydrolyzed +1 charged (chloroaqua and hydroxoqua) derivatives of cisplatin with cysteine and methionine. All possible binding centers (S, N, O atoms) in the isolated molecules of the amino acids were considered. In first step connected with the

monoadduct formation the most thermodynamically advantageous target for the platinum attack was the sulphur atom of cysteine. In the second step the reaction could proceed by the binding to the nitrogen atom forming the $\kappa^2(\text{S},\text{N})$ chelate of cysteine as the most energetically favorable structure.

Non-bonding interactions of Pt(II)-complexes are interesting due to the non-classical behavior of the central Pt(II) atom. Kozelka with coworkers showed⁴⁶⁻⁴⁸ that this atom interacts with water solvent molecules by the Pt \cdots HOH ‘inverse hydration’ interaction in neutral complexes while the classical Pt \cdots OH₂ interaction is repulsive. In **P9** we also observed the Pt \cdots HOH interaction in one optimized structure between the leaving water molecule and the Pt-DNA adduct but in this case the adduct was +2 charged. According to ETS-NOCV analysis this interaction was stabilized by orbital interaction energy of -6.9 kcal/mol. Since it could result from the existence of just a shallow local minimum in these static calculations we decided to explore this phenomena in more detail in **P11** using both static and molecular dynamical DFT calculations for cisplatin and its charged derivatives. Indeed, the Pt \cdots HOH interaction existed even for the +2 charged complex although the incidence and the strength of this interaction decreased with increasing positive charge of the complex. The interaction is stabilized mainly by the charge transfer from the 5d(z²) orbital of the platinum atom towards the inversely bound water molecule. Electrons from this orbital manifested the lowest value of average local ionization energy being more easily ionized than electrons from the chloride ligands (**P6**). The Pt \cdots OH₂ interaction was attractive only for the +2 charged diaqua complex but being very weak this interaction manifested itself only as a slight deformation of the H-bond network around the interacting water molecule. Thus, the Pt(II) atom in cisplatin and its +1 charged derivatives either formed Pt \cdots HOH interaction(s) with water solvent molecules or was surrounded by a hydrophobic cage of non-interacting water molecules which was anchored to ligands of the Pt(II) complex by a system of H-bond interactions. We are going to explore an impact of this behavior on the course of cisplatin hydrolysis in future studies.

Some other properties of cisplatin were also discussed in studies **P6** and **P10** where this complex was used as a reference molecule. These studies are described in the next section.

2.2. Hydrolysis reactions of piano-stool Ru(II)-complexes

Success of Pt(II) complexes in cancer treatment stimulated the search for complexes of other

metals with a wider range of anticancer properties but fewer side effects and which circumvent developed and intrinsic resistance. Ruthenium complexes may represent attractive alternatives to Pt drugs since they exhibit a similar reactivity but are less toxic. Two Ru(III) complexes have entered clinical trials, $\text{trans}[\text{RuCl}_4(\text{DMSO})(\text{Im})]\text{ImH}$ (NAMI-A, Im = imidazole) and $\text{trans}[\text{RuCl}_4(\text{Ind})_2]\text{IndH}$ (KP1019, Ind = indazole).⁴⁹ In vivo these drugs are reduced to more reactive Ru(II) counterparts. We were interested in Ru(II)(arene) octahedral complexes where the arene ring occupies three binding positions giving a ‘piano-stool’ or ‘half-sandwich’ shape to these compounds. Their biotransformation is considered to follow a similar mechanism as cisplatin: they are also delivered as neutral compounds and then inside the cells are hydrolyzed on more reactive positively charged complexes. All three papers **P6**, **P10** and **P12** deal with the hydrolysis reaction of Ru(II)-complexes and were done in a close collaboration with prof. Burda (Charles University, Prague).

In **P6** the hydrolysis reactions of the monofunctional $[\text{Ru}(\text{benzene})(\text{en})\text{Cl}]^+$ (en = ethylenediamine) and bifunctional $[\text{Ru}(\text{benzene})(\text{pta})\text{Cl}_2]^0$ (RAPTA-B, pta = 1,3,5-triaza-7-phosphatricyclo[3,3,1,1]decane) complexes were studied and compared with cisplatin. Both drugs were hydrolyzed by about one order of magnitude faster than cisplatin. Substitution reactions of these complexes may proceed by two competing associative interchange and dissociative mechanisms. Their relative preference strongly depended on the nature of the ligands. The dissociative mechanism was not possible in the presence of the bidentate *en* ligand. The two coordinated nitrogen atoms of the *en* ligand were not able to occupy positions in which the perpendicular Ru-N-N plane with respect to the plane of the benzene ring would have been formed. This arrangement of non-leaving ligands was typical for the geometries of an intermediate structure in the dissociative mechanism (cf. structure Int1 in Figure 4).

On the other hand, the hydrolysis of the RAPTA-B derivative with the negatively charged OH⁻ group tightly bound to the Ru(II) atom as a non-leaving ligand proceeded only by the dissociative mechanism. The ligands in the RAPTA-B complex were much more destabilized by the OH⁻ ligand than by the Cl⁻ ligand(s) which led to an intermediate structure with very long Ru-water and Ru-Cl distances minimizing the inter-ligand repulsion.

The hydrolysis of the Ru(arene) complexes with Cl⁻ and water ligands (and with nalidixic acid or its derivatives studied later: see below) could proceed by both mechanisms since they showed very similar reaction rates for all substitution reactions studied (Figure 4; cf. **P12**).

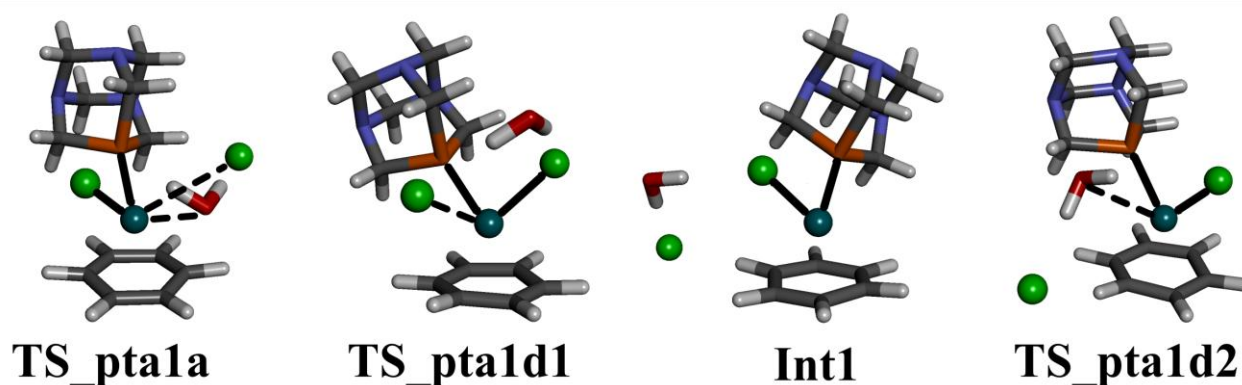


Figure 4: Structures relevant for the first hydrolysis reaction of the RAPTA-B complex. TS for the associative interchange mechanism (TS_pta1a); the structures for the dissociative mechanism: the first TS (TS_pta1d1), the intermediate (Int1) and the second TS (TS_pta1d2). The designation of the structures is taken from **P6**. Standard coordination bonds and Ru interactions with loosely bound ligands (Ru-ligand distance < 3.0 Å) are shown by black solid and dashed lines, respectively. Benzene, pta and water ligands are shown by a stick model; Ru(II) atom and Cl⁻ ligands are highlighted by a ball model. All these structures lie within the free energy range of 2.2 kcal/mol.

In the subsequent **P10** study we analyzed the hydrolysis reactions from **P6** in more detail using HF, DFT and more expensive MP_x ($x = 2, 3, 4$) and CCSD(T) ab initio methods. The evaluation of electronic properties and reaction descriptors was done for all stationary structures and selected intrinsic reaction coordinate (IRC) points along the reaction coordinates. Only the dissociative mechanism was considered for RAPTA-B but we were not able to confirm the existence of the reaction intermediate by CCSD(T) and MP_x methods. These methods gave only a flat area on the respective part of the potential energy surface instead of a true minimum. CCSD(T) and MP_x optimized geometries probably differ from the B3LYP ones used for the analyses. Since CCSD(T) energy profiles were analyzed this discrepancy influenced mainly the course of reaction force and force constant. These descriptors enabled a division of the reaction course into several stages with predominant either structural or electronic changes of the structures. Maximum/minimum values of average local ionization energies and molecular electrostatic potential and their position on the molecular isosurface reflected changes in the character of the metal complexes during hydrolysis reactions. Values of chemical potential and reaction electronic flux enabled us to obtain a closer insight on exact timing of the creation/disruption of bonding and non-bonding interactions in the course of these reactions.

In **P12** we studied hydrolysis reactions of piano-stool Ru(II) complexes containing nalidixic

acid or its derivatives (thionalidixic acid, ofloxacin or cinoxacin). Anticancer and antibacterial activities of these compounds were revealed by Turel et al.^{50,51}

Firstly we determined the reaction mechanism on the model compound with benzene as an arene ligand and nalidixic acid as a quinolone bidentate ligand. Both associative and dissociative mechanisms were considered for substitution reactions on all three coordination sites in the complex: the chloro ligand and the keto and carboxyl groups of the nalidixic acid. The carboxyl group was modeled in both protonated and deprotonated states. Dechlorination was found to be the most probable reaction in the acidic and especially in the basic environment. The associative and dissociative mechanisms gave similar rate constants for all hydrolysis reactions.

In the second part we studied kinetic and thermodynamic parameters of the hydrolysis of the Ru-Cl bond in the complexes with nalidixic and thionalidixic acids, cinoxacin and ofloxacin considering only the dissociative mechanism. The reaction rate was dependent on the nature of the quinolone ligand and in the basic environment it decreased in the order: cinoxacin > nalidixic acid > thionalidixic acid > ofloxacin. In neutral solution the reaction rates were approximately by four orders of magnitude slower and followed the order nalidixic acid > cinoxacin > thionalidixic acid > ofloxacin.

2.3. Mg²⁺ ions in the RNA environment

Interactions with metal ions are essential for the stability of secondary and tertiary structure of nucleic acids. Monovalent cations are bound non-specifically with nucleic acids creating ‘a cloud’ around the negatively charged phosphate groups. In addition to that due to their high charge density the divalent cations are also able to influence the chemistry of nucleic acids: these ions may shift the tautomer equilibrium of the bases,⁵² shift acidity of the functional groups⁵³ and participate in a cleavage reaction of the sugar-phosphate chain in case of RNA.⁵⁴ We were interested in all these phenomena to some extent.

In **P7** we studied the influence of the Mg²⁺ ion on the activation (deprotonation) of the 2’OH group of the ribose. This is the first step of the cleavage of the sugar-phosphate backbone in the self-cleaving ribozymes since the activated 2’O⁻ group acts as a nucleophile attacking the neighboring phosphate group which may lead to the disruption of the P-O5’ bond. The outer-sphere coordination of the Mg²⁺ ion to 2’OH lowered the pK_a value of this group by more than three log units and the inner-sphere coordination of the metal further stabilized the developing

negative charge on the 2'O center. The change from the inner-sphere to the outer-sphere coordination appeared to be driven by the energy cost of the first coordination shell reorganization rather than by the electrostatic repulsion between the ligands.

We considered several reaction mechanisms of the 2'OH activation and tried to understand the role of the Mg^{2+} ion with respect to the nature and the position of the nucleophile. The metal-ion catalysis was more effective with a specific base and the inner-sphere coordination of the metal stabilizing "long-lived" intermediates. In presence of a nucleobase (guanine G12 in case of the hammerhead ribozyme⁵⁵) that acted as a general base and the metal ion bound by the outer-sphere coordination the 2'OH activation was catalyzed purely by the electrostatic influence of the metal ion.

Influence of the environment and the metal Mg^{2+} ion on the tautomeric equilibrium of the uracil base was studied in **P8**. The rare keto-enol form was strongly stabilized in the isolated system of uracil with the bare metal ion. On the other hand, the environmental effects such as the presence of the metal ion's hydration shell, bulk water, and possibly also of the phosphate group in the first coordination shell of the metal, shielded the electrostatic field of the metal contributing to the stabilization of the canonical diketo tautomer of uracil. Bulk water solvent represented by the polarizable continuum model decreased the polarization of uracil by the hydrated metal ion by more than 50 % while the charge transfer between the two subsystems remained almost unchanged (decreased by less than 10 % in most cases).

3. Future perspectives

Currently we are studying the influence of the ligand substitution effects on the reactivity of the Pt(II) and Ru(II) complexes with the goal to understand their structure-activity relationships. This experience should be useful not only with respect to cytotoxic properties of these compounds but also with respect to the understanding of their catalytic activities which represent another important field of chemistry of metal complexes^{56,57} but was not described in the previous text. Homogeneous and later also heterogeneous catalysis should be next steps of our research.

4. Summary

We were interested mainly in the properties of short lived structures (the reaction intermediates and/or TS structures) which are formed during reactions of metal compounds but are hardly detectable experimentally.

The hydrolysis reactions of metallodrugs were described in four papers: in **P2** for cisplatin and in **P6**, **P10**, **P12** for piano-stool Ru(II)-complexes. In **P11** which dealt with non-bonding interactions of cisplatin and its hydrolyzed derivatives we showed that Pt \cdots OH₂ interaction was in fact repulsive for neutral and +1 charged complexes. Reactions of hydrolyzed Pt(II) complexes with the model compounds which represented the most important cellular targets were described in **P3** (nucleobases guanine and adenine), **P5** (amino acids cysteine and methionine) and **P9** (1,2-pGpG dinucleotide). Reactivity of Pt(II) complexes was also studied more generally in **P4** dealing with the trans effect. The ligand in the trans position influenced not only the energetics but also the mechanism of the substitution reaction. A small contribution **P1** to the force field development of Pt(II) complexes showed the importance of the puckering of the bound purine base for MD simulations of Pt-DNA adducts.

In **P7** we studied the role of the Mg²⁺ ion in the 2'OH activation as the first step in the ribozyme self-cleavage. Since both inner-sphere and outer-sphere binding modes of the Mg²⁺ ion were considered this study could represent a more general description of the role of the metal ion in the deprotonation reaction shifting the acid-base equilibrium. Finally, in **P8** we dealt with the influence of individual environmental factors (metal ion, hydration, phosphate group) on the tautomer equilibrium of the uracil nucleobase.

5. References

- (1) Schnabl, J.; Suter, P.; Sigel, R. K. O. *Nucleic Acids Res.* **2012**, *40* (D1), D434–D438.
- (2) Arnér, E. S. J.; Nakamura, H.; Sasada, T.; Yodoi, J.; Holmgren, A.; Spyrou, G. *Free Radic. Biol. Med.* **2001**, *31* (10), 1170–1178.
- (3) Lin, Z. Y.; Hall, M. B. *Inorg. Chem.* **1991**, *30* (4), 646–651.
- (4) Wendt, O. F.; Elding, L. I. *J. Chem. Soc.-Dalton Trans.* **1997**, No. 24, 4725–4731.
- (5) Khoroshun, D. V.; Musaev, D. G.; Morokuma, K. *J. Comput. Chem.* **2007**, *28* (1), 423–441.
- (6) Kapoor, P. N.; Kakkar, R. *J. Mol. Struct.-Theochem* **2004**, *679* (3), 149–156.
- (7) Zhu, J.; Lin, Z. Y.; Marder, T. B. *Inorg. Chem.* **2005**, *44* (25), 9384–9390.

- (8) Pinter, B.; Van Speybroeck, V.; Waroquier, M.; Geerlings, P.; De Proft, F. *Phys. Chem. Chem. Phys.* **2013**, *15* (40), 17354.
- (9) Manojlovic-Muir, L. J.; Muir, K. W. *Inorganica Chim. Acta* **1974**, *10*, 47–49.
- (10) Rosenberg, B.; Camp, L. V.; Krigas, T. *Publ. Online 13 Febr. 1965 Doi101038205698a0* **1965**, *205* (4972), 698–699.
- (11) Florea, A.-M.; Büsselberg, D. *Cancers* **2011**, *3* (1), 1351–1371.
- (12) Deeth, R. J.; Elding, L. I. *Inorg. Chem.* **1996**, *35* (17), 5019–5026.
- (13) Yang, D.; van Boom, S. S. G. E.; Reedijk, J.; van Boom, J. H.; Wang, A. H.-J. *Biochemistry (Mosc.)* **1995**, *34* (39), 12912–12920.
- (14) Gelasco, A.; Lippard, S. *Biochemistry (Mosc.)* **1998**, *37* (26), 9230–9239.
- (15) Dunham, S. U.; Dunham, S. U.; Turner, C. J.; Lippard, S. J. *J. Am. Chem. Soc.* **1998**, *120* (22), 5395–5406.
- (16) Wing, R. M.; Pjura, P.; Drew, H. R.; Dickerson, R. E. *EMBO J.* **1984**, *3* (5), 1201–1206.
- (17) Williams, K. M.; Scarcia, T.; Natile, G.; Marzilli, L. G. *Inorg. Chem.* **2001**, *40* (3), 445–454.
- (18) Jung, Y.; Lippard, S. *Chem. Rev.* **2007**, *107* (5), 1387–1407.
- (19) Ohndorf, U.-M.; Rould, M. A.; He, Q.; Pabo, C. O.; Lippard, S. J. *Nature* **1999**, *399* (6737), 708–712.
- (20) Baik, M. H.; Friesner, R. A.; Lippard, S. J. *J. Am. Chem. Soc.* **2003**, *125* (46), 14082–14092.
- (21) Costa, L. A. S.; Hambley, T. W.; Rocha, W. R.; De Almeida, W. B.; Dos Santos, H. F. *Int. J. Quantum Chem.* **2006**, *106* (9), 2129–2144.
- (22) Raber, J.; Zhu, C. B.; Eriksson, L. A. *J. Phys. Chem. B* **2005**, *109* (21), 11006–11015.
- (23) Sarmah, P.; Deka, R. C. *J. Mol. Struct. THEOCHEM* **2010**, *955* (1–3), 53–60.
- (24) Ranaldo, R.; Margiotta, N.; Intini, F.; Pacifico, C.; Natile, G. *Inorg. Chem.* **2008**, *47* (7), 2820–2830.
- (25) Mantri, Y.; Lippard, S. J.; Baik, M. H. *J. Am. Chem. Soc.* **2007**, *129* (16), 5023–5030.
- (26) Wheate, N. J.; Walker, S.; Craig, G. E.; Oun, R. *Dalton Trans.* **2010**, *39* (35), 8113–8127.
- (27) Legendre, F.; Bas, V.; Kozelka, J.; Chottard, J.-C. *Chem. – Eur. J.* **2000**, *6* (11), 2002–2010.
- (28) Kozelka, J. *Inorg. Chim. Acta* **2009**, *362* (3), 651–668.
- (29) Spingler, B.; Whittington, D.; Lippard, S. *Inorg. Chem.* **2001**, *40* (22), 5596–5602.
- (30) Malina, J.; Novakova, O.; Vojtiskova, M.; Natile, G.; Brabec, V. *Biophys. J.* **2007**, *93* (11), 3950–3962.
- (31) Vrána, O.; Mašek, V.; Dražan, V.; Brabec, V. *J. Struct. Biol.* **2007**, *159* (1), 1–8.
- (32) Wu, Y.; Bhattacharyya, D.; King, C. L.; Baskerville-Abraham, I.; Huh, S.-H.; Boysen, G.; Swenberg, J. A.; Temple, B.; Campbell, S. L.; Chaney, S. G. *Biochemistry (Mosc.)* **2007**, *46* (22), 6477–6487.
- (33) Robertazzi, A.; Platts, J. A. *Inorg. Chem.* **2005**, *44* (2), 267–274.

- (34) Carloni, P.; Sprik, M.; Andreoni, W. *J. Phys. Chem. B* **2000**, *104* (4), 823–835.
- (35) Gkionis, K.; Platts, J. *J. Biol. Inorg. Chem.* **2009**, *14* (8), 1165–1174.
- (36) Magistrato, A.; Ruggerone, P.; Spiegel, K.; Carloni, P.; Reedijk, J. *J. Phys. Chem. B* **2006**, *110* (8), 3604–3613.
- (37) Robertazzi, A.; Platts, J. *Chem. - Eur. J.* **2006**, *12* (22), 5747–5756.
- (38) Elizondo-Riojas, M.; Kozelka, J. *J. Mol. Biol.* **2001**, *314* (5), 1227–1243.
- (39) Hambley, T.; Jones, A. *Coord. Chem. Rev.* **2001**, *212*, 35–59.
- (40) Teletchea, S.; Skauge, T.; Sletten, E.; Kozelka, J. *Chem. - Eur. J.* **2009**, *15* (45), 12320–12337.
- (41) Melchior, A.; Martínez, J. M.; Pappalardo, R. R.; Sánchez Marcos, E. *J. Chem. Theory Comput.* **2013**, *9* (10), 4562–4573.
- (42) Šebesta, F.; Sláma, V.; Melcr, J.; Futera, Z.; Burda, J. *J. Chem. Theory Comput.* **2016**, *12* (8), 3681–3688.
- (43) Cubeddu, L. X.; Hoffmann, I. S.; Fuenmayor, N. T.; Finn, A. L. *N. Engl. J. Med.* **1990**, *322* (12), 810–816.
- (44) Ranganath, P.; Einhorn, L.; Albany, C. *BioMed Res. Int.* **2015**, *2015*, e943618.
- (45) Reedijk, J.; Teuben, J. M. In *Cisplatin*; Lippert, B., Ed.; Verlag Helvetica Chimica Acta, 1999; pp 339–362.
- (46) Berges, J.; Caillet, J.; Langlet, J.; Kozelka, J. *Chem. Phys. Lett.* **2001**, *344* (5–6), 573–577.
- (47) Rizzato, S.; Bergès, J.; Mason, S. A.; Albinati, A.; Kozelka, J. *Angew. Chem. Int. Ed.* **2010**, *49* (41), 7440–7443.
- (48) Bergès, J.; Fourré, I.; Pilmé, J.; Kozelka, J. *Inorg. Chem.* **2013**, *52* (3), 1217–1227.
- (49) Levina, A.; Mitra, A.; Lay, P. A. *Metallomics* **2009**, *1* (6), 458–470.
- (50) Turel, I.; Kljun, J.; Perdih, F.; Morozova, E.; Bakulev, V.; Kasyanenko, N.; Byl, J. A. W.; Osheroff, N. *Inorg. Chem.* **2010**, *49* (23), 10750–10752.
- (51) Kljun, J.; Bytzeck, A. K.; Kandioller, W.; Bartel, C.; Jakupec, M. A.; Hartinger, C. G.; Keppler, B. K.; Turel, I. *Organometallics* **2011**, *30* (9), 2506–2512.
- (52) Kabeláč, M.; Hobza, P. *J. Phys. Chem. B* **2006**, *110* (29), 14515–14523.
- (53) Sigel, H. *J. Am. Chem. Soc.* **1975**, *97* (11), 3209–3214.
- (54) Schnabl, J.; Sigel, R. K. *Curr. Opin. Chem. Biol.* **2010**, *14* (2), 269–275.
- (55) Thomas, J. M.; Perrin, D. M. *J. Am. Chem. Soc.* **2008**, *130* (46), 15467–15475.
- (56) Kumar, P.; Gupta, R. K.; Pandey, D. S. *Chem. Soc. Rev.* **2013**, *43* (2), 707–733.
- (57) Labinger, J. A. *Chem. Rev.* **2017**, doi: 10.1021/acs.chemrev.6b00583

LETTERS

Force Field for Platinum Binding to Adenine and Guanine Taking into Account Flexibility of Nucleic Acids Bases**Zdenek Chval and Miroslav Sip****Faculty of Biological Sciences, University of South Bohemia, and Institute of Plant Molecular Biology, Academy of Sciences, Branišovská 31, 370 05 České Budejovice, Czech Republic**Received: October 15, 1997; In Final Form: January 5, 1998*

Many metal-based antitumor drugs such as *cis*-diamminedichloroplatinum(II) (cisplatin) bind to purine nucleic acid (NA) bases via N7. On the basis of ab initio quantum mechanics calculations using $[\text{Pt}(\text{NH}_3)_3 \text{purine}]^{2+}$ (where purine = adenine or guanine) as a model system, we show that the common assumption of planarity of NA bases leads to an overestimation of the platinum out-of-plane bending molecular mechanics constant in certain cases by more than 50%. New values of force-field parameters are given, and some of the implications on molecular mechanics computations of platinum nucleic acid adducts are discussed.

Introduction

Molecular modeling largely depends on a correct set of parameters defining the so-called force field of the molecular object. For platinum binding to DNA, for a long time only approximate estimates of the molecular mechanics energy constants were used. The growing interest in these compounds resulting from their antitumor activity led to exact evaluation of force-field parameters using mainly ab initio calculations.^{1–5} The major DNA–*cis*-diamminedichloroplatinum(II) (cisplatin) adduct is the intrastrand GpG chelate.^{6–8} Upon cisplatin binding, the B-DNA structure is altered with a resulting kink and double-helix unwinding.^{9,10} The changed structure and its recognition on the molecular level is thought to be responsible for the antitumor action of cisplatin and its analogues. The geometry of the resulting adducts is largely given by the square planar geometry of cisplatin. The relative position of the guanines and cisplatin is defined by the rotation angle about the Pt–N7 bond and the direction of this bond with respect to the guanine residue. Whereas the free rotation about the single covalent bond is hindered only sterically, by noncovalent

interactions, the second characteristic—the direction—has an equilibrium value situated in the plane of the purine rings and every excursion of the platinum atom out of this direction is penalized by an increase of the steric energy of the adduct. The increase of the angle-bending contribution to the steric energy is usually approximated in molecular mechanics by the quadratic term

$$E_{\alpha} = K_{\alpha} \alpha^2 \quad (1)$$

where α is the bond angle deviation from the equilibrium value and k_{α} is the bending constant corresponding to the angle α . The direction of the N7–Pt bond with respect to its equilibrium value may be decomposed into two components: bending in the plane of the base and the out-of-plane bending. The former parameter is usually taken from the values computed for the N-glycosidic bond.¹ The latter one, the out-of-plane bending, is the key factor determining the geometry of platinum–DNA adducts and is not directly accessible to experimental measurement. The out-of-plane bending was first computed by Kozelka et al. by ab initio methods.¹ The parameters derived from these studies yielded in molecular mechanics a realistic behavior of DNA–platinum adducts.^{11,12}

* To whom the correspondence should be addressed at the University of South Bohemia. E-mail: sip@umbr.cas.cz.

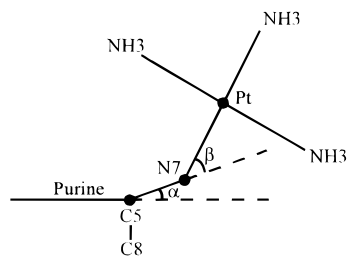


Figure 1. 1. Schematic drawing of the $[\text{Pt}(\text{NH}_3)_3 \text{ purine}]^{2+}$ adduct showing the out-of-plane bending angles α and β .

The question we essayed to answer in this work was whether the purine ring is stiff enough to withstand large out-of-plane bending of the N7–Pt bond without deformation (puckering) of the five-membered cycle and what would become the platinum out-of-plane deviation if such puckering occurs.

Computational Methods

Quantum calculations employ the GAMESS program.¹³ Valence basis sets (VBSs) and effective core potentials (ECPs) were used for heavy atoms and a -31G basis for hydrogens. The GAMESS ECPs¹⁴ take into account relativistic effects, which become important for the platinum atom. Transition-metal VBS is quadruple and triple- ξ for sp and d shells, respectively, while main group elements are valence double- ξ .¹⁴ Geometries are optimized at the restricted Hartree–Fock (RHF) level for closed-shell singlets.

The total excursion of the platinum atom out of the nucleobase plane is given in general by both the out-of-plane bending of the N7–Pt bond (angle β in Figure 1) and the puckering of the purine base. The puckering of course concerns the whole purine ring and will be given not only by the stress imposed by covalent bonds (Pt–N7 and N-glycosidic bonds) and hydrogen bonds but also by numerous other interactions, for example, stacking interactions. Simple geometrical considerations show that the component of puckering that is by far the most important for the conformation of cisplatin adducts is the deviation of the purine N7 atom from the plane of the base. This deviation may be quantified by the angle of the rotation of the N7 atom about the axis C5–C8.

Results and Discussion

The first set of calculations, which practically reproduced the results published by Kozelka et al.,¹ was performed for a fixed value of $\alpha = 0$ and β varying stepwise from 0 to 40° (curve 1 in Figures 2, 3). The second set of energy values was obtained for $\beta = 0$ and α varying from 0 to 20° (curve 2 in Figures 2, 3).

All calculations were done with eight constraints, and all other coordinations were fully optimized.

When the Pt–N7 bond alone was bent ($\alpha = 0$), six of the constraints were used to keep purine rings planar, the seventh one was used to keep the PtN₄ plane perpendicular to that of the purine plane, and the eighth one was used to keep the desired value of the angle β constant in the course of optimization.

When the N7 atom was allowed to deviate out of the nucleobase plane along with the platinum atom, five constraints were used to keep the rest of the purine rings planar, one constraint was used to keep the PtN₄ plane perpendicular to that of the purine, and the last one was used to keep the desired value of the angle α constant in the course of optimization.

The resulting angular dependencies of ab initio energies for the guanine adduct plotted in Figure 3 are quadratic in the

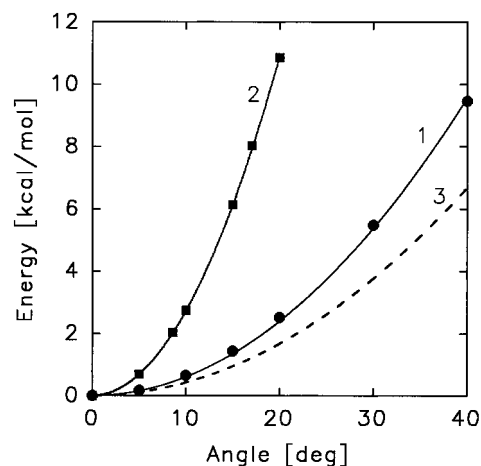


Figure 2. 2. Ab initio energies of $[\text{Pt}(\text{NH}_3)_3 \text{ adenine}]^{2+}$: (1) E_β (for $\alpha = 0$); (2) E_α (for $\beta = 0$); (3) $E_{\beta\alpha}$ (for $\alpha = 0$).

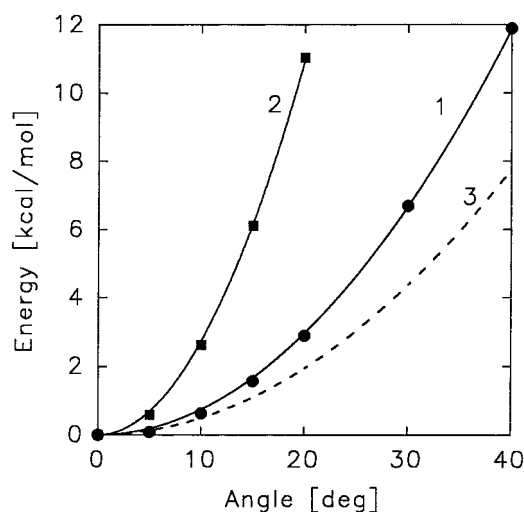


Figure 3. 3. Ab initio energies of $[\text{Pt}(\text{NH}_3)_3 \text{ guanine}]^{2+}$: same characteristics as for Figure 2.

investigated interval of angles and may be fitted by quadratic functions

$$E_\alpha = k_\alpha \alpha^2 \quad \text{with} \quad k_\alpha = 90.0 \text{ kcal}\cdot\text{mol}^{-1}\cdot\text{rad}^{-2}$$

$$E_\beta = k_\beta \beta^2 \quad \text{with} \quad k_\beta = 24.3 \text{ kcal}\cdot\text{mol}^{-1}\cdot\text{rad}^{-2}$$

Similar calculations were performed for the adenine adduct. Results are depicted in Figure 2. The corresponding parameter values for adenine are

$$k_\alpha = 89.7 \text{ kcal}\cdot\text{mol}^{-1}\cdot\text{rad}^{-2}$$

$$k_\beta = 19.6 \text{ kcal}\cdot\text{mol}^{-1}\cdot\text{rad}^{-2}$$

To assess the influence of electron correlation, we performed test single-point calculations on the MP2 level, which indicate only a slight lowering of force constants with respect to the values obtained by HF calculations. Similar results were obtained by Kozelka¹⁵ for the comparison of HF and DFT calculations of the out-of-plane bending energies.

The harmonic terms can be readily used in molecular mechanics and molecular dynamics force fields.^{1,3} A convenient way of implementing the new parameters with only minor changes of the existing force fields for platinum binding to adenine would be the use of the Pt–N7 out-of-plane bending

constant corrected for nonplanarity of the bases while keeping the other parameters intact. Indeed, allowing the N7 atom to deviate out of the nucleobase plane makes possible a better distribution of the bending deformation within the platinum adduct resulting in a lower bending energy and an increased elasticity of the adduct. For small deviations typical of the platinum adducts, an equivalent molecular mechanics description consists of increasing the elasticity of the Pt–N7 bond (by lowering the value of k_β) while keeping the purine rings stiff.

Supposing that at a given deviation of Pt of the nucleobase plane the angles α and β minimize the bending energy, we obtain in the approximation of small angles ($\sin x \approx \tan x \approx x$) for k_β a corrected value $k_{\beta r}$

$$k_{\beta r} = \frac{b^2 k_\alpha k_\beta}{k_\alpha b^2 + k_\beta (a + b)^2} \quad (2)$$

where a is the distance of the N7 atom from the rotation axis C5–C8 (0.83 Å for adenine, 0.823 Å for guanine), b is the Pt–N7 distance (2.066 Å for adenine, 2.076 Å for guanine) and k_α , k_β are the previously calculated bending constants.

For adenine $k_{\beta r} = 13.7 \text{ kcal}\cdot\text{mol}^{-1}\cdot\text{rad}^{-2}$ and for guanine $k_{\beta r} = 15.9 \text{ kcal}\cdot\text{mol}^{-1}\cdot\text{rad}^{-2}$. The curves $E_{\beta r} = k_{\beta r} \beta^2$ are depicted for comparison in Figures 2 and 3.

The considerable increase of flexibility of the nucleobase–platinum binding when the flexibility of the purine ring is taken into consideration may modify some results of molecular mechanics calculations. The Pt out-of-plane bending constant influences the extent of distortion of the double helix in the cisplatin GpG and ApG cross-links. A lower value of the constant should better accommodate the square planar geometry of cisplatin with the B-DNA structure and should result in a smaller kink angle. Indeed, gel electrophoresis experiments¹⁶

indicated kink angle values lower than those obtained by molecular modeling.¹⁷

The presented parameters for platinum binding to guanine and adenine will provide a basis for molecular mechanics and molecular dynamics studies of the metal-modified nucleic acid structures and simultaneously may stimulate a more systematic study of the flexibility of heterocyclic molecules.

Acknowledgment. The project was supported by the Grant No. ID 96 029 of the Ministry of Education of the Czech Republic.

References and Notes

- (1) Kozelka, J.; Savinelli, R.; Berthier, G.; Flament, J.-P.; Lavery, R. *J. Comput. Chem.* **1993**, *14*, 45.
- (2) Yao, S.; Plataras, J. P.; Marzilli, L. G. *Inorg. Chem.* **1994**, *33*, 6061.
- (3) Cundari, T. R.; Fu, W.; Moody, E. W.; Slavin, L. L.; Snyder, L. A.; Sommerer, S. O.; Klinckman T. R. *J. Phys. Chem.* **1996**, *100*, 18057.
- (4) Miller; et al. *J. Biomol. Struct. Dyn.* **1985**, *2*, 1157.
- (5) Herman; et al. *Eur. J. Biochem.* **1990**, *194*, 119.
- (6) Fichtinger-Schepman, A. M. J.; van der Veer, J. L.; den Hartog, J. H. J.; Lohman, P. H. M.; Reedijk, J. *Biochemistry* **1985**, *24*, 707.
- (7) Fichtinger-Schepman, A. M. J.; van Osterom, A. T.; Lohman, P. H. M.; Berends, F. *Cancer Res.* **1987**, *47*, 3000.
- (8) Eastman, A. *Biochemistry* **1986**, *25*, 3912.
- (9) Bellon, S. F.; Coleman, J. H.; Lippard, S. J. *Biochemistry* **1991**, *30*, 8026.
- (10) Rice, A. J.; Crothers, J. M.; Pinto, A. M.; Lippard, S. J. *Proc. Nat. Acad. Sci. U.S.A.* **1988**, *81*, 53158.
- (11) Sip, M.; Schwartz, A.; Vovelle, F.; Ptak, M.; Leng, M. *Biochemistry* **1992**, *31*, 2508.
- (12) Brabec, V.; Sip, M.; Leng, M. *Biochemistry* **1993**, *32*, 11676.
- (13) Schmidt, M. W.; Baldrige, K. K.; Boatz, J. A.; Jensen, J. H.; Koseki, S.; Matsunaga, N.; Gordon, M. S.; Nguyen, K. A.; Su, S.; Windus, T. L.; Elberts, S. T.; Montgomery, J.; Dupuis, M. *J. Comput. Chem.* **1993**, *14*, 1347.
- (14) Stevens, W. J.; Krauss, M.; Basch, H.; Jasien, P. G. *Can J. Chem.* **1992**, *70*, 612.
- (15) Kozelka, J. Private communication.
- (16) Bellon, S. F.; Lippard, S. J. *Biophys. Chem.* **1990**, *35*, 179.
- (17) Kozelka, J.; Chottard, J. C. *Biophys. Chem.* **1990**, *35*, 165.

Pentacoordinated transition states of cisplatin hydrolysis— ab initio study

Z. Chval, M. Sip*

Department of Chemistry, Faculty of Biological Sciences, University of South Bohemia, and Institute of Plant Molecular Biology,
Academy of Sciences, Branisovska 31, 370 05 Ceske Budejovice, Czech Republic

Received 12 January 2000; received in revised form 29 February 2000; accepted 10 March 2000

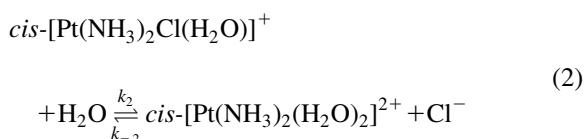
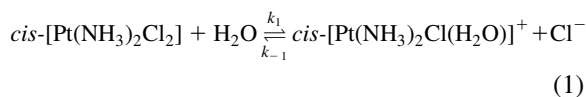
Abstract

Pentacoordinated platinum transition state (TS) geometries for both steps of cisplatin S_N2 hydrolysis reaction were fully optimized using Möller–Plesset second order perturbation (MP2) and density functional (DFT) calculations. Both reactions proceed by one step mechanism and relevant TS's adopt the shape of a substantially distorted trigonal bipyramid with considerably prolonged bonds to the leaving and entering ligands (Pt–O bond of about 0.3 Å, Pt–Cl bond of about 0.4 Å). Only negligible distortions were recognized for the remaining ligands (including the ligand in the *trans*-position). Influence of the liquid phase on the energetics of the reaction was considered using the SCIPCM model implemented in GAUSSIAN94. Both steps of hydrolysis are endothermic. The activation barrier of the first step attains 21.3 kcal/mol. For the second step the values of 26.1 kcal/mol relative to the absolute minimum structure and of 21.6 kcal/mol for the local minimum confirmed by the IRC method were obtained. © 2000 Elsevier Science B.V. All rights reserved.

Keywords: Cisplatin; Transition states; Hydrolysis; Reaction mechanism; Antitumor drugs

1. Introduction

Cisplatin (*cis*-diamminedichloroplatinum, *cis*-DDP) and related antitumor drugs need one or more hydrolysis steps prior to binding to nucleic acids, their supposed pharmacological target. The so-called leaving groups (chloride ions for cisplatin) are displaced by water molecules in two steps:



The experimental rate constants of the hydrolysis reactions k_1 and k_2 depend on experimental conditions. The value of k_1 was in the range of $2.5 - 8.51 \times 10^{-5} \text{ s}^{-1}$ (see Ref. [1] and cited references) and k_2 was determined [2] to be $2.5 \times 10^{-5} \text{ s}^{-1}$. Only the mono-aquated or diaquated species react with DNA and therefore hydrolysis is the rate-limiting step in the binding of cisplatin to DNA.

Structure and electronic properties of cisplatin and its water-substituted complexes were already theoretically studied [3,4] and the changes connected with the substitution of chloride anions by water molecules

* Corresponding author.

E-mail address: sip@umbr.cas.cz (M. Sip).

were shown [3]. However, both steps of hydrolysis and binding to DNA are supposed to pass through a pentacoordinated platinum structure whose geometry has been so far ignored or hypothetical, although it may bring a new insight into the reaction dynamics, spectrum of DNA adducts and modes of binding of cisplatin and its derivatives.

Some structural aspects of cisplatin hydrolysis were treated by Nikolov et al. in a molecular mechanics and extended Hückel methods based study [5]. However, ab initio methods are required when calculating TS structures exactly, since any parametric approach employs experimental data to determine values for the relevant adjustable parameters and these data are not available for TS's. The ab initio methods were already used for the determination of a water exchange TS structure of the $[\text{Pt}(\text{H}_2\text{O})_4]^{2+}$ complex [6], but due to imposed symmetry restrictions only a hypothetical TS structure was obtained. TS's of substitution reactions on square planar d^8 -complexes have been so far modeled only in idealized shapes of a regular trigonal bipyramid (tb) [5,6] or as a square pyramid (sp)⁵ which did not, however, correspond to the true TS structures but were supposed to be 'close to' them. In this contribution we present fully optimized ab initio geometries of pentacoordinated platinum TS's for both the steps of cisplatin hydrolysis.

2. Computational methods

Quantum calculations employ the GAMESS [7] and GAUSSIAN94 [8] program packages. LANL2DZ [9] and SBK [10] valence basis (VB) sets and relativistic effective core potentials (ECP's) were used for the platinum atom. Pt is treated as an 18-electron system in all calculations, with both the $n = 5$ and $n = 6$ shells considered as valence electron shells. Both types of ECP's give similar results for our system. Modification of LANL2DZ valence basis set with an extra set of f functions of exponent 0.78 [11] improves the bonding overlap of orbitals of the Pt atom and the donor atoms of ligands. We denote such a modified VB set as LANL2DZ*. For the main group elements the split valence 6-31G* [12] basis set were mostly used. All geometries were fully optimized at the HF, MP2 (with only valence electrons included in correlation) and DFT levels. The nature of the obtained

stationary points was always checked by vibrational analysis.

For every TS the corresponding structures of reactants and products were confirmed by the intrinsic reaction coordinate (IRC) method implemented in the used programs [7,8].

To evaluate the influence of the liquid phase on the energetics of the reaction, single point calculations were performed using Self-Consistent Isodensity Polarized Continuum Model (SCIPCM) model implemented in G94 (The SCIPCM method has not yet been published (at least to our knowledge). For a brief description see the GAUSSIAN94 manual and Ref. [13]. For a description of the underlying PCM and IPCM methods, see Refs. [14,15]). Compared with other continuum solvation models, the size and shape of the cavity depend only on actual electron density here and no other parameters such as atom sphere radii are needed. The default value of electron density of 0.004 was chosen as the border value of the isodensity surface.

3. Comparison of computational methods

Reliability of the methods was checked by comparing the results of our computations with experimental and theoretical data that are available for cisplatin and its water derivatives. For cisplatin, experimental values (see Ref. [3] and references cited therein) of the Pt–N and Pt–Cl bonds measured in solvent-free crystals attain 2.01 ± 0.04 and 2.33 ± 0.01 Å, respectively. Corresponding stretch modes are 512 and 520 cm^{-1} for the Pt–N bonds, 317 and 324 cm^{-1} for the Pt–Cl bonds. Cisplatin was optimized in the C_S symmetry. The HF/SBK/SBK method gives too long bond lengths of 2.13 Å (439 and 452 cm^{-1}) and 2.39 Å (330 and 342 cm^{-1}), respectively. Inclusion of correlation in the DFT methods based on gradient-corrected Becke's [16,17] functionals results in only moderate shortening with a good description of the Pt–Cl bond length of 2.33 Å but still yielding a Pt–N bond about 0.09 Å longer, which is in agreement with the findings of Deeth et al. [6].

Relatively best results were achieved by using B3P86 functional [17,18] with bond lengths of 2.09 Å (460 and 468 cm^{-1}) for the Pt–N bonds and 2.33 Å (337 and 350 cm^{-1}) for the Pt–Cl bonds.

Table 1

The main characteristics of the transition state *TSI* (bond distances and activation energy ΔH_0^\ddagger) optimized by different methods (note, that in all SBK and LANL2DZ* optimizations the Cartesian sets of 6d (10f) functions were used). For comparison we show also in parentheses changes of *TSI* bond distances with respect to cisplatin (for Pt–N and Pt–Cl bonds) or to monoaquacisplatin (for Pt–O bond)

	Pt–O (Å)	Pt–N(1) (Å)	Pt–N(2) (Å)	Pt–Cl(1) (Å)	Pt–Cl(2) (Å)	ΔH_0^\ddagger (kcal/mol)
HF/SBK/SBK	2.451 (+ 0.333)	2.122 (– 0.010)	2.112 (– 0.020)	2.396 + 0.009	2.801 + 0.414	22.3
MP2/LANL2DZ/6-31G*	2.386 + 0.273	2.068 – 0.025	2.078 – 0.015	2.356 + 0.011	2.716 + 0.371	23.5
MP2/LANL2DZ*/6-31G*	2.360 + 0.288	2.013 – 0.045	2.045 – 0.013	2.291 + 0.014	2.687 + 0.410	28.2 ^a
B3P86/LANL2DZ/6-31G*	2.400 + 0.296	2.067 – 0.023	2.073 – 0.017	2.335 + 0.010	2.745 + 0.420	23.7
LSDA/LANL2DZ/6-31G*	2.358 + 0.289	2.033 – 0.017	2.037 – 0.013	2.308 + 0.008	2.661 + 0.361	21.9

^a Value is not corrected with respect to ZPE.

Table 2

Selected geometrical parameters of *TSI* and *TSII* optimized at B3P86, MP2, LSDA/LANL2DZ/6-31G* and HF/SBK/SBK levels

	B3P86	MP2	LSDA	HF		B3P86	MP2	LSDA	HF
<i>TSI: bond lengths—see Table 1: bond angles (°)</i>									
N(1)–Pt–N(2)	98.8	97.6	100.2	96.0	N(2)–Pt–Cl(2)	75.4	77.2	75.5	77.3
N(1)–Pt–Cl(1)	84.8	85.3	84.1	86.0	N(2)–Pt–O	89.6	88.9	90.9	86.4
N(1)–Pt–Cl(2)	141.8	139.2	144.4	140.6	Cl(1)–Pt–Cl(2)	102.3	101.8	101.5	103.4
N(1)–Pt–O	150.0	150.8	146.7	149.4	Cl(1)–Pt–O	86.9	87.6	85.0	90.0
N(2)–Pt–Cl(1)	176.4	176.5	175.7	175.8	Cl(2)–Pt–O	68.6	70.0	68.8	70.0
<i>TSII: bond lengths (Å)</i>									
Pt–N(1)	2.069	2.073	2.033	2.130	Pt–O(1)	2.089	2.107	2.059	2.106
Pt–N(2)	2.030	2.035	2.004	2.070	Pt–O(2)	2.347	2.316	2.349	2.323
Pt–Cl	2.722	2.688	2.649	2.715					
<i>Bond angles (°)</i>									
N(1)–Pt–N(2)	97.5	96.5	98.9	95.6	N(2)–Pt–O(1)	173.8	173.3	174.0	172.7
N(1)–Pt–Cl	132.2	128.7	136.5	127.4	N(2)–Pt–O(2)	76.5	78.5	73.4	84.6
N(1)–Pt–O(1)	85.6	85.6	84.8	88.7	Cl–Pt–O(1)	72.5	76.2	72.4	81.8
N(1)–Pt–O(2)	158.9	160.5	155.1	160.2	Cl–Pt–O(2)	68.8	70.9	68.3	72.3
N(2)–Pt–Cl	101.6	97.6	101.8	90.9	O(1)–Pt–O(2)	102.4	101.5	105.2	93.2

B3P86 works slightly better than MP2 with bond lengths of 2.09 Å (457 and 464 cm⁻¹) and 2.34 Å (342 and 354 cm⁻¹), respectively, but the difference is in our opinion negligible. The Pt–N distance is overestimated by 0.02 Å in comparison with the best available theoretical results [3]. Inclusion of polarization f functions on Pt atom using MP2/LANL2DZ*/6-31G* method results in Pt–N bond length decrease to 2.06 Å (491 and 499 cm⁻¹) and a very good agreement with experiment but we were not able to compute all the stationary points by this time consuming method.

Following the idea proposed by Deeth et al. [6] we have tried performing optimization using Local Spin

Density Approximation (LSDA) functional (which is a combination of VWN correlation functional [19] with Slater exchange functional [20–22]). This method gives an excellent agreement with the experiment. The Pt–N and Pt–Cl distances are 2.05 Å (503 and 512 cm⁻¹) and 2.30 Å (350 and 364 cm⁻¹).

For cisplatin water derivatives LSDA and MP2/LANL2DZ*/6-31G* calculations give bond lengths¹

¹ For monoaquacisplatin LSDA gives (all values in Angstroms) Pt–N = 2.00, 2.06; Pt–O = 2.07; Pt–Cl = 2.28; MP2 gives Pt–N = 2.00, 2.07; Pt–O = 2.07; Pt–Cl = 2.26. For diaquacisplatin LSDA gives Pt–N = 2.00; Pt–O = 2.07; MP2 gives Pt–N = 2.00; Pt–O = 2.08.

of the same quality as the results of Carloni et al. [3]; B3P86 again gives slightly overestimated bond lengths of about 0.02 Å.

The main aim of our study is to describe properly the character of the TS for the substitution reaction of cisplatin. Most currently published studies about transition metals chemistry are done using DFT methods. Many different DFT functionals have been constructed so far and their performance evaluated for species at equilibrium geometries. But only limited attention was paid to the performance of these functionals for calculations of transition states. Therefore, this time, we have tested all the methods on the transition state structure. If we compare the values of relative changes of bond lengths with respect to cisplatin (or for Pt–O bond to monoaquacisplatin), all the methods (even including HF) give similar results (see Tables 1 and 2).

Although the LSDA method gives excellent Pt–ligand distances, it seems to overestimate the importance of intermolecular (in our case) H-bonds. It results in too small N–Pt–O and N–Pt–Cl angles and larger N–Pt–N, O–Pt–O and Cl–Pt–Cl angles for cisplatin and its water derivatives (comparing with results of Carloni et al. [3]). Maximum deviations are of 3°, but square planar complexes cannot be expected to be sensitive cases. For less rigid structures of the transition states the deviations of bond angles were up to 5 and 8° comparing B3P86 and MP2 methods (see Table 2), resulting in up to 0.2 and 0.3 Å, respectively, shorter H-bonds. Taking into account the good description of relative changes of the Pt–ligand bonds, MP2 and B3P86 methods should give satisfactory results. Therefore, we preferred them to the LSDA method, however, that was used in our calculations for a comparison, too.

For continuum solvation models a good description of electric properties is crucial. It was already shown by Kozelka et al. [23] that the MP2 and DFT methods tend to overestimate the size of the dipole moment. It was shown [23] that by using the BLYP functional [16,24,25] dipole moment approaches the experimental value asymptotically with increasing basis set. Since our testing calculations have also shown that the BLYP functional gives the lowest value of dipole moment for a given geometry of all gradient-corrected func-

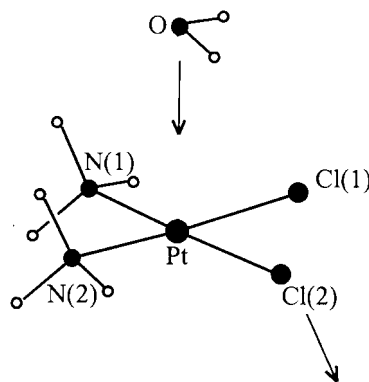


Fig. 1. Schematic representation of a hypothetical pre-reaction situation for the first step of hydrolysis with corresponding atom labeling.

tionals we used the BLYP functional in the following single point calculation using continuum SCIPCM solvation model implemented in GAUSSIAN94.

4. Results

4.1. Conformational space searching

We have performed a detailed search of *cis*-[Pt(NH₃)₂Cl₂] \cdots H₂O (for **1**) (Figs. 1 and 2) and of *cis*-[Pt(NH₃)₂Cl(H₂O)]⁺ \cdots H₂O (for **2**) (Fig. 3) conformational spaces. The only minima we have found are with the H₂O molecule bound to the Pt(II)-complex by two H-bonds. There are three symmetrically different positions of the H₂O molecule in the case of *cis*-[Pt(NH₃)₂Cl₂] and four positions in the case of *cis*-[Pt(NH₃)₂Cl(H₂O)]⁺. The most stabilized structures are shown in Figs. 2 and 3 as the structure denoted *R1* for **1** (structure of reactants for the first step of hydrolysis) and analogically as *R2-1* and *R2-2* for **2** (the two possible structures for the second step). These structures are stabilized only through H-bonds since the interaction with the central Pt(II)-atom is negligible (Pt \cdots OH₂ distances being above 3.5 Å in all cases). Similar properties are observed for products of the first and second step of hydrolysis *P1* and *P2*.

No intermediate of the *sp*-shape was found. The only structures that resemble the *sp*-intermediates are not minima on the PES, but true transition states

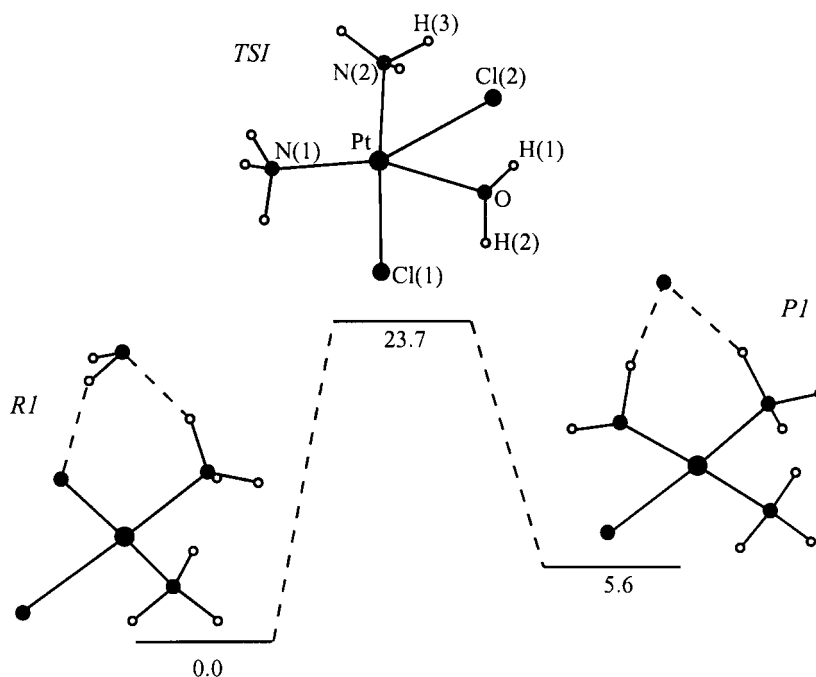


Fig. 2. Schematic drawing of structures *R1*, *TSI* and *P1* of the reaction $(1)^2$ and its in vacuo B3P86-energetical profile. See also Fig. 4 for stereo-pair picture of *TSI*.

corresponding to the transitions between the above-mentioned H-bonded structures (therefore their importance for the reaction mechanism is low) as for example transition state structure TS ($1 \leftrightarrow 2$) (see Fig. 3) corresponding to the transition between reactants $R2-1 \leftrightarrow R2-2$. However, the Pt(II) atom can hardly be considered pentacoordinated here due to the long Pt(II)···O distance of 2.967 Å.

The main feature of Pt(II) stereochemistry is the tendency to form square planar diamagnetic complexes. Our calculations have shown that a deviation of a ligand (for example NH_3) from planarity destabilizes both the deviated ligand and the ligand in the *trans*-position (in this case the Cl^- ligand). But when another ligand (such as H_2O) is available, destabilization occurs only to the ligand that is closer to the

entering ligand but not to the ligand in the *trans*-position. It leads directly to the TS structure of the *tb*-shape. The entering ligand just tries to compensate the decreasing *trans*-influence of the leaving ligand. The distortion of the complex from planarity (caused e.g. by a symmetrical out-of-plane deformation) is in our opinion the substance of the ligand substitution reaction for similar Pt(II)-square planar complexes.

The transition state structure found for the first step of hydrolysis (**1**) (denoted *TSI*) served us as a good starting point for the following second cisplatin hydrolysis (**2**) (the corresponding TS was denoted as *TSII*) and for substitution with guanine [26] since the corresponding TS's have similar main structural characteristics.

4.2. Structural and electronic properties of TS structures

Water substitutions of cisplatin and monoaquacisplatin proceed in one step over pentacoordinated TS structures, there are true transition states and no metastable reaction intermediates were found.

² Structures of *R1*, *P1*, *R2-1*, *R2-2*, *P2* are standard Pt(II)-minima with H_2O or Cl^- bound by H-bond. It was not the purpose of this study to describe their structures. Optimized Cartesian coordinates of all structures are available in ASCII format (tables containing the total energies, thermal corrections and Cartesian coordinates of all stationary points (minima and transition states) discussed in this study are available in ASCII format and can be sent on request).

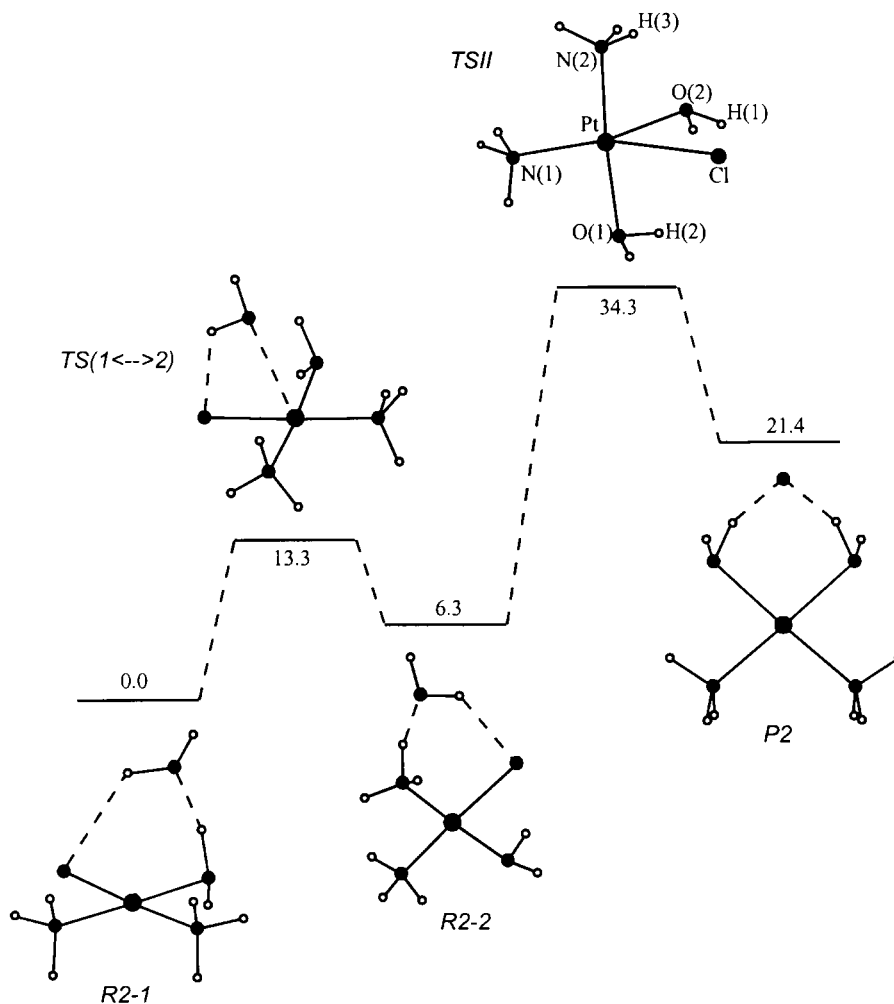


Fig. 3. Schematic drawing of structures of R2-1, TS(1 ↔ 2), R2-2, TSI and P2 of the reaction (2)^{2,3} and its in vacuo B3P86-energetical profile.

The resulting TS structures can be described as a substantially distorted trigonal bipyramid. In TSI the angle between the platinum atom and the entering and leaving ligands is only 68.6°. Furthermore, the Pt–O–Cl(2) plane is not perpendicular to that of the original complex (N(2), N(1), Cl(1)), but forms with this plane an angle of 77°. This deviation is caused by the formation of intramolecular H-bonds between water and ammonia hydrogens with chloro-ligands ($r_{\text{H}(1)-\text{Cl}(2)} =$

2.095 Å, $r_{\text{H}(2)-\text{Cl}(1)} = 2.731$ Å, $r_{\text{H}(3)-\text{Cl}(2)} = 2.268$ Å) and the repulsion between chloro ligands (see Figs. 2 and 4). The geometry of TSI is very similar. The O(2)–Pt–Cl angle is 68.8°. The deviation of the Pt–O(2)–Cl plane from perpendicular orientation is approximately 25°, but in opposite sense in comparison with the rotation in TSI, forming an angle of 115° with the original complex ((N(1), N(2), O(1)), see Fig. 3). The stabilization occurs through H-bonds between water hydrogens and Cl⁻ ($r_{\text{H}(1)-\text{Cl}} = 2.121$ Å, $r_{\text{H}(2)-\text{Cl}} = 2.091$ Å) and between water and ammonia ($r_{\text{H}(3)-\text{O}(2)} = 2.180$ Å).

Bonds leading from the central Pt atom to the

³ Note, that structures of R2-1, TS(1 ↔ 2) and R2-2 differ mainly in the position of the H-bonded H₂O. Differences of the geometry of *cis*-[Pt(NH₃)₂Cl(H₂O)]⁺ complexes alone are negligible.

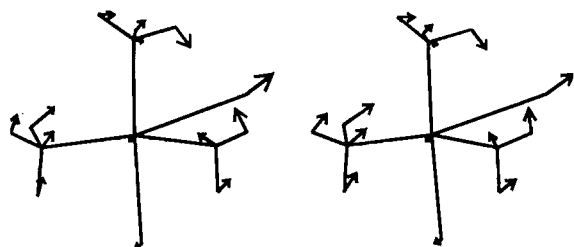


Fig. 4. Stereo-pair picture of the *TSI* (same orientation as in Fig. 2—see atom labeling). Arrows represent its imaginary frequency of 186 cm^{-1} .

leaving and entering ligands are considerably lengthened by approximately 0.3 \AA for the Pt–O bond and by approximately 0.4 \AA for the Pt–Cl bond comparing to the stable Pt(II) compounds. The lengthening in *TSI* attains up to 2.745 \AA for the Cl^- ligand and up to 2.400 \AA for the H_2O ligand, respectively. For *TSII* the corresponding values are shorter: 2.722 and 2.347 \AA .

The movement of the entering and leaving ligands and the corresponding movement of the NH_3 group in the *trans*-position correspond to the directions of imaginary frequency of *TSI* depicted in Fig. 4. The NH_3 group ‘sees’ the movement of interchanging ligands and changes its position in order to keep the Pt(II)-complex as planar as possible during the reaction.

The main structure characteristics of both TS’s are shown in Figs. 2 and 3 and in Table 2. An interesting point for future studies of similar more complex systems is the fact that main features, such as bond angles and relative prolongation of the bonds of the TS structure, seem not to be sensitive of the method used. The HF calculations yield results comparable with the DFT and MP2 methods (see Tables 1 and 2).

In Fig. 5 HOMO and LUMO of the *TSI* are depicted and compared with analogous orbitals of cisplatin. With respect to cisplatin we can consider the TS structure as an electronically slightly perturbed system where the character of the d-orbitals on the central atom remains unchanged. The distortion of the complex from planarity increases the electron repulsion from the z -direction and decreases the electron repulsion in the xy plane, which is why relative energies of corresponding orbitals are shifted. It leads to a higher relative energy mainly of the d_{z^2} orbital and to a lower energy of the d_{xy} orbital. The energy of the d_{xz}

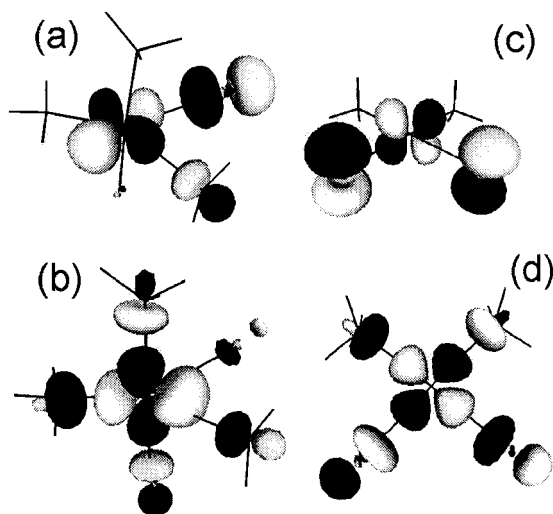


Fig. 5. Isodensity surfaces of the HOMO and LUMO of the *TSI* ((a) and (b) respectively) and HOMO and LUMO of cisplatin ((c) and (d) respectively) calculated at MP2 level.

orbital (HOMO) is slightly increased and the energy of the $d_{x^2-y^2}$ orbital (LUMO) is slightly decreased, which contributes to narrow the HOMO–LUMO gap from 3.43 eV in cisplatin to 2.41 eV in the *TSI*.

4.3. Energetics

All the results are summarized in Table 3. For (2), two reactant structures are considered, since the IRC found structure (*R2-2*) differs from the most stable one (*R2-1*) (see Fig. 3). Since the TS structure for the *R2-1* \leftrightarrow *R2-2* transition lies more than 20 kcal/mol under *TSII* we consider both structures as thermodynamically possible reactants. The value corresponding to *R2-2* is shown in brackets after the value corresponding to *R2-1*. Our discussion is based mainly on B3P86 relative energies; MP2 gives very similar results (see Tables 3 and 4) but LSDA energies alone may not be adequate.⁴

Since the hydrolysis of cisplatin is in principle a charge separation process it is, in both steps, endothermic of 5.6 kcal/mol for (1) and of 21.4 kcal/mol

⁴ Although the LSDA geometries are adequate, the LSDA energies alone may be not [6]. However they give an identical trend to gradient corrected methods. We show them for a comparison in Table 3. LSDA optimized geometries were used directly in the BLYP-SCIPCM single point calculation.

Table 3
Relative energies for both steps of hydrolysis

Method	Relative energy (kcal/mol)				
	MP2 ^a	B3P86 ^a	LSDA ^a	SCIPCM//B3P86 ^b	SCIPCM//LSDA ^c
<i>Step (1)</i>					
Cisplatin + H ₂ O	7.6	9.2	16.7		
R1	0.0	0.0	0.0	0.0	0.0
TSI	23.5	23.7	21.9	21.3	20.2
P1	7.9	5.6	2.6	1.5	−0.6
Pt[(NH ₃) ₂ (H ₂ O)Cl] ⁺ + Cl [−]	123.1	128.5	136.9		
<i>Step (2)</i>					
Pt[(NH ₃) ₂ (H ₂ O)Cl] ⁺ + H ₂ O	17.0	19.3	29.9		
R2-1	0.0	0.0	0.0	0.0	0.0
TS(1 ↔ 2)	10.0	13.3	19.0	11.2	9.7
R2-2	5.3	6.3	9.6	4.5	4.5
TSII	33.4	34.3	31.9	26.1	26.9
P2	24.9	21.4	15.6	8.2	9.3
Pt[(NH ₃) ₂ (H ₂ O) ₂] ²⁺ + Cl [−]	224.5	234.8	249.0		

^a LANL2DZ/6-31G* basis set used.

^b BLYP-SCIPCM/LANL2DZ*/6-31G*//B3P86/LANL2DZ/6-31G* calculation.

^c BLYP-SCIPCM/LANL2DZ*/6-31G*//LSDA/LANL2DZ/6-31G* calculation.

(15.1 kcal/mol for R2-2) for (2). The activation energies are 23.7 and 34.3 kcal/mol (28.0 kcal/mol), respectively. Considering the influence of the solvent all the values become substantially lower (mainly for (2)): an endothermicity of only 1.5 kcal/mol and an activation energy of 21.3 kcal/mol for (1) and an endothermicity of 8.2 kcal/mol (3.7 kcal/mol) and an activation energy of 26.1 kcal/mol (21.6 kcal/mol) for (2). Using LSDA optimized geometries results in exothermicity of 0.6 kcal/mol with an activation energy of 20.2 kcal/mol for (1) and endothermicity of 9.3 kcal/mol (4.8 kcal/mol) with an activation energy of 26.9 kcal/mol (22.3 kcal/mol)

for (2). Our results are in good agreement with the experiment (see Table 4).

5. Discussion

The point to stress is that the pentacoordinated transition state was determined as a saddle point between the valley of reactants and the valley of products. The question concerns the stability of the pentacoordinated species in the Pt(II) chemistry.

As it is well known, the kinetics of substitution reactions on square-planar d⁸-complexes is not

Table 4
Calculated thermodynamic activation parameters at $T = 298.15$ K for both steps of hydrolysis

Method	(1)		(2)	
	ΔH^\ddagger_{298} kcal/mol	ΔS^\ddagger (cal/K mol)	ΔH^\ddagger_{298} kcal/mol	ΔS^\ddagger (cal/K mol)
MP2/LANL2DZ/6-31G*	22.9	5.1	32.7 (27.1)	6.6 (8.6)
B3P86/LANL2DZ/6-31G*	23.2	4.1	33.6 (27.0)	5.7 (8.6)
BLYP-SCIPCM//B3P86 ^a	20.9	4.1	22.5 (20.6)	5.7 (8.6)
BLYP-SCIPCM//LSDA ^b	19.9	2.2	26.5 (21.4)	3.8 (8.7)
Experiment—see Ref. [1]	19.5–21.5	13.9		

^a B3P86/LANL2DZ/6-31G* 'vacuum phase' thermal corrections are used.

^b LSDA/LANL2DZ/6-31G* 'vacuum phase' thermal corrections are used.

dependent on the nature of entering and leaving ligands but it is dependent on the nature of the ligand in the *trans*-position [27]. It leads to the well known concept in Pt(II) chemistry known as the ‘*trans*-effect’. A number of ligands have been investigated with respect to this property. Unlike for the described stable five-coordinated Pt(II) complexes with strong π -acceptor ligands such as olefins [28] exhibiting two-step mechanism of the relevant substitution reactions with five-coordinated intermediate [29], no five-coordinated structures or intermediates have been detected so far in case of cisplatin substitution reactions. Here, the NH_3 -ligand, which is known to have a very weak *trans*-effect with prevailing σ contribution, is in the *trans*-position. None or only minor stabilization of the five-coordinated structure can be therefore expected in this case. Our calculations confirm such an expected finding of no minimum in this region of the PES and showing that five-coordinated structure exists only as a true (with one imaginary frequency) transition state.

A related question is how the *in vacuo* geometries correspond to solvated geometries. A stabilization of the pentacoordinated TS's occurs in our case only through interligand hydrogen bonds and through nonbonding interactions with solvent molecules. It was already mentioned by Deeth et al. [6] that solvent interactions probably little affect the geometry of Pt(II)-complexes even at the TS structure.

Our results (both geometries and vibrational frequencies of minimas and energetics of the reaction) are in good agreement with all the available experimental data.

The agreement of relative energies with liquid phase experimental data is surprisingly good which can be explained by only little changes in the solvation of the complex during the reaction. Such an assumption can be supported by the results of kinetic measurements [30] of the reaction of $[\text{Pt}(\text{phen})\text{Me}(\text{MeSO})]^+$ with Cl^- yielding $[\text{Pt}(\text{phen})\text{MeCl}]$. The authors, who performed this reaction in various solvents, concluded that the observed rate differences stem entirely from the differences of solvation energy of the anionic nucleophile, the solvation of the cationic substrate making little if any contribution [30]. In this work we study similar reactions, but in backward direction compared with the cited study. A neutral molecule of H_2O , on which

changes in solvation are small compared to anions used in the cited article, is the nucleophile. The anionic nucleophile Cl^- is then released, but relevant relative energies are calculated with respect to the product structure where Cl^- is closely bound by H-bonds to the complex, thus remaining in its solvation shell.

Elongation of the bonds to the leaving and entering ligands (Pt–O bond of about 0.3 Å, Pt–Cl bond of about 0.4 Å) in the pentacoordinated bipyramid TS structures is in agreement with the calculations of Deeth et al. [6] who optimized the TS structure for water exchange of $[\text{Pt}(\text{H}_2\text{O})_4]^{2+}$ complex in the idealized shape of the *trb* and they predicted 0.25–0.30 Å prolongation of the bonds in the equatorial plane of the complex (i.e. also of ligand in the *trans*-position). However, no weakening of the ligand in the *trans*-position were observed in our calculations. On the contrary, this ligand is slightly strengthened (see Table 1) since the entering ligand does not fully compensate the decreasing *trans*-influence of the leaving ligand in the TS structure. In the cited work, the weakening is probably an artifact due to imposed symmetry restrictions. In agreement with the cited work, only negligible distortions were observed for the *cis*-ligands.

6. Conclusions

A theoretical model of the substitution reactions of cisplatin is presented showing good agreement with the available experimental and theoretical data.

The results have importance not only for Pt(II)-chemistry concerning especially the activation steps and the binding to nucleic acids of antitumor platinum drugs, but to our knowledge they also represent the first published structure of the true transition state of substitution reactions on a square-planar d^8 -complex with weak *trans*-effect ligands.

Acknowledgements

The project was supported by the Ministry of Education of the Czech Republic and by Volkswagen Stiftung. We are very grateful to Supercomputing centers of the Charles University and of the Czech Technical University in Prague and of the Masaryk

University in Brno for providing their computational facilities.

References

- [1] S.E. Miller, D.A. House, *Inorg. Chim. Acta* 161 (1989) 131.
- [2] S.E. Miller, D.A. House, *Inorg. Chim. Acta* 166 (1989) 189.
- [3] P. Carloni, W. Andreoni, J. Hutter, A. Curioni, P. Giannozzi, M. Parrinello, *Chem. Phys. Lett.* 234 (1995) 50.
- [4] H. Basch, M. Krauss, W.J. Stevens, D. Cohen, *Inorg. Chem.* 24 (1985) 3313.
- [5] G.S. Nikolov, N. Trendafilova, I. Georgieva, H. Schöenberger, R. Gust, J. Kritzenberger, H. Yersin, *Monatshefte für Chemie* 128 (1997) 443.
- [6] R.J. Deeth, L.I. Elding, *Inorg. Chem.* 35 (1996) 5019.
- [7] M.W. Schmidt, K.K. Baldrige, J.A. Boatz, S.T. Elbert, M.S. Gordon, J.J. Jensen, S. Koseki, N. Matsunaga, K.A. Nguyen, S. Su, T.L. Windus, M. Dupuis, J.A. Montgomery, *J. Comput. Chem.* 14 (1993) 1347.
- [8] M.J. Frisch, G.W. Trucks, H.B. Schlegel, P.M.W. Gill, B.G. Johnson, M.A. Robb, J.R. Cheeseman, T.A. Keith, G.A. Petersson, J.A. Montgomery, K. Raghavachari, M.A. Al-Laham, V.G. Zakrzewski, J.V. Ortiz, J.B. Foresman, C.Y. Peng, P.A. Ayala, M.W. Wong, J.L. Andres, E.S. Replogle, R. Gomperts, R.L. Martin, D.J. Fox, J.S. Binkley, D.J. Defrees, J. Baker, J.P. Stewart, M. Head-Gordon, C. Gonzalez, J.A. Pople, GAUSSIAN94 (Revision D.4), Gaussian Inc., Pittsburgh, PA, 1995.
- [9] P.J. Hay, W.R. Wadt, *J. Phys. Chem.* 82 (1985) 299.
- [10] W.J. Stevens, M. Krauss, H. Basch, P.G. Jasien, *Can. J. Chem.* 70 (1992) 612.
- [11] K.K. Irikura, W.A. Goddard III, *J. Am. Chem. Soc.* 116 (1994) 8733.
- [12] W.J. Pietro, M.M. Francl, W.J. Hehre, D.J. DeFrees, J.A. Pople, J.S. Binkley, *J. Am. Chem. Soc.* 104 (1982) 5039.
- [13] J.B. Foresman, A. Frisch, *Exploring Chemistry with Electronic Structure Methods*, 2 ed., Gaussian Inc., Pittsburgh, PA, 1995–1996 (pp. 237–249).
- [14] S. Miertus, E. Scrocco, J. Tomasi, *Chem. Phys.* 55 (1981) 117.
- [15] J.B. Foresman, T.A. Keith, K.B. Wiberg, J. Snoonlan, M.J. Frisch, *J. Phys. Chem.* 100 (1996) 16 098.
- [16] A.D. Becke, *Phys. Rev. A* 38 (1988) 3098.
- [17] A.D. Becke, *J. Chem. Phys.* 98 (1993) 5648.
- [18] J.P. Perdew, *Phys. Rev. B* 33 (1986) 8822.
- [19] S.H. Vosko, L. Wilk, M. Nusair, *Can. J. Phys.* 58 (1980) 1200.
- [20] P. Hohenberg, W. Kohn, *Phys. Rev.* 136 (1964) B864–B871.
- [21] W. Kohn, L.J. Sham, *Phys. Rev.* 140 (1965) A1133–A1138.
- [22] J.C. Slater, *Quantum Theory of Molecular and Solids. Vol. 4: The Self-Consistent Field for Molecular and Solids*, McGraw-Hill, New York, 1974.
- [23] J. Kozelka, J. Berges, *J. Chim. Phys.* 95 (1998) 2226.
- [24] C. Lee, W. Yang, R.G. Parr, *Phys. Rev. B* 37 (1988) 785.
- [25] B. Miehlich, A. Savin, H. Stoll, H. Preuss, *Chem. Phys. Lett.* 157 (1989) 200.
- [26] Z. Chval, M. Sip, in preparation.
- [27] F. Basolo, J. Chatt, H.B. Gray, R.G. Pearson, B.L. Shaw, *J. Chem. Soc.* (1961) 2207.
- [28] V.G. Albano, G. Natile, A. Panunzi, *Coord. Chem. Rev.* 133 (1994) 67.
- [29] F. Basolo, R.G. Pearson, *Mechanisms of Inorganic Reactions*, Wiley, New York, 1967 (chap. 5).
- [30] R. Romeo, G. Arena, L.M. Scolaro, M.R. Plutino, *Inorg. Chim. Acta* 240 (1995) 81.

TRANSITION STATES OF CISPLATIN BINDING TO GUANINE AND ADENINE: *ab initio* REACTIVITY STUDYZdenek CHVAL^a and Miroslav ŠÍP^{b,*}^a Department of Chemistry, Faculty of Biological Sciences, Branišovská 31, 370 05 České Budějovice, Czech Republic; e-mail: chval@jcu.cz^b Department of Health Physics and Biophysics, Faculty of Health and Social Studies, University of South Bohemia, Jírovcova 24, 370 04 České Budějovice, Czech Republic; e-mail: sip@zsf.jcu.cz

Received September 18, 2002

Accepted March 11, 2003

Fully optimised HF and DFT transition states of cisplatin binding to adenine and guanine are presented for the first time. They have similar structure as the recently published transition states for cisplatin hydrolysis with the angle of about 70° between entering and leaving ligands and corresponding bonds prolonged up to 0.5 Å. Calculated activation energies are in the range of 10.5–18 kcal/mol. The lowest activation energies were found for the binding of *cis*-Pt[(NH₃)₂(H₂O)(OH)]⁺ to guanine. The role of hydrogen bonds in recognition of binding sites, stabilisation of reactants and final yields of individual cisplatin–DNA adducts is discussed.

Keywords: Nucleobases; Purines; Platinum; Antitumor drugs; Hydrogen bonds; Chelates; DNA; Recognition; Reaction mechanisms; *Ab initio* calculations; DFT.

In recent years much work has been done to improve the understanding of cisplatin–DNA reactivity and recognition. It is known that 60–65% of cisplatin is bound to d(GG) moiety^{1,2}. Experimental results show that the rate of the platination reaction is higher for double-stranded oligonucleotides than for the single stranded ones³, and it is increasing with the length of the oligonucleotide^{4,5}. Furthermore binding to 5′-G is slightly preferred before 3′-G in GG sequences^{3,4,6}. Therefore the DNA environment influences substantially the binding of cisplatin. The nature of the adduct is given mostly by structural properties of both Pt(II)-complex and DNA. Structurally very distinct adducts can be formed. However in all cases the first target of the complex attack is the same – the guanine base.

The dichloro form of cisplatin is not able to attack DNA and has to be modified by hydrolysis or by some S-bound groups of proteins before binding to DNA. Hydrolytic changes were already studied by Miller *et al.*⁷ under physiological conditions. It was concluded that the most probable species inter-

acting with DNA are mono-charged complexes of *cis*-Pt[(NH₃)₂(H₂O)Cl]⁺ (**1**) and *cis*-Pt[(NH₃)₂(H₂O)(OH)]⁺ (**2**). Ratio of double-charged *cis*-Pt[(NH₃)₂(H₂O)₂]²⁺ complex (**3**) is negligible (less than 1%)⁷ under physiological pH of 7.4 (compare also with pK_a values of 5.37 and 7.21⁸). However it was shown for Co-complexes by Black *et al.*⁹ that with increasing positive charge the affinity of metal species increases by an order of magnitude or even more. That is why double-charged cisplatin can be important in the DNA binding and we have considered it in our study.

Despite the relative simplicity of the cisplatin molecule, the above-mentioned aspects of DNA–cisplatin reactivity result from complex interactions, where besides the role of the DNA double helix the influence of solvent should be considered, too. Water and counterions play an important role in cisplatin binding to DNA.

COMPUTATIONAL METHODS

Choice of Model System

The choice of the model system always reflects a compromise between computational possibilities and natural complexity of the molecular system. Our model system includes the whole nucleic acid base (adenine or guanine) and one of the three above-mentioned platinum structures (**1**, **2**, **3**).

Computational Details

Quantum calculations employ the GAMESS¹⁰ and GAUSSIAN94¹¹ program packages. LANL2DZ¹² and SBK¹³ valence basis (VB) sets and corresponding relativistic effective core potentials (ECPs) were used for the platinum atom. Pt is treated as the 18-electron system in all calculations, with both the $n = 5$ and $n = 6$ shells considered as valence electron shells. Due to complexity of our system we performed all optimisations only on HF/SBK/SBK level, it means we replaced also all core electrons of main group elements and described them by SBK pseudopotentials. Valence electrons are described by split valence -31G SBK basis set. HF method was also recommended for cisplatin calculations on larger systems by Pavankumar *et al.*¹⁴ It gives very reasonable agreement with MP2 and DFT calculations for bond and dihedral angles. Pt–X (X = Cl, N, O) were overestimated by about 0.1 Å but relative bond changes were well preserved when comparing minima and transition-states structures¹⁵. To prove this statement we have also performed B3P86/LANL2DZ/6-31G* optimisations for selected TS structures.

To give consistent and comparable picture for all transition states we based our results on HF structures. B3P86/LANL2DZ/6-31G* and HF/SBK/SBK optimised structures are compared in a special paragraph.

Relative energies were evaluated by single point MP2/LANL2DZ*/6-31G* calculations. LANL2DZ valence basis set on the platinum atom was modified by an extra set of *f* functions of exponent 0.78¹⁶.

The procedure of determining the transition states has been described elsewhere¹⁵. All structures were carefully optimised (with the maximum gradient of 0.00001 a.u.) and the nature of the stationary points obtained was always checked by frequency analysis.

The activation energies are computed with respect to the appropriate H-bonded minima structures that we call “pre-substitution” complexes.

Labelling Scheme

Structures are referred to as XxxYz, where Xxx is either Ade (adenine) or Gua (guanine), Y is one of the three above-defined platinum structures **1**, **2**, **3** and the italic letter *z* distinguishes various conformers of the same structure. Transition states are referred to as TS_XxxYz, adopting the same scheme as the corresponding structures. The TS structure corresponding to guanine O6 atom bonding in the first step is designated as TS_Gua1a-O6.

RESULTS

Interaction of **1** with Guanine

The “pre-substitution” complex Gua1a can be formed before reaction. In Gua1a structure the first H-bond connects the N7 atom of guanine with a H₂O ligand ($r_{\text{N7-H}} = 1.602 \text{ \AA}$) and the second one connects O6 atom of guanine with the NH₃ ligand ($r_{\text{O6-H}} = 1.786 \text{ \AA}$) (Fig. 1). The first H-bond helps to keep the platinum central atom of the complex in a relative vicinity of the future reaction center of guanine – the N7 atom ($r_{\text{Pt-N7}} = 4.099 \text{ \AA}$). Thus, a good relative position with respect to the transition-state geometry is also ensured and the probability of the reaction is increased effectively. The chloro ligand is a “bad” leaving ligand since its interaction with N7 atom of guanine is repulsive. Although in the X-ray and NMR studies of the 1,2-intrastrand adduct cisplatin–DNA the second H-bond O6...NH₃ has not been observed^{17,18} its formation is well known in the monofunctional complexes of cisplatin with guanine³. This H-bond is preserved in the course of the substitution and it further stabilises the complex. In the reaction with

DNA there is also the third H-bond to the oxygen of the phosphate which was observed^{17,18}. Its stabilising role is important¹⁹ but it is in our opinion well preserved in the course of the reaction due to flexibility of the phosphate chain and it should not affect the mechanism of the substitution. It may only change the relative conformation of the platinum complex with the purine base.

The shape of the transition-state structure TS_Gua1a is a distorted trigonal bipyramid with longer bonds to the entering guanine ($r_{\text{Pt-N7}} = 2.588 \text{ \AA}$ comparing with 2.091 \AA in the *cis*-Pt[(NH₃)₂GuaCl]⁺ complex) and to the leaving water ($r_{\text{Pt-O}}$ changes from 2.022 to 2.451 \AA). The angle entering ligand, platinum atom, leaving ligand is only 71.7° . The angle between the plane of guanine and that of Pt(II)-complex is about 51° . However this value can be very different in a real DNA environment (compare also ϕ values in Table I). The structure is stabilised by a strong O6...HNH₂ H-bond.

An internal rotation around the Pt-N7 bond gives another (by about 0.5 kcal/mol less stable) conformation of the transition state TS_Gua1b with two weaker and non-linear H-bonds resulting from the interaction of O6 atom with the NH₃ ligand of cisplatin and the hydrogen of the leaving water molecule (see Table I).

We have also checked for possibility of formation of the Pt-O6 adduct in the first step. Formation of the Pt-O6 bond causes significant changes in the interaction between guanine and cytosine compared to the Watson-Crick H-bonding pattern²⁰. It may lead to a point mutation of DNA²¹. The corresponding transition state TS_Gua1a-O6 is by about 2.9 kcal/mol less

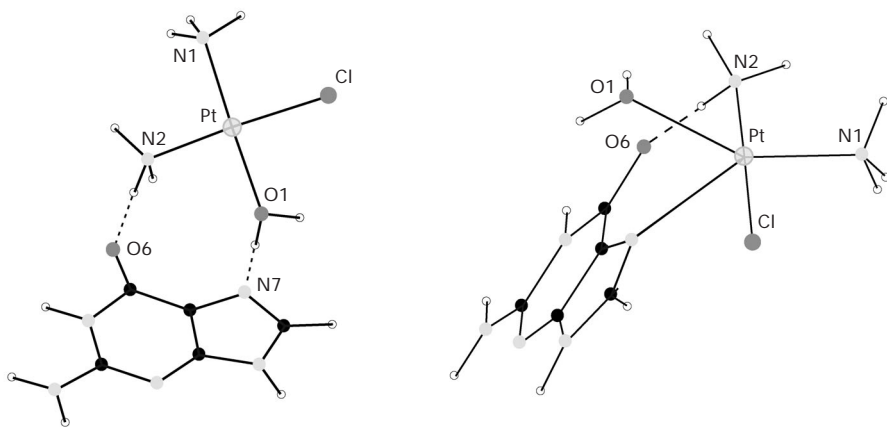


FIG. 1

Structure of the “pre-substitution” complex 1a (left) and the transition state TS1a (right)³⁵

TABLE I

Comparison of main structural characteristics of transition states for the cisplatin bonding with guanine and adenine computing by HF/SBK/SBK method (Structures denoted by DFT are optimised by B3P86/LANL2DZ/6-31G* method. See Fig. 1 for numbering of atoms of TS1-3a structures; Fig. 2 for numbering of TS1a-O6 and TSII-O6 structures; Fig. 3 for numbering of TSAdel structures. Pt-displacement, displacement of platinum atom from the guanine (adenine) base plane; ϕ , angle between planes of guanine (or adenine) and Pt(II)-complex; E_a , activation energy for corresponding substitution.)

Transition states	Pt-N7	Pt-O1	H-bonds Å	N7-Pt-O1 °	Pt-displacement Å	ϕ °	E_a kcal/mol
TS1a	2.59	2.45	1.75 ^a	71.7	0.4	51	14.0
TS1b	2.57	2.40	1.91 ^a ; 2.17 ^b	74.5	0.0	50	14.5
TS1b-DFT	2.48	2.38	1.90 ^a ; 1.90 ^b	73.1	0.5	56	-
TS2a	2.55	2.43	1.84 ^a	71.1	0.6	55	10.4
TS2b	2.58	2.41	1.91 ^b ; 2.14 ^a	74.6	0.2	53	11.5
TS3a	2.59	2.45	1.42 ^b	71.2	0.6	70	17.9
TS3b	2.50	2.48	2.02 ^a ; 2.47 ^{a,g}	78.2	0.4	79	21.1
TSAdel1a	2.59	2.44	1.87 ^c ; 2.58 ^d	75.1	0.0	66	14.5
TSAdel1a-DFT	2.50	2.38	1.75 ^c ; 2.39 ^d	74.8	0.1	67	-
TSAdel1b	2.59	2.44	2.56 ^d	69.6	0.7	88	16.1
TSAdel1c	2.62	2.42	2.09 ^e	73.6	0.5	37	16.7

	Pt-O6 Å	Pt-O1 Å	H-bonds Å	O6-Pt-O1 °	Pt-displacement Å	ϕ °	E_a kcal/mol
TS1a-O6	2.43	2.49	1.77 ^f ; 2.55 ^b	74.9	1.4	76	16.9
TS1b-O6	2.46	2.50	2.06	63.1	0.6	79	17.1
TSII-O6	2.51	2.55	-	66.2	0.0	31	-

^a O6...HNH₂ distance; ^b O6...HOH distance; ^c N6...HOH distance; ^d Cl...HN6 distance; ^e NH₃...N6 distance; ^f N7...HOH distance; ^g O6 atom forms H-bonds with both NH₃ groups of cisplatin.

stable than TS_Gua1a structure. Substitution reactions of cisplatin are kinetically driven giving only a minor importance to the thermodynamic stability of the product structures. In spite of that we would like to mention that the reaction on the O6 atom is slightly endothermic (by about 2.2 kcal/mol) while the reaction on the N7 atom it is exothermic for all species. Our data clearly support the N7 atom as the preferential binding site for platinum but they are not able to explain fully the zero occurrence of Pt-O6 adducts. Other factors such as steric hindrance that is not included in our model can influence the results.

Very similar conclusions are probably also valid for the O6-binding in the second step after a previous binding of cisplatin to N7 atom to form N7-Pt-O6 chelate (with corresponding TSII-O6 transition-state structure) although in this case an increase of energy connected with the deformation of DNA has to be taken into account for the competitive GpG chelate. Structures of both transition states for the O6-adduct formation are shown in Fig. 2 and in Table I.

Interaction of 2 with Guanine

This reaction needs the lowest barrier of about 10.4 kcal/mol to proceed. **2** is more stable than **1**²² and it is also the most probable species to attack guanine according to our results. OH⁻ group is able to polarize more its bond with central platinum atom comparing to Cl⁻. The Mulliken population analysis at the MP2/LANL2DZ*/6-31G* level shows that the charges on the Pt atom for **2a** and TS**2a** (or **b**) structures are approximately by +0.25 e

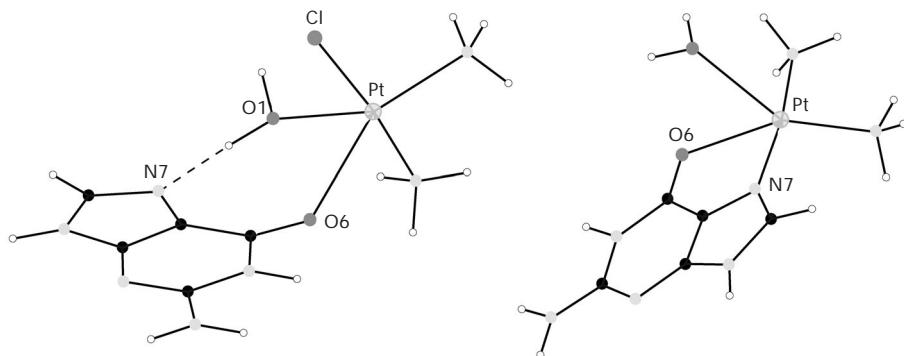


FIG. 2

Structure of transition states for the cisplatin binding on the O6 atom of guanine in the first step TS1a-O6 (left) and in the second chelation step TSII-O6 (right)

higher than those for corresponding chlorine complexes **1a** and TS**1a** (or *b*) (+0.99 comparing to +0.72 e). However, this difference is overestimated for the 6-31G* basis set and it is expected to be lower with the extended basis set²².

Otherwise, as expected, the substitution of the Cl⁻ ligand by an OH⁻ ligand does not change significantly the picture described in the previous section. Main structure characteristics of the transition states TS**2a** and TS**2b** for substitution of **2** with guanine are given and compared in Table I. The “pre-substitution” complex **2a** can be found in Supporting Information.

Interaction of 3 with Guanine

The diaqua species **3** bearing two positive charges has the biggest affinity to guanine. However this structure differs not only in its charge but also in its capability to form H-bonds. The chloride and hydroxo ligands in **1** and **2**, respectively, are potential H-bond acceptor whereas the aqua ligand in **3** is a H-bond donor. Therefore there is one more ligand that is able to form an H-bond with O6 atom of guanine and several conformers of **3** with guanine can be formed. Only the most stable conformer with H-bonds to two aqua ligands was considered – **3a** and **3aw** structures (see further text). It leads to the TS**3a** TS structure. The transition state TS**3b** is less stable by about 3.2 kcal/mol due to a weaker O6...HNH₂ H-bond.

Due to the double positive charge of **3** the H₂O hydrogens are highly acidic here (pK_a value of 5.4⁸) comparing with free water molecule hydrogens. It can lead to artificial differences between primarily equal hydrogens in our vacuum-phase calculations if the first of these acidic hydrogens is involved in hydrogen bonding to *e.g.* guanine or free water molecule and the second hydrogen is not. To make again both hydrogens equivalent, an additional water molecule, bound by H-bond to the second hydrogen of the water ligand, was included to our quantum chemical system. This approach was used with success for **3a** complex to give complex designated as **3aw** (see Supporting information).

No hydrogen transfer occurs in the TS structures since the H₂O...N7 hydrogen bond is already disrupted. We were able therefore to perform full TS optimisations without an additional water molecule (structures TS**3a** and TS**3b**). Optimisations with an additional water molecule were done only for TS**3a** to give TS**3aw** for a comparison with the **3aw** minimum.

We have to note, however, that these structures are computed with the highest error due to the highest unscreened charge. Besides the previously described problems, it results in short H-bonds (HOH...O6 being only 1.42 Å

in the TS3a structure). However, what is in our opinion more important, the covalent bonds are described properly as can be seen from the comparison in Table I.

The energy barrier for this substitution is according to our calculations the highest: 17.9 kcal/mol. The reason may be a better stabilisation of the double-charged 3aw structure comparing to the stabilisation of the mono-charged 1a and 2a structures.

Interaction of 1 with Adenine

Amino group of adenine is intrinsically pyramidal due to a partial sp^3 hybridisation of its nitrogen atom, which allows forming non-classical interactions: out-of-plane H-bonds and amino-acceptor interactions²³. It was already observed *e.g.* for the hydrated Mg^{2+} -Deoxyadenosine Monophosphate complex¹⁹. Another example is shown in Fig. 3. The transition state TS_Ade1a for N7 binding to adenine has H1 atom of the NH_2 group substantially deviated by about 50° from the adenine plane. A double H-bond stabilisation of the TS structure and a little higher angle between entering and leaving ligands of about 75° are observed (see Fig. 3 and Table I). There is no out-of-plane force acting on the H2 hydrogen of the amino group. The AT base pair structure will not be therefore influenced. The activation energy is 14.5 kcal/mol.

Other possible TS-structure conformers are a little less stabilised by only one H-bond: TSAde1b structure with the $NH_2 \cdots Cl$ hydrogen bond and TSAde1c structure with the $NH_3 \cdots NH_2$ hydrogen bond are about 1.6 and 2.2 kcal/mol less stable, respectively. However, differences are not important and the most stable conformation will result from the stabilisations and/or destabilisations coming from the real DNA environment. The important feature of our model is the fact that all the structures have the same main structural characteristics as it is shown in Table I.

Comparing our results for guanine and adenine, it is clear that different reactivity is not caused by the difference in stability of their Pt-N7 bond. The difference of 100 kJ/mol of interaction energies of cisplatin adducts with guanine and adenine, respectively, was already calculated²⁴. Our calculated value of activation energy for the platinum substitution of adenine is only by about 0.5 kcal/mol higher than the corresponding value of guanine. TSAde1a structure is very well stabilised by $NH_2 \cdots Cl$ and $H_2N \cdots H_2O$ H-bonds. In 2 OH^- group does not offer such an advantageous pattern, we expect a little higher difference of about 2.0 kcal/mol²⁵. Anyway the "pre-substitution" complexes already include the large portion of electro-

static interaction, which was shown to be responsible for the stronger stabilisation of guanine adducts when compared to adenine²⁶.

DFT Optimised Structures

We have reoptimised TS_Gua1b and TS_Ade1a transition states using B3P86/LANL2DZ/6-31G* method. As shown in Table I, the DFT computations provide structures essentially identical with the Hartree-Fock results despite some systematic differences in bond lengths¹⁹. HF bond lengths Pt-X (X = Cl, N, O) are overestimated by about 0.1 Å what is in a good

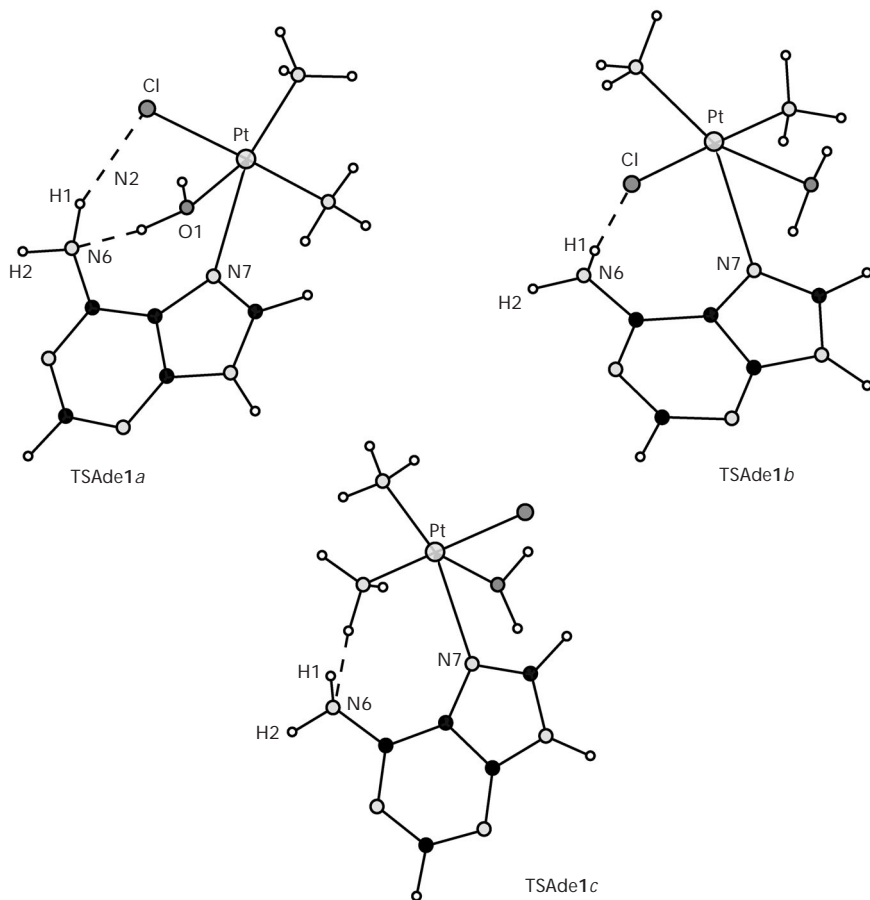


FIG. 3

Three different conformers of transition states for the cisplatin-adenine binding

agreement with results of our previous study¹⁵. H-Bonds are considerably shorter, too. The 6-31G* basis set enables much better orbital overlap between donor and acceptor atoms. TS_Gua1b structure is stabilised by two strong H-bonds of 1.9 Å.

DISCUSSION

An agreement of *ab initio* calculation results of an isolated vacuum-phase molecular system with a real liquid-phase experiment is often achieved. It seems to be the case of Pt(II) transition-states structures as was already proposed by Deeth *et al.*²⁷, too. The question is whether and to what extent the results of the present study concerning a system formed by a whole nucleic acid base (adenine or guanine) and one of the three platinum structures (1, 2, 3) can be extrapolated to a real environment of DNA in solution.

First we would like to stress that all our results (including those from our previous study¹⁵ concerning cisplatin hydrolysis) are in a good agreement with available experimental data. The second point is the conserved structure of these transition states, which does not seem to be dependent on the nature of leaving and entering ligands and of the ligands in the *cis*-positions. The TS structure does not even depend on the charge of the system – compare *e.g.* transition states for the first and the second step of cisplatin hydrolysis in our previous study¹⁵ – or results shown in Table I of this study. In spite of large differences in the description of H-bonds, the double-charged system TS3a has the same main structure characteristics which are connected with the Pt(II)-complex itself as the mono-charged complexes TS1a and TS2a or TSAde1.

Although nonbonding interactions do not have significant influence on the structure of transition states, they have a key role in molecular recognition affecting thus reactivity. We would like to touch this interesting and important theme from the point of view of our results.

In the “pre-substitution” complex structure, the H-bond, which connects the leaving ligand with N7 atom of guanine, can be significant in this particular geometry for two reasons: (i) helps to keep the platinum central atom of the complex relatively close to the future reaction center of atom N7 which may increase effectively the probability of the reaction and (ii) right mutual position of the reactants with respect to the structure of transition state is ensured in this case. To support the second point we would like to stress that the angle entering ligand-Pt-leaving ligand is low (about 70°) in the TS structures. We have not found any attempt of cisplatin to spread its coordination sphere. Even in the critical pentacoordinated struc-

ture of the TS, its electronic structure is indeed that of a slightly disturbed four-coordinated complex (see also Fig. 4 in our previous study¹⁵). Therefore the reaction could be more precisely described like "pushing away" of the leaving ligand by the entering one rather than a direct attack of the entering ligand from the direction perpendicular to the coordination plane.

The high electron density associated with N7 atoms in GG pairs appears to provide major driving force for these reactions with positively charged complexes²⁸. And it was also stated that H-bonding plays a role in stabilisation of intermediates formed during the course of the reactions of cisplatin with nucleotides and it may provide a kinetic driving force toward GpG cross-links in oligonucleotides²⁹. The question is the relative importance of different H-bonds, mainly of the H-bond with the O6 atom of guanine.

The H-bond to the O6 atom is well known from the monofunctional cisplatin–DNA adducts and its possible stabilisation role was already proposed³. Interaction with NH₂ group of adenine has a much lower stabilising effect²⁴. The H-bond towards the O6 atom was not observed in the bifunctional adducts of cisplatin with DNA^{17,18} but already bonded guanine may play its stabilisation role for the chelation step. In this case the Pt(II)-complex is already well anchored to the chain and the O6 atom is not necessary for the stabilisation. Therefore cisplatin can chelate very easily also to adenine if it is close enough. This is the case, indeed, for 1,2-intra-strand ApG adducts with the 25% occurrence ratio.

Previous consideration is in a good agreement with the common hypothesis that the presence of at least one N–H group to bind O6 atom of guanine is a prerequisite for the drug anticancer activity³⁰. However this hypothesis was scrutinised recently. It was shown²⁶ that a net stabilisation due to this H-bond formation is only 4.2 kcal/mol for [Pt(NH₃)₃(9-methyl-guanine)]²⁺. After experiments on DNA adducts with dichloro-*N,N'*-dimethylpiperazineplatinum(II), which lacks N–H functionalities, it was concluded that the very small size of the NH group, not its H-bonding ability, is responsible for the good activity exhibited by Pt compounds with ammine carrier ligands with multiple NH groups³¹.

Moreover the theoretical study of interactions of hydrated divalent cations with purine nucleotides reveals that the interaction with the O6 atom of guanine is apparently weaker¹⁹ comparing to strong bridges between the cation and anionic oxygen atoms of the phosphate group.

The H-bonding to the phosphate oxygen was observed for adducts of mononucleotides³² up to adducts of real DNA^{17,18}. It was shown *e.g.* that 5'-GMP reacts with *cis*-[Pt(H₂O)₂(NH₃)₂]²⁺ more rapidly than 3'-GMP, G, or dG³³. The interaction with the phosphate backbone changes certainly con-

formations of our optimised structures. We expect mainly some internal rotation of the platinum complex around Pt–N7 bond and the angle between the purine base plane and the plane of the platinum complex will be changed. However, the high flexibility of the phosphate chain should allow neglecting changes of interaction energies connected with these H-bonds in the course of the reactions.

The higher strength of the H-bond of N7 atom of guanine is directly connected with its higher electron density comparing to the electron density of N7 atom of adenine.

To conclude this section, we should like to stress the importance of the H-bonding with N7 atom in the “pre-substitution” complex followed by H-bonds with phosphate oxygens and the O6 (NH₂) atom. The latter two are well preserved during the reaction. The main role of the O6 atom in guanine is in our opinion in the enhancement of a negative electric field in the vicinity of the N7 atom as can be seen from a molecular electrostatic potential comparison³⁴. N6 atom of adenine is a nucleophile, too, when the amino group becomes pyramidal-rotated but in the adenine plane the N6 atom is shielded by its hydrogens.

CONCLUSIONS

Our reaction model of the cisplatin binding to guanine supposes:

1) Formation of the “pre-substitution” complex which is stabilised by three H-bonds connecting N7, O6 and phosphate with proper ligands of Pt(II)-complex. However the H-bond to phosphate is neglected in our study supposing to be well preserved in the course of the reaction and not having significant influence on the mechanism of the reaction. The H-bond connecting the leaving ligand with the reacting center of the guanine (N7 atom) ensures a good mutual position of reactants with respect to the TS structure.

2) Substitution proceeds *via* a pentacoordinated transition state with a low angle of about 70° between entering and leaving ligands and corresponding bonds prolonged up to 0.5 Å. It has the same structural characteristics as our previously reported transition states for cisplatin hydrolysis¹⁵.

3) The activation energy for Pt–adenine binding is slightly higher by about 0.5–2.0 kcal/mol than the activation energy for Pt–guanine binding. This number reflects mainly differences in orbital energy stabilisations and only a small portion of electrostatic contribution. The preferential binding site for Pt(II)-complexes resulting from our calculations is as expected the N7 atom of guanine.

Supporting Information Available

Tables containing HF total energies, thermal corrections, and Cartesian coordinates of all stationary points discussed in this study, in ASCII format, are available on request.

The research was partly supported by the Aktion 27p15 and Kontakt 2001-24 projects of scientific cooperation between Czech Republic and Austria and was included into the COST Action D20. We are very grateful to Supercomputing centers of the Technical University in Prague; the Masaryk University in Brno and the Charles University in Prague for providing their computational facilities. We are indebted to Dr J. V. Burda for helpful discussions and to Dr M. Kabeláč for the help with time-consuming DFT optimisations.

REFERENCES AND NOTES

1. Eastman A.: *Biochemistry* **1985**, *24*, 5027.
2. Fichtinger-Schepman A. M. J., Van der Veer J. L., Den Hartog J. H. J., Lohman P. H. M., Reedijk J.: *Biochemistry* **1985**, *24*, 707.
3. Reeder F., Guo Z., Murdoch P. S., Corazza A., Hambley T. W., Berners-Price S. J., Chottard J. C., Sadler P. J.: *Eur. J. Biochem.* **1997**, *249*, 370.
4. Gonnet F., Reeder F., Kozelka J., Chottard J. C.: *Inorg. Chem.* **1996**, *35*, 1653.
5. Elmroth S. K. C., Lippard S. J.: *J. Am. Chem. Soc.* **1994**, *116*, 3633.
6. Gonnet F., Kocher F., Blais J. C., Bolbach G., Tabet J. C., Chottard J. C.: *J. Mass Spectrom.* **1996**, *31*, 802.
7. Miller S. E., House D. A.: *Inorg. Chim. Acta* **1990**, *173*, 53; and references therein.
8. Berners-Price S. J., Frenkiel T. A., Frey U., Ranford J. D., Sadler P. J.: *J. Chem. Soc., Chem. Commun.* **1992**, 789.
9. Black C. B., Cowan J. A.: *J. Am. Chem. Soc.* **1994**, *116*, 1174.
10. Schmidt M. W., Baldrige K. K., Boatz J. A., Elbert S. T., Gordon M. S., Jensen J. J., Koseki S., Matsunaga N., Nguyen K. A., Su S., Windus T. L., Dupuis M., Montgomery J. A.: *J. Comput. Chem.* **1993**, *14*, 1347.
11. Frisch M. J., Trucks G. W., Schlegel H. B., Gill P. M. W., Johnson B. G., Robb M. A., Cheeseman J. R., Keith T. A., Petersson G. A., Montgomery J. A., Raghavachari K., Al-Laham M. A., Zakrzewski V. G., Ortiz J. V., Foresman J. B., Peng C. Y., Ayala P. A., Wong M. W., Andres J. L., Replogle E. S., Gomperts R., Martin R. L., Fox D. J., Binkley J. S., Defrees D. J., Baker J., Stewart J. P., Head-Gordon M., Gonzalez C., Pople J. A.: *Gaussian 94* (Revision D.4). Gaussian, Inc., Pittsburgh (PA) 1995.
12. Hay P. J., Wadt W. R.: *J. Phys. Chem.* **1985**, *82*, 299.
13. Stevens W. J., Krauss M., Basch H., Jasien P. G.: *Can. J. Chem.* **1992**, *70*, 612.
14. Pavankumar P. N. V., Seetharamulu P., Yao S., Saxe J. D., Reddy D. G., Hausheer F. H.: *J. Comput. Chem.* **1999**, *20*, 365.
15. Chval Z., Šíp M.: *J. Mol. Struct. (THEOCHEM)* **2000**, *532*, 59.
16. Irikura K. K., Goddard III, W. A.: *J. Am. Chem. Soc.* **1994**, *116*, 8733.
17. Takahara P. M., Frederick C. A., Lippard S. J.: *J. Am. Chem. Soc.* **1996**, *118*, 12309.
18. Gelasco A., Lippard S. J.: *Biochemistry* **1998**, *37*, 9230.

19. Šponer J., Sabat M., Gorb L., Leszczynski J., Lippert B., Hobza P.: *J. Phys. Chem. B: At., Mol. Opt. Phys.* **2000**, *104*, 7535.
20. Pelmeshnikov A., Zilberberg I., Leszczynski J., Famulari A., Sironi M., Raimondi M.: *Chem. Phys. Lett.* **1999**, *314*, 496.
21. Zilberberg I. L., Avdeev V. I., Zhidomirov G. M.: *J. Mol. Struct. (THEOCHEM)* **1997**, *418*, 73.
22. Burda J. V., Zeizinger M., Šponer J., Leszczynski J.: *J. Chem. Phys.* **2000**, *113*, 2224.
23. Hobza P., Šponer J.: *Chem. Rev. (Washington, D. C.)* **1999**, *99*, 3247.
24. Burda J. V., Šponer J., Leszczynski J.: *J. Biol. Inorg. Chem.* **2000**, *5*, 178.
25. Estimated by comparison of structures with only one H-bond: e.g. TSAd $\mathbf{e1b}$ with TS $\mathbf{1a}$.
26. Deubel D. V.: *J. Am. Chem. Soc.* **2002**, *124*, 5834.
27. Deeth R. J., Elding L. I.: *Inorg. Chem.* **1996**, *35*, 5019.
28. Pullman A., Pullman B.: *Q. Rev. Biophys.* **1981**, *14*, 289.
29. Laoui A., Kozelka J., Chottard J.-C.: *Inorg. Chem.* **1988**, *27*, 2751.
30. Reedijk J.: *Chem. Commun.* **1996**, 801.
31. Sullivan S. T., Ciccarese A., Fanizzi F. P., Marzilli L. G.: *J. Am. Chem. Soc.* **2001**, *123*, 9345.
32. Berners-Price S. J., Frey U., Ranford J. D., Sadler P. J.: *J. Am. Chem. Soc.* **1993**, *115*, 8649.
33. Green M., Garner M., Orton D. H.: *Transition Met. Chem. (London)* **1992**, *17*, 164.
34. Bonnacorsi R., Scrocco E., Tomasi J., Pullman A.: *Theor. Chim. Acta* **1975**, *36*, 339.
35. $\mathbf{2a}$ and TS $\mathbf{2a}$, TS $\mathbf{3b}$ structures are the same except for the chloro ligand in the *cis*-position. $\mathbf{3a}$ and TS $\mathbf{3a}$ structures have O6 \cdots H $_2$ O H-bond; TS $\mathbf{3b}$ structure has two O6 \cdots NH $_3$ hydrogen bonds.

The Trans Effect in Square-Planar Platinum(II) Complexes—A Density Functional Study

ZDENEK CHVAL,¹ MIROSLAV ŠÍP,¹ JAROSLAV V. BURDA²

¹Department of Biophysics, Faculty of Health and Social Studies, University of South Bohemia, J. Boreckého 27, 370 11 České Budejovice, Czech Republic

²Department of Chemical Physics and Optics, Faculty of Mathematics and Physics, Charles University, Ke Karlovu 3, 121 16 Prague 2, Czech Republic

Received 25 October 2007; Revised 12 February 2008; Accepted 17 February 2008

DOI 10.1002/jcc.20980

Published online 28 April 2008 in Wiley InterScience (www.interscience.wiley.com).

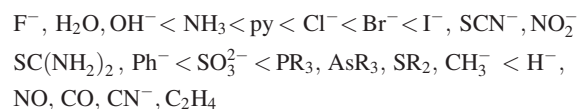
Abstract: The mechanism of substitution water exchange reactions in square planar trans-Pt[(NH₃)₂T(H₂O)]ⁿ⁺ complexes is studied (T=H₂O, NH₃, OH⁻, F⁻, Cl⁻, Br⁻, H₂S, CH₃S⁻, SCN⁻, CN⁻, PH₃, CO, CH₃⁻, H⁻, C₂H₄). The trans effect is explained in terms of σ -donation and π -back-donation whose relative strengths are quantified by the changes of electron occupations of 5d platinum atomic orbitals. The σ -donation strength is linearly correlated with the Pt–H₂O (leaving ligand) bond length (trans influence). The kinetic trans effect strength correlates proportionally with the σ -donation ability of the trans-ligand except the ligands with strong π -back-donation ability that stabilizes transition state structure. The σ -donation ability of the ligand is dependent on the σ -donation strength of the ligand in the trans position. Therefore the trans effect caused by σ -donation can be understood as a competition between the trans-ligands for the opportunity to donate electron density to the central Pt(II) atom. The influence of the trans effect on the reaction mechanism is also shown. For ligands with a very strong σ -donation (e.g. CH₃⁻ and H⁻), the substitution proceeds by a dissociative interchange (*I_d*) mechanism. Ligands with strong π -back donation ability (e.g. C₂H₄) stabilize the pentacoordinated intermediate and the substitution proceeds by a two step associative mechanism. For ligands with weak σ -donation and π -back-donation abilities, the highest activation barriers have to be overcome and substitutions can be described by an associative interchange (*I_a*) mechanism. The results are supported by the energy decomposition and the natural orbital analysis.

© 2008 Wiley Periodicals, Inc. J Comput Chem 29: 2370–2381, 2008

Key words: trans effect; reaction mechanism; square planar platinum(II) complexes; σ -donation; π -back-donation

Introduction

The ligand substitution reactions in square-planar Pt(II) complexes comprise a very intensively investigated class of processes. The trans effect was already observed by Chernyaev in the twenties of the last century.¹ Since then the kinetics of many other systems has been explained by the trans effect.² By the trans effect is meant the labilization of a ligand in trans position to certain other ligand. For platinum complexes there is a number of experimental studies available comparing trans effects of different ligands.³ The intensity of the trans effect (as measured by the increase in the rate of substitution of the trans ligand) follows this sequence:



Since the trans effect is a kinetic phenomenon, its origin lies in reactant destabilization and/or in the transition state stabilization. The first effect is usually expressed by the Pt–trans ligand bond elongation and it is sometimes called as the trans influence.

The finding of the anticancer activity of cisplatin (cis-diamminedichloroplatinum(II)) and its derivatives further enhanced the interest of this class of compounds.⁴ Cisplatin is one of the best theoretically described systems.^{5–14} The mode of

Additional Supporting Information may be found in the online version of this article.

Correspondence to: Z. Chval; e-mail: chval@jcu.cz or J.V. Burda; e-mail: burda@karlov.mff.cuni.cz

Contract/grant sponsors: COST and Ministry of Education of the Czech Republic; contract/grant number: D20.005

Contract/grant sponsor: GA-AV; contract/grant number: IAA400550701

Contract/grant sponsor: MSM; contract/grant number: 0021620835

action of cisplatin includes hydrolysis in the first step followed by the binding to the guanine N7 atom of DNA. Both these steps were described theoretically in number of studies during recent years.^{6,9,14–22} In the hydrolysis step the chloride ligand is replaced by a water ligand which is exchanged by the guanine in the next step. Both substitution reactions have a similar one-step mechanism and go via pentacoordinated transition states.^{6,15} The NH_3 group with a weak trans effect inheres in the *trans* position with respect to these substitutions. A thorough study of substitution reactions in the square planar $\text{Pt}[(\text{NH}_3)_x(\text{H}_2\text{O})_y\text{Cl}_z]^{+2-z}$ ($x + y + z = 4$) complexes was done by Cooper and Ziegler.²³ Since all ligands considered in the cited study have a weak trans effect strengths, all possible substitution reactions were described by a facilitated dissociative mechanism (or an associative interchange (I_a) mechanism as it is denoted in this contribution) overcoming one pentacoordinated transition state.

Trans effect of biologically active ligands was studied by Lau and Deubel.²⁴ The kinetic trans effect of the biomolecules significantly differs from the thermodynamic trans influence. The sulfur ligands show a larger trans effect than nitrogen ligands and water.

In the theoretical paper dealing with boryl ligands,²⁵ i.e. ligands with very strong trans influence, results were analyzed by the natural orbital analysis. A good correlation between the trans influence strength and the percentage contribution of Pt in Pt–B σ bond was found. These properties are also correlated with the ratio of the boron p- to s-orbital population in the Pt–B σ bond. Very recently trans- influence of boryl ligands was also studied experimentally by Braunschweig et al.²⁶

In this contribution we show how the ligands with different trans effect strengths influence not only the value of activation energy (i.e. kinetics) of substitution reactions but also the reaction mechanism itself. We use similar systems as were used in the pioneer study of Lin and Hall.²⁷ However this time electron correlation is included, all the stationary points including transition states are fully optimized and influence of much larger number of ligands in the trans position is compared. Moreover theoretical methods for the analysis of the nature of bonding interactions (such as the natural bond orbital analysis and the energy decomposition analysis) are currently available. Thus we are able to show details about the substitution reactions that could not be revealed in the cited study.

Computational Details

The calculations were performed with the Gaussian 03 (G03) program package.²⁸ All geometries were fully optimized using B3LYP functional.²⁹ LANL2DZ valence basis set with an extra set of f functions of exponent 0.78 and relativistic effective core potentials (ECP's) were used for the platinum atom. Pt is treated as an 18-electron system with both $n = 5$ and $n = 6$ shells considered as valence electron shells. This basis set on the Pt atom is designated as LANL2DZ*. For the main group elements the split valence 6-31G* basis set was used. These calculations are designated as B3LYP/BSI in the further text. Selected structures were optimized by a substantially improved MWB-60(2f)/6-311++G(2d,2p) basis set. It means platinum atom was treated

using Dresden-Stuttgart pseudopotentials.³⁰ The suggested basis set was extended with two extra sets of f functions with exponents of 1.4193 and 0.4662.¹⁰ The main group elements are described by 6-311++G(2d,2p) basis set. These calculations are designated as B3LYP/BSII in the further text.

The nature of the obtained stationary points was always checked by a vibrational analysis. Thermal contributions to the energetic properties were calculated using microcanonical ensemble of statistical mechanics at standard conditions ($T = 298$ K, $p = 101.325$ kPa). Single point energy evaluations on the optimized geometries were carried out with a more flexible MWB-60(2fg)/6-311++G(2df,2dp) basis set. Platinum basis set was augmented by an extra set of g functions with the exponent 1.2077.

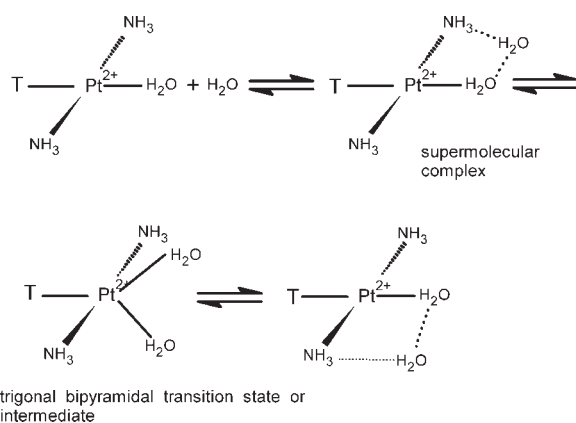
To evaluate the solvent influence on the energetics of the reaction, single point calculations on the gas phase optimized geometries were performed using CPCM continuum solvation model on the B3LYP/MWB-60(2fg)/6-311++G(2df,2dp) level of theory (the same level as the gas-phase single points). All solvation calculations were carried out in water ($\epsilon = 78.39$). Default CPCM parameterization as implemented in G03 was used.

Atomic charges were derived by Weinhold's natural population analysis (NPA) using the natural bond orbital (NBO) partitioning scheme.^{31,32}

In this study we deal with substitution reactions $\text{trans-Pt}[(\text{NH}_3)_2(\text{H}_2\text{O})\text{T}]^{n+} + \text{H}_2\text{O} \leftrightarrow \text{trans-Pt}[(\text{NH}_3)_2(\text{H}_2\text{O})\text{T}]^{n+} + \text{H}_2\text{O}$. Water ligand that is in the trans position with respect to the T ligand (T=H₂O, NH₃, OH⁻, F⁻, Cl⁻, Br⁻, H₂S, CH₃S⁻, SCN⁻, CN⁻, PH₃, CO, CH₃⁻, H⁻, C₂H₄) is exchanged for another water molecule. In further text entering and leaving water molecules will be designated as E and L, respectively (the entering ligand is supposed to be the water ligand which is more distant from the central Pt(II) atom in the transition state structure than the leaving ligand (of course the same assumption is valid for the reactant region). However in most TS–T structures the difference between the two Pt–OH₂ bond lengths is small or negligible). This experimental arrangement enables us to use principle of microscopic reversibility and also the symmetry in the preparatory stage of optimizations. However the final structures are optimized with no symmetry restrictions. Although such reactions do not have a practical importance, differences in the strength of the trans- effect of selected ligands can be evaluated and compared.

The starting reactant square- planar complexes $\text{trans-Pt}[(\text{NH}_3)_2(\text{H}_2\text{O})\text{T}]^{n+}$ will be designated as R–T structures while pentacoordinated transition states and/or intermediates $\text{trans-Pt}[(\text{NH}_3)_2\text{T}(\text{H}_2\text{O})_2]^{n+}$ will be designated as TS–T and INT–T, respectively.

The reaction mechanism suggests the formation of a supermolecular complex R–T··H₂O in the first stage. Then reaction proceeds via one TS–T transition state structure or via INT–T intermediate structure surrounded by two transition states (see Scheme 1 and Fig. 1). The activation barriers are calculated as the energy difference between TS–T and R–T··H₂O structures (the same approach was used with success in a number of studies (refs. 6, 9, 17, 18). Although it was shown recently by Lau and Deubel (ref. 14) that agreement of activation energies with



Scheme 1. Proposed reaction mechanism of substitution reactions.

experiment in the cited studies is due to large cancellation of errors, this approach is fully acceptable in our case since we are interested only in the relative (not absolute) activation energies of the reactions of the same class).

Energy Decomposition Analysis of Pt–H₂O Bond

Additional single-point calculations on the optimized structures were conducted using the Amsterdam Density Functional 2001.01 package (ADF)³³ to calculate fragment energy decompositions according to the extended transition state theory.³⁴ In these calculations, a triple- ζ STO basis set is utilized, with one set of polarization functions as provided in the ADF, together with the BLYP functional.^{29a,c} Relativistic effects on Pt are included using the “zero order regular approximation” (ZORA).³⁵

The fragment calculations available in ADF provide a decomposition of the binding energies in a chemically meaningful manner.³³ Reactant structures were considered to consist of Pt[(NH₃)₂T] and H₂O fragments. The TS structures were considered to be divided into the two fragments in a number of ways: (1) Pt[(NH₃)₂T] and L water ligand when E water ligand is neglected; (2) Pt[(NH₃)₂T] and E water ligand when L water ligand is neglected (this analysis is done only when Pt–E and Pt–L bond lengths differ significantly); (3) Pt[(NH₃)₂T] and both L and E water ligands being considered as one fragment; (4) Pt[(NH₃)₂TL] and E water ligand. This enables us to make a comparison of interaction energies of E and L ligands with Pt[(NH₃)₂T] fragment. The Pt[(NH₃)₂TL]–E decomposition gives additional information about the possible stabilization of the pentacoordinated transition states or intermediate structures.

Note that interaction energy ΔE_{int} corresponds to the bond energy of the fragments with geometries as found in original molecule. Thus the fragments are not at their equilibrium geometry resulting in higher bond energies comparing with that of true overall bond energy (the energy difference is usually called the deformation (or preparation) energy and it is the energy needed to deform the equilibrium geometries of the separate fragments to that found in the adduct structure. In case of energy decomposition analysis of R–T structures, the deformation energy of the two fragments ranges between -1.7 (R–NO₂) and -0.4 kcal/mol (R–H)—see Table 1S in the Supplementary

material). The interaction energy can be further decomposed into three terms:

$$\Delta E_{\text{int}} = \Delta E_{\text{Pauli}} + \Delta E_{\text{el-st.}} + \Delta E_{\text{orb-int}}$$

The term ΔE_{Pauli} comprises the destabilizing interactions between occupied orbitals in accord with the Pauli principle. The second term $\Delta E_{\text{el-st}}$ corresponds to the classical electrostatic interaction between the charge distributions of the two fragments. These two terms can be summed to form the so called nonorbital interaction energy $\Delta E_{\text{non-orb}}$. Finally, the orbital interaction $\Delta E_{\text{orb-int}}$ accounts for charge-transfer and polarization interactions.

The R–T Complexes

Structural Features and Trans-Influence

Although the R–T structures were optimized without any constraints of symmetry they are planar. Geometrical parameters of the square planar R–T complexes are shown in the Table 1. H₂O ligand is in the trans position with respect to the T ligand. According to the decreasing Pt–OH₂ bond lengths we can order the ligands by the decreasing trans influence:

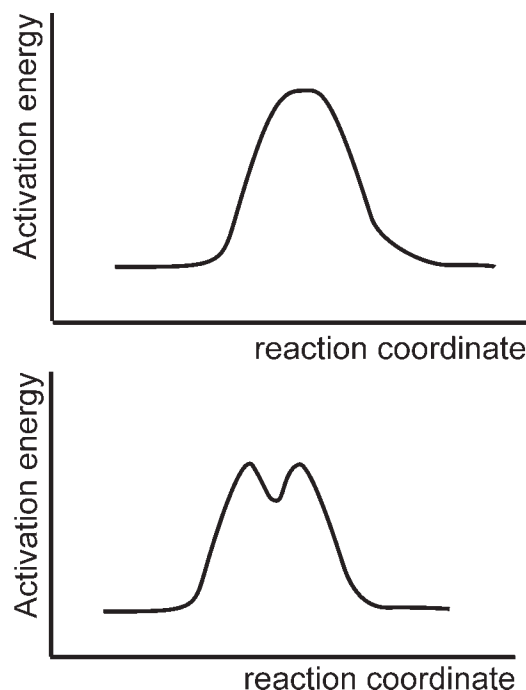
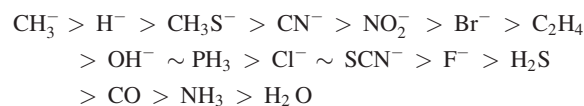


Figure 1. Possible energy profiles of substitution reactions.

Table 1. B3LYP/BSI and B3LYP/BSII Distances (in Å) in R–T Structures.

T/basis set	Pt–H ₂ O		Pt–T		Pt–NH ₃			
	BSI	BSII	BSI	BSII	BSI	BSII	BSI	BSII
H ₂ O	2.066	2.065	2.066	2.065	2.087	2.086	2.087	2.086
F	2.140	2.129	1.904	1.922	2.064	2.074	2.073	2.066
OH	2.190	2.180	1.946	1.952	2.066	2.068	2.073	2.074
NH ₃	2.109	2.108	2.053	2.053	2.094	2.092	2.085	2.087
SCN	2.179	2.171	1.955	1.958	2.087	2.085	2.070	2.071
Cl	2.180	2.181	2.288	2.266	2.081	2.078	2.066	2.069
Br	2.203	2.202	2.408	2.409	2.082	2.079	2.067	2.069
H ₂ S	2.136	2.143	2.339	2.313	2.083	2.085	2.094	2.094
NO ₂	2.219	2.208	1.998	2.000	2.092	2.089	2.081	2.081
CN	2.224	2.215	1.915	1.919	2.085	2.083	2.071	2.074
PH ₃	2.189	2.196	2.275	2.260	2.091	2.090	2.087	2.091
SCH ₃	2.281	2.292	2.308	2.290	2.081	2.079	2.070	2.072
CO	2.125	2.122	1.876	1.881	2.099	2.097	2.091	2.093
H	2.319	2.334	1.527	1.530	2.079	2.076	2.067	2.069
CH ₃	2.335	2.351	2.029	2.028	2.068	2.070	2.084	2.081
C ₂ H ₄	2.197	2.195	2.084	2.070	2.082	2.084	2.091	2.089

The Pt–OH₂ bond trans to CH₃[−] (i.e. to the ligand with the strongest trans influence) is almost by 0.3 Å longer than the Pt–OH₂ bond trans to H₂O (i.e. to the ligand with the weakest trans influence). Pt–NH₃ bond lengths are influenced significantly less by the nature of the T ligand (which is in the cis-position) ranging from 2.069 (T=F[−]) to 2.095 Å (T=CO). We have not found any correlation between Pt–OH₂ and Pt–NH₃ bond lengths.

Almost the same order of ligands has been achieved after reoptimizations using substantially improved B3LYP/BSII level (see Table 1). C₂H₄, OH[−], PH₃, Cl[−] ligands, i.e. ligands in the middle of the row, are mutually interchanged giving slightly modified order PH₃ ~ C₂H₄ > Cl[−] ~ OH[−]. The same is the case for F[−] and H₂S ligands, trans-influence of the H₂S ligand is stronger than of the F[−] ligand on B3LYP/BSII level. However these changes are subtle and give us the evidence that B3LYP/BSI method offers fairly reliable geometries.

Electronic Properties and σ -Donation

Molecular orbitals of cisplatin and related square planar Pt(II) complexes have been analyzed in a number of previous studies.^{5a,7,10,27,36} Supposing that the ligands lie on the *x,y* axis then according to the classical ligand field theory, the 5d_{x²-y²} atomic orbital (AO) becomes LUMO of the Pt(II) fragment due to its largest repulsion with σ -donating electron pairs of ligands. The stability of the complex arises from the bonding interaction of the vacant 5d_{x²-y²} orbital of the metal with the HOMO of the ligands' fragment which is the linear combination of p_x and p_y orbitals. Since it is two-electron/two-orbital interaction, the antibonding combination of these orbitals becomes the LUMO of the complex. As electrons are donated from the filled ligand orbital to the vacant metal orbital, this kind of interaction is called σ -donation (a simplified picture for one ligand orbital is shown in Fig. 2a). It decreases the total (positive) NBO charge of the

Pt(II) atom by an increase of electron density in the *xy* plane. According to the classical explanation, trans effect causes electrostatic destabilization of the ligand in the trans position and it is observable experimentally as Pt–H₂O bond length elongation (see above).

The character of the remaining 5d orbitals of the Pt(II) atom becomes nonbonding. According to the classical ligand field theory these filled nonbonding orbitals provide a repulsive interaction with the entering ligand.

NBO analysis shows that occupancies of 5d_{xy}, 5d_{yz}, and 5d_{z²} orbitals are almost the same for different R-T structures with

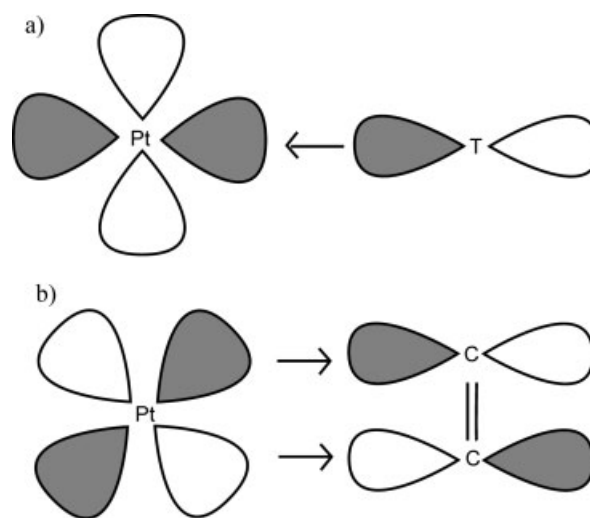


Figure 2. (a) σ -donation from the filled ligand p_x orbital to vacant metal 5d_{x²-y²} orbital. (b) π -back-donation from the filled metal d_{xz} orbital to the antibonding linear combination of carbons' p_x orbitals in C₂H₄.

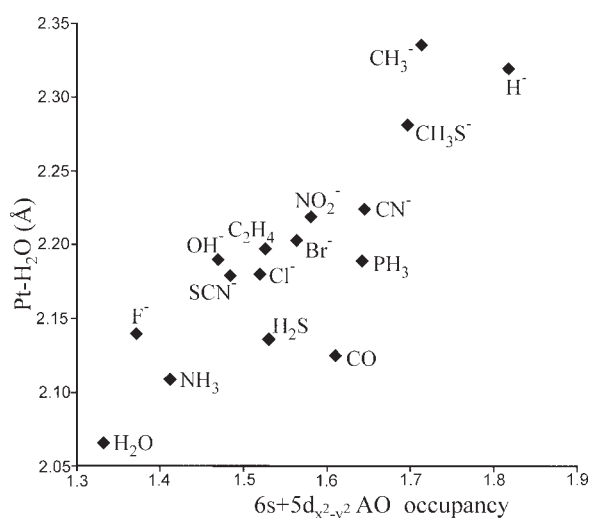
Table 2. Total NBO Charges Q and AO Occupancies on Pt(II) Atom in R–T Structures.^a

T	Q	5d _{x²-y²}	5d _{xz}	5d _{xy}	5d _{yz}	5d _{z²}	6s
H ₂ O	0.845	0.815	1.989	1.970	1.987	1.855	0.517
F	0.828	0.819	1.989	1.980	1.983	1.822	0.551
OH	0.737	0.895	1.986	1.979	1.982	1.822	0.574
NH ₃	0.763	0.865	1.987	1.979	1.986	1.855	0.546
SCN	0.721	0.924	1.972	1.969	1.984	1.846	0.560
Cl	0.634	0.948	1.991	1.981	1.984	1.860	0.572
Br	0.581	0.981	1.992	1.982	1.984	1.866	0.582
H ₂ S	0.644	0.965	1.974	1.970	1.986	1.879	0.565
NO ₂	0.653	0.970	1.937	1.979	1.985	1.847	0.611
CN	0.595	1.031	1.952	1.948	1.985	1.864	0.614
PH ₃	0.550	1.048	1.963	1.958	1.986	1.886	0.594
SCH ₃	0.481	1.070	1.979	1.980	1.982	1.857	0.627
CO	0.726	1.013	1.884	1.894	1.989	1.887	0.598
H	0.359	1.132	1.995	1.979	1.981	1.855	0.686
CH ₃	0.495	1.088	1.985	1.973	1.982	1.840	0.626
C ₂ H ₄	0.794	1.022	1.811	1.970	1.986	1.900	0.504

^aAO's are ordered by their importance for the trans effect strengths, not by their relative energies.

mean values of 1.968 ± 0.021 , 1.984 ± 0.002 , and 1.859 ± 0.021 , respectively (see Table 2). On the other hand the occupancies of 5d_{x²-y²} differ substantially ranging between 0.815 (R–H₂O) and 1.132 (R–H). The 5d_{x²-y²} orbital is sd¹ hybridized with 6s orbital. Occupancy of 6s orbital increases linearly with that of 5d_{x²-y²} orbital with exception of R–C₂H₄. Figure 3 shows that the dependence of Pt–H₂O distances on 5d_{x²-y²} and 6s occupancies is linear in agreement with the theory of trans influence (see also a linear dependence of Pt–Cl bond lengths on the total platinum charge in trans-[PtClX(dms)₂] complexes³⁷ (dms = dimethylsulfide)).

The deviation of the value for R–CO complex is caused by a partial hybridization of the 5d_{x²-y²} orbital with 5d_{xy} orbital.

**Figure 3.** Dependence of Pt–H₂O distance on the occupancy of 6s and 5d_{x²-y²} AOs in R–T structures.

The latter has unusually low occupancy of 1.884. The same situation can be also seen to a smaller extent in all R–T complexes and it may be caused by the fact that the ligand–Pt–ligand angles differ from the ideal value of 90° therefore the ligands do not lay exactly on the x,y axis.

Summing up occupancy numbers of the 6s, 5d_{xy}, and 5d_{x²-y²} AOs the following sequence of trans ligands can be constructed what may be used as a measure of the trans influence strength:

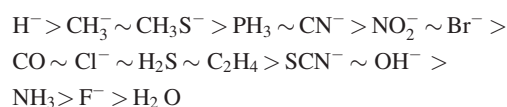


Figure 4 shows that the relationship between the occupancies of 6s, 5d_{xy}, 5d_{x²-y²} AOs and the total H₂O ligand charge is inverse proportional. The total H₂O ligand charge reflects the amount of the charge transferred by σ-donation from H₂O ligand to the 5d_{x²-y²} orbital. Thus one would expect the above relationship should be proportional. The inverse proportional relationship between the two amounts of charges means that σ-donation ability of H₂O ligand is given by the population of the 5d_{x²-y²} orbital. The higher is the occupancy of the 5d_{x²-y²} AO the lower amount of charge can be donated by H₂O ligand to this orbital and the weaker (and longer- compare Figs. 3 and 4) is the Pt–H₂O dative bond.

Therefore we can conclude that trans influence can be understood basically as a competition between the ligands in the trans direction for the ability to donate their electron density to the 5d_{x²-y²} AO.

Further evidence for this assumption provides NBO analysis of cis- and trans- isomers of Pt[(NH₃)₂(H₂O)₂]. The trans- isomer shows only a slight increase of 5d_{x²-y²} orbital occupancy with respect to R–H structure. On the other hand in the cis- isomer there is a substantial increase of 5d_{x²-y²} orbital occupancy with respect to both the trans- isomer and R–H structure (see Table 3 and Table 2).

According to our results, a classical opinion²⁷ that σ-donation increases electrostatic and Pauli repulsion between electrons in the metal 5d_{x²-y²} AO and electron pairs in the H₂O trans ligand

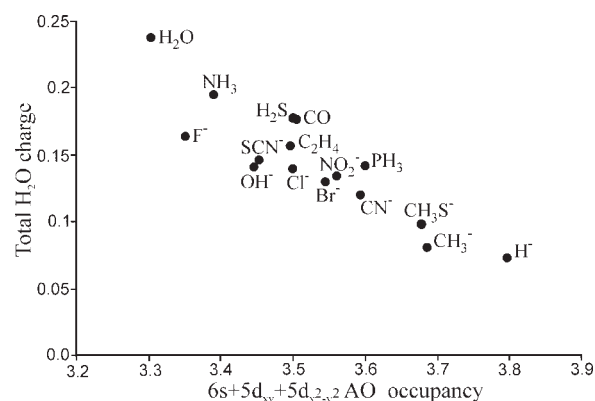
**Figure 4.** Dependence of total NBO charge of H₂O ligand on the AO occupancy of 6s, 5d_{xy} and 5d_{x²-y²} orbitals in R–T structures.

Table 3. Total NBO Charges Q and AO Occupancies on Pt(II) Atom in cis/trans-[Pt(NH₃)₂X₂] Structures.

cis/trans	X	Q	5d _{x²-y²}	5d _{xz}	5d _{xy}	5d _{yz}	5d _{z²}	6s
Trans	H	0.288	1.169	1.976	1.977	1.996	1.868	0.704
Cis	H	0.017	1.333	1.991	1.983	1.991	1.872	0.793
Trans	C ₂ H ₄	0.704	1.072	1.813	1.983	1.987	1.908	0.514
Cis	C ₂ H ₄	0.731	1.094	1.862	1.982	1.862	1.938	0.513

should be modified. Besides the electrostatic term also the orbital-interaction term of increases proportionally to the σ -donation. Mutual dependence of these two terms is shown in Figure 6 below. It means that relative strengths of Pt–H₂O bonds in all R-T structures studied can be also described by differences in orbital interaction energies (see below an energy decomposition analysis for more details).

π -Back-Donation

Ligands such as CO and C₂H₄ stabilize the complex also by the π -back-donation. It is interaction of the filled 5d_{xz} orbital (supposing the trans ligand lies on the *x* axis) with empty π (p_x) orbitals of the ligand. Thus π -back-donation increases the total positive charge of the Pt(II) atom by a decrease of electron density in the *xz* plane. It facilitates a nucleophilic attack in the *xz* plane and stabilizes corresponding pentacoordinated transition state.

The occupancies of 5d_{xz} orbital are equal to almost 2.0 for most of the R-T structures (1.989 ± 0.003 for T=H₂O, NH₃, OH⁻, F⁻, Cl⁻, Br⁻, CH₃⁻, H⁻). Very slight lowering of the electron population of 5d_{xz} orbital (δ (d_{xz})) was observed for R–CH₃S (1.979), R–H₂S (1.974), R–SCN (1.972) and R–PH₃ (1.963), i.e. for atoms with low-lying 3d vacant orbitals. More pronounced decrease of δ (d_{xz}) occurs for R–CN (1.952) and R–NO₂ (1.937) ligands with “improperly” oriented π -system, and the most apparent reduction of δ (d_{xz}) is visible for the R–CO (1.884) and especially for R–C₂H₄ (1.813). Since the *xz* plane is the plane where ligand exchange takes place the lowering of the 5d_{xz} orbital population enables σ -donation from filled orbitals of E and L ligands to the antibonding Pt–C orbitals. These antibonding orbitals can be characterized as linear combinations of 6s, 5d_{x²-y²} and 5d_{xz} platinum orbitals, however character of 5d_{xz} AO prevails (expansion coefficient 0.7 in case of INT–C₂H₄). The electron-repulsion decrease of the entering and leaving ligands with the orbitals of central Pt(II) atom plays slightly more significant role than in R-T structures but $\Delta E_{\text{non-orb}}$ still comprises not more than 25% of ΔE_{int} (see below).

Only for C₂H₄ ligand the lowering of 5d_{xz} orbital population is sufficient to enable the formation of the pentacoordinated intermediate minimum structure. For other trans ligands the pentacoordinated structures exist only as true transition states in case that both E and L ligands are water molecules. If E and L are e.g., OH⁻ ligands, minimum pentacoordinated structure was optimized also for CO ligand. The OH⁻ ligand forms much stronger dative bond with Pt(II) atom than the H₂O ligand as can be seen from a comparison of second order NBO energies

(E²) for LP(1)O → σ^* (Pt–C) electron donations (101.6 kcal/mol vs. 26.8 kcal/mol).

A comparison of NBO charges of cis- and trans- isomers of Pt[(NH₃)₂(C₂H₄)₂]²⁺ shows that a higher positive partial charge on the platinum atom is in the cis isomer³⁸ since two orbitals (5d_{xz} and 5d_{yz}) are involved in π -back-donation. Only one (5d_{xz}) orbital is available for the two π -back-donating ligands in the trans isomer (see Table 3).

Energy Decomposition Analysis of Pt[(NH₃)₂T] ... H₂O Interaction

The results are summarized in the Table 1S in the Supplementary Material. Values of ΔE_{int} for Pt[(NH₃)₂T] · H₂O interaction are dependent mainly on the total charge of the complex. The +2 charged systems (i.e. systems with a neutral T ligand) offer generally much lower values of ΔE_{int} than the +1 charged systems. Considering the systems with the same charge, ΔE_{int} is linearly correlated with Pt–H₂O intermolecular distances (see Fig. 5a and also refs. 13 and 39). It suggests simple electrostatic nature of the Pt–H₂O bond. However in water solvent environment ($\epsilon_r =$

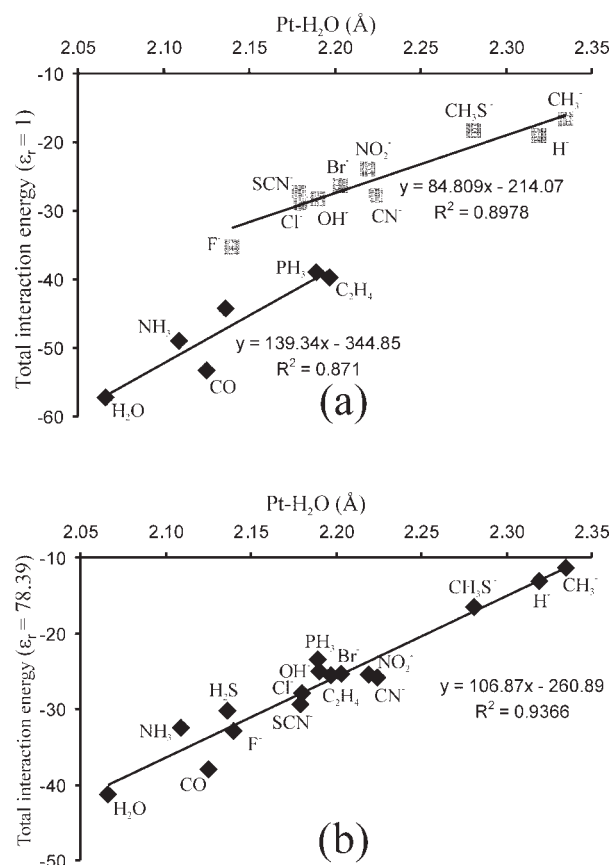


Figure 5. Total interaction ΔE_{int} and $\Delta E_{\text{int}}(w)$ energies dependence on Pt–H₂O distances in R–T structures in (a) vacuum and (b) water environment. Note that $\Delta E_{\text{int}}(w)$ energies are corrected by the deformation energies of the fragments. They are not lower than –1.7 kcal/mol (see Table 1S in the Supplementary Material) not having an important influence on the results (energies in kcal/mol).

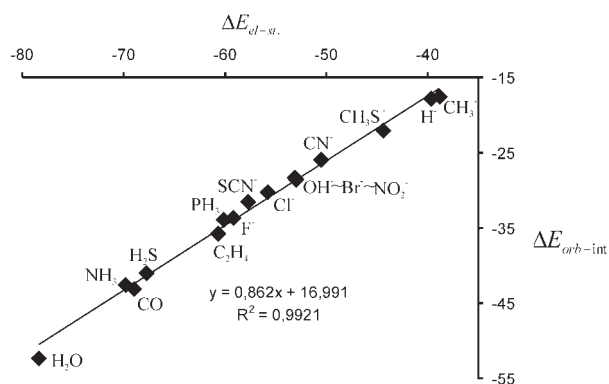


Figure 6. A mutual dependence of $\Delta E_{\text{el-st}}$ and $\Delta E_{\text{orb-int}}$ terms for $\text{Pt}[(\text{NH}_3)_2\text{T}] \cdots \text{H}_2\text{O}$ decomposition in R-T structures (in kcal/mol).

78.39) the total interaction energy $\Delta E_{\text{int}}(w)$ dependence on $\text{Pt}-\text{H}_2\text{O}$ distance becomes linear (Fig. 5b). It is well known that long range electrostatic effects are essentially eliminated by the solvent and the dependence is then dominated by the density distribution changes (polarization and charge transfer contributions) that should not be markedly influenced by the solvent.⁴⁰

ΔE_{int} is calculated as the sum of ΔE_{Pauli} , $\Delta E_{\text{el-st}}$, and $\Delta E_{\text{orb-int}}$ terms [Eq. (1)]. To compensate the repulsive ΔE_{Pauli} term, the $\Delta E_{\text{el-st}}$ term is usually used to form the so-called nonorbital interactions. In this case nonorbital interactions contribute only up to 20% to the total interaction energy ΔE_{int} . However in many other studies (see e.g. ref. 41 and references cited therein) instead of the $\Delta E_{\text{el-st}}$ term, $\Delta E_{\text{orb-int}}$ is used to compensate ΔE_{Pauli} term. Since the $\Delta E_{\text{orb-int}}$ term is linearly correlated with the $\Delta E_{\text{el-st}}$ term (see Fig. 6), these two ways are equivalent for R-T structures (interestingly when we have studied the dependence of the fragment energy decomposition terms on the $\text{Pt}-\text{H}_2\text{O}$ distance for the points along the IRC pathway, for +2 charged complexes ΔE_{Pauli} was well compensated by $\Delta E_{\text{el-st}}$ in the reactant region while in the TS region it was compensated by $\Delta E_{\text{orb-int}}$ (Figs. 1Sa) and 1Sb) in the Supplementary material). For +1 charged complexes ΔE_{Pauli} was compensated by $\Delta E_{\text{el-st}}$ on the whole reaction coordinate and ΔE_{int} follows well the $\Delta E_{\text{orb-int}}$ (Fig. 1Sc) in the Supplementary material). $\Delta E_{\text{orb-int}}$ includes a polarization term and a charge transfer component that are, indeed, closely related with the electrostatics. Figure 6 shows that for the considered R-T structures the dependence is almost exactly linear.

The covalent/ionic ratio, expressed by the ratio $\Delta E_{\text{orb-int}}/\Delta E_{\text{el-st}}$, does not differ significantly for R-T structures being 0.45 for R-H and R- CH_3 , 0.54 ± 0.02 for the other +1 charged complexes and 0.61 ± 0.03 for the +2 charged complexes. Note that energy decomposition analysis is performed in the gas phase, in solution the $\Delta E_{\text{orb-int}}$ term can be expected to be the main contributor to the $\Delta E_{\text{int}}(w)$ energy (see above).

Structures Relevant for the Course of Substitution Reactions and Energetics

In the previous sections we have seen how electronic properties of R-T structures influence the mechanism of the substitution reac-

tions. In this section let us describe the mechanism of the reaction pathways together with the relevant structures and the energetics.

The Associative Mechanism: The Trigonal Bipyramidal (TBP) INT- C_2H_4 Intermediate Structure

From the range of ligands studied, only the C_2H_4 ligand was able to stabilize both E and L water ligands in the pentacoordinated INT- C_2H_4 intermediate structure. This structure has the C_S symmetry and it is a true minimum on the potential energy surface. A similar structure was found by partial optimization in the previous study of Lin and Hall²⁷ but it could not be recognized as a minimum since it is a true transition state on the HF level²⁷ (see also ref. 42). Electron correlation effects are responsible for the stabilization of this intermediate structure as it has been proven also by the optimization on the MP2/BSI level.

Note that TBP structures of general formula $[\text{M}(\text{N}-\text{N})(\text{olefin})\text{XY}]$ (M = metal; N-N = bidentate N-donor ligand; X, Y = monodentate ligands) are well experimentally described complexes.^{42,43}

In the INT- C_2H_4 intermediate the E-Pt-L angle has the value of 74.0° and Pt, E, L, C_2H_4 lie in the plane which is perpendicular to the NH_3-Pt bonds. Pt-E and Pt-L bond lengths are equal to 2.39 Å, i.e. Pt- H_2O bond is elongated by 0.19 Å with respect to the R- C_2H_4 structure.

Structure and geometrical parameters of the transition state TS- C_2H_4 connecting INT- C_2H_4 intermediate with the square planar reactant R- $\text{C}_2\text{H}_4 \cdots \text{H}_2\text{O}$ are shown on the Figure 7 and in the Table 4. The Pt-E and Pt-L distances are 2.268 and 2.734 Å, respectively.

The Dissociative Interchange (I_d) Mechanism: The T-Shaped $\text{Pt}[(\text{NH}_3)_2\text{T}(\text{H}_2\text{O})_2]^\ddagger$ ($\text{T}=\text{H}^-$, CH_3^-) Transition State Structures

Structure of transition states for ligands with the strongest trans influence, i.e. for H^- and CH_3^- , differ substantially from the other transition state structures.

H^- and CH_3^- ligands have the strongest σ -donation ability and no π -back-donation ability. It results in high populations of $5d_{x^2-y^2}$ and $5d_{xz}$ orbitals that destabilize the Pt-L bond in both the reactant and transition states structures. The substitution in the trans position proceeds clearly by a dissociative interchange (I_d) mechanism via transition state of the T-shape. Unlike the other transition states TS-H and TS- CH_3 structures are planar with E and L ligands in the plane of the complex. It is enabled by very long Pt-E and Pt-L distances being 3.075 and 3.294 Å, respectively, in TS-H; 3.684 and 3.785 Å, respectively, in TS- CH_3 (see Table 4). Pt-L and Pt-E distances are already too long to cause any interactions with filled d- orbitals on the platinum atom and they are comparable with Pt-ligand distances reported for the ligands in the first solvation shell of cisplatin-like complexes.^{44,45} The position of E and L ligands in the plane of the complex is more advantageous than in the perpendicular plane since it offers ligand stabilization by the H-bond formation with NH_3 ligands. The weaker is the Pt-L (or Pt-E) interaction the stronger is the H-bonding with NH_3 ligand. In case of TS- CH_3 both E and L ligands are involved in the

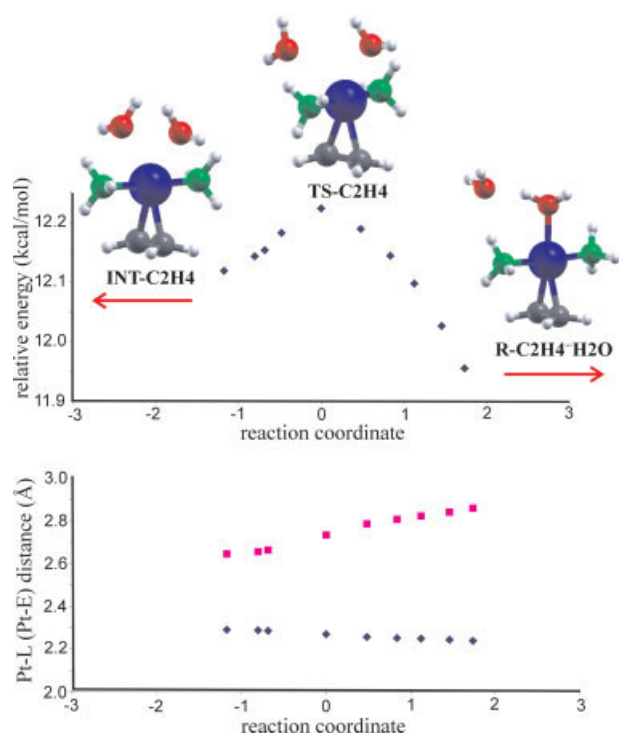


Figure 7. The IRC profile of the substitution reaction of R—C₂H₄ structure. Only a few points could be found on both directions. Their relative B3LYP/BSI energies (the upper graph) are given with respect to R—C₂H₄·H₂O structure (which has the relative energy 0.0 kcal/mol). INT—C₂H₄ structure has relative energy 11.15 kcal/mol. The direction of the INT—C₂H₄ and R—C₂H₄·H₂O structures are indicated by arrows. On the graph below Pt—E and Pt—L distances are shown.

Table 4. B3LYP/BSI Geometries of TS—T and INT—C₂H₄ Structures (Distances in Å, O—Pt—O Angles in Degrees).

T	Pt—L	Pt—E	Pt—T	Pt—NH ₃	O—Pt—O	
H ₂ O	2.408	2.426	2.110	2.070	2.084	67.2
F	2.561	2.562	1.921	2.065	2.065	60.9
OH	2.689	2.688	1.953	2.062	2.075	59.5
NH ₃	2.470	2.476	2.063	2.082	2.083	66.1
SCN	2.570	2.583	1.965	2.078	2.073	62.3
Cl	2.566	2.566	2.297	2.068	2.068	63.5
Br	2.581	2.581	2.416	2.069	2.069	63.7
H ₂ S	2.446	2.450	2.316	2.081	2.082	68.8
NO ₂	2.564	2.564	1.987	2.084	2.084	62.6
CN	2.581	2.581	1.904	2.076	2.076	63.8
CN ^a	2.610	2.610	1.906	2.075	2.075	64.1
PH ₃	2.483	2.484	2.246	2.086	2.082	68.9
SCH ₃	2.826	2.880	2.299	2.064	2.081	57.1
CO	2.396	2.396	1.853	2.089	2.089	68.5
CO ^a	2.407	2.407	1.856	2.089	2.089	69.5
H	3.075	3.294	1.151	2.075	2.060	53.5
CH ₃	3.684	3.785	2.023	2.069	2.074	79.1
CH ₃ ^a	3.488	4.191	2.025	2.069	2.072	81.3
C ₂ H ₄	2.268	2.734	2.031	2.079	2.084	76.3
INT—C ₂ H ₄	2.39	2.393	2.005	2.082	2.082	74.0

^aB3LYP/BSII geometries.

H—bonding towards to NH₃ groups. It results in the fairly large E—Pt—L angle of 79.1°. In case of TS—H only E is H—bonded with the NH₃ group. E is also involved in the H—bond with L ligand. It results in the lowest E—Pt—L angle of 53.5°. L is the H—bond acceptor group while E is the H—bond donor group.

Since Pt—E and Pt—L distances are not the same, E and L ligands are not fully equivalent in the TS—H and TS—CH₃ structures. As a result IRC profile is not symmetric for reverse and forward directions as both E and L ligands keep their H—bonding pattern as found in the transition state structure (see Fig. 8). However both directions lead to the same R—T·H₂O structure with oxygen atom of water involved in two H—bonds. The other H—bond pattern is not stable (structure on the reverse (negative) direction side of reaction coordinate in the Fig. 8) and rearranges to the structure R—H·H₂O upon optimization.

The Associative Interchange (*I_a*) Mechanism: The TBP Pt[(NH₃)₂T(H₂O)₂] Transition State Structures

For all the trans directors other than H[−], CH₃[−], and C₂H₄, the substitution has to overcome one TS—T transition state (T=H₂O, NH₃,

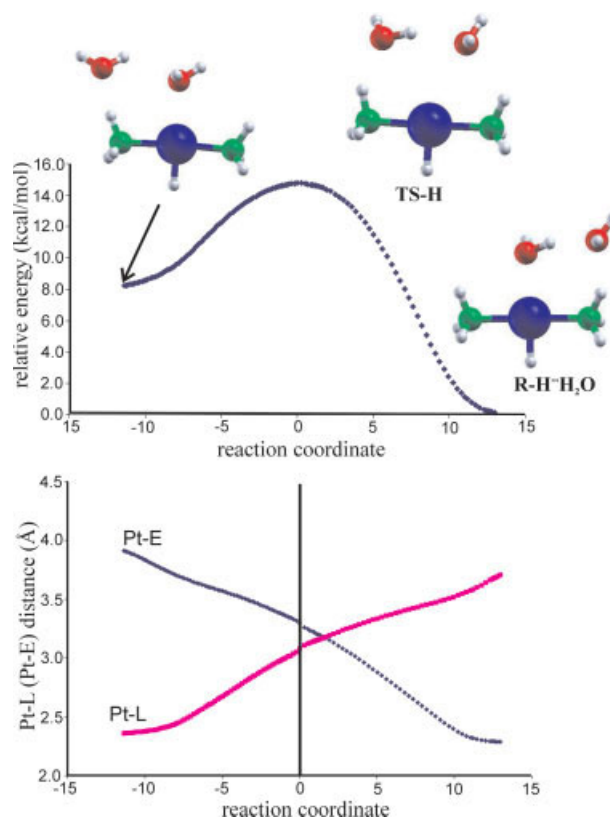


Figure 8. The IRC profile of the substitution reaction of R—H structure. B3LYP/BSI energy (the upper graph) is given with respect to R—H·H₂O structure (which has the relative energy 0.0 kcal/mol). The structure on the reverse side rearranges to R—H·H₂O structure upon optimization. On the graph below Pt—E and Pt—L distances are shown.

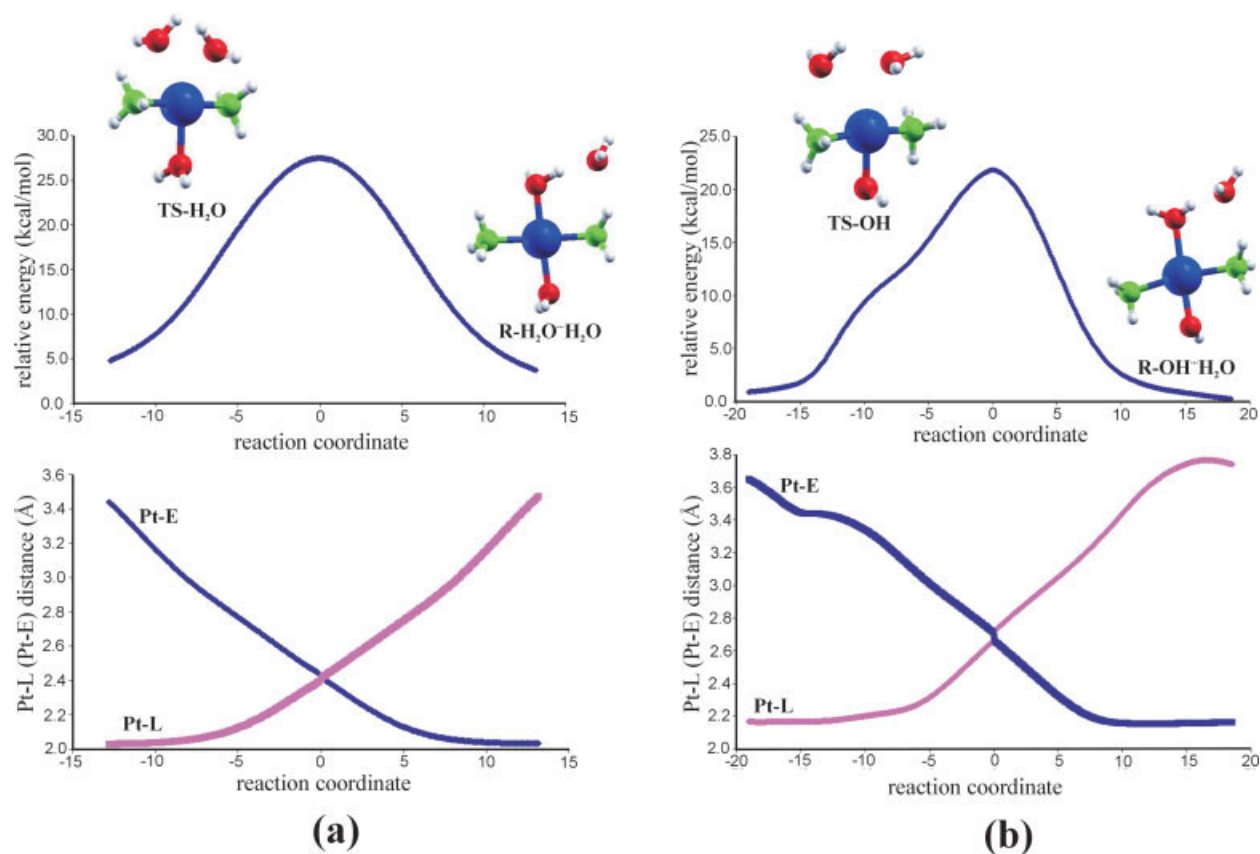


Figure 9. The IRC profiles of the substitution reactions of (a) R—H₂O and (b) R—OH structures. B3LYP/BSI energies (the upper graphs) are given with respect to R—H₂O ··· H₂O and R—OH ··· H₂O structures (what have relative energies 0.0 kcal/mol), respectively. On the graphs below Pt—E and Pt—L distances are shown. Note a steep change of these distances in the region of the TS—OH transition state.

OH[−], F[−], Cl[−], Br[−], H₂S, SCN[−], CN[−], PH₃, CH₃S[−], CO) what have the TBP structure with substantially elongated bonds towards to E and L ligands. Similar structures have already been optimized several times for cisplatin and its derivatives.^{6,15,17,20,46} The elongation of Pt—L bond in TS—T structures with respect to R—T structures ranges between 0.271 (CO) and 0.545 Å (CH₃S[−]) with a mean value of 0.377 Å. The other bond lengths are almost unaffected comparing to the corresponding R—T complexes. The Pt—L and Pt—E bond lengths are very similar in most of the structures (see Table 4). Thus E and L ligands can be considered to be fully equivalent in the transition state structures. The reaction can be described by an associative interchange (*I_a*) mechanism and a typical reaction profile is shown on the Figure 9a.

Regardless the structural similarity of the TS geometries, the calculated differences in activation barriers correspond to a ratio of reaction rates of up to seven orders of magnitude.

In the TS—OH structure E and L ligands interact by an H—bond with each other. The formation of the H—bond disturbs the symmetry of the forward reaction with respect to the reverse one as it is shown by IRC calculation (see Fig. 9b). However it has no practical importance for the general mechanism of the substitution. The H—bond formation is the reason

of a fairly low E—Pt—L angle of 59.5° and of a relatively higher stabilization of E in the pentacoordinated transition state according to energy decomposition analysis.

The E ligand is rather distorted from the equatorial T—Pt—L plane in TS—CH₃S structure forming a nonlinear H—bond with NH₃ ligand (N—H···O distance of 2.018 Å and angle of 128.2°). The E ligand is also involved in additional H—bonding with L ligand leading to a fairly small E—Pt—L angle of 57.1°. The Pt—L and Pt—E bonds are rather long, more than 2.8 Å (compare with the TS structure in Fig. 1 in ref. 24). Similar geometrical features are found in TS—T (T=H[−], CH₃[−]) structures, however in TS—CH₃S structure the H—bonds of E ligand are much weaker and Pt—L interaction is still strong enough to keep the L ligand in the equatorial plane of the TBP structure. Therefore for CH₃S ligand as the trans director, the ligand exchange proceeds by *I_a* rather than *I_d* mechanism.

The reaction mechanism may also depend on the nature of the leaving and entering ligands. For CO ligand as the trans director we have shown that strong nucleophiles (e.g. OH[−] ligands as E and L) are able to stabilize minimum pentacoordinated TBP intermediate (see above) and reaction proceeds via associative mechanism.

Table 5. Relative Energies, Zero Point Energies, Enthalpy, Entropy and Solvation Corrections; and Free Energies (at 298 K) of the TS—T and INT—C₂H₄ Structures with Respect to Corresponding R—T· ·H₂O Structures for Ligand Exchange Reactions.

	$\Delta E(\text{DFT})^a$	ΔE_{ZPE}^b	ΔE_{TRV}^b	$-T\Delta S^b$	$\Delta E_{\text{solv}} - \text{CPCM}^c$	ΔG^\ddagger -DFT/CPCM
TS—H ₂ O	26.10	-1.67	0.46	0.70	-1.57	22.63
TS—F	24.81	-1.93	0.47	1.15	0.07	22.27
TS—OH	21.33	-1.60	0.21	0.23	1.37	21.07
TS—NH ₃	24.41	-1.89	0.52	1.17	-1.64	20.23
TS—SCN	21.48	-2.02	0.50	0.80	0.68	19.83
TS—Cl	20.57	-1.98	0.50	1.02	-0.04	18.02
TS—Br	19.07	-1.92	0.46	0.71	0.06	16.96
TS—H ₂ S	19.25	-1.62	0.40	0.51	-1.42	16.10
TS—NO ₂	17.65	-1.93	0.52	1.24	0.28	15.28
TS—CN	17.97	-2.04	0.54	1.19	-0.62	14.65
TS—PH ₃	16.59	-1.63	0.42	0.50	-1.44	13.44
TS—SCH ₃	14.64	-1.50	1.28	3.69	2.41	13.15
TS—CO	17.44	-1.28	0.31	0.25	-3.27	12.95
TS—H	12.77	-1.81	0.21	0.64	0.79	11.31
TS—CH ₃	10.06	-2.02	0.65	3.38	5.43	10.74
TS—C ₂ H ₄	11.01	-1.49	0.30	0.43	-1.15	8.24
INT—C ₂ H ₄	10.27	-1.18	0.68	1.27	-2.76	5.74

All energies are in kcal/mol.

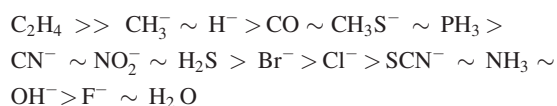
^aB3LYP/ MWB-60(2fg)/6-311++G(2df,2dp)//B3LYP/6-31G* values.

^bB3LYP/6-31G* corrections.

^cB3LYP-CPCM/ MWB-60(2fg)/6-311++G(2df,2dp)// B3LYP/6-31G* corrections.

Activation Free Energies and the Kinetic Trans-Effect

Activation free energies ΔG^\ddagger are directly related with the kinetic constant of the reaction by a factor $e^{-\Delta G^\ddagger/RT}$. Since the trans effect is a kinetic phenomenon relative activation free energies correspond to the expected relative strengths of the trans effect. We can order the ligands according to the activation energies (see Table 5), which these ligands provoke in the trans position:



The water H₂O ligand and the ethylene C₂H₄ ligand show the weakest and the strongest trans effect, respectively.

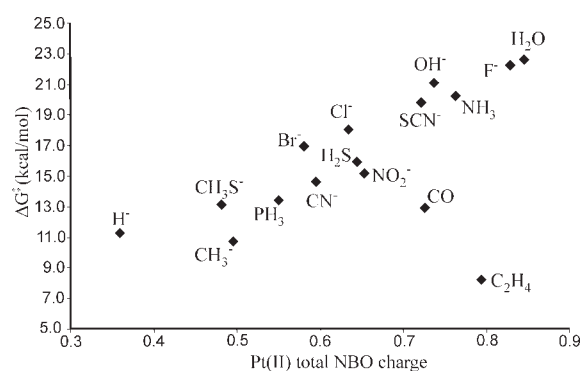
The total NBO charges on the central Pt(II) atom in the reactant structures correlate proportionally with the heights of the activation barriers (see Fig. 10). The lower is the total NBO charge on the Pt(II) atom the lower is the activation free energy. This dependence is almost linear with important exceptions of CO and C₂H₄ ligands. Their activation energies are too low with respect to their total NBO charges. It suggests that σ -donation is the prevailing effect for all the ligands except of CO and C₂H₄ ligands, which deviation reflects the extent of the π -back donation (see also a dependence of the activation free energies on the 6s, 5d_{xy} and 5d_{x²-y²} AOs occupancies in Fig. 2S).

Since the NBO charges correlate linearly with activation energies and simultaneously also with the Pt—H₂O trans- ligand distances in R-T structures, it is not surprising that there is a linear dependence between Pt—H₂O distances and heights of activation barriers (see Fig. 11). It is in accord with the trans

influence theory and it suggests Pt—H₂O (or Pt—L) bond breaking energy is a dominant contribution to activation free energy (see also ref. 23). Again the C₂H₄ and CO ligands are exceptions where the TS structure stabilization by π -back donation plays important role.

TS Geometry: Energy Decomposition Analysis for Pt((NH₃)₂T] and L Fragments when E Water Ligand is Neglected

Values of ΔE_{int} for the transition states are linearly correlated with ΔE_{int} energies in the reactant structures, i.e. the stronger is ΔE_{int} energy in the reactant structure the stronger it is also in

**Figure 10.** Activation free energy dependence on the total NBO charge of the Pt atom in R—T structures.

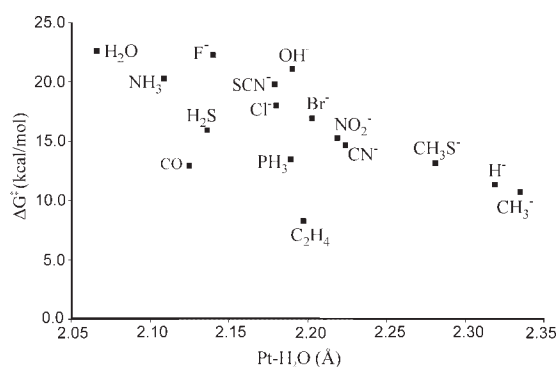


Figure 11. Dependence of activation free energies on Pt–H₂O distances in R–T structures.

the corresponding transition state (compare Tables 1S and 2S in the Supplementary Material). Absolute value of ΔE_{int} energy increases linearly with the decreasing Pt–H₂O distance with exception of CH₃ and H ligands where stabilization of L through the H–bonding with the NH₃ group is important.

Relative importance of $\Delta E_{\text{non-orb}}$ terms is higher in TS–T structures than in R–T structures. It is caused by a relatively higher decrease of the ΔE_{Pauli} term comparing to $\Delta E_{\text{el-st}}$ and $\Delta E_{\text{orb-int}}$ terms. For TS–H, $\Delta E_{\text{non-orb}}$ energy makes even 62% of ΔE_{int} energy showing a strong H–bond formation between the E water molecule and the complex but it is substantially less for the other TS–T structures.

Since L and E water ligands are equivalent in most of the TS structures, energy decomposition analysis for Pt[(NH₃)₂T] and both L and E water ligands being considered as one fragment gives results that are exactly in line with the above described ones (see Table 3S and Fig. 3S in the Supplementary Material).

TS Geometry: Energy Decomposition Analysis for Pt[(NH₃)₂TL] and E Water Ligand Fragments

As in previous cases, value of ΔE_{int} for the Pt[(NH₃)₂TL]...E interaction is dependant mainly on the charge of the complex. The +2 charged systems offers generally much lower ΔE_{int} values (see Table 4S in the Supplementary Material). The lowest ΔE_{int} values were calculated for INT–C₂H₄ and TS–CO structures suggesting the highest stabilization of the fifth ligand in the complex. ΔE_{int} values in other +2 charged systems are lower by about 20 kcal/mol.

Values of ΔE_{int} for +1 charged systems are about half of that for +2 charged systems. From +1 charged systems the lowest ΔE_{int} values offer structures with additional H–bond E ligand stabilization such as TS–OH and surprisingly also TS–H and TS–CH₃ where H–bonding can be considered as the only source of stabilization. This statement can be supported by a comparison of these results with the Pt[(NH₃)₂T]...E decompositions. ΔE_{int} values for Pt[(NH₃)₂TL]...E structures are increased substantially except the Pt[(NH₃)₂HL]...E decomposition. Increase of ΔE_{int} values is caused by both (1) an increase of ΔE_{Pauli} repulsion term due to presence of L water molecule and (2) a decrease of $\Delta E_{\text{orb-int}}$. The $\Delta E_{\text{el-st}}$ term is almost unchanged what shows that E and L water ligands do not inter-

act with each other. For the Pt[(NH₃)₂HL]...E decomposition, an increase of $\Delta E_{\text{el-st}}$ and $\Delta E_{\text{orb-int}}$ terms fully compensates the increase in ΔE_{Pauli} repulsion term suggesting an H–bond formation between E and L water ligands.

Conclusions

In this contribution we show that reactivity of Pt(II) square planar complexes is driven by two effects: σ -donation and π -back-donation. Their importance can be quantified by the population of 5d_{x²-y²} and 5d_{xz} AOs, respectively (in case the ligands lie in the xy plane with trans-directing ligands on the x axis). The first effect is linearly correlated with the Pt–H₂O (leaving ligand) bond length prolongations (i.e. trans-influence, see Fig. 3). In solution the Pt–H₂O bond lengths are linearly correlated with the total interaction energies between the leaving H₂O ligand and the rest of the complex (see Fig. 5b). Nearly linear dependence was found also for dependence of activation free energies on Pt–H₂O distances (see Fig. 11) with exceptions of C₂H₄ and CO ligands. It means that the kinetic trans effect is determined by the strength of the trans influence (i.e. by σ -donation ability—see Fig. 10) except the ligands with strong π -back-donation ability such as C₂H₄ and CO that stabilize transition state structure.

Pt(II)-ligand bonds are described as typical donor-acceptor bonds, non-orbital interactions contribute only up to 20% to the total interaction energy. The σ -donation ability of the ligand is dependant on the σ -donation ability of the ligand in the trans position (but not in the cis-position). Therefore there is a competition between the ligands in the trans-position for the opportunity to donate their electron density to the central Pt(II) atom (see Fig. 4 and Table 3). Similarly two π -back-donating ligands in trans position compete with each other to some extent since the two ligands withdraw electron density from the same (5d_{xz}) orbital.

The influence of the trans-effect on the reaction mechanism is also shown. When a ligand with a very strong σ -donation (such as CH₃[−] and H[−]) is present the total electron occupation in the 5d_{x²-y²} orbital is higher. It prevents the trans-ligand to form a strong dative bond with the central Pt(II) atom by σ -donation. Only formation of a very weak Pt–H₂O bond is allowed. Substitution proceeds by a dissociative interchange (*I_d*) mechanism.

On the other hand ligands such as ethylene C₂H₄ and CO show only a moderate trans-effect but they lower electron occupation in the 5d_{xz} orbital by a π -back donation. It decreases electron density on the Pt(II) atom in the xz plane and it leads to the stabilization of the pentacoordinated transition state/intermediate and the substitution proceeds by an associative mechanism. Existence of the stable pentacoordinated intermediate structure on the potential energy surface depends on the nucleophilicity of the entering and leaving ligands. In case of CO ligand the pentacoordinated intermediate structure exists for OH[−] ligands being the entering and leaving ligands but not for a weak nucleophile such as H₂O ligand. C₂H₄ ligand is able to stabilize pentacoordinated intermediate structure for both H₂O and OH[−] ligands being the entering and leaving ligands.

The other ligands (T=H₂O, NH₃, OH[−], H₂S, F[−], Cl[−], Br[−], SCN[−], CN[−], PH₃, CH₃S[−]) in the trans-position show weak or

moderate σ -donation and π -back-donation abilities. The substitution reactions have to overcome higher activation barriers and they proceed via one transition state of the TBP shape with substantially elongated bonds towards to leaving and entering ligands. Their mechanism corresponds to a associative interchange (I_a) mechanism.

References

1. Chernyaev, I. I. *Ann Inst Platine (USSR)* 1926, 4, 423.
2. (a) Fleischhacker, A. S.; Matthews, R. G. *Biochemistry* 2007, 46, 12382; (b) Albeniz, A. C.; Espinet, P.; Martin-Ruiz, B. *Dalton Trans* 2007, 33, 3710; (c) Berezin, D. B.; Toldina, O. V.; Berezin, B. D. *Russ J Inorg Chem* 2006, 51, 1728; (d) Chermette, H.; Rachedi, K.; Volatron, F. *J Mol Struct (Theochem)* 2006, 762, 109; (e) Randaccio, L.; Geremia, S.; Nardino, G.; Wuerges, J. *Coord Chem Rev* 2006, 250, 1332; (f) Sergienko, V. S. *Crystallogr Rep* 2004, 49, 907.
3. (a) Banerjee, D.; Basolo, F.; Pearson, R. G. *J Am Chem Soc* 1957, 79, 4055; (b) Basolo, F.; Gray, H. B.; Pearson, R. G. *J Am Chem Soc* 1960, 82, 4200; (c) Gosling, R.; Tobe, M. L. *Inorg Chem* 1983, 22, 1235; (d) Wendt, O. F.; Elding, L. I. *Inorg Chem* 1997, 36, 6028; (e) Wendt, O. F.; Elding, L. I. *J Chem Soc Dalton Trans* 1997, 4725; (f) Kuznik, N.; Wendt, O. F. *J Chem Soc Dalton Trans* 2002, 15, 3074; (g) Otto, S.; Elding, L. I. *J Chem Soc Dalton Trans* 2002, 11, 2354.
4. (a) Melnik, M.; Holloway, C. E. *Coord Chem Rev* 2006, 250, 2261; (b) Dedieu, A. *Chem Rev* 2000, 100, 543; (c) Wong, E.; Giandomenico, C. M. *Chem Rev* 1999, 99, 2451; (d) Fuertes, M. A.; Alonso, C.; Perez, J. M. *Chem Rev* 2003, 103, 645; (e) Jamieson, E. R.; Lippard, S. J. *Chem Rev* 1999, 99, 2467; (f) Hush, N. S.; Schamberger, J.; Bacskaý, G. B. *Coord Chem Rev* 2005, 249, 299.
5. (a) Basch, H.; Krauss, M.; Stevens, W. J.; Cohen, D. *Inorg Chem* 1985, 24, 3313; (b) Carloni, P.; Andreoni, W.; Hutter, J.; Curioni, A.; Giannozzi, P.; Parrinello, M. *Chem Phys Lett* 1995, 234, 50; (c) Wysokinski, R.; Michalska, D. *J Comput Chem* 2001, 22, 901; (d) Deubel, D. V. *J Am Chem Soc* 2004, 126, 5999; (e) Michalska, D.; Wisokinski, R. *Chem Phys Lett* 2005, 403, 211.
6. Chval, Z.; Sip, M. *J Mol Struct (Theochem)* 2000, 532, 59.
7. Pavankumar, P. N. V.; Seetharamulu, P.; Yao, S.; Saxe, J. D.; Reddy, D. G.; Hausheer, F. H. *J Comput Chem* 1999, 20, 365.
8. Burda, J. V.; Leszczynski, J. *Inorg Chem* 2003, 42, 7162.
9. Burda, J. V.; Zeizinger, M.; Leszczynski, J. *J Comput Chem* 2005, 26, 907.
10. Burda, J. V.; Zeizinger, M.; Sponer, J.; Leszczynski, J. *J Chem Phys* 2000, 113, 2224.
11. Zeizinger, M.; Burda, J. V.; Leszczynski, J. *Phys Chem Chem Phys* 2004, 6, 3585.
12. Lopes, J. F.; Menezes, V. S. D.; Duarte, H. A.; Rocha, W. R.; De Almeida, W. B.; Dos Santos, H. F. *J Phys Chem B* 2006, 110, 12047.
13. Deubel, D. V. *J Am Chem Soc* 2002, 124, 5834.
14. Lau, J. K.-C.; Deubel, D. V. *J Chem Theory Comput* 2006, 2, 103.
15. Chval, Z.; Sip, M. *Collect Czech Chem Commun* 2003, 68, 1105.
16. Costa, L. A. S.; Hambley, T. W.; Rocha, W. R.; De Almeida, W. B.; Dos Santos, H. F. *Int J Quantum Chem* 2006, 106, 2129.
17. Costa, L. A. S.; Rocha, W. R.; De Almeida, W. B.; Dos Santos, H. F. *J Chem Phys* 2003, 118, 10584.
18. Raber, J.; Zhu, C. B.; Eriksson, L. A. *J Phys Chem B* 2005, 109, 11006.
19. Zhang, Y.; Guo, Z. J.; You, X. Z. *J Am Chem Soc* 2001, 123, 9378.
20. Baik, M. H.; Friesner, R. A.; Lippard, S. J. *J Am Chem Soc* 2003, 125, 14082.
21. Deubel, D. V. *J Am Chem Soc* 2006, 128, 1654.
22. Mantri, Y.; Lippard, S. J.; Baik, M. H. *J Am Chem Soc* 2007, 129, 5023.
23. Cooper, J.; Ziegler, T. *Inorg Chem* 2002, 41, 6614.
24. Lau, J. K.-C.; Deubel, D. V. *Chem Eur J* 2005, 11, 2849.
25. Zhu, J.; Lin, Z. Y.; Marder, T. B. *Inorg Chem* 2005, 44, 9384.
26. Braunschweig, H.; Brenner, P.; Müller, A.; Radacki, K.; Rais, D.; Uttinger, K. *Chem Eur J* 2007, 13, 7171.
27. Lin, Z. Y.; Hall, M. B. *Inorg Chem* 1991, 30, 646.
28. Gaussian 03, Revision C. 02, Frisch, M. J.; Trucks, G. W.; Schlegel, H. B.; Scuseria, G. E.; Robb, M. A.; Cheeseman, J. R.; Montgomery, J. A., Jr.; Vreven, T.; Kudin, K. N.; Burant, J. C.; Millam, J. M.; Iyengar, S. S.; Tomasi, J.; Barone, V.; Mennucci, B.; Cossi, M.; Scalmani, G.; Rega, N.; Petersson, G. A.; Nakatsuji, H.; Hada, M.; Ehara, M.; Toyota, K.; Fukuda, R.; Hasegawa, J.; Ishida, M.; Nakajima, T.; Honda, Y.; Kitao, O.; Nakai, H.; Klene, M.; Li, X.; Knox, J. E.; Hratchian, H. P.; Cross, J. B.; Adamo, C.; Jaramillo, J.; Gomperts, R.; Stratmann, R. E.; Yazyev, O.; Austin, A. J.; Cammi, R.; Pomelli, C.; Ochterski, J. W.; Ayala, P. Y.; Morokuma, K.; Voth, G. A.; Salvador, P.; Dannenberg, J. J.; Zakrzewski, V. G.; Dapprich, S.; Daniels, A. D.; Strain, M. C.; Farkas, O.; Malick, D. K.; Rabuck, A. D.; Raghavachari, K.; Foresman, J. B.; Ortiz, J. V.; Cui, Q.; Baboul, A. G.; Clifford, S.; Cioslowski, J.; Stefanov, B. B.; Liu, G.; Liashenko, A.; Piskorz, P.; Komaromi, I.; Martin, R. L.; Fox, D. J.; Keith, T.; Al-Laham, M. A.; Peng, C. Y.; Nanayakkara, A.; Challacombe, M.; Gill, P. M. W.; Johnson, B.; Chen, W.; Wong, M. W.; Gonzalez, C.; Pople, J. A. *Gaussian, Inc.: Pittsburgh PA*, 2003.
29. (a) Becke, A. D. *Phys Rev A* 1988, 38, 3098; (b) Vosko, S. H.; Wilk, L.; Nusair, M. *Can J Phys* 1980, 58, 1200; (c) Lee, C. T.; Yang, W. T.; Parr, R. G. *Phys Rev B* 1988, 37, 785; (d) Becke, A. D. *J Chem Phys* 1993, 98, 5648.
30. Andrae, D.; Haussermann, U.; Dolg, M.; Stoll, H.; Preuss, H. *Theor Chim Acta* 1990, 77, 123.
31. Reed, A. E.; Weinhold, F. *J Chem Phys* 1983, 78, 4066.
32. Weinhold, F.; Landis, C. R. *Chem Ed Res Pract (CERP; special "Structural Concepts" issue)* 2001, 2, 91.
33. Velde, G. T.; Bickelhaupt, F. M.; Baerends, E. J.; Guerra, C. F.; Van Gisbergen, S. J. A.; Snijders, J. G.; Ziegler, T. *J Comput Chem* 2001, 22, 931.
34. (a) Ziegler, T.; Rauk, A. *Theor Chim Acta* 1977, 46, 1; (b) Ziegler, T.; Rauk, A. *Inorg Chem* 1979, 18, 1558; (c) Ziegler, T.; Rauk, A. *Inorg Chem* 1979, 18, 1755.
35. (a) van Lenthe, E.; Baerends, E. J.; Snijders, J. G. *J Chem Phys* 1993, 99, 4597; (b) van Lenthe, E.; van Leeuwen, R.; Baerends, E. J.; Snijders, J. G. *Int J Quantum Chem* 1996, 57, 281.
36. Baik, M. H.; Friesner, R. A.; Lippard, S. J. *J Am Chem Soc* 2002, 124, 4495.
37. Kapoor, P. N.; Kakkar, R. *J Mol Struct (Theochem)* 2004, 679, 149.
38. Hofmann, A.; Jaganyi, D.; Munro, O. Q.; Liehr, G.; van Eldik, R. *Inorg Chem* 2003, 42, 1688.
39. Mrázek, J.; Burda, J. V. *J Chem Phys* 2006, 125, 194518.
40. Burda, J. V.; Sponer, J.; Hrabakova, J.; Zeizinger, M.; Leszczynski, J. *J Phys Chem B* 2003, 170, 5349.
41. Frenking, G.; Frohlich, N. *Chem Rev* 2000, 100, 717.
42. Albano, V. G.; Natile, G.; Panunzi, A. *Coord Chem Rev* 1994, 133, 67.
43. Albano, V. G.; Monari, M.; Orabona, I.; Ruffo, F.; Vitagliano, A. *Inorg Chim Acta* 1997, 265, 35.
44. Berges, J.; Caillet, J.; Langlet, J.; Kozelka, J. *Chem Phys Lett* 2001, 344, 573.
45. Naidoo, K. J.; Klatt, G.; Koch, K. R.; Robinson, D. J. *Inorg Chem* 2002, 41, 1845.
46. Burda, J. V.; Zeizinger, M.; Leszczynski, J. *J Chem Phys* 2004, 120, 1253.

Cisplatin Interaction with Cysteine and Methionine in Aqueous Solution: Computational DFT/PCM Study

Tomáš Zimmermann,[†] Zdeněk Chval,[‡] and Jaroslav V. Burda^{*,†}

Department of Chemical Physics and Optics, Faculty of Mathematics and Physics, Charles University, Ke Karlovu 3, 121 16 Prague 2, Czech Republic, and Department of Biophysics, Faculty of Health and Social Studies, University of South Bohemia, J. Boreckeho 27, 370 11 Ceske Budejovice, Czech Republic

Received: August 27, 2008; Revised Manuscript Received: December 2, 2008

In this paper we explore cisplatin interactions with sulfur-containing amino acids in a polarizable continuum model. Two cisplatin hydrated complexes were considered as reactants (chloro complex, cis -[Pt(NH₃)₂Cl(H₂O)]⁺; hydroxo complex, cis -[Pt(NH₃)₂(OH)(H₂O)]⁺). We considered the following reaction mechanism: first step, substitution of the aqua ligand by amino acid; second step, dissociative chelate formation. For the optimized complex (at the B3LYP/6-31+G(d)/COSMO level), the energy profile was determined using the B3LYP/6-311++G(2df,2pd) level and two different PCM models—COSMO and UAKS/DPCM methods which were adapted for use on transition metal complexes. The results show thermodynamic preference for bonding by cysteine sulfur followed by the amino group nitrogen, methionine thioether sulfur, and carboxyl-group oxygen. Methionine slightly prefers the Pt–N(Met) coordination in the chloro complex, but in the hydroxo complex it prefers the Pt–S(Met) coordination. A similar trend follows from the bonding energies: BE(Pt–S(Cys)) = 80.8 kcal/mol and BE(Pt–N(Met)) = 76 kcal/mol. According to the experimental observations, the most stable structures found are κ^2 (S,N) chelates. In the case of methionine, the same thermodynamic stability is predicted also for the κ^2 (N,O) chelate. This differs from the gas-phase results, where κ^2 (S,N) and even κ^2 (S,O) were found to be more stable than κ^2 (N,O) complex.

Introduction

Cisplatin (*cis*-diamminedichloroplatinum(II)) is one of the most commonly used anticancer agents. It is administered intravenously, and on its way into the cell it can interact with blood proteins¹ and other macromolecules. Inside the cellular environment with a significantly lower chloride concentration cisplatin undergoes hydrolysis, which leads to the formation of more reactive positively charged aqua complexes. These complexes can further interact with a wide spectrum of biomolecules including RNA, DNA, cellular proteins, peptides, and others.² A crucial step in the cisplatin antitumor activity is (most probably) formation of DNA–platinum bifunctional adducts. The most preferred platinum DNA binding sites are the N7 positions of guanine nucleobases. Cisplatin isomer—*trans*-diamminedichloroplatinum(II)—is inactive. This could be attributed to the fact that due to the 180° angle between the leaving groups *trans*-platin forms different adducts with DNA. In particular, unlike cisplatin, it is unable to create a bridge between two adjacent guanine bases.^{3,4}

Cisplatin and its hydrated products interact with proteins either by direct interaction⁵ or by protein recognition of platinum–DNA adducts.^{4,6–11} One of the most frequently studied platinum binding sites of proteins are sulfur atoms of cysteine or methionine residues.³ In both residues sulfur atom is present in different chemical contexts. In cysteine, sulfur belongs to the terminal thiol group, which is capable of deprotonation. At physiological pH some fraction is due to its pK_a (8.3) present in the anionic deprotonated form. In methio-

nine, sulfur is present as thioether with slightly positive partial charge. As will be shown in this work, this difference is a crucial factor that affects the behavior of both amino acids toward cisplatin.

One of the most abundant molecules containing cysteine is glutathione. Glutathione (GSH) is a cellular tripeptide which is inside the cell present in high (0.1–10 mM) concentrations.¹² It has various functions; most notably it serves as a thiol–disulfide redox buffer of the cell,¹³ protects from oxidative stress, participates in detoxification mechanism, and takes part in leukotriene synthesis. The platinum–glutathione complex represents a major cisplatin metabolite which accounts for approximately 60% of the intracellular platinum.¹⁴ Several cisplatin–glutathione structures were reported, including dinuclear Pt₂S₂ complexes or κ^2 (S,N) chelates.¹⁵ It was shown that these adducts irreversibly inhibit thioredoxin, glutaredoxin, and thioredoxin reductase enzyme,^{16,17} and in this manner worsens the ability of the cell to resist oxidative stress. Moreover, metabolism of the cisplatin–glutathione adduct in proximal tubule cells contributes to a strong cisplatin nephrotoxicity. In the respective metabolic pathway, the cisplatin–glutathione adduct is first cleaved by γ -glutamyl transpeptidase and aminopeptidase to yield cysteine κ (S) monodentate platinum complex, which is further cleaved in the reaction catalyzed by cysteine–S-conjugate β -lyase.^{18,19} Reactive thiol species which are final products of this pathway bind to the macromolecules, triggering an increase of the free cytosolic calcium and finally the cell death. Interestingly, glutathione adduct of a cisplatin non-nephrotoxic analogue carboplatin is probably not metabolized through this pathway.¹⁹ On the other hand, glutathione is also a vital part of cisplatin detoxification mechanism and ATP-dependent GS–Pt efflux is supposed to contribute to its elimination from the cell.¹⁴ Suppression of GSH synthesis can

* To whom correspondence should be addressed. Phone: +420 221 911 246. Fax: +420 221 911 249. E-mail: burda@karlov.mff.cuni.cz.

[†] Charles University.

[‡] University of South Bohemia.

even revert cisplatin resistance.^{20,21} Other thiol group containing molecules which in vivo interact with cisplatin are cysteine itself and various proteins. The interaction with cysteine residues of many proteins probably contributes to the cisplatin side effects.²²

With methionine, cisplatin forms various monodentate and bidentate compounds, mainly *cis*-[Pt(NH₃)₂Met-(S,N)]^{1+/2+} chelates.^{23,24} In strongly acidic conditions (pH < 0.5) initial formation of *cis*-[Pt(NH₃)₂Met-(S,O)]²⁺ was observed, which was subsequently slowly replaced by a more stable *cis*-[Pt(NH₃)₂Met-(S,N)]²⁺ complex.²⁵ [Pt(Met-(S,N))₂] bischelates were also observed in the urine of patients treated with cisplatin.^{26,27} In the competitive experimental studies was shown that platinum and the thioether group of methionine forms a weaker bond than platinum and the thiol and even displacement of κ^2 (S,N) chelated methionine from a model platinum complex by GSH was observed.²⁶ Similar result was obtained in a competition study of thioether glutathione analogue GSMe with 5-GMP. The platinum bond to N7 of 5-GMP was found to be more stable than the platinum–thioether bond in Pt(dien)–GSMe, and prior formation of Pt–S bonds even accelerated the Pt–GMP coordination.²⁸ Nevertheless, in reaction with macromolecular DNA oligomers, the methionine presence inhibits Pt–DNA binding.²⁹ The interaction with methionine-containing peptides can, similarly to the cysteine case, lead to a disruption of their function, and even hydrolytic cleavage of methionine-containing peptides mediated by cisplatin was reported in recent works.^{30,31} During a reaction with both cysteine and methionine, the release of ammonia was observed, which is faster for cysteine.^{15,23,25,32} Strong sulfur trans effect and trans influence can contribute to the ammonia release,^{33,34} and this mechanism can possibly lead to cisplatin inactivation.³³

The kinetics of cisplatin bonding to S-donor atoms of glutathione, cysteine, and methionine is experimentally relatively well-documented,^{32,35–39} and computational study on this theme was published recently.⁴⁰ On the other hand, knowledge of equilibrium thermodynamics of these interactions is mediated mainly through the competitive studies performed on model systems. In this work we used the methods of computational chemistry to obtain information about thermodynamics of bonding of cisplatin aquation products to free cysteine and methionine, which can be hardly accessible by other methods.

Many other computational works were devoted to the study of the Pt(II) interaction in bioenvironment. A recent work studying the influence of GC base pairing on the Pt complexes was published,⁴¹ where the possibility of the interbase proton transfer from G to C is discussed. The structural and spectroscopic data for novel platinum-based anticancer drugs are discussed by Dal Peraro⁴² using Carr-Parinello molecular dynamics (CPMD) and hybrid molecular mechanics/CPMD techniques. The calculation of the Pt(II) adduct with thiazole was performed by Chang.⁴³ Dos Santos et al.⁴⁴ have studied the structure and properties of a anhydrotetracycline–platinum(II) complex. These authors also dealt with the description of cisplatin in explicit water solution using the Monte Carlo method⁴⁵ and the interaction of cisplatin with guanine.⁴⁶ Robertazzi et al. have carried out the QM/MM calculations of the cisplatin adduct with an octamer of double-stranded DNA sequence.^{47–49} Wysokinski has investigated characterization of the structural and vibrational spectra of (orotato)platinum(II) complex.⁵⁰ He has compared the calculated (DFT/mPW1PW91) vibration transitions with experimental data. Some novel trans-platinum(II) anticancer drugs (with aliphatic amines) were studied at the B3LYP level,⁵¹ where also the aquation process was examined. Recently also dinuclear⁵² and trinuclear⁵³

(BBR3464) platinum(II) complexes were studied using the computational approach. Aquation study of carboplatin was performed by Pavelka,⁵⁴ where a relatively high activation barrier of 30 kcal/mol was suggested on the basis of the B3LYP/6-31++G(2df,2pd) computational level. Discussion about correlation between thermodynamic and kinetic data and theoretical calculations of the Pt(II) complexes was published by Hofmann et al.⁵⁵ A lot of studies on behavior and properties of the platinum complexes were published by Ziegler and co-workers.⁵⁶ In one of these studies the activation of methane by [PtCl₄]²⁻ was examined in the acidic aqueous solution. The authors have shown that the complex with two water molecules is the most active in the H/D exchange reaction.⁵⁷ Some aspects of the cisplatin hydrolysis are discussed by Tsipis.⁵⁸ Some other recent studies on the interaction of Pt(II) complexes should be also mentioned.^{25,59–63}

In this work we focus our attention on the interaction of hydrated cisplatin with the sulfur-containing amino acids methionine and cysteine since both are important in vivo cisplatin targets. Taking into account the HSAB principle,⁶⁴ a strong platinum affinity to the sulfur sites could be expected.

Computational Details

In our previous work we have explored the cisplatin interactions with sulfur-containing amino acids in the gas-phase model.³⁴ We chose the DFT/B3LYP computational level and compared it with several other methods (including the CCSD(T)) on model system *cis*-[Pt(NH₃)₂(H₂S)(OH)]⁺. In the present work we use the DFT/B3LYP method for both geometry optimizations and single-point calculations. Combination of the B3LYP functional method with the COSMO solvation model was successfully used in the study comparing the relative stability of cis and trans cisplatin isomers.⁶⁵ On the other hand, in the study,⁶⁶ where several computational methods were compared with experimental geometric parameters and vibrational frequencies of cisplatin and carboplatin, the mPW1PW functional was suggested as the best computational tool for these systems. However, the differences in calculated geometric parameters between the B3LYP and mPW1PW functionals were small. Moreover in our previous study, the B3LYP functional reproduced the CCSD(T) bonding energy of the Pt–S bond significantly better than mPW1PW.

The Stuttgart-Dresden quasi-relativistic energy-averaged pseudopotentials were used to describe core electrons of platinum (MWB-60⁶⁷), chlorine, and sulfur (MWB-10⁶⁸). The 6-31+G* basis set was chosen, and the original pseudoorbitals of Pt, Cl, and S atoms were augmented by appropriate diffuse and polarization functions ($\alpha_f(\text{Pt}) = 0.980$, $\alpha_d(\text{Cl}) = 0.618$, and $\alpha_d(\text{S}) = 0.498$).⁶⁹ For the single-point (SP) calculations the triple- ζ 6-311++G(2df,2pd) basis set was used with pseudoorbitals of heavy elements augmented by the same diffuse functions and the following set of polarization functions: $\alpha_{f1}(\text{Pt}) = 1.419$, $\alpha_{f2}(\text{Pt}) = 0.466$, $\alpha_g(\text{Pt}) = 1.208$; $\alpha_{d1}(\text{Cl}) = 1.500$, $\alpha_{d2}(\text{Cl}) = 0.375$, $\alpha_f(\text{Cl}) = 0.700$; $\alpha_{d1}(\text{S}) = 0.918$, $\alpha_{d2}(\text{S}) = 0.289$, and $\alpha_f(\text{S}) = 0.568$.⁶⁹

To include the effects of water as a high-permittivity solvent, we utilized the SCRF computational framework. Geometry optimizations were performed using the COSMO method with sphere radii proposed by Klamt.⁷⁰ In SP calculations two implicit solvation models were applied: (a) the COSMO method as specified above and (b) the DPCM model^{71,72} with modified UAKS cavities.⁷³ In the latter case, the polarization charges were compensated by means of an additional effective charge distributed according to the solute electronic density (ICOMP

= 4 keyword in Gaussian 03 program). It should be mentioned that the study⁷³ introduces the UAHF model optimized for the HF/6-31G* level of theory and not the UAKS model, which is optimized for the PBE0/6-31G(d) level. But the only difference between both (in our case) consists of the sphere radii of sp₂ hybridized oxygen. Since UAKS cavities were not optimized for the transition metal complexes, small modifications were necessary to appropriately describe solvation of platinum complexes. Sphere radii in ref 73 were calculated considering the atom type, number of bonded hydrogens, hybridization, atomic charge and effects of neighboring groups. The originally used atomic charge is a formal charge carried by atoms in ions or zwitterions (for example oxygens of the deprotonated carboxyl group both possess formal charge $-1/2$). For groups of platinum complexes this model due to the lack of the parametrization assigns charges which are equal to the total charge of the complex divided by the number of groups. Instead we attempted to assign formal partial charges of platinum ligands in a manner similar to UAKS of organic molecules. This approximation appeared to be too crude. Therefore, more realistic NPA partial charges from the COSMO single-point calculations were applied instead of the formal charges. However, NPA partial charges cannot be used directly in the UAKS model since it is parametrized using formal charges (the original atomic radii, beside other criteria, reflects the (semi-)integer charge localized on the atom, e.g., for sulfur: $R_S = 1.980 + fn$, where n is the formal charge and f is some fitted factor ($f(S) = 0.3$)). Therefore we have introduced a scaling procedure for NPA partial charges of platinum ligands (containing sulfur, chlorine, nitrogen, and oxygen) based on the actual NPA charges of reference molecules, which were used or were similar to molecules used for parameterization of the original model. [For instance, sulfur atom bonded to platinum has a charge from the range between the neutral CH₃SH ($n = 0$) and the anion CH₃S⁻ ($n = -1$) states. In the scaling procedure, the NPA charge of S atom from the Pt complex (with cysteine or methionine) was determined first, then projected into the range of NPA charges of sulfur in CH₃SH and CH₃S⁻ particles, and linearly rescaled into the $-1 - 0$ range of formal charges. This procedure gives a better estimation for n in R_S parametrization when compared to the original article.⁷³] The performance of this modification of the UAKS model was verified by means of comparison with experimental pK_a values of the *cis*-[Pt(NH₃)₂(H₂O)₂]²⁺, *cis*-[Pt(NH₃)₂(OH)(H₂O)]⁺, and *cis*-[Pt(NH₃)₂Cl(H₂O)]⁺ complexes. The details of the procedure together with the comparison with other methods and experimental values can be found in the article.⁷⁴ Superior performance of the original DPCM/UAHF method in this type of calculation was also observed by da Silva et al.⁷⁵ in calculations of pK_a of nitrous acid.

Calculating the thermochemical data, we have found that although all the structures were properly optimized using standard convergence criteria, some vibrational spectra (even after subsequent optimization attempts) still contained very low imaginary frequencies. This is the most probably due to the numerical instability of PCM method caused by a discretization of a cavity surface. Therefore in determination of the Gibbs free energies, the vibrational analyses were taken from gas-phase (reoptimized) calculations at the HF/6-31+G* level of theory. The average gas phase – solvent difference of thermal corrections to the Gibbs free energy determined for all molecules, where the solvent vibrational spectrum without imaginary frequencies was obtained, is 9.4 kcal/mol (thermal corrections to Gibbs free energy taken from solvated molecules are always

lower). This averaged difference correlates well with the number of degrees of freedom of a particular molecule with an average value of 0.14 kcal/mol per degree of freedom (neglecting error in rotational frequencies) and variance of 0.017 kcal/mol (average absolute deviation is only 10% of the mean). Thus, the probable error introduced to the reaction Gibbs free energies by using the HF gas-phase frequencies instead of the COSMO frequencies is approximately 1.5 kcal/mol (deviations in reactants and products are taken as mutually uncorrelated). The true COSMO frequencies were used in two cases (where no imaginary eigenvalues occurred): First, in a detailed discussion of solvent influence on properties of both *cis*-[Pt(NH₃)₂Cl(H₂O)]⁺ and *cis*-[Pt(NH₃)₂(H₂O)(OH)]⁺ reactant complexes. Second, in the discussion of the relative stability of κ²(S,N) methionine chelates, where higher accuracy is needed in comparison of subtle energy differences of various nearly degenerated conformers, which were observed in the NMR measurements.

Another source of error arises from the fact that in a solvent a mixture of several geometric conformers of a same complex is usually present. The ratio of their concentrations is determined by the Maxwell–Boltzmann statistics. In our calculations, only global minima are, however, used. This error affects more results obtained within supermolecular approach, because of the higher number of conformations available for weakly bound supermolecules. Structures of global minima were obtained from several (usually above 10) local minima examined at the B3LYP/6-31+G* level. Usually, for both reactant and product four to five other structures were within 2–3 kcal/mol from a global minimum. Therefore, large cancelation of errors can be expected on the basis of this similarity. To estimate the error numerically, we consider a reaction where reactant can take only one conformation, whereas product can take either one conformation or 10 degenerated but distinguishable conformations. Standard reaction Gibbs free energy in the first case is equal to

$$\Delta G_1 = -RT \ln(K_1) = -RT \ln\left(\frac{Q_p}{Q_r}\right) \quad (1)$$

where Q_r and Q_p are partition functions of reactant and of the product. In the second case 10 times more states are accessible to the product, so the standard reaction free energy is

$$\Delta G_2 = -RT \ln(K_2) = -RT \ln\left(\frac{10Q_p}{Q_r}\right) = \Delta G_1 - RT \ln(10) \quad (2)$$

The error caused by neglecting nine conformers of product at 298.15 K is therefore equal to 1.36 kcal/mol. If that nine conformers had higher formation Gibbs free energies than the global minimum, their contribution to the partition function would be exponentially suppressed and the error greatly reduced. For example if all nine conformers had 1 kcal/mol higher formation Gibbs free energy, then the error caused by neglecting them would be only 0.35 kcal/mol. From this and aforementioned large cancelation of errors between reactant and products, it can be expected that the error caused by neglecting all local minima is safely well beyond 0.5 kcal/mol.

Three energy characteristics were calculated in the COSMO approach to investigate a weak association of the monomers in supermolecules: (a) association energy without the deformation energy

$$\Delta E_S^{\text{af}} = E_{\text{supermol}}^{\text{el}} + G_{\text{supermol}}^{\text{sol}} - \sum_m^{\text{monomers}} (E_m^{\text{el}} + G_m^{\text{sol}}) \quad (3)$$

where G^{sol} represents electrostatic, cavitation, dispersion, and repulsion solvation free energy terms calculated in the SCRf framework. Monomer energies are calculated in the frozen supermolecular geometry. Subscript S denotes that both supermolecule and monomers were surrounded by the solvent. Adding the G^{sol} terms to E^{el} actually creates a mixed quantity, which does not have a direct thermodynamic sense (it is neither the Gibbs free energy nor energy since it does contain part of the work necessary to introduce the molecule into the dielectric). But it is useful in this context, and in our model it also has a convenient property of temperature independence.

(b) association energy with deformation corrections

$$\Delta E_S^{\text{a}} = \Delta E_S^{\text{af}} + \sum_m^{\text{monomers}} \Delta E_m^{\text{deform}} \quad (4)$$

(c) association Gibbs free energy (ΔG_S^{a}) by adding thermodynamic quantities of nuclear motion to association energy.

The bonding energies (BE) of the Pt–L bonds (calculated for isolated Pt complexes) are determined according to eq 3 where instead of monomers two fragments partitioned according to the corresponding Pt–L bond were regarded.

To correct for the basis set superposition error,^{76,77} the electronic energies of separated molecules were calculated using a complete set of basis functions of all atoms present in the supermolecule. Two counterpoise-like procedures were employed. In the first one, energies of fragments enclosed in appropriate cavities were calculated in the basis set of a complete supermolecule with the ghost atoms placed mainly outside the fragment cavity. Unfortunately this leads to the incorrect values of solute–solvent energies of nonelectrostatic origin (at least in our version of Gaussian03 Rev.C2). Nevertheless these energies can be taken from calculations of, e.g., the deformation energy corrections where an isolated monomer without ghost atoms must be employed. In the second approach to the BSSE corrections, a sum of differences of monomer electronic energies computed in the basis set of the supermolecule (with ghost atoms) and in the basis set of the monomer (without ghost atoms) was determined where both energies were calculated in the cavity of the supermolecule. This BSSE correction was added to the association energy computed as a simple difference of electronic energy of a supermolecule and sum of electronic energies of monomers without ghost atoms. Both methods are illustrated in Figure 1.

The average absolute BSSE correction in the whole set of calculated complexes is 0.93 kcal/mol (using the first method), and the average absolute difference between both methods is 0.09 kcal/mol. The largest difference between both BSSE approaches is 0.5 kcal/mol in the case of strongly bonded Pt(II) and –1 charged cysteine, where the bonding energy is 127.6 kcal/mol and the BSSE correction using the first method is 1.6 kcal/mol. The estimation of BSSE corrections using the first approach is used in further discussion.

Partial charges analysis was done using the natural bond orbitals program NBO v. 5.0⁷⁸ at the B3LYP/6-311++G(2df,2pd) level of theory in the COSMO solvation model.

Results and Discussion

The two most important cisplatin hydrolysis products *cis*-[Pt(NH₃)₂Cl(H₂O)]⁺ and *cis*-[Pt(NH₃)₂(OH)(H₂O)]⁺ were chosen

as mono- and dihydrated reactants. The studied reaction mechanism leading to formation of chelate product through a monodentate intermediate was studied in the model of isolated molecules and in the supermolecular model where reactants and products form the associated complex. In the first reaction step (the least firmly) bound aqua ligand of the hydrated cisplatin cation is replaced by the amino acid. Preference of the aqua ligand is also suggested by results of numerous experimental studies, e.g., in refs 32 and 79. All three possible active sites (S, N, and O atoms) of the amino acid were considered for the formation of dative bonds with the platinum atom. In the second step, one of the two remaining free active sites of the amino acid further replaces the second Pt–ligand (either chloride or hydroxyl group) forming the chelate structure. Other possible reaction paths (e.g., replacement of the NH₃ ligands) were not considered, although these species were also observed in the reaction of methionine with nonhydrated cisplatin²³ with more labile leaving ligands such as aqua in *cis*-[Pt(NH₃)₂(H₂O)₂]²⁺. Nevertheless, these structures were not observed in significant quantities.¹⁵ Since the reactions take place in an aqueous solution, a rapid establishment of equilibrium with respect to the proton-transfer reactions is assumed. All possible internal proton transfers were taken into account. Generalization of this approach to the case where protons are exchanged also with solvent will be the subject of our subsequent study.

Structures. Structures of the most stable conformers discussed in the study are presented in Figures 2–4. In contrast to the gas-phase calculations, solvation introduces several structural changes. When solvated, amino acids adopt zwitterionic structure. The calculated cysteine structure can be compared to the global minimum found in the computational study devoted to the solvation of cysteine.⁸⁰ The accordance is qualitative and the main reason of the quantitative disagreement can be seen in fact that, in the Fernandez-Ramos' study,⁸⁰ the Onsager solvation model was used for geometry optimization. In the platinum chloro complex, solvation leads to weakening of the Pt–Cl bond accompanied by bond elongation by approximately 0.06 Å and a 40 cm^{–1} red shift of the bond stretch frequency to 309 cm^{–1}. Also, the NPA negative charge of chlorine increases by 0.14 e. Other coordination distances are consequently shortened, most notably the platinum–ammine ligand in the trans position to Cl[–] anion is shortened by 0.06 Å. Its stretch frequency is shifted up by approximately 50 cm^{–1} due to the weakening of chlorine trans influence. Also the Pt–O bond in the hydroxo complex is lengthened by approximately 0.04 Å accompanied with a bond stretch frequency shift down by 50 cm^{–1} to 548 cm^{–1}. The NPA negative charge of the oxygen atom is increased by approximately 0.05 e. In analogy with the chloro complex the trans Pt–NH₃ bond is shortened by approximately 0.04 Å with the frequency shifted up by approximately 40 cm^{–1}.

Although charged systems do not have an invariant dipole moment under translation, keeping the origin of the coordinate system in the center of the mass of structures, some interesting features can be shown. In both complexes, the changes related to the solvation lead to an increase of the molecular dipole moment by approximately a half—to 11.1 (chloro complex) and 8.9 D (hydroxo complex). As for amino acids; an increase of the dipole moment is further enhanced by adoption of the zwitterionic structure; the solution values are 2.5 (cysteine) and 3 (methionine) times higher than the gas-phase ones. This trend is conserved in all first- and second-step products, and the average dipole moment of solvated molecules is approximately 2.5 times larger than in the gas phase.

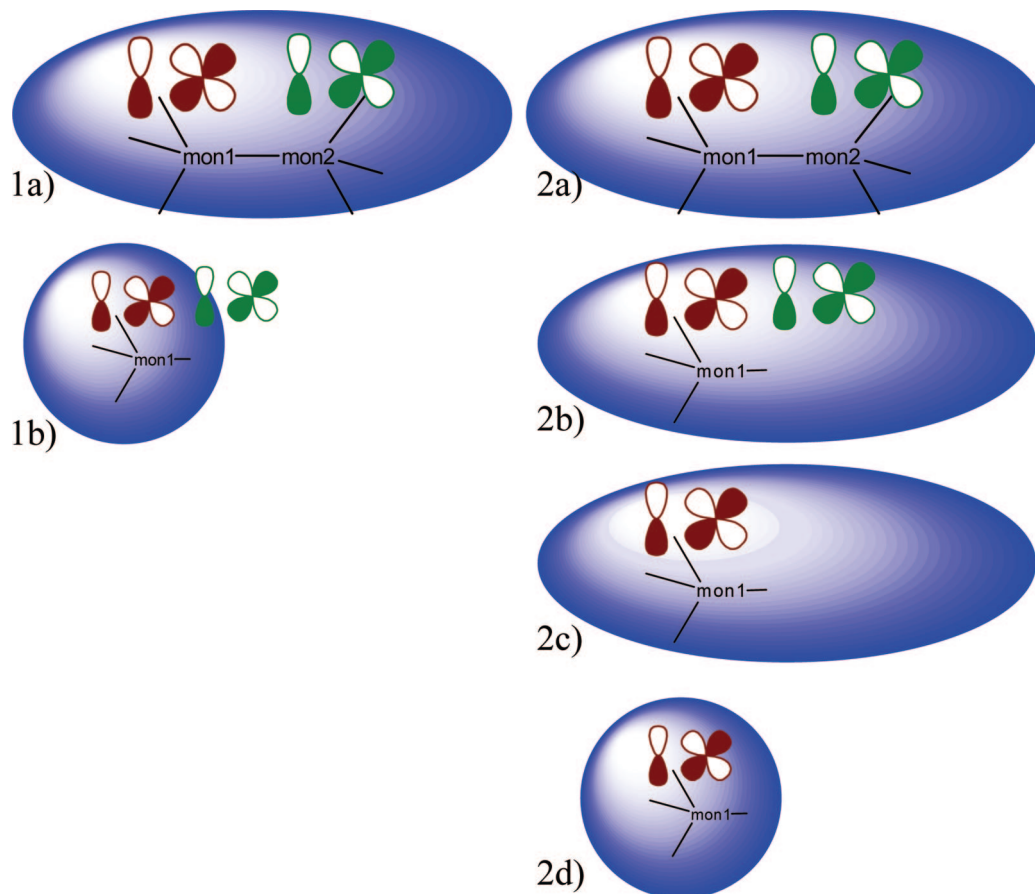


Figure 1. Counterpoise-like BSSE calculations. In the first method, $\Delta E_{\text{S}}^{\text{cf}}$ is calculated as a difference between the energy of supermolecule 1a and a sum of fragment energies calculated in supermolecular basis set using fragment cavities 1b. In the second approach, $\Delta E_{\text{S}}^{\text{cf}} - E^{\text{BSSE}}$ is calculated as a difference between the energy of supermolecule 2a and a sum of fragment energies calculated in the fragment basis set using fragment cavities 2b. E^{BSSE} is calculated as a sum of differences of fragment energies calculated in supermolecular 2b and fragment 2c basis sets both in the supermolecular cavity.

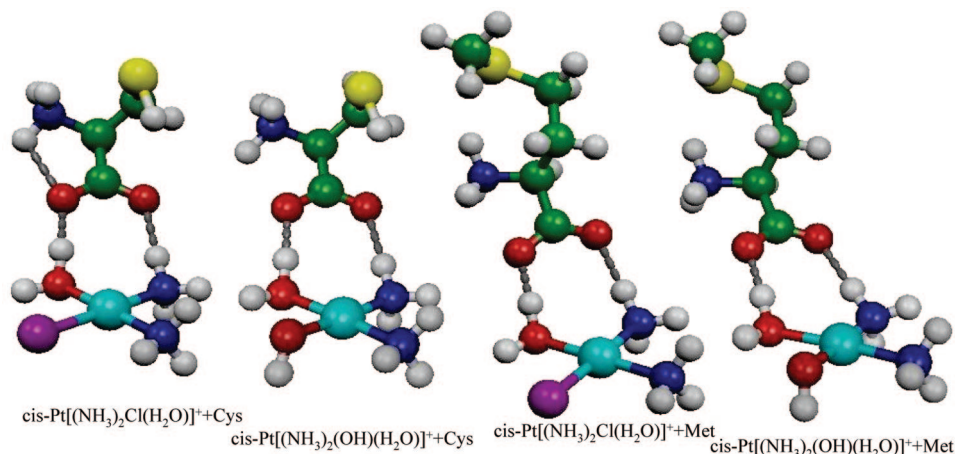


Figure 2. First-step reactants in the supermolecular approach.

In the products of the first reaction step, the aqua ligand is substituted by the amino acid donor atom. The most stable supermolecular structures are displayed in Figure 2. The coordination distances of the platinum atom are presented in Table 1. Partial charges of platinum and its ligands are summarized in Table 2.

The sulfur coordination is accompanied by a charge transfer from the sulfur to platinum atom whose partial charge is decreased by approximately 0.17 e. This value is similar for both cysteine and methionine, suggesting that the extent of electron donation is comparable for both amino acids. The main

difference between the thiol and thioether dative bonds lies in the different ionic character of both bonds. Whereas the positive partial charge of methionine sulfur is increased during the bond formation by 0.28 to 0.48 e, the partial charge of cysteine sulfur is decreased by +0.25 to -0.28 e due to additional proton transfer from very acidic platinum-bonded sulfur to carboxyl oxygen. This way, the Pt–S bond in cysteine complexes gains significantly more ionic character. This fact can be demonstrated also on the example of two point charges (using the NBO charges of platinum and sulfur atoms of cysteine or methionine) in the optimized bond distances. The gas-phase difference of

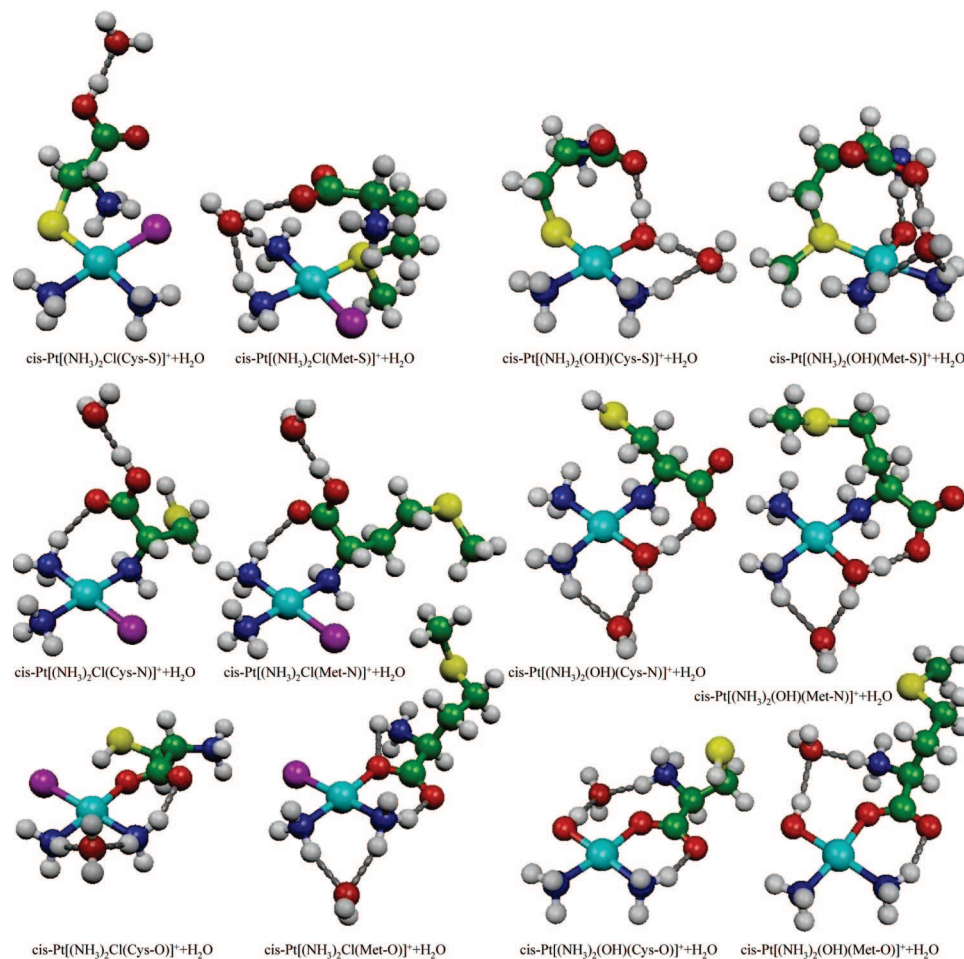


Figure 3. First-step products in the supermolecular approach.

electrostatic energies of point charges representing cysteine and methionine complexes is approximately 50 kcal/mol, which is very similar to the difference of the gas-phase bonding energies calculated in our previous paper.³⁴ The Pt–S bond length of 2.35 Å is unaffected by the solvent and is practically independent of the complex type. A similar insensitivity of the Pt–S bond length on the type of the sulfur ligand can also be observed in the results of the study,⁸¹ where the *cis*-[Pt(NH₃)₃L]²⁺ complexes were explored (L is a small ligand containing either S, N, or O donor atoms). The Pt–S bond length obtained for all the complexes calculated in ref 81 was 2.32 Å, and the same value is also an average of the Pt–S distances found in the X-ray diffraction study of +2 charged platinum complex [Pt(tu)₄]Cl₂ (tu = thiourea).⁸² All these data give a fair confidence in our results. Previously mentioned internal proton transfer from platinum-bonded sulfur to carboxylic oxygen occurs only in chloro complexes, since in the hydroxo complex *cis*-[Pt(NH₃)₂(OH)(Cys-S)]⁺, the higher acidity of cysteine carboxylic group leads to a proton transfer to the platinum hydroxo ligand instead, so that the most stable structure is actually *cis*-[Pt(NH₃)₂(H₂O)(Cys-S)]⁺. This effect was not observed in the gas-phase calculations.

Nitrogen coordination causes only a slight decrease of the platinum charge by approximately 0.04 e (in comparison to the original reactant complexes), demonstrating a lower donation of the amino group compared to sulfur. The Pt–N bond length is approximately 2.1 Å, which is also the gas-phase value. The structures of chloro complexes (with both amino acids) are stabilized by internal hydrogen bonds between the platinum

ammine ligand and the carboxyl group of amino acid. The hydroxo complexes undergo an internal proton transfer from the carboxyl groups, transforming the hydroxo ligands into aqua ligands. The aqua ligand remains H-bonded to the carboxyl group (cf. Figure 3).

Coordination of oxygen does not affect the platinum partial charge. The Pt–O bond distance is 2.07 Å, which is approximately by 0.03 Å longer than in the corresponding gas-phase structures. In the chloro complexes, one of the ammine ligand forms a hydrogen bond with the carboxyl group, which is tilted by approximately 35° out of the platinum complex plane. In the hydroxo complexes a stronger hydrogen bond is formed between the hydroxo ligand and carboxyl group in the plane of the platinum complex.

In the second reaction step, the remaining leaving ligand (either chloride or (possibly protonated) hydroxide) is replaced by the second amino acid donor atom and the chelate structure is formed. The Pt–X distances (where X is a donor atom of amino acid) are usually shortened in comparison to monodentate complexes. This is most significant in the case of +1 e charged κ^2 (N,O) complexes where both Pt–N and Pt–O bonds are by 0.04 Å shorter than in the corresponding monodentate complexes. All the κ^2 (N,O) structures contain a rigid five-membered ring with the plane of the carboxyl group practically coplanar with the plane of the platinum ligands. The carboxyl group is protonated in the +2 complexes and deprotonated in the +1 e charged complexes (cf. structures in the middle part of Figure 4).

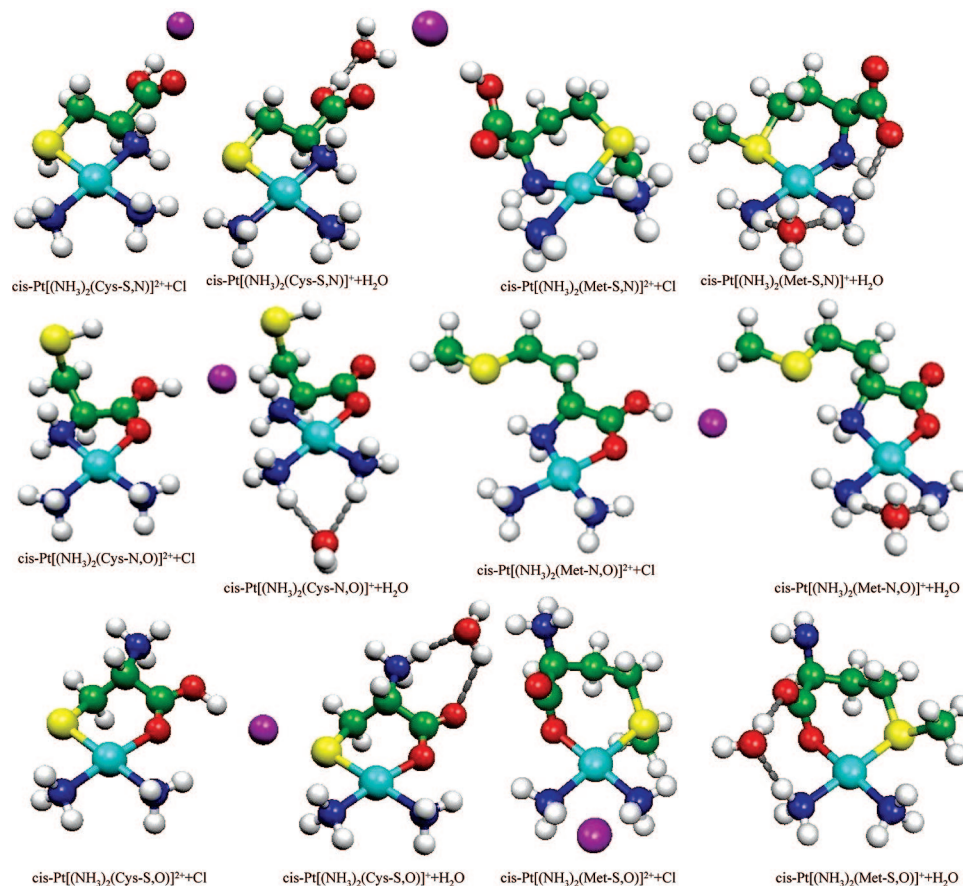


Figure 4. Second-step products in the supermolecular approach.

Regarding the $\kappa^2(\text{S,N})$ chelates, each amino acid adopts a different conformation. Since cysteine has a shorter side chain, the five-membered ring with the carboxyl group in equatorial position is formed in accord with the structure proposed for *S*-methyl-L-cysteine in the study of Appleton et al.²⁵ The most stable methionine (+2) $\kappa^2(\text{S,N})$ chelate is a six-membered ring in a chairlike conformation with both carboxy and *S*-methyl groups in axial positions. Slightly twisted boatlike conformation has approximately 1.3 kcal/mol higher energy. In the case of +1 charged chelates (the charge also depends on the pH of the surrounding solvent), practically the same energy was obtained for both conformers. The boatlike conformation is very slightly preferred (the difference is less than 0.2 kcal/mol) due to a stronger H-bond between the deprotonated carboxyl group and the platinum ammine ligand (in boatlike conformation H-bond is shorter and, also, the $\text{N}\cdots\text{H}-\text{O}$ bond is closer to 180°). This contrasts to the structure found in the X-ray diffraction study of *cis*-[Pt(Cl)₂(Met-S,N)],⁸³ where the chairlike conformation with equatorial carboxyl and *S*-methyl groups was observed. Subsequently in the NMR experimental study of cisplatin methionine chelate,¹⁵ the equatorial position of the carboxyl group is assumed. However, our calculations show that interaction with the ammine ligand stabilizes the carboxyl group in axial position. Similarly, the *S*-methyl group is stabilized in the axial position by interaction of the sulfur lone pair with hydrogen of the second ammine ligand. A difference in the Gibbs free energies between both *S*-methyl positions (corresponding to the *S* and *R* sulfur atom chiralities) is relatively small—approximately 0.5 kcal/mol for +1 chelate and 0.4 kcal/mol for +2 chelate (using the more accurate COSMO vibrational frequencies). At room temperature these differences represent a concentration ratio of 2.7:1 and 2:1, respectively. In the mentioned NMR

TABLE 1: Platinum Coordination Distances (\AA)^a

complex ^b	Pt-S	Pt-N(AA)	Pt-O	Pt-X	Pt-Nt	Pt-Nc
[Pt-a ₂ Cl(H ₂ O)] ⁺			2.11	2.36	2.03	2.07
[Pt-a ₂ (OH)(H ₂ O)] ⁺			2.10	2.01	2.03	2.09
[Pt-a ₂ Cl(Cys-S)] ⁺	2.35			2.38	2.12	2.07
[Pt-a ₂ Cl(Met-S)] ⁺	2.35			2.37	2.09	2.07
[Pt-a ₂ (OH)(Cys-S)] ⁺	2.35			2.10	2.12	2.04
[Pt-a ₂ (OH)(Met-S)] ⁺	2.34			2.03	2.08	2.08
[Pt-a ₂ Cl(Cys-N)] ⁺		2.09		2.36	2.07	2.07
[Pt-a ₂ Cl(Met-N)] ⁺		2.09		2.36	2.07	2.07
[Pt-a ₂ (OH)(Cys-N)] ⁺		2.10		2.08	2.07	2.05
[Pt-a ₂ (OH)(Met-N)] ⁺		2.10		2.07	2.07	2.05
[Pt-a ₂ Cl(Cys-O)] ⁺			2.07	2.37	2.05	2.07
[Pt-a ₂ Cl(Met-O)] ⁺			2.07	2.37	2.05	2.07
[Pt-a ₂ (OH)(Cys-O)] ⁺			2.07	2.01	2.04	2.09
[Pt-a ₂ (OH)(Met-O)] ⁺			2.07	2.01	2.04	2.09
[Pt-a ₂ (Cys-S,N)] ²⁺	2.33	2.08			2.09	2.07
[Pt-a ₂ (Cys-S,N)] ⁺	2.32	2.08			2.13	2.08
[Pt-a ₂ (Met-S,N)] ²⁺	2.34	2.08			2.09	2.08
[Pt-a ₂ (Met-S,N)] ⁺	2.35	2.08			2.09	2.09
[Pt-a ₂ (Cys-S,O)] ²⁺	2.33		2.08		2.12	2.04
[Pt-a ₂ (Cys-S,O)] ⁺	2.33		2.05		2.12	2.06
[Pt-a ₂ (Met-S,O)] ²⁺	2.35		2.05		2.08	2.06
[Pt-a ₂ (Met-S,O)] ⁺	2.36		2.04		2.08	2.07
[Pt-a ₂ (Cys-N,O)] ²⁺		2.08	2.07		2.07	2.04
[Pt-a ₂ (Cys-N,O)] ⁺		2.06	2.03		2.07	2.07
[Pt-a ₂ (Met-N,O)] ²⁺		2.08	2.07		2.07	2.04
[Pt-a ₂ (Met-N,O)] ⁺		2.06	2.03		2.07	2.07

^a AA means amino acid; X stands for either Cl or O (of hydroxo ligand); Nt refers to the ammine ligand in the trans position to the aqua ligand in reactant complexes, to the amino acid in the first-step products, to the sulfur atom in $\kappa^2(\text{S,N})$ and $\kappa^2(\text{S,O})$ chelate complexes, and to the nitrogen atom in $\kappa^2(\text{N,O})$ chelates; Nc refers to the remaining ammine ligand. ^b In all chemical formulas, a₂ means (NH₃)₂.

TABLE 2: NPA Partial Charges (e) from the COSMO Approach^a

complex ^c	Pt	S	X	N ^t	N ^c	N ^a	O ⁿ	O ^s
[Pt-a ₂ Cl(H ₂ O)] ⁺	0.67		-0.59	-0.89	-0.94			
[Pt-a ₂ (OH)(H ₂ O)] ⁺	0.75		-1.08	-0.90	-0.95			
cysteine		-0.03				-0.69	-0.80	-0.82
methionine		0.20				-0.71	-0.81	-0.83
[Pt-a ₂ Cl(Cys-S)] ⁺	0.49	-0.28	-0.59	-0.97	-0.92	-0.70	-0.65	-0.68
[Pt-a ₂ Cl(Met-S)] ⁺	0.48	0.49	-0.59	-0.95	-0.94	-0.69	-0.80	-0.81
[Pt-a ₂ (OH)(Cys-S)] ⁺	0.58	-0.28	-0.90 ^b	-0.98	-0.90	-0.68	-0.77	-0.85
[Pt-a ₂ (OH)(Met-S)] ⁺	0.59	0.47	-1.05	-0.95	-0.94	-0.74	-0.81	-0.82
[Pt-a ₂ Cl(Cys-N)] ⁺	0.62	-0.01	-0.60	-0.92	-0.94	-0.76	-0.66	-0.68
[Pt-a ₂ Cl(Met-N)] ⁺	0.62	0.20	-0.60	-0.93	-0.94	-0.75	-0.67	-0.68
[Pt-a ₂ (OH)(Cys-N)] ⁺	0.72	-0.05	-0.91 ^b	-0.93	-0.92	-0.77	-0.77	-0.82
[Pt-a ₂ (OH)(Met-N)] ⁺	0.72	0.18	-0.91 ^b	-0.93	-0.93	-0.77	-0.77	-0.82
[Pt-a ₂ Cl(Cys-O)] ⁺	0.67	-0.01	-0.61	-0.91	-0.94	-0.68	-0.74	-0.72
[Pt-a ₂ Cl(Met-O)] ⁺	0.67	0.20	-0.61	-0.91	-0.94	-0.70	-0.74	-0.73
[Pt-a ₂ (OH)(Cys-O)] ⁺	0.74	-0.02	-1.10	-0.91	-0.95	-0.68	-0.75	-0.73
[Pt-a ₂ (OH)(Met-O)] ⁺	0.74	0.19	-1.10	-0.91	-0.95	-0.70	-0.75	-0.73
[Pt-a ₂ (Cys-S,N)] ²⁺	0.56	0.30		-0.95	-0.93	-0.76	-0.64	-0.68
[Pt-a ₂ (Cys-S,N)] ⁺	0.52	-0.25		-0.98	-0.93	-0.76	-0.66	-0.69
[Pt-a ₂ (Met-S,N)] ²⁺	0.54	0.49		-0.96	-0.93	-0.76	-0.66	-0.68
[Pt-a ₂ (Met-S,N)] ⁺	0.54	0.48		-0.97	-0.94	-0.76	-0.84	-0.81
[Pt-a ₂ (Cys-S,O)] ²⁺	0.59	-0.23		-0.98	-0.89	-0.67	-0.62	-0.64
[Pt-a ₂ (Cys-S,O)] ⁺	0.57	-0.25		-0.98	-0.91	-0.67	-0.74	-0.74
[Pt-a ₂ (Met-S,O)] ²⁺	0.61	0.48		-0.95	-0.92	-0.67	-0.69	-0.76
[Pt-a ₂ (Met-S,O)] ⁺	0.60	0.47		-0.95	-0.92	-0.89	-0.71	-0.78
[Pt-a ₂ (Cys-N,O)] ²⁺	0.74	-0.01		-0.93	-0.90	-0.77	-0.62	-0.63
[Pt-a ₂ (Cys-N,O)] ⁺	0.72	-0.03		-0.94	-0.93	-0.77	-0.71	-0.74
[Pt-a ₂ (Met-N,O)] ²⁺	0.74	0.20		-0.93	-0.90	-0.79	-0.63	-0.63
[Pt-a ₂ (Met-N,O)] ⁺	0.71	0.19		-0.94	-0.93	-0.78	-0.72	-0.74

^a X stands for Cl or O (in hydroxo ligand); N^a is the nitrogen of the amino acid, Oⁿ the carbonyl oxygen and O^s the hydroxyl oxygen of the carboxyl group, N^t the nitrogen from the ammine ligand in the trans position to the aqua ligand in reactant complexes, to the amino acid in the first-step products, to the sulfur atom in κ^2 (S,N) and κ^2 (S,O) chelate complexes, and to the nitrogen atom in κ^2 (N,O) chelates; N^c refers to the nitrogen atom from the remaining ammine ligand. ^b Aqua ligand formed by the proton transfer to the hydroxyl group. ^c In all chemical formulas, a₂ means (NH₃)₂.

studies two sets of ¹H δ CH₃ and ¹⁹⁵Pt resonances are described and assigned to isomers with different sulfur chiralities with ratios of 5.3:2⁵ and 1.3:1²³ (both measurements were performed in a solution with pH > 5, where +1 charged chelate dominates). Discussed structures are drawn in Figure 5.

Finally in cysteine κ^2 (S,O) chelates, planarity of the carboxyl group imposes the six-membered ring flat boatlike structure with the amino group in the equatorial position. Methionine κ^2 (S,O) chelate forms a seven-membered ring in a chairlike conformation with the amino and S-methyl groups in axial positions.

Reaction Energetics. Reaction energies and reaction Gibbs free energies were calculated using both COSMO and modified DPCM/UAKS solvation models with vibrational frequencies taken from the reoptimized gas-phase structures as discussed in Computational Details. COSMO Gibbs free energies are collected in Table 8 in the Supporting Information; DPCM/UAKS values, in Table 3.

Since the modified DPCM/UAKS model performs much better than COSMO in comparison of calculated and experimental pK_a values, as shown in ref 74, we will concentrate on the DPCM/UAKS results in the discussion of reaction energies. The DPCM/UAKS and COSMO Gibbs free energies usually differ by up to 8 kcal/mol. One exception is the second reaction step in the noninteracting approach (of isolated molecules), where small ions (hydroxide and chlorine) are released. In this case the difference is up to 25 kcal/mol for reactions leading to +2 charged platinum chelates and hydroxide ions (these reactions are always thermodynamically more demanding than the formation of the +1 charged chelate and water molecule; therefore, their Gibbs free energies are not presented hereinafter) and up to 15 kcal/mol for reactions releasing chloride ions. A

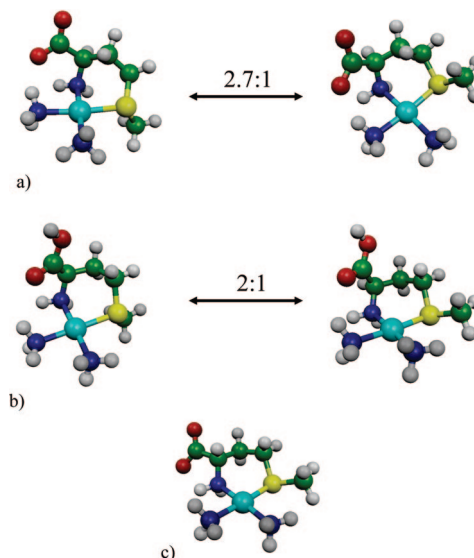


Figure 5. Structures and room temperature concentration ratios of +1 charged (a) and +2 charged (b) *cis*-[Pt(NH₃)₂(Met-S,N)]⁺²⁺ chelates differing in the position of S-methyl groups. Notice the boatlike conformation of the 1+ chelate and the chairlike conformation of the 2+ chelate. In the bottom, the structure originally proposed in ref 25 (c) is depicted.

qualitative difference between both models occurs in the chelation step of cysteine chloro complexes and in the reaction leading to methionine κ^2 (N,O) chelate, where formation of +2 chelate is predicted in DPCM/UAKS, while +1 chelate and HCl is the most stable product in the COSMO approach. The main source of this discrepancy lies in the difference of solvation

TABLE 3: Reaction Gibbs Free Energies (kcal/mol) at 298.15 K Using the DPCM Approach with Modified UAKS Cavities

reactants ^a	products ^a	isolated molecules				supermolecules	
		Cys	Met	Cys	Met	Cys	Met
[Pt-a ₂ Cl(H ₂ O)] ⁺ + AA	[Pt-a ₂ Cl(AA-S)] ⁺ + H ₂ O	-8.9	1.0			-11.8	5.9
	[Pt-a ₂ Cl(AA-N)] ⁺ + H ₂ O	-2.2	-1.7			-6.0	-3.4
	[Pt-a ₂ Cl(AA-O)] ⁺ + H ₂ O	2.9	1.2			1.1	2.1
[Pt-a ₂ (OH)(H ₂ O)] ⁺ + AA	[Pt-a ₂ (OH)(AA-S)] ⁺ + H ₂ O	-14.0	-3.9			-16.1	2.7
	[Pt-a ₂ (OH)(AA-N)] ⁺ + H ₂ O	-3.1	-2.3			-7.2	-4.2
	[Pt-a ₂ (OH)(AA-O)] ⁺ + H ₂ O	2.8	1.1			3.4	5.5
[Pt-a ₂ Cl(AA-S)] ⁺	[Pt-a ₂ (AA-S,O)] ²⁺ + Cl ⁻	4.2	-7.7	-4.7	-4.9	9.1	8.7
	[Pt-a ₂ (AA-S,N)] ²⁺ + Cl ⁻	-5.3	-10.0	-14.2	-7.2	5.1	0.9
[Pt-a ₂ (OH)(AA-S)] ⁺	[Pt-a ₂ (AA-S,O)] ⁺ + H ₂ O	-13.4	-0.8	-27.4	-4.7	-4.3	5.9
	[Pt-a ₂ (AA-S,N)] ⁺ + H ₂ O	-22.5	-16.8	-36.5	-20.7	-15.8	-6.1
[Pt-a ₂ Cl(AA-N)] ⁺	[Pt-a ₂ (AA-N,O)] ²⁺ + Cl ⁻	-1.8	1.1	-4.0	-0.6	4.2	4.8
	[Pt-a ₂ (AA-S,N)] ²⁺ + Cl ⁻	-11.9	-5.6	-14.2	-7.2	-1.5	5.3
[Pt-a ₂ (OH)(AA-N)] ⁺	[Pt-a ₂ (AA-N,O)] ⁺ + H ₂ O	-21.7	-18.5	-24.8	-20.8	-14.1	-11.5
	[Pt-a ₂ (AA-S,N)] ⁺ + H ₂ O	-33.4	-18.4	-36.5	-20.7	-26.6	-7.6
[Pt-a ₂ Cl(AA-O)] ⁺	[Pt-a ₂ (AA-S,O)] ²⁺ + Cl ⁻	-7.6	-6.1	-4.7	-4.9	-2.6	10.3
	[Pt-a ₂ (AA-N,O)] ²⁺ + Cl ⁻	-6.9	-1.8	-4.0	-0.6	-0.9	1.9
[Pt-a ₂ (OH)(AA-O)] ⁺	[Pt-a ₂ (AA-S,O)] ⁺ + H ₂ O	-30.2	-5.8	-27.4	-4.7	-21.1	0.9
	[Pt-a ₂ (AA-N,O)] ⁺ + H ₂ O	-27.7	-21.9	-24.8	-20.8	-20.0	-15.1

^a In all chemical formulas, a₂ means (NH₃)₂.

free energies of the hydroxide and chloride ions. Solvation free energies (neglecting geometry relaxation and shift in vibrational frequencies) of hydroxide ion are -106.2 kcal/mol in the DPCM/UAKS approach and -87.1 kcal/mol in the COSMO model; for chloride anion DPCM/UAKS the solvation free energy is -75.6 kcal/mol and the COSMO solvation free energy is -68.7 kcal/mol. The difference between the Cl⁻ and OH⁻ solvation free energies in the DPCM/UAKS model is therefore 30.6 kcal/mol, which almost perfectly fits the (average) experimental value of 30.3 kcal/mol.⁸⁴ However, in the COSMO model this value is about 12 kcal/mol lower.

The question whether the model of isolated molecules or the supermolecular model is more suitable for the discussion of reaction thermodynamics in aqueous environment is addressed in the next section on association and bonding energies. As will be shown later the association Gibbs free energies of all supermolecular complexes at 298.15 K are positive and thus a bigger fraction of reactants and products will not form an H-bonded complex but rather stay separated (solvated). Therefore, the results of the model of isolated molecules are more appropriate, and we refer mainly to them in the discussion.

When compared with the gas-phase results, the Gibbs free energies of the first reaction step are often very significantly reduced in absolute values. As in the gas phase, coordination of cysteine sulfur is the most exergonic for both chloro- and hydroxo-Pt complexes. Formation of the Pt-N(Cys) bond is by 6-10 kcal/mol less exergonic. The difference is higher in the case of hydroxo complexes. In the case of methionine, the Pt-S coordination is preferred only in the reaction with the hydroxo complex. With the chloro complex, the formation of the Pt-N bond is connected with a higher energy release and Pt-S coordination is even very slightly endergonic. The platinum preference for nitrogen over thioether sulfur in certain conditions was also observed in an experimental study.⁸⁵ Again the sulfur donor atom prefers the hydroxo to chloro complex more than amino group nitrogen.

The chelate-forming dissociation reactions are mostly exergonic and are usually facilitated by the presence of the solvent. This fact is the most significant in the case of reactions leading to κ²(N,O) chelates, whose ΔG are by approximately 10 kcal/mol lower than in the gas phase. In our model, in the case of chloro complexes a +2 charged platinum chelate is formed

releasing a Cl⁻ anion. In the case of hydroxo complexes the acidity of the +2 charged chelates is higher than that of water so that formation of a deprotonated Pt(II) +1 charged complex plus water molecule is thermodynamically preferred. The most stable structure is, similarly to the gas-phase results, the κ²(S,N) chelate. However, in the case of the methionine, the κ²(N,O) chelate has practically the same stability (in both COSMO and modified DPCM/UAKS models). Unlike κ²(S,N), the methionine κ²(N,O) chelate was not experimentally observed. The reason possibly lies in a too-high activation barrier of its formation in connection with the fact that most experimental studies were conducted at a lower pH, where the amino groups are fully protonated and thus less readily available for bonding than sulfur of the thioether. Stability of the cysteine κ²(N,O) complex is similar to methionine also enhanced by the presence of the solvent, but the stronger sulfur bond still makes formation of the κ²(S,N) and κ²(S,O) chelates energetically more preferable.

The complete reaction of free amino acid with the platinum complex leading to a chelate structure is strongly exergonic. For the hydroxo complexes the released Gibbs free energy amounts up to 37 kcal/mol for cysteine and 21 kcal/mol for methionine. For the chloro complexes, these values are approximately by one-half lower. Notice that the complete platinum hydration (i.e., the hydroxo-aqua complexes in our case) strongly thermodynamically enhances formation of the chelate structures.

Bonding Energies and Association Energy Analysis. The bonding energies and association energies were calculated according to eq 3 only in the COSMO approach, and they are presented in Table 4. The DPCM/UAKS method adapted for transition metal complexes was not used mainly due to its present-time complexity, since the cavity radii modifications had to be done manually. Therefore slightly lower accuracy can be expected in comparison to reaction Gibbs free energies; nevertheless general trends should be preserved as shown later in this section. Solvation of the given system (molecule or supermolecule) and components arising from it after dissociation brings some new aspects into interpretation of the results. First, electrostatic work necessary to bring the charged (or polarized) components apart is greatly reduced, and second, in the BEs

TABLE 4: Bonding Energies (BE; kcal/mol) Calculated in the COSMO Approach

complex ^a	BE	
	Cys	Met
[Pt-a ₂ Cl(AA-S)] ⁺	-64.2	-50.5
[Pt-a ₂ (OH)(AA-S)] ⁺	-80.8	-51.6
[Pt-a ₂ Cl(AA-N)] ⁺	-50.1	-50.6
[Pt-a ₂ (OH)(AA-N)] ⁺	-73.8	-76.0
[Pt-a ₂ Cl(AA-O)] ⁺	-42.7	-43.3
[Pt-a ₂ (OH)(AA-O)] ⁺	-43.1	-43.8
[Pt-a ₂ (AA-N,O)] ⁺	-122.8	-123.8
[Pt-a ₂ (AA-S,O)] ⁺	-134.6	-115.4
[Pt-a ₂ (AA-S,N)] ⁺	-144.0	-127.5
[Pt-a ₂ (AA-N,O)] ²⁺	-97.2	
[Pt-a ₂ (AA-S,O)] ²⁺	-115.2	-107.3
[Pt-a ₂ (AA-S,N)] ²⁺		-119.6

^a In all chemical formulas, a₂ means (NH₃)₂.

calculation, direct solvation of atoms which participated in broken bond can be an unwanted effect, which actually never occurs.

All the BEs are generally smaller in their absolute value when compared with the gas-phase counterparts. Lowering of the absolute BE values during transition from the gas phase to solvent occurs systematically to a higher extent in the chloro complexes (by approximately 10 kcal/mol). This effect is mainly caused by an energetically more advantageous solvation of the chloride-containing fragment in comparison to the entire complex (due to a larger accessible surface of chloride in the fragment). Generally, BEs of solvated chelates are reduced to roughly one-third of gas-phase values since the electrostatic work required for the separation of charged parts is substantially diminished (proportionally to 1/ε_r). The only exceptions to this rule are Pt-N bonds in monodentate hydroxo complexes, which will be discussed later.

Comparing the BE of the weakest Pt-O bond, a similar bonding energy of about 43 kcal/mol is obtained for all forms of monodentate Pt complexes with both amino acids in hydroxo and chloro structures (cf. Table 4). In the case of the nitrogen adducts, the BE(Pt-N) values are similar for both amino acids—approximately 75 kcal/mol in the hydroxo complexes and approximately 50 kcal/mol in the chloro complexes. The Pt-S bonds demonstrate the highest variation. They are the strongest in the cysteine adducts. In the methionine hydroxo complex the BE(Pt-S) is weaker than the corresponding Pt-N energy. In the semihydrated (chloro) complex, both (BE(Pt-N) and BE(Pt-S)) energies are comparable. The trend for the BE energies of the Pt-X bond in the hydroxo complexes does not correlate completely with the trend of reaction energies. The higher BEs (in absolute values) of Pt-N bonds result from the proton transfer from amino acid to hydroxo ligand of the Pt complex. This proton transfer causes (a) a stronger electrostatic interaction between the -1 charged amino acid and +2 platinum moiety, which is only partially compensated by higher solvation energies of both parts (AA⁻ and Pt²⁺), and (b) a lower competitive donation ability of the (neutral) aqua ligand to the Pt atom in comparison with the negatively charged OH⁻ group. In this way a stronger Pt-N(AA) interaction is obtained. In the chelate complexes, the BEs could be quite successfully used to predict their relative thermodynamic preferences. Nevertheless, in the case of κ²(N,O) complexes, the relatively low BEs seems to slightly underestimate the resulting thermodynamic stability of the complexes. In the case of +2 charged complexes there is a quite large difference between the relative BEs and

TABLE 5: Bonding Energies (kcal/mol) of the Ammine Ligands in the COSMO Approach^a

complex ^b	BE(Pt-NH ₃ [†])		BE(Pt-NH ₃ ^c)	
	Cys	Met	Cys	Met
<i>cis</i> -[Pt-a ₂ Cl(H ₂ O)] ⁺	-66.0	-66.0	-53.2	-53.2
<i>cis</i> -[Pt-a ₂ (OH)(H ₂ O)] ⁺	-62.0	-62.0	-49.2	-49.2
<i>cis</i> -[Pt-a ₂ Cl(AA-S)] ⁺	-37.5	-58.6	-48.9	-53.9
<i>cis</i> -[Pt-a ₂ (OH)(AA-S)] ⁺	-47.4	-45.4	-57.2	-51.4
<i>cis</i> -[Pt-a ₂ Cl(AA-N)] ⁺	-54.6	-53.7	-53.0	-53.1
<i>cis</i> -[Pt-a ₂ (OH)(AA-N)] ⁺	-55.4	-54.9	-63.7	-62.5
<i>cis</i> -[Pt-a ₂ Cl(AA-O)] ⁺	-56.8	-56.7	-51.9	-52.1
<i>cis</i> -[Pt-a ₂ (OH)(AA-O)] ⁺	-54.6	-54.1	-44.6	-54.1
<i>cis</i> -[Pt-a ₂ (AA-N,O)] ⁺	-54.2	-53.4	-55.8	-54.8
<i>cis</i> -[Pt-a ₂ (AA-S,O)] ⁺	-36.0	-45.9	-55.4	-54.8
<i>cis</i> -[Pt-a ₂ (AA-S,N)] ⁺	-37.1	-50.0	-52.8	-52.5
<i>cis</i> -[Pt-a ₂ (AA-N,O)] ²⁺	-59.5		-66.2	
<i>cis</i> -[Pt-a ₂ (AA-S,O)] ²⁺	-39.0	-48.0	-63.3	-58.4
<i>cis</i> -[Pt-a ₂ (AA-S,N)] ²⁺		-49.8		-55.0

^a NH₃[†] is the ammine ligand trans to aqua ligand in the reactant complexes, the amino acid donor atom in the monodentate complexes, the sulfur donor atom in κ²(S,N) and κ²(S,O) chelates, and the amino group nitrogen in the κ²(N,O) complexes. NH₃^c is the second ammine ligand. ^b In all chemical formulas, a₂ means (NH₃)₂.

relative reaction Gibbs free energies, but the qualitative trend is still preserved.

BEs of platinum—ammine ligand bonds are collected in Table 5. The largest trans influence leading to the weakening of the Pt-NH₃[†] bond by up to 30 kcal/mol is induced by S(Cys) in monodentate chloro and chelate complexes. In hydroxo complexes, the trans influence of cysteine sulfur is comparable to methionine—it causes a reduction of the BE(Pt-NH₃[†]) by ca. 15 kcal/mol in comparison with the reactant complex. A remarkably smaller trans influence of the methionine S-donor atom can be seen in the Pt—chloro—methionine complex, where even nitrogen of the amino group and oxygen of the carboxyl group exhibit larger weakening of the Pt-NH₃[†] bond. This is in very good accord with the above-mentioned thermodynamics of methionine monodentate coordination. Trans influence of the carboxyl group oxygen and nitrogen from amino group of methionine is generally similar and causes a weakening of the Pt-NH₃[†] bond by about 10 kcal/mol. No significant change of trans influence of individual groups was observed upon the chelation step, except for the fact that protonation to the +2 species generally leads to a strengthening of Pt-NH₃ bonds.

The association energies of H-bonded parts of supermolecule calculated from eq 4 are reduced more than twice in comparison to the gas-phase values. As follows from Table 6, the highest association energies are in the reactant supermolecules of the first reaction step: *cis*-[Pt(NH₃)₂Cl-(H₂O)]⁺ and *cis*-[Pt(NH₃)₂(OH)(H₂O)]⁺, where two H-bonds are present between the carboxylic group oxygens and hydrogens of aqua and ammine Pt ligands (cf. Figure 2). This coordination differs from the reactant arrangement in the gas phase where carboxyl oxygen forms an H-bond with the NH₃ ligand and the amino group forms an H-bond with the aqua ligand. Protonation of the amino group in solvent prevents such an H-bonding pattern. The association energies of monodentate complexes and water molecule released in the first reaction step are approximately 3–6 kcal/mol. The lowest values are seen in supermolecules composed of water and κ(O) complexes where the “best sites” to create an H-bond (the carboxyl group or aqua ligand) are not available. A similar situation occurs in the supermolecules representing products of the second reaction step of the hydroxo com-

TABLE 6: Association Energies (kcal/mol) at 298.15 K, in the COSMO Approach

complex ^a	ΔE_s^a		ΔG_s^a	
	Cys	Met	Cys	Met
<i>cis</i> -[Pt-a ₂ Cl(H ₂ O)] ⁺ + AA	-12.0	-12.5	1.9	1.5
<i>cis</i> -[Pt-a ₂ (OH)(H ₂ O)] ⁺ + AA	-10.7	-11.4	3.2	2.7
<i>cis</i> -[Pt-a ₂ Cl(AA-S)] ⁺ + H ₂ O	-5.3	-8.2	4.1	6.5
<i>cis</i> -[Pt-a ₂ (OH)(AA-S)] ⁺ + H ₂ O	-4.4	-8.2	6.4	7.8
<i>cis</i> -[Pt-a ₂ Cl(AA-N)] ⁺ + H ₂ O	-5.2	-4.8	3.9	4.5
<i>cis</i> -[Pt-a ₂ (OH)(AA-N)] ⁺ + H ₂ O	-4.4	-5.1	6.4	4.8
<i>cis</i> -[Pt-a ₂ Cl(AA-O)] ⁺ + H ₂ O	-3.6	-3.2	7.3	7.4
<i>cis</i> -[Pt-a ₂ (OH)(AA-O)] ⁺ + H ₂ O	-2.4	-1.5	9.9	12.8
<i>cis</i> -[Pt-a ₂ (AA-N,O)] ²⁺ + Cl ⁻	-10.2	-9.9	-7.1	-7.5
<i>cis</i> -[Pt-a ₂ (AA-N,O)] ⁺ + H ₂ O	-3.4	-3.1	7.0	7.5
<i>cis</i> -[Pt-a ₂ (AA-S,O)] ²⁺ + Cl ⁻	-10.0	-6.0	-6.1	4.0
<i>cis</i> -[Pt-a ₂ (AA-S,O)] ⁺ + H ₂ O	-3.1	-4.0	7.6	6.5
<i>cis</i> -[Pt-a ₂ (AA-S,N)] ²⁺ + Cl ⁻	-7.0	-7.4	-0.6	1.6
<i>cis</i> -[Pt-a ₂ (AA-S,N)] ⁺ + H ₂ O	-5.0	-3.2	4.2	10.2

^a In all chemical formulas, a₂ means (NH₃)₂.

TABLE 7: Association Free Energies (kcal/mol) of the Second Reaction Step Products at 298.15 K Calculated in the COSMO and DPCM/UAKS Approach without BSSE Corrections

complex ^a	ΔG_s^a (COSMO)		ΔG_s^a (DPCM)	
	Cys	Met	Cys	Met
<i>cis</i> -[Pt-a ₂ (AA-N,O)] ²⁺ + Cl ⁻	-7.7	-8.1	4.9	3.7
<i>cis</i> -[Pt-a ₂ (AA-N,O)] ⁺ + H ₂ O	6.4	7.0	6.8	6.9
<i>cis</i> -[Pt-a ₂ (AA-S,O)] ²⁺ + Cl ⁻	-6.9	3.1	6.0	16.4
<i>cis</i> -[Pt-a ₂ (AA-S,O)] ⁺ + H ₂ O	7.2	6.0	9.1	6.7
<i>cis</i> -[Pt-a ₂ (AA-S,N)] ²⁺ + Cl ⁻	-1.2	1.0	10.4	10.9
<i>cis</i> -[Pt-a ₂ (AA-S,N)] ⁺ + H ₂ O	3.9	9.7	7.6	10.7

^a In all chemical formulas, a₂ means (NH₃)₂.

plexes, where association energies of the water molecule are comparatively low. The exceptions are the *cis*-[Pt(NH₃)₂(Cys-S,N)]⁺ + H₂O and *cis*-[Pt(NH₃)₂(Met-S,O)]⁺ + H₂O supermolecules, where the carboxyl group is available to participate in the H-bonding. The chloride anion associations are stronger with energies around -10 kcal/mol.

When contributions of nuclear motion are taken into account, we obtain the true association Gibbs free energies (ΔG_s^a). They are collected in the last two columns of Table 7. From these values it follows that the ΔG_s^a association energies are positive in all cases except of the supermolecules representing products of the second reaction step, where the chloride anion is released and H-bonded to the metal complex. Association energy analysis was not performed in DPCM/UAKS approach, but it is possible to obtain BSSE uncorrected association energies of final product supermolecules from the difference between the reaction energies of the second reaction step in the model of isolated molecules and the supermolecular approach. Contrary to the COSMO results, positive association ΔG_s^a were obtained also for supermolecules containing chloride ion. This difference basically lies in a significantly lower COSMO chlorine ion solvation free energy as discussed above. The comparison of BSSE uncorrected COSMO and DPCM/UAKS association Gibbs free energies is summarized in Table 8 of the Supporting Information. In the case of supermolecules representing the final products of reactions of hydroxo complexes (consisting of a +1 e charged chelate and a water molecule) both methods match fairly well. But for the +2 charged complexes with a chloride anion, the DPCM/UAKS values are higher by slightly more than 10 kcal/mol. Therefore, we can conclude that when no small anion such as chloride or hydroxide is present, the COSMO

values are relatively reliable and similar to results obtained using the modified DPCM/UAKS model. Correcting the value obtained for the chloride ion containing supermolecules, all association Gibbs free energies of all molecules are thus positive. On the basis of this fact, we propose that the model of isolated (solvated) molecules is more appropriate for description of reaction thermodynamics in this case.

Conclusions

In the present study we explored cisplatin interactions with sulfur-containing amino acids in the polarizable continuum model. Optimizations of semihydrated and fully hydrated cisplatin complex with cysteine and methionine were performed at the B3LYP/6-31+G(d)/COSMO level of calculations. We suggested a two-step reaction mechanism: the first substitution step where the aqua ligand was replaced by one of the three active amino acid sites (N, O, or S), and the second dissociation process forming chelate and water or chloride anion. All the reactants and products were treated as supermolecular complexes as well as an approximation of isolated molecules. Energy characteristics and electronic properties were determined at the B3LYP/6-311++G(2df,2pd) level using two different PCM models—the COSMO and DPCM techniques with different cavities. Obtained results were compared with the gas-phase data from our previous study where a similar computational model was used.

The first reaction step is exergonic for both amino acids and both platinum complexes. The reaction Gibbs free energies released in formation of the Pt–N adduct are roughly comparable for both amino acids; the same also holds for the Pt–O adducts. However, in the case of Pt–S coordination, the energy of the cysteine-complex formation is more exergonic than for methionine (by 7–10 kcal/mol). Generally, cysteine strongly prefers the $\kappa(S)$ coordination over $\kappa(N)$. Creation of the $\kappa(O)$ complex is thermodynamically the least convenient reaction outcome. Thermodynamics of reaction with methionine is dependent on the cisplatin hydration state. In the case of the monohydrated chloro complex, the $\kappa(N)$ coordination is the most exergonic. On the other hand, the $\kappa(S(\text{Met}))$ bonding is more preferable in the hydroxo complex. A similar (but less pronounced) behavior was observed also in the gas phase.

Among products of the chelation process the $\kappa^2(S,N)$ chelate of cysteine clearly prevails followed by almost an equivalent presence of the $\kappa^2(S,O)$ and $\kappa^2(N,O)$ structures. This is in qualitative agreement with gas-phase calculations. In the methionine case, the highest ΔG release occurs in the formation of the $\kappa^2(N,O)$ and $\kappa^2(S,N)$ chelates. The $\kappa^2(S,O)$ structure is predicted to be the least stable using both SCRF methods. This preference however differs from the gas-phase results, where $\kappa^2(S,O)$ and $\kappa^2(S,N)$ complexes are more stable than the $\kappa^2(N,O)$ complex.

Two procedures for calculation of BSSE-corrected bonding and association energies were explored. The first calculates the BSSE correction directly with ghost functions placed outside of a solute cavity, whereas the second calculates the correction separately in the cavity of the original supermolecule. Analysis of Gibbs free association energies showed that the model of isolated molecules is more suitable for discussion of thermodynamics of considered reactions in aqueous solution than the supermolecular model due to the positive Gibbs free association energies of all supermolecules. Basic thermodynamic preferences of considered reactions are relatively well-reflected in bonding energies of Pt–AA bonds. Some care must be, however, taken due to the effects of intermolecular proton transfers and solvation of residues.

Acknowledgment. This study was supported by the MSM 0021620835 grant of the Ministry of Education, Youth and Sport and the IAA400550701 grant of the Grant Agency of the Academy of Sciences of the Czech Republic. We are grateful for access to the excellent computational resources from our department supercomputer cluster administered by Dr. Šimánek.

Supporting Information Available: Table showing reaction Gibbs free energies using the COSMO approach. This material is available free of charge via the Internet at <http://pubs.acs.org>.

References and Notes

- Eastman, A. The Mechanism of Action of Cisplatin: From Adducts to Apoptosis. In *Cisplatin*; Lippert, B., Ed.; Wiley-VCH: Weinheim, Germany, 1999; p 111.
- Pascoe, J. M.; Roberts, J. J. *Biochem. Pharmacol.* **1974**, *23*, 1345.
- Lippert, B. *Cisplatin: Chem. and Biochemistry of a Leading Anticancer Drug*; Wiley-VCH: Weinheim, Germany, 1999; p 1999.
- Donahue, B. A.; Augot, M.; Bellon, S. F.; Treiber, D. K.; Toney, J. H.; Lippard, S. J.; Essigmann, J. M. *Biochemistry* **1990**, *29*, 5872.
- Peleg-Shulman, T.; Najajreh, Y.; Gibson, D. *J Inorg. Biochem.* **2002**, *91*, 306.
- Kartalou, M.; Essigmann, J. M. *Mutat. Res.* **2001**, *478*, 1.
- Fojta, M.; Pivonkova, H.; Brazdova, M.; Kovarova, L.; Palecek, E.; Pospisilova, S.; Vojtesek, B.; Kasparkova, J.; Brabec, V. *Biochem. Pharmacol.* **2003**, *65*, 1305.
- Pivonkova, H.; Pecinka, P.; Ceskova, P.; Fojta, M. *FEBS J* **2006**, *273*, 4693.
- Andrews, P. A.; Jones, J. A. *Cancer Commun.* **1991**, *3*, 1.
- Burger, A. M.; Double, J. A.; Newell, D. R. *Eur. J. Cancer* **1997**, *33*, 638.
- Zamble, D. B.; Lippard, S. J. The Responce of Cellular Proteins to Cisplatin-Damaged DNA. In *Cisplatin*; Lippert, B., Ed.; Wiley-VCH: Weinheim, Germany, 1999; p 73.
- Meister, A. *J. Biol. Chem.* **1988**, *263*, 17205.
- Schafer, F. Q.; Buettner, G. R. *Free Radical Biol. Med.* **2001**, *30*, 1191.
- Ishikawa, T.; Aliosman, F. *J. Biol. Chem.* **1993**, *268*, 20116.
- Appleton, T. G.; Connor, J. W.; Hall, J. R.; Prenzler, P. D. *Inorg. Chem.* **1989**, *28*, 2030.
- Witte, A. B.; Anestalt, K.; Jerremalm, E.; Ehrsson, H.; Arner, E. S. J. *Free Radical Biol. Med.* **2005**, *39*, 696.
- Arner, E. S. J.; Nakamura, H.; Sasada, T.; Yodoi, J.; Holmgren, A.; Spyrou, G. *Free Radical Biol. Med.* **2001**, *31*, 1170.
- Townsend, D. M.; Deng, M.; Zhang, L.; Lopus, M. G.; Hanigan, M. H. *J Am. Soc. Nephrol.* **2003**, *14*, 1.
- Zhang, L.; Hanigan, M. H. *Pharmacol. Exp. Ther.* **2003**, *306*, 988.
- Rudin, C. M.; Yang, Z.; Schumaker, L. M.; VanderWeele, D. J.; Newkirk, K.; Egorin, M. J.; Zuhowski, E. G.; Cullen, K. J. *Cancer Res.* **2003**, *63*, 312.
- Nagata, J.; Kijima, H.; Hatanaka, H.; Asai, S.; Miyachi, H.; Takagi, A.; Miwa, T.; Mine, T.; Yamazaki, H.; Nakamura, M.; Kondo, T.; Scanlon, K. J.; Ueyama, Y. *Biochem. Biophys. Res. Commun.* **2001**, *286*, 406.
- Reedijk, J.; Teuben, J. M. Platinum-Sulphur Interaction Involved in Antitumor Drugs, Rescue Agents and Biomolecules. In *Cisplatin*; Lippert, B., Ed.; Wiley-VCH: Weinheim, Germany, 1999.
- Norman, R. E.; Ranford, J. D.; Sadler, P. J. *Inorg. Chem.* **1992**, *31*, 877.
- Williams, K. M.; Rowan, C.; Mitchell, J. *Inorg. Chem.* **2004**, *43*, 1190.
- Appleton, T. G.; Connor, J. W.; Hall, J. R. *Inorg. Chem.* **1988**, *27*, 130.
- Wei, H. Y.; Liu, Q.; Lin, J.; Jiang, P. J.; Guo, Z. J. *Inorg. Chem. Commun.* **2004**, *7*, 792.
- Riley, C. M.; Sternson, L. A.; Repta, A. J. *J. Pharm. Sci.* **1983**, *72*, 351.
- Reedijk, J. *Chem. Rev.* **1999**, *99*, 2499.
- Vrana, O.; Brabec, V. *Biochemistry* **2002**, *41*, 10994.
- Manka, S.; Becker, F.; Hohage, O.; Sheldrick, W. S. *J Inorg. Biochem.* **2004**, *98*, 1947.
- Hohage, O.; Sheldrick, W. S. *J Inorg. Biochem.* **2006**, *100*, 1506.
- Bose, R. N.; Ghosh, S. K.; Moghaddas, S. *J Inorg. Biochem.* **1997**, *65*, 199.
- Lau, J. K. C.; Deubel, D. V. *Chem.-Eur. J* **2005**, *11*, 2849.
- Zimmermann, T.; Zeizinger, M.; Burda, J. V. *J. Inorg. Biochem.* **2005**, *99*, 2184.
- Hagman, D.; Goodisman, J.; Souid, A.-K. *J. Pharm. Exp. Ther.* **2004**, *308*, 658.
- Dabrowiak, J. C.; Goodisman, J.; Souid, A.-K. *Drug Metab. Dispos.* **2002**, *30*, 1378.
- Dedon, P. C.; Borch, R. F. *Biochem. Pharmacol.* **1987**, *36*, 1955.
- Bose, R. N.; Moghaddas, S.; Weaver, E. L.; Cox, E. H. *Inorg. Chem.* **1995**, *34*, 5878.
- Zou, J.; Yang, X. D.; An, F.; Wang, K. *J. Inorg. Biochem.* **1998**, *70*, 227.
- Da Silva, V. J.; Costa, L. A. S.; Dos Santos, H. F. *Int. J. Quantum Chem.* **2008**, *108*, 401.
- Matsui, T.; Shigeta, Y.; Hirao, K. *Chem. Phys. Lett.* **2006**, *423*, 331.
- Dal Peraro, M.; Ruggerone, P.; Raugeri, S.; Gervasi, F. L.; Carloni, P. *Curr. Opin. Struct. Biol.* **2007**, *17*, 149.
- Chang, G. R.; Zhou, L. X.; Chen, D. *Chin. J. Struct. Chem.* **2006**, *25*, 533.
- Dos Santos, H. F.; Marcial, B. L.; De Miranda, C. F.; Costa, L. A. S.; De Almeida, W. B. *J. Inorg. Biochem.* **2006**, *100*, 1594.
- Lopes, J. F.; Menezes, V. S. D.; Duarte, H. A.; Rocha, W. R.; De Almeida, W. B.; Dos Santos, H. F. *J. Phys. Chem. B* **2006**, *110*, 12047.
- Costa, L. A.; Hambley, T. W.; Rocha, W. R.; Almeida, W. B.; Dos Santos, H. F. *Int. J. Quantum Chem.* **2006**, *106*, 2129.
- Robertazzi, A.; Platts, J. A. *J. Comput. Chem.* **2004**, *25*, 1060.
- Robertazzi, A.; Platts, J. A. *Inorg. Chem.* **2005**, *44*, 267.
- Robertazzi, A.; Platts, J. A. *Chem.-Eur. J* **2006**, *12*, 5747.
- Wysokinski, R.; Hernik, K.; Szostak, R.; Michalska, D. *Chem. Phys.* **2007**, *333*, 37.
- Yuan, Q. H.; Zhou, L. X. *Chin. J. Struct. Chem.* **2007**, *26*, 962.
- Erturk, H.; Hofmann, A.; Puchta, R.; van Eldik, R. *Dalton Trans.* **2007**, 2295.
- Hao, L.; Zhang, Y.; Tan, H. W.; Chen, G. J. *Chem. J. Chin. Univ. (Chinese)* **2007**, *28*, 1160.
- Pavelka, M.; Lucas, M. F. A.; Russo, N. *Chem. Eur. J.*, in press.
- Hofmann, A.; Jaganyi, D.; Munro, O. Q.; Liehr, G.; van Eldik, R. *Inorg. Chem.* **2003**, *42*, 1688.
- Cooper, J.; Ziegler, T. *Inorg. Chem.* **2002**, *41*, 6614.
- Zhu, H. J.; Ziegler, T. *J. Organomet. Chem.* **2006**, *691*, 4486.
- Tsipis, A. C.; Sigalas, M. P. *J. Mol. Struct.* **2002**, *584*, 235.
- Zhu, C.; Raber, J. A., E. L. *J. Phys. Chem. B* **2005**, *109*, 12195.
- Song, T.; Hu, P. *J. Chem. Phys.* **2006**, *125*, 091101.
- Jia, M.; Qu, W.; Yang, Z.; Chen, G. *Int. J. Mod. Phys. B* **2005**, *19*, 2939.
- Zhang, Y.; Guo, Z.; You, X.-Z. *J. Am. Chem. Soc.* **2001**, *123*, 9378.
- Lau, J. K. C.; Deubel, D. V. *J. Chem. Theor. Comput.* **2006**, *2*, 103.
- Parr, R. G.; Pearson, R. G. *J. Am. Chem. Soc.* **1983**, *105*, 7512.
- Hush, N. S.; Schamberger, J.; Bacskey, G. B. *Coord. Chem. Rev.* **2005**, *249*, 299.
- Wysokinski, R.; Michalska, D. *J. Comput. Chem.* **2001**, *22*, 901.
- Andrae, D.; Haussermann, U.; Dolg, M.; Stoll, H.; Preuss, H. *Theor. Chim. Acta* **1990**, *77*, 123.
- Bergner, A.; Dolg, M.; Kuchle, W.; Stoll, H.; Preuss, H. *Mol. Phys.* **1993**, *80*, 1431.
- Burda, J. V.; Zeizinger, M.; Sponer, J.; Leszczynski, J. *J. Chem. Phys.* **2000**, *113*, 2224.
- Klamt, A.; Schuurmann, G. *J. Chem. Soc., Perkin Trans. 2* **1993**, 799.
- Miertus, S.; Scrocco, E.; Tomasi, J. *Chem. Phys.* **1981**, *55*, 117.
- Miertus, S.; Tomasi, J. *Chem. Phys.* **1982**, *65*, 239.
- Barone, V.; Cossi, M.; Tomasi, J. *J. Chem. Phys.* **1997**, *107*, 3210.
- Zimmermann, T.; Burda, J. V. *PCCP*, submitted for publication.
- da Silva, G.; Kennedy, E. M.; Dlugogorski, B. Z. *J. Phys. Chem. A* **2006**, *110*, 11371.
- Boys, S. F.; Bernardi, F. *Mol. Phys.* **1970**, *19*, 553.
- van Duijneveldt, F. B.; van Duijneveldt-van de Rijdt, J. G. C. M.; van Lenthe, J. H. *Chem. Rev.* **1994**, *94*, 1873.
- Weinhold, F. *NBO 5.0 Program*, 5.0 ed.; University of Wisconsin: Madison, WI, 2001.
- Heudi, O.; Cailleux, A.; Allain, P. *J Inorg. Biochem.* **1998**, *71*, 61.
- Fernandez-Ramos, A.; Cabaleiro-Lago, E.; Hermida-Ramon, J. M.; Martinez-Nunez, E.; Pena-Gallego, A. *J. Mol. Struct.* **2000**, *498*, 191.
- Deubel, D. V. *J. Am. Chem. Soc.* **2002**, *124*, 5834.
- Fuks, L.; Sadlej-Sosnowska, N.; Samochocka, K.; Starosta, W. J. *J. Mol. Struct.* **2005**, *740*, 229.
- Wilson, C.; Scudder, M. L.; Hambley, T. W.; Freeman, H. C. *Acta Cryst., Sect. C: Cryst. Struct. Commun.* **1992**, *48*, 1012.
- Tissandier, M. D.; Cowen, K. A.; Feng, W. Y.; Gundlach, E.; Cohen, M. H.; Earhart, A. D.; Coe, J. V.; Tuttle, T. R. *J. Phys. Chem. A* **1998**, *102*, 7787.
- Lempers, E. L. M.; Reedijk, J. *J. Inorg. Chem.* **1990**, *29*, 1880.

Comparison of hydration reactions for “piano-stool” RAPTA-B and $[\text{Ru}(\eta^6\text{-arene})(\text{en})\text{Cl}]^+$ complexes: Density functional theory computational study

Zdeněk Chval,¹ Zdeněk Futera,² and Jaroslav V. Burda^{2,a)}

¹Department of Laboratory Methods and Medical Technology, Faculty of Health and Social Studies, University of South Bohemia, J. Boreckého 27, 370 11 České Budějovice, Czech Republic

²Department of Chemical Physics and Optics, Faculty of Mathematics and Physics, Charles University, Ke Karlovu 3, 121 16 Prague 2, Czech Republic

(Received 10 June 2010; accepted 22 October 2010; published online 12 January 2011)

The hydration process for two Ru(II) representative half-sandwich complexes: $\text{Ru}(\text{arene})(\text{pta})\text{Cl}_2$ (from the RAPTA family) and $[\text{Ru}(\text{arene})(\text{en})\text{Cl}]^+$ (further labeled as Ru_en) were compared with analogous reaction of cisplatin. In the study, quantum chemical methods were employed. All the complexes were optimized at the B3LYP/6-31G(d) level using Conductor Polarizable Continuum Model (CPCM) solvent continuum model and single-point (SP) energy calculations and determination of electronic properties were performed at the B3LYP/6-311++G(2df,2pd)/CPCM level. It was found that the hydration model works fairly well for the replacement of the first chloride by water where an acceptable agreement for both Gibbs free energies and rate constants was obtained. However, in the second hydration step worse agreement of the experimental and calculated values was achieved. In agreement with experimental values, the rate constants for the first step can be ordered as $\text{RAPTA-B} > \text{Ru_en} > \text{cisplatin}$. The rate constants correlate well with binding energies (BEs) of the Pt/Ru–Cl bond in the reactant complexes. Substitution reactions on Ru_en and cisplatin complexes proceed only via pseudoassociative (associative interchange) mechanism. On the other hand in the case of RAPTA there is also possible a competitive dissociation mechanism with metastable penta-coordinated intermediate. The first hydration step is slightly endothermic for all three complexes by 3–5 kcal/mol. Estimated BEs confirm that the benzene ligand is relatively weakly bonded assuming the fact that it occupies three coordination positions of the Ru(II) cation. © 2011 American Institute of Physics. [doi:10.1063/1.3515534]

I. INTRODUCTION

Despite cisplatin is a very effective anticancer metallo-drug, an intensive research of some other metal complexes is carried out. The reason is based on the fact that cisplatin is very toxic with many side effects.¹ Another problem consists in low or even no activity for some kinds of carcinomas.² Therefore many studies appeared on complexes, which are active against cancer cells. Various biophysical and biochemical properties of rhodium,^{3–7} titanium,^{8–10} ruthenium,^{11–24} and many other metal complexes^{25,26} were explored.

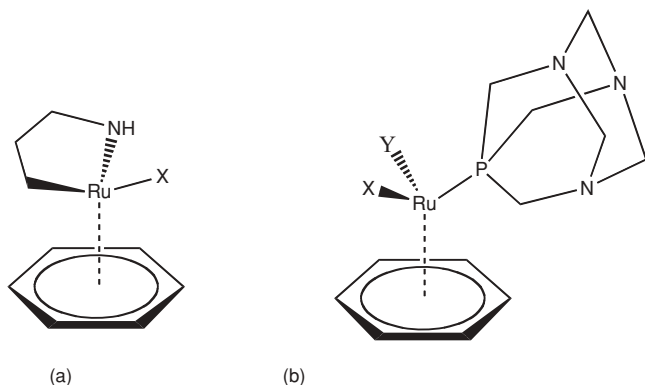
Computational studies usually concentrate on coordination and structural effects. Description of the reaction mechanisms and electronic properties of cisplatin and its analogs were examined in several papers.^{27–31} Some studies concerned the aquation process of platinum complexes, which is crucial in the activation step,^{32–39} interactions with nucleobases,^{40–51} or other competitive reactions with cellular components, such as side chains of amino acids.^{52–56}

Ruthenium compounds also attract a lot of attention as can be noticed in recent computational chemistry literature.^{19,57–64} A lot of interesting features, hypotheses and conclusions, which would be worth of computational

confirmations or deserve a more detailed insight based on molecular modeling can be found in many experimental works.^{18,21,24,25,65–72} An interesting paper on stacking interaction of Ru(II) complexes with guanine and adenine using density functional theory (DFT) study was presented by Platts.⁷³

There are two basic families of half-sandwich ruthenium(II) complexes. First class (further labeled as Ru_en) is represented by $[\text{Ru}(\eta^6\text{-arene})(\text{en})\text{Cl}]^+$ complexes^{67,74} (en = ethylenediamine, arene = benzene), which can coordinate to DNA helix in the form of monofunctional adducts (at least in the first step). This is one of the basic differences compared to Pt-complexes where bifunctional adducts are believed to be the key structure coordinated to the genomic sequence. The role of the size of the arene ligand was examined, too.¹⁷ It was found that larger arene ligands like anthracene or biphenyl increase the drug efficiency due to possible intercalation into DNA helix via π – π stacking interaction. This interaction is reduced in the case of smaller aromatic ligands with a single benzene ring. Also, a pronounced selectivity (higher affinity) of these Ru(II) complexes to guanine was discussed in Refs. 17 and 19. The explanation was searched in a formation of an additional H-bond between O6 and the amine group of the ethylenediamine ligand. Such a strong binding can be created neither with N7-adenine nor with N3-cytosine adduct. However, in our previous paper it was shown⁷⁵ that this is only

^{a)} Author to whom correspondence should be addressed. Electronic mail: burda@karlov.mff.cuni.cz. Tel.: +420 221 911 246. Fax: +420 221 911 249.

SCHEME 1. Structural formulas of (a) Ru_{en} and (b) RAPTA-B complexes.

partially true since some (weaker) H-bond can be formed also in the case of adenine. We confirmed that the size of arene ring does not play any role in the activation reaction so that the extent of aromatic system does not substantially change the coordination strength of the Ru-arene part of the complex.⁷⁵ Also, the H-bonding between ethylenediamine and exocyclic N6 amino group of adenine is markedly weaker than analogous interaction in the guanine complex (at least according to N6...H/O6...H distance which is 2.07 and 1.83 Å, respectively) or according to electron density of the bond critical points obtained from Bader's Atoms-in-Molecules (AIM) analysis.⁷⁶

The second class of the Ru(II) "piano-stool" compounds examined in this study is the so-called RAPTA family. We used a model complex RAPTA-B (further called just RAPTA), which contain monofunctional pta ligand (1.3.5-triaza-7-phosphatricyclo[3.3.1]decane),^{77,78} benzene, and two chloride anions. In this way, some similarities with cisplatin can be expected concerning the mechanism of the drug activity in the cancer cells.

The general structures of both Ru(II) classes are drawn in Scheme 1.

In the present study we compare activation process, e.g., hydration reactions of basic representatives of both classes of half-sandwich ruthenium complexes together with the frequently studied cisplatin complex. The DFT computational level and the CPCM continuum solvent model were employed for determination of all explored structures in reactants, products and transition states. Besides energy profiles, also some physicochemical and electronic characteristics were determined for the deeper insight into the reaction mechanism.

II. COMPUTATIONAL DETAILS

In the present study, the compounds of [Ru(η^6 -arene)(en)X]^{+2/+} and [Ru(η^6 -arene)(pta)XY]^{0/1/+2/+} (X, Y = Cl⁻, OH, H₂O) were examined. The general structures of both classes of Ru(II) complexes contain the pseudo-octahedral arrangement of the Ru atom. For the comparison cisplatin hydration is also included.

All the explored systems were optimized both in the gas phase and in water environment using the Klamt's COSMO (CPCM) implicit solvent approach^{79,80} with dielectric con-

stant $\epsilon = 78$. In chosen model, default Klamt's cavities were used.

In the reaction course of the pseudoassociative mechanism (PAM), the Cl⁻ ligand(s) was/were replaced by water. In order to describe the reaction kinetics of the hydration reactions, the supermolecular approach was considered. In the reactant state, the Ru-complexes and water are associated by H-bonding. The transition states for the replacement of chloro ligand by water were found where formation of a seven-coordinated structure was revealed. In the Ru_{en} complexes, only one step is possible while activation of the RAPTA and cisplatin complexes can occur in two subsequent steps replacing both chloride ligands. Moreover in the RAPTA complex also a dissociative mechanism was explored where two reaction steps in each dechloration were determined. The first TS structure is linked with Ru-Cl bond breaking. Then the five-coordinated intermediate is formed with both chloride and water particles detached from the RAPTA complex. Finally, the second TS complex follows where oxygen of water is approaching and forming a new coordination bond.

All the geometries were optimized at the DFT level with the hybrid B3LYP functional and 6-31G(d) basis set (further labeled as BS1) with the description of heavy elements Pt, Ru, P, and Cl atoms by Stuttgart energy averaged pseudopotentials.^{81,82} The original pseudo-orbital basis set was extended by polarization functions (with exponents $\alpha_f(\text{Pt}) = 0.98$, $\alpha_f(\text{Ru}) = 1.29$, $\alpha_d(\text{P}) = 0.51$, and $\alpha_d(\text{Cl}) = 0.62$) in the optimization part. The same level was used for the determination of the ΔG contributions (thermal and entropy terms) and also for confirmation of the proper character of the optimized geometries of TS structures as well as reactant and product supermolecules in both gas phase and CPCM approach. The energy profiles were determined at the B3LYP/6-311++G(2df,2pd)/CPCM level (BS2) expression where original pseudo-orbitals of metals were consistently augmented by a set of diffuse and polarization (2fg) functions optimized for neutral atoms at CCSD level, as mentioned elsewhere.^{75,83}

As it can be noticed from Scheme 1 the complexes are composed from three/four ligands and the metal cation. The total stabilization energy (ΔE^{Stab}) of the complex is defined as

$$\Delta E^{\text{Stab}} = - \left(E_{\text{compl}} - \sum_i^{\text{Ligands}} E_i - E_{\text{Me}} + \Delta E^{\text{deform}} \right). \quad (1)$$

Here E_{compl} is total energy of the whole complex, E_i and E_{Me} are BSSE corrected energies of a given ligand i and Me—the metal cation. In this case, the ligand deformation energies were included

$$\Delta E^{\text{deform}} = \sum_i^{\text{Ligands}} (E_i^{\text{compl}} - E_i^{\text{opt}}). \quad (2)$$

In the equation the superscripts compl and opt denote calculations for the frozen ligand structure (taken from geometry of the complex) and for the optimized (isolated) ligand, respectively. The ligand binding and/or association energies (ΔE^{BE}) were evaluated according to equation

$$\Delta E^{\text{BE}}(L) = (E_{\text{compl}} - E_L - E_{\text{rest}}). \quad (3)$$

TABLE I. Metal-ligand coordination distances (in Å) within the hydration reactions for $[\text{Ru}(\text{arene})(\text{en})\text{Cl}]^+$, $[\text{Ru}(\text{arene})(\text{pta})\text{Cl}_2]$, and $[\text{Pt}(\text{NH}_3)_2\text{Cl}_2]$ complexes. The optimized bond lengths were obtained at the B3LYP/BS1/CPCM and $T = 298$ K level.

	Ru-Cl	Ru-Ben	Ru-N1	Ru-N2	Ru-O
Ru_en_Cl+w	2.479	1.713	2.146	2.151	4.218
TS_en	3.238	1.700	2.137	2.142	2.883
Ru_en_w+Cl	4.288	1.714	2.143	2.143	2.166
	Ru-Cl	Ru-Ben	Ru-P	Ru-O	Ru-O
Ru_pta_Cl2+w	2.473	1.740	2.343	3.810	
TS_pta1a	2.447	1.716	2.359	2.918	
TS_pta1d1	2.397	1.714	2.362	4.391	
Int1	2.380	1.717	2.365	4.794	
TS_pta1d2	2.358	1.711	2.382	3.584	
Ru_pta_Cl_w+Cl	2.448	1.741	2.348	2.159	
Ru_pta_Cl_w+w	2.458	1.743	2.347	2.175	4.070
TS_pta2a	3.206	1.715	2.367	2.199	2.724
TS_pta2d1	3.598	1.714	2.376	2.153	3.862
Int2	6.970	1.738	2.375	1.945	4.468
TS_pta2d2	5.137	1.703	2.398	2.16	3.461
Ru_pta_w2+Cl	4.207	1.740	2.362	2.176	2.148
Ru_pta_Cl_OH+w	2.496	1.763	2.335	2.087	
TS_pta2d1+OH	6.970	1.738	2.375	1.945	4.468
Int2_OH	4.397	1.711	2.387	1.957	3.090
TS_pta2d2_OH	4.477	1.734	2.352	2.064	2.18
Ru_pta_OH_w+Cl	2.496	1.763	2.335	2.087	
	Pt-Cl	Pt-N	Pt-N	Pt-O	Pt-O
Pt_a2_Cl2+w	2.361	2.066	2.065	3.862	
TS_cis1	2.354	2.058	2.045	2.467	
Pt_a2_Cl_w+Cl	2.349	2.070	2.034	2.082	
Pt_a2_Cl_w+w	2.360	2.068	2.074	2.021	3.738
TS_cis2	2.908	2.043	2.031	2.119	2.653
Pt_a2_2w+Cl	4.016	2.045	2.045	2.107	2.107
Pt_a2_Cl_OH+w	2.357	2.083	2.039	2.102	3.768
TS_cis2_OH	3.009	2.057	2.094	2.004	2.405
Pt_a2_OH_w+Cl	4.103	2.087	2.026	2.005	2.086

Similarly, the E_L and E_{rest} energies mean the BSSE corrected values of the given ligand and the remaining part of the complex, respectively. In these energies, deformation corrections were not considered.

The ground state of all the explored complexes is a closed-shell singlet. In the calculations of BSSE corrections within the CPCM regime, the ghost atomic orbital functions are localized inside the cavity, which has the same size as the whole complex. This is the simplest approach and discussion on other possibilities for determination of BSSE corrections within the PCM model can be found in Ref. 55.

The kinetic parameters of the studied reactions were determined according to Eyring's transition state theory. Because vibration modes, energies, and geometries are available from the above-described calculations, the rate constants can be estimated from the formula

$$k(T) = (k_B T/h) \exp(-\Delta G^\ddagger/RT). \quad (4)$$

The calculations of electronic properties [Natural Bond Orbital (NBO) and AIM analyses, and dipole moments] were performed at the same computational level as SP calculations (B3LYP/BS2). AIM analysis was performed by AIMALL program of T. Keith⁸⁴ and natural population analysis (NPA) par-

tial charges were determined by NBO v.5 program from University of Wisconsin.⁸⁵

A. Structures

All structures of the stationary points on the reaction profiles of the hydration reactions were optimized in both gas phase and CPCM levels. The obtained metal-ligand distances in water environment are collected in Table I. Longer distances between the metal and the arene ring can be noticed in the case of the RAPTA complexes compared to the Ru_en complexes due to higher steric crowding. The Ru-P bond of the pta ligand is about 2.34 Å in neutral reactant and it slightly increases with total charge of the complex up to 2.36 Å in the diaqua product. It means that origin of this bond is basically nonelectrostatic. In the product states of the both classes of Ru complexes, Ru-O distance (≈ 2.17 Å) is visibly longer than analogous Pt-O coordination bonds in cisplatin. The same is also true for the Ru-N bonds in Ru-en complexes and Ru-Cl bonds in Ru-pta reactants. All these distances are about 0.1 Å shorter in the Pt(II) complexes. The simplest possible explanation follows from a general study on covalent radii published recently⁸⁶ where the difference of covalent radii of Pt and Ru atoms is about

0.1 Å. The binding energy unambiguously correlates with electron density of the bond critical point, as it will be discussed below.

Transition states of Ru(II) piano-stool complexes in the ‘pseudoassociative mechanism’ are represented by the hepta-coordinated structures where one can easily expect relatively large sterical repulsion. However the exchanging ligands are practically nonbonded (see the part on binding energies below) in TSs so that lower binding competition occurs and visibly shorter Ru–arene distances can be noticed (in comparison with both reactant and product states). This effect is a little bit more pronounced in PCM geometries than in gas phase. Similar shortening is observed for the Ru–N coordination distances of the ethylenediamine ligand in TS of the Ru–en complex (TS_{en}) and for the equatorial amino ligands in the trigonal-bipyramidal TSs structures of cisplatin. On the contrary, in the case of the RAPTA TS structures, the Ru–P bond of the pta ligand is elongated. Similarly the Ru–O distance of the aqua ligand in second reaction step elongates in TS geometry (TS_{pta2a}) where the Ru–O bond is about 2.199 Å (despite of H-bonding between both water molecules and chloride) and in second hydration step (TS_{cis2}) where the axial Pt–N bond is also elongated (2.094 Å). The shortening can be explained by a lower competition to Pt–N bond in equatorial plane of trigonal-bipyramid due to very weakly bounded exchanging ligands. On the contrary, the coordination of the axial ligands is generally known to be always a little bit longer (and weaker).

Another reaction mechanism was revealed in the case of RAPTA complexes. The competitive dissociation mechanism is linked with two TS structures and one metastable penta-coordinated intermediate in each dechloration reaction. This intermediate has the two pta and Cl/aqua/hydroxo ligands oriented in a plane perpendicular to the arene ring. Such an arrangement minimizes the interligand repulsion. In this way it is obvious why this direct dissociative mechanism (dDM) could not occur in the Ru_{en} complex. The ethylenediamine bidentate ligand cannot form similar kind of structure (where en ligand would be perpendicular to arene ring) due to high-energy penalty caused by deviation of the donating electron lone-pairs of nitrogens from the ideal sp³ orientation and by increased arene...H(en) steric repulsion. Basically all the structural trends from the discussion on TS of pseudoassociative mechanism are also valid for geometries of the intermediates and TS’s of the dissociative pathway.

B. Energy profile of hydration reactions

All the energy characteristics of the explored complexes are summarized in Table II and corresponding reaction energy profiles are drawn in Fig. 1 for PAM and in Fig. 2 for dDM. In the first reaction step of PAM, all the explored reactions are endoergic with $\Delta G_r \approx 3\text{--}6$ kcal/mol and have comparable activation barrier of about 20 kcal/mol for the replacement of the first chloride.

In the second reaction step of the RAPTA and cisplatin complexes, much higher activation energy (over 25 kcal/mol) was determined for pseudoassociative mechanism together with more pronounced endoergic reaction course of about

TABLE II. Gibbs energy reaction surface (in kcal/mol) and rate constants (in s⁻¹ in gray) at the B3LYP/BS2/CPCM level.

	Calc.	Expt.
Ru _{en} _Cl+w	0.00	
TS _{en}	20.01	
Ru _{en} _w+Cl	2.79	
	1.32E-02	(1.98 ± 0.02) E-03 ^a
Ru _{pta} _Cl2+w	0.00	
TS _{pta1_a}	18.95	
Ru _{pta} _Cl_w+Cl	3.31	
	7.98E-02	(3.33 ± 0.02) E-03 ^b
Ru _{pta} _Cl2+w	0.00	
TS _{pta1_d1}	18.72	
Int ₁	18.46	
TS _{pta1_d2}	20.59	
Ru _{pta} _Cl_w+Cl	4.12	
	4.72E-03 ^d	
Ru _{pta} _Cl_w+w	0.00	
TS _{pta2a}	26.49	
Ru _{pta} _w2+Cl	10.83	
	2.37E-07	(5.5 ± 0.2) E-02 ^b
Ru _{pta} _Cl_w+w	0.00	
TS _{pta2_d1_w}	19.90	
Int _{2_w}	17.90	
TS _{pta2_d2_w}	27.98	
Ru _{pta} _2w+Cl	6.23	
	1.87E-08 ^d	
Ru _{pta} _Cl_OH+w	0.00	
TS _{pta2_d1_OH}	11.88	
Int _{2_OH}	6.96	
TS _{pta2_d2_OH}	12.56	
Ru _{pta} _OH_w+Cl	4.58	
	2.90E+03 ^d	
Pt _{a2} _Cl2+w	0.00	
TS _{cis1}	23.86	
Pt _{a2} _Cl_w+Cl	5.24	
	1.99E-05	(1.9 ± 0.2)E-04 ^c
Pt _{a2} _Cl_w+w	0.00	
TS _{cis2}	28.95	
Pt _{a2} _2w+Cl	10.99	
	3.73E-09	
Pt _{a2} _Cl_OH+w	0.00	
TS _{cis2}	25.90	
Pt _{a2} _OH_w+Cl	10.51	
	6.94E-07	(2.3 ± 0.3)E-04 ^c

^aReference 19.

^bReference 88.

^cReference 89.

^d $k_1 k_2 / (k_1 + k_2)$ for subsequent reversible reactions.

8–11 kcal/mol. This feature can be explained by the fact that in the mono aqua reactant the remaining chloro ligand is more strongly bonded as follows from higher binding energy of the Ru–Cl in Table III (compare BE of 52 kcal/mol for monochloro reactant in the second hydration step with BE of 42 kcal/mol for dichloro-reactant in the first step). The same conclusion also follows from Table IV where the AIM critical points are displayed [corresponding Bond Critical Point (BCP) values of Ru–Cl are 0.065 versus 0.062 *e/a.u.*³ (Ref. 3)].

The higher extent of similarity between the RAPTA complex and cisplatin follows not only from a structural factor but

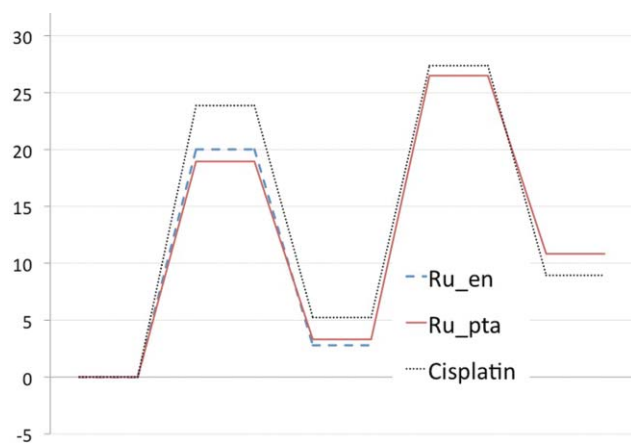


FIG. 1. Energy profile of pseudoassociative hydration reactions of $[\text{Ru}(\text{arene})(\text{en})\text{Cl}]^+$, $[\text{Ru}(\text{arene})(\text{pta})\text{Cl}_2]$, and $[\text{Pt}(\text{NH}_3)_2\text{Cl}_2]$ complexes at the B3LYP/6-31++G(2dp,2pd)/CPCM(UA0) level.

also from the shape of the reaction energy profile. In the case of cisplatin, the activation barrier of the first step is a little higher than in RAPTA (23 vs 19 kcal/mol) but otherwise the shape is more or less the same (energy of all the other stationary points on the reaction coordinate differs at most by 2 kcal/mol). However, one should keep in mind that the similarity deals only with the hydration reaction and (probably) does not concern the subsequent reactions since the role of arene ligand is believed to be important in stacking interactions with nucleobases in genomic code. This aspect was not considered in the study and it is not fully enlightened even *in vitro* and *in vivo* experiments at present. Our previous calculations⁷⁵ on this topic as well as results from other groups^{57,87} seem to confirm this assumption.

In the neutral or basic solutions the hydroxo ligand should be considered instead of the aqua ligand (for cisplatin the experimental pK_a is 5.5; calculated value ≈ 6.2 (Ref. 54) and analogous calculations for Ru_pta_wCl complex lead to estimation of ca 7.7 (Ref. 19). This leads to lower activation barrier (by about 3 kcal/mol) due to higher competition of negatively charged OH group in comparison with neutral aqua ligand. Moreover, in the case of RAPTA_OH complex the second dechlorination step cannot occur within the PAM mechanism. Instead, the direct dissociation mechanism was found with two lower reaction barriers (≈ 12 and 6 kcal/mol). The

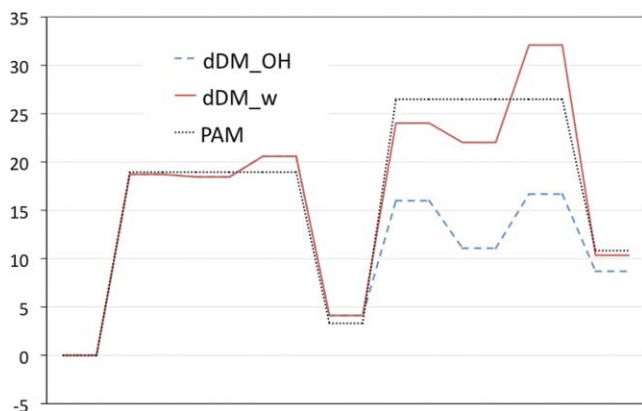


FIG. 2. Reaction coordinate for the dissociative mechanism of RAPTA dechlorination at the B3LYP/6-31++G(2dp,2pd)/CPCM level.

same dissociation mechanism was also determined for hydrated RAPTA complex in presence of aqua ligand. Here, the activation barriers were found 19 and 10 kcal/mol. It means that lower reaction barrier was also confirmed for dissociation mechanism in acidic and neutral solutions. The dDM pathway has practically the same activation energy for the first dechlorination reaction as PAM ($\Delta G_a^1 \approx 19$ kcal/mol). No dDM was found in cisplatin hydration.

C. Binding energies

Table III summarizes the stabilization and binding energies evaluated according to Eqs. (1) and (3), respectively. Two different kinds of stabilization energies are present. Besides standard definition (ΔE^{Stab}) based on Eq. (1) the other energy (ΔE^{Stex}) represents total coordination energy of the metal cation with the ligands fixed in their optimal positions in the given complex. The ΔE^{Stex} energy is determined according to Eq. (3) supposing E_L is energy of the metal cation and E_{rest} represents the frozen structure of all the ligands. In this way, mutual repulsion of the ligands is not included from the obtained value and this repulsion basically forms the main difference between both ΔE^{Stab} and ΔE^{Stex} values (besides deformation correction involved in ΔE^{Stab} value). As to deformation energies, it can be seen that the smallest values were obtained in the case of cisplatin where smallest number of ligands (small molecules—water and ammonia) is present. The largest deformations are in the Ru_en complexes mainly due to deformation of the en-ligand (about 5 kcal/mol). The deformation of the benzene ligand is ≈ 3 kcal/mol in the both Ru complexes. The repulsion energy of the ligands (as a $E^{\text{Stab}} - E^{\text{Stex}}$ difference) clearly shows the highest values in cisplatin complexes where values up to 30 kcal/mol can be seen. Substantially smaller values were gained in the RAPTA complexes and the smallest repulsion was determined in the Ru_en complexes since only one negatively charged ligand is present there.

Comparing the metal-am(m)ino binding energies, it can be noticed that the en ligand is slightly less coordinated in the Ru_en complex than amines in cisplatin. Confirmation of this fact can be observed from a comparison of BCP in Table IV where all the densities in BCP of Pt-N(H₃) are higher than 0.1 *e* a.u.⁻³ while the Ru-N(en) densities are always lower than this value. The BE of benzene is slightly higher in the Ru_en complex than in RAPTA which is in accord with the larger number of BCP's of the Ru-C bonds in the Ru_en complexes. In this case also smaller partial charge of Ru(II) cation of the RAPTA complexes (cf. Table V) can be responsible for the lower electrostatic cation- π system contribution. In these complexes it can be noticed that the pta ligand is coordinated with similar BE as both chloride ligands. Electrostatic enhancement of Ru-Cl bond is compensated by a larger coordination character of the Ru-P bond as follows from BCP analysis. The Ru-P bond has by about 50% higher electron density in the BCP (0.097 vs 0.063 in the Ru-Cl BCP).

D. Rate of hydration process

Activation barriers can give an estimation of the rate constants using Eyring's transition state theory [Eq. (4)].

TABLE III. Stabilization and binding energies of the ligands (in kcal/mol), a = NH₃, w = H₂O, ben = benzene, en and pta ligands are defined in the text. The calculations were done at the B3LYP/BS2/CPCM level.

	Stab	Stex	Repulsion	Deformation		
Ru_en_Cl+w	409.4	435.1	18.2	7.6		
TS_en	394.3	417.6	14.3	9.0		
Ru_en_w+Cl	403.3	426.7	15.0	8.4		
Ru_pta_Cl2+w	417.8	444.5	21.7	5.0		
TS_pta1a	397.4	422.9	19.2	6.3		
TS_pta1d1	387.1	414.9	17.4	6.1		
Int1	392.7	416.2	15.7	5.9		
TS_pta1d2	394.5	422.4	16.9	7.4		
Ru_pta_Cl_w+Cl	404.9	435.0	23.3	6.8		
Ru_pta_Cl_w+w	398.8	423.7	19.6	5.3		
TS_pta2a	378.3	403.4	18.4	6.6		
TS_pta2d1	369.6	408.8	11.1	6.4		
Int2	375.5	411.5	16.5	6.6		
TS_pta2d2	381.1	409.2	16.9	7.1		
Ru_pta_w2+Cl	385.7	414.6	21.4	7.5		
Ru_pta_Cl_OH+w	426.8	449.5	19.7	5.8		
TS_pta2d1+OH	418.3	433.4	18.3	6.5		
Int2_OH	414.7	428.3	13.1	6.9		
TS_pta2d2_OH	415.2	431.2	16.3	7.4		
Ru_pta_OH_w+Cl	422.1	445.8	22.9	7.8		
Pt_a2_Cl2+w	407.1	440.5	32.6	0.8		
TS_cis1	391.8	423.2	30.6	0.8		
Pt_a2_Cl_w+Cl	399.1	423.1	21.3	2.6		
Pt_a2_Cl_w+w	395.6	415.1	19.5	1.0		
TS_cis2	371.2	390.8	19.6	1.0		
Pt_a2_2w+Cl	385.7	398.9	13.3	2.7		
Pt_a2_Cl_OH+w	435.1	454.3	17.7	1.6		
TS_cis2_OH	413.5	443.0	28.3	1.2		
Pt_a2_OH_w+Cl	422.1	449.8	25.2	2.5		
	Cl		ben	en	w	
Ru_en_Cl+w	46.7		72.7	99.3	4.4	
TS_en	21.3		87.4	104.8	7.0	
Ru_en_w+Cl	19.2		81.5	110.0	34.1	
	Cl	Cl	ben	pta	w/h	w
Ru_pta_Cl2+w	42.0	42.0	59.1	42.0	5.2	
TS_pta1a	47.6	16.8	71.6	46.9	4.9	
TS_pta1d1	49.1	12.5	78.4	48.2	5.9	
Int1	51.2	5.6	92.7	53.6	5.6	
TS_pta1d2	48.1	5.8	90.9	50.1	4.6	
Ru_pta_Cl_w+Cl	46.6	16.7	65.7	45.8	31.4	
Ru_pta_Cl_w+w	51.7		67.1	45.8	30.0	10.4
TS_pta2a	22.7		81.8	47.9	21.0	13.5
TS_pta2d1	39		67.7	49.0	20.7	1.5
Int2	13.1		86.6	55.3	37.8	14.1
TS_pta2d2	8.4		93.8	52.4	26.4	12.4
Ru_pta_w2+Cl	20.1		76.2	51.4	24.0	38.8
Ru_pta_Cl_OH+w	12.0		73.6	52.9	24.1	17.1
TS_pta2d1+OH	26.6		57.1	37.8	67.5 ^a	9.0
Int2_OH	5.6		77.7	43.2	83.1 ^a	7.5
TS_pta2d2_OH	4.1		85.5	46.6	91.9 ^a	7.5
Ru_pta_OH_w+Cl	5.1		86.6	41.7	85.8 ^a	5.1
	Cl	Cl	NH3	NH3	w/h	w
Pt_a2_Cl2+w	48.7	48.7	54.8	54.8	7.7	
TS_cis1	15.0	53.8	54.1	51.1	3.4	
Pt_a2_Cl_w+Cl	19.7	57.8	59.4	66.8	42.9	

TABLE III. (Continued).

	Cl	Cl	NH3	NH3	w/h	w
Pt_a2_Cl_w+w		60.7	59.8	69.1	41.7	13.7
TS_cis2		27.7	62.3	72.6	37.0	7.8
Pt_a2_2w+Cl		28.8	73.2	73.2	45.9	45.9
Pt_a2_Cl_OH+w		50.6	54.8	51.8	89.4 ^a	10.4
TS_cis2_OH		12.1	53.1	50.1	86.8 ^a	10.1
Pt_a2_OH_w+Cl		18.2	54.4	62.6	84.5 ^a	40.1

^aHydroxo ligand.

Based on this equation, rate constants for pseudo-first order hydration process were evaluated and collected in the gray lines of Table II. According to these constants the fastest hydration in the first reaction step occurs in the case of RAPTA complex; hydration of the Ru_en complex is about one order of magnitude slower. Hydration of cisplatin is, according to our calculations, the slowest process.

Rate constants can be easily compared with experimental values. Recently published rate constants for hydra-

tion of RAPTA-C ($k_1=3.33 \pm 0.02 \times 10^{-3}$ and $k_2=5.5 \pm 0.2 \times 10^{-2} \text{ s}^{-1}$) can give a good estimation of hydration of structurally similar complexes of RAPTA-B.⁸⁸ Slightly lower rate constant ($k_{e1}=1.98 \pm 0.02 \times 10^{-2} \text{ s}^{-1}$) was obtained for hydration of Ru(arene)(en)Cl₂ complexes was obtained in Sadler's group.¹⁹ As to cisplatin hydration, several measurements were performed,⁸⁹⁻⁹³ estimating the k_{1c} constant between 5.2×10^{-5} and $1.9 \pm 0.2 \times 10^{-4} \text{ s}^{-1}$. Measurements of the second hydration step lead to the k_{2c}

TABLE IV. Critical points of all the M-L bonds (in e/a.u.³). The analyses were done at the B3LYP/B2/CPCM level.

	Ru-N1 ^a	Ru-N2	Ru-Cl	Ru-C ^b	Ru-O	
Ru_en_Cl+w	0.090	0.088	0.061	0.082		
TS_en	0.092	0.093	0.016	0.086	0.018	
Ru_en_w+Cl	0.091	0.092		0.082	0.068	
	Ru-P	Ru-Cl	Ru-Cl	Ru-C ^d	Ru-O	Ru-O
Ru_pta_Cl2+w	0.098	0.062	0.062	0.082		
TS_pta1a	0.097	0.067	0.014	0.090	0.017	
TS_pta1d1	0.096	0.075	0.007	0.089		
Int1	0.096	0.078		0.088		
TS_pta1d2	0.093	0.082		0.090		
Ru_pta_Cl_w+Cl	0.098	0.066		0.082	0.071	
Ru_pta_Cl_w+w	0.098	0.065		0.082	0.067	
TS_pta2a	0.096	0.017		0.089	0.064	0.023
TS_pta2d1	0.095	0.008		0.089	0.074	
Int2	0.093			0.089	0.086	
TS_pta2d2	0.091			0.089	0.072	
Ru_pta_w2+Cl	0.096			0.083	0.066	0.074
Ru_pta_Cl_OH+w	0.100	0.059		0.083	0.092	
TS_pta2d1+OH	0.093	0.010		0.089	0.119	
Int2_OH	0.093			0.089	0.132	
TS_pta2d2_OH	0.092			0.090	0.129	
Ru_pta_OH_w+Cl	0.097			0.082	0.099	0.068
	Pt-N ^c	Pt-N ^d	Pt-Cl	Pt-Cl	Pt-O	Pt-O ^e
Pt_a2_Cl2+w	0.117	0.117	0.086	0.085		
TS_cis1	0.124	0.118	0.086	0.038	0.043	
Pt_a2_Cl_w+Cl	0.126	0.116	0.088		0.093	
Pt_a2_Cl_w+w	0.113	0.125	0.087			0.088
TS_cis2	0.126	0.127	0.031		0.030	0.085
Pt_a2_2w+Cl	0.124	0.124			0.088	0.088
Pt_a2_Cl_OH+w	0.116	0.112	0.085			0.115
TS_cis2_OH	0.121	0.107	0.025		0.048	0.122
Pt_a2_OH_w+Cl	0.127	0.109			0.092	0.122

^aN atom involved in H-bond interactions.^bAveraged value of BCPs.^cN atom in equatorial plane of TS or in H-bond interactions.^dN atom in axial position of TS.^eO from hydroxo ligand.

TABLE V. Natural population analysis of the key atoms (in e). The analyses were done at the B3LYP/B2/CPCM level.

	Ru	Cl		N1	N2	O	Benzene ^a
Ru_en_Cl+w	0.394	-0.590		-0.802	-0.790	-1.027	0.493
TS_en	0.553	-0.838		-0.812	-0.808	-1.030	0.577
Ru_en_w+Cl	0.493	-0.869		-0.803	-0.787	-0.942	0.531
	Ru	Cl	Cl	P	O	O	Benzene ^a
Ru_pta_Cl2+w	0.095	-0.568	-0.561	1.153		-1.046	0.483
TS_pta1a	0.260	-0.544	-0.831	1.101		-1.032	0.568
TS_pta1d1	0.242	-0.512	-0.907	1.035		-1.014	0.625
Int1	0.233	-0.494	-0.951	1.013		-1.012	0.646
TS_pta1d2	0.234	-0.481	-0.948	1.010		-0.994	0.634
Ru_pta_Cl_w+Cl	0.200	-0.548	-0.880	1.131		-0.929	0.513
Ru_pta_Cl_w+w	0.204		-0.546	1.122	-0.935	-1.010	0.536
TS_pta2a	0.354		-0.796	1.065	-0.924	-1.030	0.639
TS_pta2d1	0.372		-0.855	1.006	-0.990	-0.896	0.674
Int2	0.390		-0.918	0.968	-0.992	-0.889	0.713
TS_pta2d2	0.398		-0.942	0.967	-0.998	-0.882	0.746
Ru_pta_w2+Cl	0.311		-0.858	1.094	-0.940	-0.907	0.593
Ru_pta_Cl_OH+w	0.206		-0.601	1.173	-1.034	-1.002	0.392
TS_pta2d1+OH	0.377		-0.912	1.031	-1.029	-0.966	0.519
Int2_OH	0.352		-0.968	0.995	-1.030	-0.926	0.554
TS_pta2d2_OH	0.359		-0.957	1.015	-0.995	-0.935	0.533
Ru_pta_OH_w+Cl	0.294		-0.916	1.118	-0.892	-1.014	0.440
	Pt	Cl	Cl	N	N	O	O ^b
Pt_a2_Cl2+w	0.542	-0.615	-0.613	-1.027	-1.030	-1.035	
TS_cis1	0.710	-0.607	-0.839	-1.026	-1.007	-1.016	
Pt_a2_Cl_w+Cl	0.659	-0.602	-0.833	-1.049	-0.999	-0.961	
Pt_a2_Cl_w+w	0.669		-0.600	-0.946	-0.894	-0.976	-0.891
TS_cis2	0.812		-0.818	-0.897	-0.889	-0.975	-0.892
Pt_a2_2w+Cl	0.782		-0.801	-0.903	-0.903	-0.911	-0.911
Pt_a2_Cl_OH+w	0.645		-0.627	-1.039	-1.034	-1.072	-1.106
TS_cis2_OH	0.795		-0.881	-1.056	-1.004	-1.000	-1.105
Pt_a2_OH_w+Cl	0.735		-0.848	-1.062	-0.999	-0.964	-1.113

^aSum of partial charges of all C and H atoms.^bO of hydroxo group.

value of $1.1 \pm 0.1 \times 10^{-4}$.^{89,92,94} It is probably not necessary to mention that the differences can be made by various experimental settings. While computational estimations of the rate constants for the first reaction steps are in acceptable agreement with measured data, calculated values for the second steps are substantially worse for cisplatin. In the RAPTA case, fairly good agreement was obtained for dissociation mechanism in neutral and acidic condition where aqua ligand is present. However, a different complex is considered as a reactant under the experimental conditions where authors⁸⁸ expect a hydration of the neutral complex with the negatively charged hydroxo group instead of the aqua ligand. Calculations with the neutral RAPTA complex lead to very fast reaction cause with rate constant $k_2 \approx 3 \times 10^3 \text{ s}^{-1}$. The explanation can be searched in stronger Ru-OH coordination which represents a higher competition to the Ru-Cl interaction and facilitates a release of chloride particle and its replacement by second aqua ligand.

E. Properties of electron density

To complete the comparison of the hydration reactions of the chosen metal complexes several analyses were performed

for all the stationary points on the reaction coordinates. Electron densities of the most important BCPs are collected in Table IV and charges obtained in the framework of natural population analysis are summarized in Table V.

Correlation between BEs and BCPs was already discussed above. Nevertheless, it is worth to note that in the RAPTA complexes, only three BCPs of the Ru-C bonds were found (with exception of the reaction product of the second step where already two relatively weaker aqua ligands are coordinated so that a stronger benzene coordination can occur). On the other hand in all the Ru_en complexes four BCPs were found.

It can be also mentioned that in accord with higher coordination, lower BCP densities for metal coordination of replacing ligands were obtained in TSs of Ru(II) complexes (both Ru-O and Ru-Cl bonds have $\approx 0.02 \text{ e/a.u.}^3$) in comparison with Pt(II) complexes (where values of 0.04 were acquired). Basically all BCP densities are visibly higher in cisplatin complexes in comparison with Ru(II) complexes due to lower ligand competition. The same conclusion can be also drawn from the BE decomposition.

Results of the NPA analysis for individual metal complexes are summarized in Table V. From partial charges of

metal cations it follows that while the charge of the Pt atom varies between 0.55 and 0.8 e in dependence on donation strength of coordinated ligands, the Ru charges of the Ru_{en} complexes lie in the range of 0.4–0.55 e . The lowest metal charges were found in the RAPTA complexes with values from 0.1 to 0.35 e . (In analogous analysis at the MP2/6-31++G(d,p) computational level even negative values were obtained for most of the RAPTA complexes.)

From Table V an estimation of electrostatic strengthening of the coordination-covalent bonds can be judged based on the Coulomb law. Since the covalent character of the bond basically follows from a BCP value, at least, an approximate estimation of the prevailing contributions to the given coordination can be ensued from Tables IV and V.

III. CONCLUSIONS

In this study hydration reactions and electronic properties of three different organometallic complexes were subject to quantum chemical calculations.

All the complexes were optimized at the B3LYP/6-31G(d)/CPCM level where metal atoms were treated with Stuttgart effective core potentials (ECPs). The SP energy calculations and determination of electronic properties were performed at the B3LYP/6-311++G(2df,2pd)/CPCM level.

It was found that our hydration model works fairly well for the replacement of the first chloride by water molecule—acceptable agreement for both Gibbs free energies and rate constants was obtained. In the second hydration step a visibly underestimated value of cisplatin rate constant can be noticed. On the contrary in direct dissociation mechanism in basic environment too fast dechlorination is predicted due to more strongly coordinated hydroxo ligand.

For the comparison of the hydration reaction of all three complexes, stabilization and binding energies together with BCP electron densities and NPA partial charges were evaluated in all stationary points of the reaction coordinates. Estimated BEs confirm that the benzene ligand is relatively weakly bonded assuming the fact that arene ligand occupies three and four coordination positions of the Ru(II) cation in the RAPTA and Ru_{en} complexes, respectively. In this way, this coordination has similar strength like coordination of the aqua ligand. The strongest coordination of the chloride ligand occurs in cisplatin complex in accord with the lowest rate constants (the highest activation barrier). The BE of the Ru–Cl bond in the Ru_{en} complex is by about 2 kcal/mol lower, which correlates well with faster hydration course in this complex and the fastest activation reaction in the RAPTA case is connected with the most “loosely” interacting chloride. From the point of BEs of chloride ligands, the higher barriers in the second reaction step are not surprising.

Basically all the relations in binding energies correlate with NPA partial charges and AIM analysis of BCPs as follows from the discussion above.

ACKNOWLEDGMENTS

Authors are grateful for support provided by the MŠMT Project MSM 0021620835 and by GA ČR Project

P205/10/0228 (JVB, ZF) and MŠMT Project Nos. ME10149 (JVB) and ME09062(ZCh).

Calculations were partly performed at the Metacentrum. The access to this supercomputer center provided under the research intent MSM6383917201 is highly appreciated.

- ¹J. Reedijk and J. M. Teuben, in *Cisplatin*, edited by B. Lippert (Wiley-VCH, Weinheim, 1999).
- ²A. W. Prestayko, J. C. D'Aoust, B. F. Issell, and S. T. Crooke, *Cancer Treat. Rev.* **6**, 17 (1979).
- ³J. R. Rubin, T. P. Haromy, and M. Sundaralingam, *Acta Crystallogr. Sect. C: Cryst. Struct. Commun.* **47**, 1712 (1991).
- ⁴J. M. Asara, J. S. Hess, E. Lozada, K. R. Dunbar, and J. Allison, *J. Am. Chem. Soc.* **122**, 8 (2000).
- ⁵D. M. L. Goodgame, C. A. Omahoney, C. J. Page, and D. J. Williams, *Inorg. Chim. Acta* **175**, 141 (1990).
- ⁶N. Katsaros and A. Anagnostopoulou, *Crit. Rev. Oncol. Hematol.* **42**, 297 (2002).
- ⁷K. Sorasaene, J. R. Galan-Mascaros, and K. R. Dunbar, *Inorg. Chem.* **41**, 433 (2002).
- ⁸M. Uudsemaa and T. Tamm, *Chem. Phys. Lett.* **342**, 667 (2001).
- ⁹F. Caruso and M. Rossi, *Mini Rev. Med. Chem.* **4**, 49 (2004).
- ¹⁰B. M. zu Berstenhorst, G. Erker, G. Kehr, J. C. Wasilke, J. Muller, H. Redlich, and J. Pyplo-Schnieders, *Eur. J. Inorg. Chem.* **1**, 92 (2005).
- ¹¹M. Hartmann, A. Robert, V. Duarte, B. K. Keppler, and B. Meunier, *J. Biol. Inorg. Chem.* **2**, 427 (1997).
- ¹²P. Lincoln and B. Norden, *J. Phys. Chem. B* **102**, 9583 (1998).
- ¹³K. Gisselfaelt, P. Lincoln, B. Norden, and M. Jonsson, *J. Phys. Chem. B* **104**, 3651 (2000).
- ¹⁴J.-G. Liu, B.-H. Ye, Q.-L. Zhang, X.-H. Zou, Q.-X. Zhen, X. Tian, and L.-N. Ji, *J. Biol. Inorg. Chem.* **5**, 119 (2000).
- ¹⁵J. Malina, O. Novakova, B. K. Keppler, E. Alessio, and V. Brabec, *J. Biol. Inorg. Chem.* **6**, 435 (2001).
- ¹⁶A. Kueng, T. Pieper, R. Wissiack, E. Rosenberg, and B. K. Keppler, *J. Biol. Inorg. Chem.* **6**, 292 (2001).
- ¹⁷H. M. Chen, J. A. Parkinson, R. E. Moris, and P. J. Sadler, *J. Am. Chem. Soc.* **125**, 173 (2003).
- ¹⁸O. Novakova, H. Chen, O. Vrana, A. Rodger, P. J. Sadler, and V. Brabec, *Biochemistry* **42**, 11544 (2003).
- ¹⁹F. Wang, H. M. Chen, S. Parsons, L. D. H. Oswald, J. E. Davidson, and P. J. Sadler, *Chem. Eur. J.* **9**, 5810 (2003).
- ²⁰V. G. Vaidyanathan and B. U. Nair, *J. Inorg. Biochem.* **91**, 405 (2002).
- ²¹B. Serli, E. Zangrando, T. Gianferrara, C. Scolaro, P. J. Dyson, A. Bergamo, and E. Alessio, *Eur. J. Inorg. Chem.* **17**, 3423 (2005).
- ²²T. Bugarcic, A. Habtemariam, J. Stepankova, P. Heringova, J. Kasparikova, R. J. Deeth, R. D. L. Johnstone, A. Prescimone, A. Parkin, S. Parsons, V. Brabec, and P. J. Sadler, *Inorg. Chem.* **47**, 11470 (2008).
- ²³S. S. N. Kraft, C. Bischof, A. Loos, S. Braun, N. Jafarova, and U. Schatzschneider, *J. Inorg. Biochem.* **103**, 1126 (2009).
- ²⁴A. K. Renfrew, A. D. Phillips, E. Tapavicza, R. Scopelliti, U. Rothlisberger, and P. J. Dyson, *Organometallics* **28**, 5061 (2009).
- ²⁵A. F. A. Peacock, A. Habtemariam, R. Fernandez, V. Walland, F. P. A. Fabbiani, S. Parsons, R. E. Aird, D. I. Jodrell, and P. J. Sadler, *J. Am. Chem. Soc.* **128**, 1739 (2006).
- ²⁶A. Dorcier, P. J. Dyson, C. Gossens, U. Rothlisberger, R. Scopelliti, and I. Tavernelli, *Organometallics* **24**, 2114 (2005).
- ²⁷R. Wysokinski and D. Michalska, *J. Comput. Chem.* **22**, 901 (2001).
- ²⁸P. N. Pavankumar, P. Seetharamulu, S. Yao, J. D. Saxe, D. G. Reddy, and F. H. Hausheer, *J. Comput. Chem.* **20**, 365 (1999).
- ²⁹H. F. Dos Santos, B. L. Marcial, C. F. De Miranda, L. A. S. Costa, and W. B. De Almeida, *J. Inorg. Biochem.* **100**, 1594 (2006).
- ³⁰L. A. S. Costa, W. R. Rocha, W. B. De Almeida, and H. F. Dos Santos, *J. Inorg. Biochem.* **99**, 575 (2005).
- ³¹Z. Chval, M. Sip, and J. V. Burda, *J. Comput. Chem.* **29**, 2370 (2008).
- ³²M. Zeizinger, J. V. Burda, J. Šponer, V. Kapsa, and J. Leszczynski, *J. Phys. Chem. A* **105**, 8086 (2001).
- ³³J. Raber, C. Zhu, and L. A. Eriksson, *J. Phys. Chem.* **109**, 11006 (2005).
- ³⁴A. Robertazzi and J. A. Platts, *J. Comput. Chem.* **25**, 1060 (2004).
- ³⁵Y. Zhang, Z. Guo, and X.-Z. You, *J. Am. Chem. Soc.* **123**, 9378 (2001).
- ³⁶J. V. Burda, M. Zeizinger, and J. Leszczynski, *J. Comput. Chem.* **29**, 907 (2005).

- ³⁷J. V. Burda, M. Zeizinger, and J. Leszczynski, *J. Chem. Phys.* **120**, 1253 (2004).
- ³⁸G. Schroeder, J. Kozelka, M. Sabat, M.-H. Fouchet, R. Beyerle-Pfinur, and B. Lippert, *Inorg. Chem.* **35**, 1647 (1996).
- ³⁹J. F. Lopes, V. S. D. Menezes, H. A. Duarte, W. R. Rocha, W. B. De Almeida, and H. F. Dos Santos, *J. Phys. Chem. B* **110**, 12047 (2006).
- ⁴⁰J. V. Burda and J. Leszczynski, *Inorg. Chem.* **42**, 7162 (2003).
- ⁴¹M. Zeizinger, J. V. Burda, and J. Leszczynski, *Phys. Chem. Chem. Phys.* **6**, 3585 (2004).
- ⁴²M.-H. Baik, R. A. Friesner, and S. J. Lippard, *J. Am. Chem. Soc.* **124**, 4495 (2002).
- ⁴³M. H. Baik, R. A. Friesner, and S. J. Lippard, *Inorg. Chem.* **42**, 8615 (2003).
- ⁴⁴M. H. Baik, R. A. Friesner, and S. J. Lippard, *J. Am. Chem. Soc.* **125**, 14082 (2003).
- ⁴⁵M. Eriksson, M. Leijon, C. Hiort, B. Norden, and A. Graeslund, *Biochemistry* **33**, 5031 (1994).
- ⁴⁶M. Coll, S. E. Sherman, D. Gibson, S. J. Lippard, and A. H.-J. Wang, *J. Biomol. Struct. Dyn.* **8**, 315 (1990).
- ⁴⁷K. Spiegel, U. Rothlisberger, and P. Carloni, *J. Phys. Chem. B* **108**, 2699 (2004).
- ⁴⁸A. Robertazzi and J. A. Platts, *Inorg. Chem.* **44**, 267 (2005).
- ⁴⁹Z. Chval and M. Šíp, *J. Mol. Struct.: THEOCHEM* **532**, 59 (2000).
- ⁵⁰Z. Chval and M. Šíp, *Collect. Czech. Chem. Commun.* **68**, 1105 (2003).
- ⁵¹M. Pavelka, M. Šimánek, J. Šponer, and J. V. Burda, *J. Phys. Chem. A* **110**, 4795 (2006).
- ⁵²D. V. Deubel, *J. Am. Chem. Soc.* **126**, 5999 (2004).
- ⁵³T. Zimmermann, M. Zeizinger, and J. V. Burda, *J. Inorg. Biochem.* **99**, 2184 (2005).
- ⁵⁴T. Zimmermann and J. V. Burda, *J. Chem. Phys.* **131**, 135101 (2009).
- ⁵⁵T. Zimmermann, Z. Chval, and J. V. Burda, *J. Phys. Chem. B* **113**, 3139 (2009).
- ⁵⁶T. Zimmermann and J. V. Burda, *Dalton Trans.* **39**(5), 1295 (2010).
- ⁵⁷C. Gossens, I. Tavernelli, and U. Rothlisberger, *Chimia* **59**, 81 (2005).
- ⁵⁸D. V. Deubel and J. K. C. Lau, *Chem. Commun.* (23), 2451 (2006).
- ⁵⁹J. C. Chen, L. M. Chen, S. Y. Liao, K. Zheng, and L. N. Ji, *Dalton Trans.* (32), 3507. (2007).
- ⁶⁰J. C. Chen, L. M. Chen, S. Y. Liao, K. C. Zheng, and L. N. Ji, *J. Mol. Struct.: THEOCHEM* **901**, 137 (2009).
- ⁶¹J. C. Chen, L. M. Chen, S. Y. Liao, K. C. Zheng, and L. N. Ji, *Phys. Chem. Chem. Phys.* **11**, 3401 (2009).
- ⁶²J. C. Chen, L. M. Chen, L. C. Xu, K. C. Zheng, and L. N. Ji, *J. Phys. Chem. B* **112**, 9966 (2008).
- ⁶³C. Gossens, A. Dorcier, P. J. Dyson, and U. Rothlisberger, *Organometallics* **26**, 3969 (2007).
- ⁶⁴C. Gossens, I. Tavernelli, and U. Rothlisberger, *J. Phys. Chem. A* **113**, 11888 (2009).
- ⁶⁵R. Aird, J. Cummings, A. Ritchie, M. Muir, R. Morris, H. Chen, P. Sadler, and D. Jodrell, *Br. J. Cancer* **86**, 1652 (2002).
- ⁶⁶S. J. Berners-Price, L. Ronconi, and P. J. Sadler, *Prog. Nucl. Magn. Reson. Spectrosc.* **49**, 65 (2006).
- ⁶⁷H. Chen, J. A. Parkinson, S. Parsons, R. A. Coxal, R. O. Gould, and P. Sadler, *J. Am. Chem. Soc.* **124**, 3064 (2002).
- ⁶⁸J. Kašpárková, F. S. Mackay, V. Brabec, and P. J. Sadler, *J. Biol. Inorg. Chem.* **8**, 741 (2003).
- ⁶⁹A. Habtemariam, M. Melchart, R. Fernandez, S. Parsons, I. D. H. Oswald, A. Parkin, F. P. A. Fabbiani, J. E. Davidson, A. Dawson, R. E. Aird, D. I. Jodrell, and P. J. Sadler, *J. Med. Chem.* **49**, 6858 (2006).
- ⁷⁰F. Y. Wang, A. Habtemariam, E. P. L. Van Der Geer, R. Fernandez, M. Melchart, R. J. Deeth, R. Aird, S. Guichard, F. P. A. Fabbiani, P. Lozano-Casal, I. D. H. Oswald, D. I. Jodrell, S. Parsons, and P. J. Sadler, *Proc. Natl. Acad. Sci. U.S.A.* **102**, 18269 (2005).
- ⁷¹A. B. Chaplin, C. Fellay, G. Laurency, and P. J. Dyson, *Organometallics* **26**, 586 (2007).
- ⁷²C. A. Vock and P. J. Dyson, *Z. Anorg. Allg. Chem.* **633**, 640 (2007).
- ⁷³K. Gkionis, J. A. Platts, and J. G. Hill, *Inorg. Chem.* **47**, 3893 (2008).
- ⁷⁴R. E. Morris, R. E. Aird, P. D. Murdoch, H. M. Chen, J. Cummings, N. D. Hughes, S. Parsons, A. Parkin, G. Boyd, D. I. Jodrell, and P. J. Sadler, *J. Med. Chem.* **44**, 3616 (2001).
- ⁷⁵Z. Futera, J. Klenko, J. E. Šponer, J. Šponer, and J. V. Burda, *J. Comput. Chem.* **30**, 1758 (2009).
- ⁷⁶R. F. W. Bader, *Atoms in Molecules: A Quantum Theory* (Oxford University, Oxford, 1990).
- ⁷⁷C. S. Allardyce, P. J. Dyson, D. J. Ellis, and S. L. Heath, *Chem. Commun.* 1396 (2001).
- ⁷⁸C. S. Allardyce, P. J. Dyson, D. J. Ellis, P. A. Salter, and R. Scopelliti, *J. Organomet. Chem.* **668**, 35 (2003).
- ⁷⁹A. Klamt, *J. Phys. Chem.* **99**, 2224 (1995).
- ⁸⁰A. Klamt and G. Schuurmann, *J. Chem. Soc., Perkin Trans.* **2** (5), 799 (1993).
- ⁸¹D. Andrae, U. Haussermann, M. Dolg, H. Stoll, and H. Preuss, *Theor. Chim. Acta* **77**, 123 (1990).
- ⁸²A. Bergner, M. Dolg, W. Kuechle, H. Stoll, and H. Preuss, *Mol. Phys.* **80**, 1431 (1993).
- ⁸³J. V. Burda, M. Zeizinger, J. Šponer, and J. Leszczynski, *J. Chem. Phys.* **113**, 2224 (2000).
- ⁸⁴T. A. Keith AIMAll (Version 10.11.24) 2010 (aim.tkgristmill.com).
- ⁸⁵E. D. Glendening, J. K. Badenhoop, A. E. Reed, J. E. Carpenter, J. A. Bohmann, C. M. Morales, and F. Weinhold, *NBO 5.0* University of Wisconsin, Madison (2001).
- ⁸⁶B. Cordero, V. Gómez, A. E. Platero-Prats, M. Revés, J. Echeverría, E. Cremades, F. Barragán, and S. Alvarez, *Dalton Trans.* **21**, 2832 (2008).
- ⁸⁷A. E. Egger, C. G. Hartinger, A. K. Renfrew, and P. J. Dyson, *J. Biol. Inorg. Chem.* **15**, 919 (2010).
- ⁸⁸C. Scolaro, C. G. Hartinger, C. S. Allardyce, B. K. Keppler, and P. J. Dyson, *J. Inorg. Biochem.* **102**, 1743 (2008).
- ⁸⁹J. Arpalahti, M. Mikola, and S. Mauristo, *Inorg. Chem.* **32**, 3327 (1993).
- ⁹⁰K. Hindmarsh, D. A. House, and M. M. Turnbull, *Inorg. Chim. Acta* **257**, 11 (1997).
- ⁹¹J.-L. Jestin, B. Lambert, and J.-C. Chottard, *J. Biol. Inorg. Chem.* **3**, 515 (1998).
- ⁹²E. Segal-Bendirdjian, P. Brehin, B. Lambert, A. Laouisi, J. Kozelka, M. Barreau, F. Lavallo, J. B. LePecq, and J.-C. Chottard, *Platinum and Other Metal Coordination Compounds in Cancer Chemotherapy* (Plenum, New York, 1991).
- ⁹³D. P. Bancroft, C. A. Lepre, and S. J. Lippard, *J. Am. Chem. Soc.* **112**, 6860 (1990).
- ⁹⁴N. P. Johnson, J. D. Hoeschele, and R. O. Rahn, *Chem. Biol. Interact.* **30**, 151 (1980).

Modeling the RNA 2'OH Activation: Possible Roles of Metal Ion and Nucleobase as Catalysts in Self-Cleaving Ribozymes

Zdeněk Chval,^{*,†,§} Daniela Chvalová,[‡] and Fabrice Leclerc^{*,§}

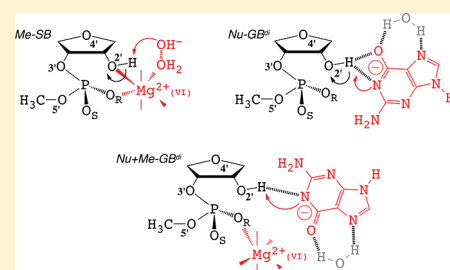
[†]Department of Laboratory Methods and Information Systems, Faculty of Health and Social Studies, University of South Bohemia, J. Boreckého 27, 370 11 České Budějovice, Czech Republic

[‡]Department of Applied Chemistry, Faculty of Agriculture, University of South Bohemia, Branišovská 31, 370 05, České Budějovice, Czech Republic

[§]Laboratoire ARN, RNP, structure-fonction-maturation, Enzymologie Moléculaire et Structurale (AREMS), UMR 7214 CNRS-UHP Nancy 1, Faculté des Sciences et Technologies, B.P. 70239, 54506 Vandoeuvre-lès-Nancy, France

Supporting Information

ABSTRACT: The RNA 2'OH activation as taking place in the first chemical step of self-cleaving ribozymes is studied theoretically by DFT and MP2 methods using a continuum solvation model (CPCM). The reaction of proton transfer is studied in the presence of two kinds of catalysts: a fully hydrated metal ion (Mg^{2+}) or partially hydrated nucleobase (guanine), taken separately or together leading to three different modes of activation. The metal ion is either directly bound (inner-sphere) or indirectly bound (outer-sphere) to the 2'OH group and a hydroxide ion acts as a general or specific base; the nucleobase is taken in anionic or in neutral enol-tautomeric forms playing itself the role of general base. The presence of a close metal ion (outer-sphere) lowers the pK_a value of the 2'OH group by several log units in both metal-ion and nucleobase catalysis. The direct metal coordination to the 2'OH group (inner-sphere) further stabilizes the developing negative charge on the nucleophile. The switching from the inner-sphere to the outer-sphere coordination appears to be driven by the energy cost for reorganizing the first coordination shell rather than by the electrostatic repulsion between the ligands. The metal-ion catalysis is more effective with a specific base in the dianionic mechanism. On the other hand, the nucleobase catalysis is more effective in the monoanionic mechanism and in the presence of a metal ion acting as a cofactor through nonspecific electrostatic interactions. The results establish a baseline to study the possible roles of metal and nucleobase catalysts and their environment in more realistic models for self-cleaving ribozymes.



INTRODUCTION

Natural RNA enzymes catalyze phosphodiester autocleavage reactions to give products with 5'-hydroxyl and 2'-3'-cyclic phosphate termini or 5'-phosphate and 3'-hydroxyl termini: a chemical signature from self-cleaving or self-splicing ribozymes, respectively. In both types of ribozymes, the cleavage reaction proceeds through a S_N2 -type in-line attack mechanism with an inversion of the stereochemical configuration of the nonbridging oxygen atoms about the scissile phosphorus atom. The S_N2 -type in-line mechanism involves a trigonal bipyramidal transition state that is formed after the nucleophilic attack (once the nucleophile is activated) on the phosphorus and before the departure of the leaving group. From the data accumulated on several ribozymes, it was suggested in review articles that self-cleaving and self-splicing ribozymes employ distinct catalytic strategies that rely on metal ions or nucleobases as catalysts, respectively.^{1–3} The active site of self-splicing ribozymes has a higher charge density because of the presence of an additional exogenous or endogenous nucleotide cofactor (a guanosine in group-I introns or an adenosine in group-II introns). It might explain the requirement for divalent metal ions in a catalytic strategy based on a two-metal-ion mechanism in group I[†] or group II self-splicing

introns.¹ In self-cleaving ribozymes, the role of nucleobases as catalysts has been generalized, although they may intervene in very different ways³ including in a cooperative way with metal ions.⁵

The two major steps of the reaction are (1) the phosphoryl transfer resulting from the nucleophilic attack and (2) the proton transfer to the 5'-oxygen leaving group. Not only the departure of the leaving group but also the nucleophilic attack involve some acid/base catalysis. A proton transfer is involved both in facilitating the departure of the leaving group and in activating the attacking nucleophile (Figure 1). In the nonenzymatic reaction, the catalysis may proceed by a specific acid/base catalysis (dianionic mechanism) or a general acid/base catalysis (monoanionic mechanism) where one of the phosphate oxygens can operate as an internal base (Figure 1A). In the enzymatic reactions, the nucleophile is either an internal 2'-hydroxyl in self-cleaving ribozymes or an external hydroxyl in self-splicing ribozymes that can be a 3'-hydroxyl (group I introns) or a 2'-hydroxyl (group II introns).

Received: January 29, 2011

Revised: August 6, 2011

Published: August 08, 2011

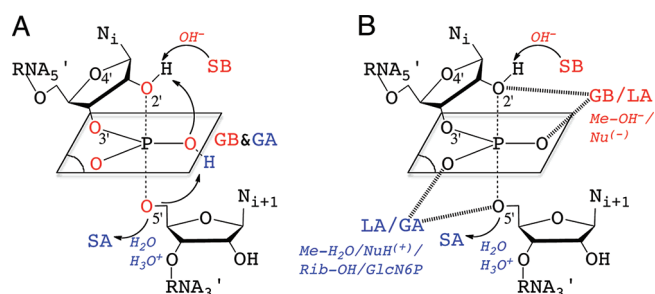


Figure 1. Acid/base activations of the 5'-oxygen leaving group and 2'-oxygen nucleophile in the catalysis by self-cleaving ribozymes: (A) nonenzymatic reaction; (B) enzymatic reaction. Abbreviations: SB, specific base; GB, general base; GA, general acid; SA, specific acid; Rib, ribose; Nu, nucleobase; Me, metal.

Table 1. Activation Modes of the Nucleophile and Leaving Group Associated with Proton Transfers^a

ribozyme	2'-hydroxyl deprotonation	5'-oxygen protonation
hammerhead	Nu-GB(G12 ⁻) ³⁴	Me-GA/Rib2'-OH-GA-(Mg ²⁺ /H ₂ O & G8-OH) ²⁰
	Me-GB(Mg ²⁺ /OH ⁻) ^{11,13,15}	
	Me-SB(Mg ²⁺ & OH ⁻) ⁵⁵	
hairpin	Nu-GB(G8 ⁻) ⁵⁶⁻⁵⁸	Nu-GA(A38H ⁺) ⁵⁶⁻⁵⁸
	Nu-SB(G8 & OH ⁻) ^{16,59,60}	Nu-SA(A38 & H ₂ O) ^{16,59,60}
HDV	Nu-GB(C75) ^{22,61}	Me-GA(Mg ²⁺ /H ₂ O) ^{22,61}
		Me-SA(Mg ²⁺ /H ₂ O)
	Me-GB(Mg ²⁺ /OH ⁻) ^{21,62-64}	Nu-GA(C75H ⁺) ^{21,62-64}
	Me-SB(Mg ²⁺ /OH ⁻) ⁶⁴	
VS	Nu-GB(G638 ⁻ /A756) ^{65,66}	Nu-GA(A756) ^{65,66}
glmS	Nu-GB(G33) ^{37,67}	Glc*-GA(GlcN6PH ⁺) ^{37,67}

^a Me: metal ion, Nu: nucleobase, Rib: ribose, GA: general acid, GB: general base, SA: specific acid, SB: specific base, Glc: glucosamine-6-phosphate.

A general or specific base catalyst can activate the nucleophile by removal of the proton from the hydroxyl group (Figure 1B). Similarly, a general or specific acid can facilitate the departure of the 5'-oxygen leaving group. Among the self-cleaving ribozymes studied (Hammerhead, Hairpin, HDV, VS, glmS), different catalytic strategies have been proposed.^{2,6} Although these strategies may be reduced to four basic ways to promote the reaction,⁷ there is still a large diversity of catalysts that may play similar roles depending on the organization and dynamics of the active site. We can classify the catalysts in different families, whether they act as general/specific acid or base and whether they are metal ion or nucleobase. As summarized in Table 1, all eight possible combinations are represented in the models proposed and are supported by some experimental data. However, metal ions are associated with either general or specific acid/base whereas nucleobases are more tightly combined as general acid or base. In the case of the hairpin and HDV ribozymes, the experimental data are consistent with either specific or general acid/base. In the hairpin ribozyme, nucleobases are the only catalysts. On the other hand, both metal ions and nucleobases are supported as catalysts in the HDV ribozyme. Opposite models were proposed depending on the roles assigned to the nucleobase (C75) and the metal ion (Mg²⁺) as base and acid, respectively or vice versa.

The nucleophile activation through the 2'-hydroxyl deprotonation is generally considered as minor because the chemical process itself is not rate-determining in the overall reaction. Besides, the possible interference with induced conformational changes related to solvent effects or presence of divalent metal ions⁸⁻¹⁰ makes it difficult to evaluate precisely the energetics of this step in the reaction mechanism. A first and simple approach is to study the elementary chemical processes associated with the nucleophile activation in solution, excluding the influence of the active site and its environment. Theoretical approaches are particularly appropriate to study the energetics of the reaction and provide a baseline for the evaluation of the contributions coming from the active site preorganization and reorganization. The extension of the study to the full ribozymes would then allow us to evaluate the influence of the active site and the catalytic efficiency resulting from their molecular evolution.

In the models proposed from theoretical calculations, different activation modes have been examined depending on the proposed reaction mechanism. All the activation modes were not fully or exhaustively explored (Figure 2). Most of the studies based on classical QM approaches systemically neglect the contributions from the metal binding to the ribose-phosphate moiety and the rearrangements associated with changes of metal coordinations occurring before the deprotonation (Figure 2A). They were also initially focused on minimalist models of self-cleaving (hammerhead) ribozymes and a general acid/base catalysis with metal ions as unique catalysts (Figure 2C).¹¹⁻¹⁵ Other activation modes using nucleobases as catalysts have been studied more recently using hybrid QM/MM approaches applied to the hairpin,^{16,17} hammerhead,¹⁸⁻²⁰ and HDV^{21,22} ribozymes (Figure 2B,F). The comparison of the results obtained using QM/MM or QM approaches, including (or not) the environment of the active site from the ribozyme structures, will be valuable to evaluate the influence of the active site reorganizations on the catalytic efficiency. However, the available data are currently too limited for such comparison. In the hammerhead ribozyme for example, the nucleophile activation is skipped in the QM/MM studies and the nucleophile is usually considered as already activated.²³

Using DFT methods, the activation barriers for the nonenzymatic and uncatalyzed reaction of activation have been calculated by Boero et al.¹² and Lopez et al.¹⁴ with a pretty good accordance giving a Gibbs free energy barrier for the nucleophile activation between 28 and 30 kcal/mol (depending on the sugar pucker) in the case of the GB^{mono} activation mode (Figure 1A). The presence of metal catalysts and their influence on the energy barrier has been studied using minimalist QM models in nonenzymatic reactions (Figure 2B,C).^{11,13,15} The presence of a metal ion close to the 2'-oxygen contributes to lowering the energy barrier even more when the metal ion is directly coordinated (Me-GB^{mono}: Figure 2B).¹² Furthermore, the presence of a second noncatalyst metal ion, in the Me-GB^{mono} activation mode, has a cooperative effect.¹³ A cooperative effect between a nucleobase and a metal ion was also suggested recently in the nucleophile activation of the hammerhead ribozyme,⁵ but no QM study on such model has been done yet (example: Figure 2G). On the other hand, the activation barrier for the nucleophile activation by a nucleobase has been calculated for the hairpin ribozyme¹⁶ but only for the monoanionic mechanism (Figure 2F).

In none of the self-cleaving ribozymes is the nucleophile activation the rate-limiting step, but the activation barrier may be underestimated when, for example, the energy barrier for

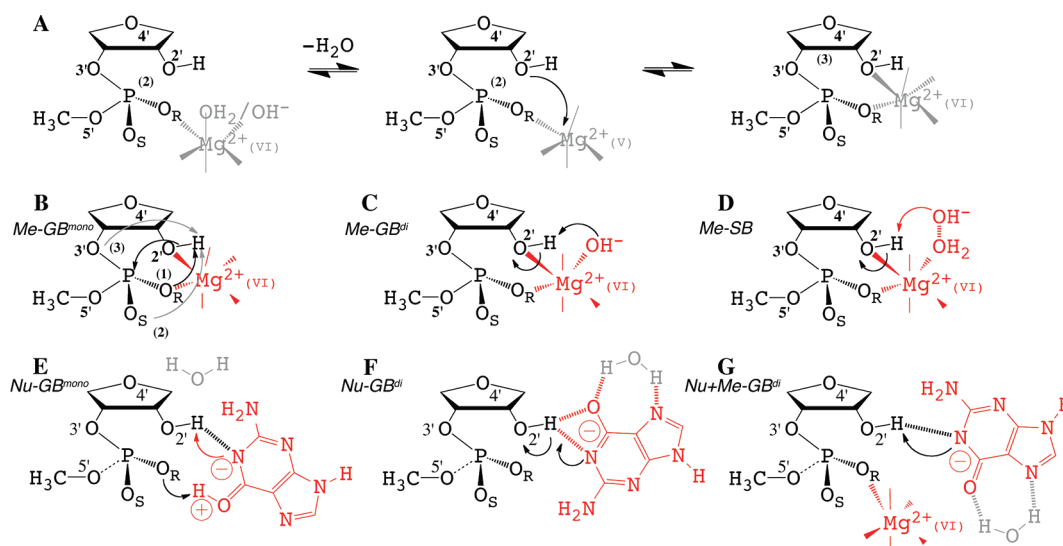


Figure 2. Activation modes of the 2'OH nucleophile. (A) Coordination change step by inner-sphere coordination to the 2'-oxygen. (B) Activation by a general base through an internal proton transfer (monoanionic mechanism). (C) Activation by a general base through a metal OH⁻ ligand (dianionic mechanism). (D) Activation by a specific base through a OH⁻ ligand. (E) Activation by a general base: a nucleobase in a tautomeric form (monoanionic mechanism). (F) Activation by a general base: a nucleobase in an ionized form (dianionic mechanism). (G) Activation by a general base: a nucleobase in an ionized form assisted by a metal.

going from a loosely bound to a tightly bound metal to the 2'OH (outer-sphere to inner-sphere coordination) in the Me-GB or Me-SB activation modes is neglected. Thus, one may misinterpret the comparison of role and influence of different catalysts when trying to predict the more favorable reaction mechanisms.

In the current study, we describe and analyze the reaction mechanisms for a selection of four different activation modes: Me-GB, Me-SB, Nu-GB, and Me+Nu-GB (Figure 2). The first three activation modes correspond to the more representative supported models in self-cleaving ribozymes, i.e., Me-GB, Me-SB and Nu-GB (Table 1); the last one corresponds to a new cooperative model between a metal ion and a nucleobase (Me+Nu-GB). In the case of Me-GB or Me-SB modes, the rearrangements necessary for metal coordination (preactivation) have also been taken into account. For the sake of comparison between mono- and dianionic mechanisms on the one hand and between general or specific base catalysis on the other hand, activation modes studied previously (Figure 2C,F) have been evaluated as well at the same level of theory. In the case of Me-GB^{mono}, both paths involving the proton transfer on either of the two nonbridging oxygens are well-known but in different contexts: the nonenzymatic and uncatalyzed reaction,¹⁴ the nonenzymatic reaction in the presence of a metal ion as catalyst¹³ (Figure 2B) or the enzymatic reaction in the hairpin ribozyme but using a nucleobase as catalyst.²⁴ This activation mode is evaluated in the presence of a metal ion as catalyst for three reaction paths: the two well-known reaction paths and a third alternative and new path where the proton is transferred to the bridging 3'-oxygen (Figure 2B). In the case of the activation by a nucleobase (Nu-GB), it has been previously studied in the context of the hairpin ribozyme²⁴ (Figure 2F) but the catalyst was a charged and thus activated nucleobase (Nu-GB^{di}); a neutral tautomeric form is considered here as well to evaluate the monoanionic mechanism of the activation reaction (Nu-GB^{mono}; Figure 2E). Finally, a cooperative model between a nucleobase and a metal ion is proposed and compared to the other activation modes. The following steps of the reaction are then considered to determine

how the activation mode orients the reaction path for the nucleophilic attack and eventually the departure of the leaving group and how it impacts the energy barriers.

THEORETICAL METHODS AND ENERGY MODELS

High level ab initio calculations (DFT and MP2) were performed with the Gaussian 03 program package.²⁵ The Molden program²⁶ was employed to visualize the geometric and electronic features of the structures and XCrySDen program²⁷ for final structure presentation. A 3'-phosphorylated ribose moiety is considered as a model system for the self-cleaving reaction. All structures were fully optimized using the B3LYP density functional theory method with a 6-31+G(d) basis set. The nature of the obtained stationary points was always checked by a vibrational analysis. Thermal contributions to the energetic properties were calculated using canonical ensemble of statistical mechanics at standard conditions ($T = 298$ K, $p = 101.325$ kPa). Single point energy calculations on the optimized geometries were carried out with a more flexible 6-311+G(2d,2p) basis set.

The optimization on the B3LYP/6-31+G* level gives a Mg–O bond length of 2.109 Å for [Mg(H₂O)₆]²⁺ that is in complete agreement with X-ray diffraction data (Mg–O = 2.11 Å).²⁸ However, when DFT and MP2 energies are compared, the latter show significantly stronger preference for hexacoordinated Mg–(H₂O)₆²⁺ ion with respect to pentacoordinated Mg(H₂O)₅·(H₂O)²⁺ ion.²⁹ Although the former ion is more stable than the latter by 2.2 kcal/mol at the B3LYP/6-311++G(d,p) level, the MP2(FULL)/6-311++G(d,p) method offers a much higher value of 6.2 kcal/mol.²⁹ Both numbers decrease while using a larger basis set but the difference of about 3–4 kcal/mol remains (1.4 kcal/mol vs 4.6 kcal/mol for the 6-311++(3df,3dp) basis set²⁹). This trend was confirmed in our calculations, although we obtained slightly higher values, because we had to use a smaller basis set due to the size of our system. At the B3LYP/6-311+G(2d,2p)//6-31+G* level the [Mg(H₂O)₆]²⁺ complex is by 2.5 kcal/mol more stable than the [Mg(H₂O)₅]²⁺(H₂O) complex.

The MP2(FC)/6-31+G**//B3LYP/6-31+G* scheme gives a difference of 6.5 kcal/mol. Because the 2'OH activation mechanism involves a Mg^{2+} coordination change, MP2(FC)/6-31+G**//B3LYP/6-31+G* single point energies are also shown for a comparison in the relevant cases. Relative free energies at the MP2 level clearly favor hexacoordinated Mg^{2+} structures; otherwise all trends of energy are consistent with DFT results.

To evaluate the solvent influence on the energetics of the reaction, single point calculations on the gas-phase optimized geometries were performed using CPCM continuum solvation model at the B3LYP/6-31+G(2d,2p) level of theory (the same level as the gas-phase single points). All solvent-phase calculations were carried out in water ($\epsilon_r = 78.39$). Default CPCM parametrization as implemented in G03 was used. These calculations are denoted as DFT-CPCM. The solvation corrections calculated by B3LYP were used also for MP2 energies. MP2 gas-phase energies combined with DFT solvation corrections are denoted as MP2-CPCM energies. The electrostatic potential-fitted atomic charges were used to describe changes in electrostatic properties.

Additional single-point calculations on selected G03-optimized structures were conducted using the Amsterdam Density Functional 2001.01 package (ADF)³⁰ to calculate fragment energy decompositions according to the extended transition state theory.³¹ In these calculations, a triple- ζ STO basis set is used, with one set of polarization functions as provided in the ADF, together with the BLYP functional.

Exact theoretical determination of $\text{p}K_a$ values is still tricky, especially for charged metal complexes. Our estimations of $\text{p}K_a$ values are based on the comparisons of relative energies using a standard expression: $\Delta\text{p}K_a = -\Delta(\Delta G)/2.303RT$.

In the model compounds, the positions of the metal and the nucleobase, with respect to the ribose–phosphate moiety, were initially determined on the basis of X-ray data: the more favorable binding site for Mg^{2+} around phosphate groups^{32,33} and the positions of the nucleobase in the catalytic pocket of a full-length hammerhead ribozyme.³⁴ Only the phospho-ribose moiety of the residue C17 and the nucleobase of the residue G8 base were extracted; the other atoms were not included (PDB ID: 2GOZ).³⁴

■ STRUCTURE LABELING

In the metal based activation models (Me-GB and Me-SB), the structures are labeled by roman numbers starting from reactants to products in the progressive order along the reaction coordinate. The basic model system is neutral and consists of 3'-phosphorylated ribose (−1), a magnesium ion (+2) with four water and one OH^- (−1) ligands. The 3'-phosphorylated ribose is a monoanion that is converted into a dianion during the nucleophile activation (the dianionic mechanism). The structures are labeled by a roman number (from I to VII) and the symbol w. In the monoanionic mechanism, the structures have one more proton than those in the dianionic mechanism, so they are labeled by an additional H symbol. The coordination number of the Mg^{2+} ion can change during the reaction, expelling one water ligand to the second hydration shell. When this happens, those water molecules are not considered in the forward chemical steps along the reaction path (see ref 2, Supporting Information) and the corresponding structures are labeled without the w symbol.

Two structures with identical roman numbers are at an equivalent stage of the reaction. For example, the starting structures, labeled “I”, correspond to the reactant with a hexacoordinated

magnesium and the 2'OH group in the second coordination shell and the final structures, labeled “VII”, correspond to the product of activation with the active $2'\text{O}^-$ group directly coordinated to magnesium. An Arabic number is added when necessary to distinguish different isomers of the same model compound.

In the Me-GB models, the possible rate-determining transition states for the cleavage reaction were also optimized. They correspond to a final proton transfer to the 5'-oxygen of the leaving group and they are designated as “TSH-Ox” and “TS-Ox” for the transition states resulting from Me-GB^{mono} and Me-GB^{di} pathways, respectively. The letter “x” refers to a proton acceptor, and it can be replaced by “w”, “R”, “S”, or “3” corresponding to the oxygen atom of a water molecule, a nonbridging oxygen from the phosphate group (pro-R_p, pro-S_p), or the bridging oxygen from the 3'OH group, respectively.

In the Nu-GB and Nu+Me-GB models the 2'OH group of the ribose moiety is activated by the guanine nucleobase. Here, the reactant (R), transition state (TS), and product (P) structures are designated as Nu-GB/R, Nu-GB/TS, and Nu-GB/P, respectively. In the Nu+Me-GB activation mode, two additional water molecules are present in the second coordination shell of the metal.

■ RESULTS

The activation modes are classified and examined depending on the catalyst (metal ion/nucleobase) and its role (general/specific base) and the reaction mechanism (dianionic/monoanionic), as shown in Figure 2. For both kinds of catalysts, the monoanionic and dianionic mechanisms are considered. The rearrangements related to changes in conformation and metal coordinations are taken into account as a preactivation step associated with the switch from an outer- to inner-sphere coordination that subsequently facilitates the activation by increasing the proton acidity (Figure 2A).

In the monoanionic mechanism, the 2'OH activation is coupled with the nucleophilic attack. In the uncatalyzed reaction, the proton is transferred to one of the nonbridging oxygens before the nucleophilic attack occurs^{14,16} as the in-line conformation is adopted. In the catalyzed reaction, a similar reaction path has been proposed for the nucleobase catalysis (Nu-GB^{mono}) in the hairpin ribozyme.^{16,24} The two chemical steps are concerted in the metal catalysis (Me-GB^{mono}) where the in-line attack and the proton transfer occur simultaneously via a late proton transfer.¹³ Unfortunately, the energy barrier for the 2'OH activation and nucleophilic attack are not specified. In this study, we consider the monoanionic mechanism as proposed for the uncatalyzed and catalyzed reactions where the 2'OH activation and the nucleophilic attack are coupled but not concerted. Thus, we can provide precise data on the 2'OH activation for Me-GB^{mono} (Figure 2B) and compare with the available data in the presence of a nucleobase catalyst: Nu-GB^{mono}_{14,16}.

In the dianionic mechanism, the 2'OH activation is supposed to be disconnected from the nucleophilic attack. We can still assume that the activation takes place either before or after some conformational rearrangement in the in-line attack for Nu-GB^{di} (Figure 2F) and Me-GB^{di} (Figure 2C), respectively. In the particular case of Me-GB^{di}, we may further distinguish two situations where the 2'-oxygen is within the first or second coordination sphere of the metal: both situations have been considered to determine the influence of the inner-sphere/outer-sphere coordinations on the 2'OH activation and the following steps of the reaction. The Me-SB activation mode follows a

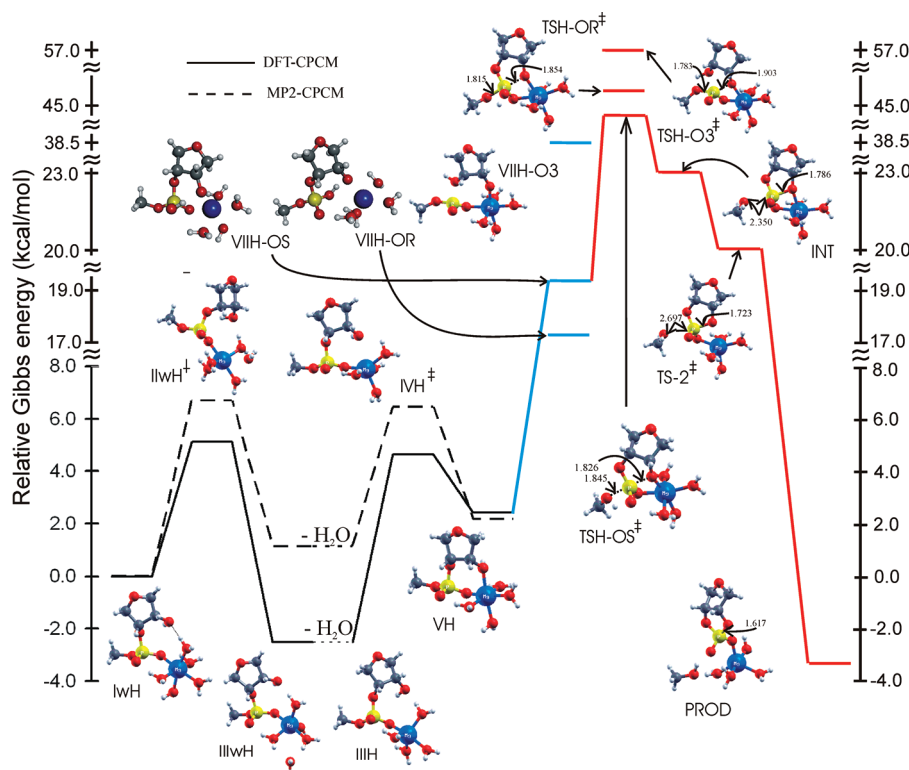


Figure 3. Gibbs free energy surface for the monoanionic pathway ($\text{Me-GB}^{\text{mono}}$ activation modes). The black lines correspond to the preactivation step (structures from IwH to VH). The blue line corresponds to the 2'OH activation, and the red line corresponds to the final cleavage reaction. Structures VH-OR, VH-OS, VIH-OR⁺, and VIH-OS⁺ are omitted for the clarity. VH can be activated also by an external base (Figure 5). See the text for a more detailed description of the stationary points. Lines: full, DFT-CPCM pathway; dashed, MP2-CPCM pathway.

preactivation similar to the step in the monoanionic mechanism described here ($\text{Me-GB}^{\text{mono}}$) for switching from an outer-sphere to an inner-sphere coordination to the 2'-oxygen. Then, a specific base (OH^-) in the second coordination sphere abstracts the proton to generate a dianion (Figure 2D). In both monoanionic and dianionic mechanisms, the 2'OH is first deprotonated (at pre-equilibrium) before the nucleophilic attack and the departure of the leaving group proceed.

The nucleobase catalysis in the 2'OH activation has been studied theoretically only in the context of the hairpin ribozyme where a guanine (G8 residue) has an active or passive role.^{16,24} Nevertheless, the results can probably be extended to the hammerhead ribozyme³⁵ or the glmS ribozyme^{36,37} in which a guanine (G12 and G33, respectively) may have exactly the same role. Up to now, only two models have been proposed: the first one where the nucleobase (in an anionic state) from residue G8 has an active role via a dianionic mechanism, the second one where the same nucleobase has only a passive role via a monoanionic mechanism. Here, the nucleobase contributes to the electrostatic reorganization of the active site without chemical participation in the proton transfer necessary for activation. So, the reaction basically follows the path corresponding to the uncatalyzed reaction with a coupling between the proton transfer and the in-line attack. On the other hand, the nucleobase charged in an anionic state has an active role and acts as a general base (Figure 2F).

When the nucleobase can act at the same time as a general base and as a proton donor (enol tautomer), the two chemical processes corresponding to the 2'OH activation and the nucleophilic attack may not be coupled in the monoanionic mechanism.

Instead, the 2'OH activation can be coupled to another proton transfer from the enol group of the nucleobase to the close nonbridging oxygen ($\text{Nu-GB}^{\text{mono}}$). This is an alternative and new model proposed here (Figure 2E). Finally, the presence of a metal ion close to the 2'OH was shown to have an effect on the acidity of the alcoholic proton.¹² Thus, the presence of two catalysts, a metal ion in the outer-sphere coordination to facilitate the proton transfer and a nucleobase to take an active role in the activation, can have a synergic effect. A new activation model is proposed on the basis of this hypothesis (Figure 2G).

1. Metal-Dependent Activation. The full reaction paths are described as decomposed into three major steps: preactivation, activation, and postactivation (in-line attack and departure of the leaving group), in the monoanionic or dianionic mechanisms (Figures 3 and 4).

1.1. Preactivation or Metal-Dependent Conformational Changes. Reaction Paths. The preactivation involves some conformational changes that are driven by the conversion from an outer-sphere to an inner-sphere metal coordination to the 2'-oxygen through a pentacoordinated metal intermediate. The starting structure involves a hexacoordinated metal where the first coordination sphere (represented explicitly) is filled with five water ligands and only one RNA-like ligand: the nonbridging oxygen pro- R_p of the phosphate group. In the preactivated structure, one of the water ligands has been displaced by the 2'-oxygen that is inserted into the first coordination sphere that thus includes one water ligand less and one RNA-like ligand more. The rate-limiting step is the decrease in the metal coordination number n from $n = 6$ to $n = 5$. In the monoanionic mechanism, the preactivation is a stepwise process with the formation of a pentacoordinated metal including four

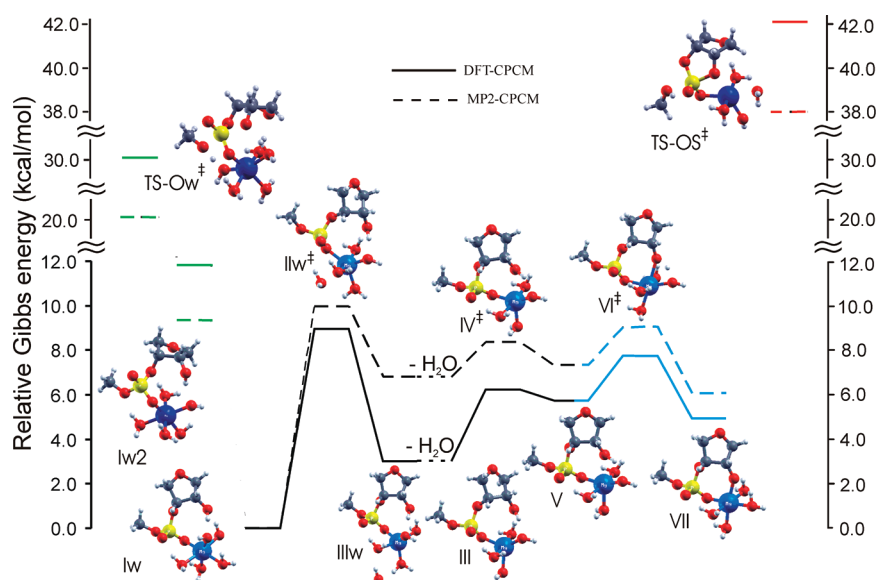


Figure 4. Gibbs free energy surface for the dianionic pathway (Me-GB^{di} activation modes). The black lines correspond to the preactivation step (structures from Iw to V). The blue lines correspond to the $2'\text{OH}$ activation, and the red line corresponds to the rate-determining transition state TS-OS^{\ddagger} for the final cleavage reaction in the $\text{Me}^{\text{i}}\text{-GB}^{\text{di}}$ pathway. The structures Iw2 and TS-Ow^{\ddagger} (green line) correspond to the $\text{Me}^{\text{o}}\text{-GB}^{\text{di}}$ mechanism of the cleavage reaction.¹¹ See the text for a more detailed description of the stationary points. Lines: full, DFT-CPCM pathway; dashed, MP2-CPCM pathway.

water ligands in the first shell and one excluded water ligand in the second shell (Figure 3, IwH to IIIwH). The second step restores a hexacoordinated metal through the inner-sphere coordination to the $2'$ -oxygen (IIIH to VH). In the dianionic mechanism (Figure 4), one of the water ligands is replaced by a hydroxide ion but the reaction path remains unchanged with respect to the monoanionic mechanism (Iw to IIIw and III to V); an additional step leads to the deprotonation of the $2'\text{OH}$ by the metal–hydroxide complex (V to VII). The structural and energetic changes involved in both the mono- and dianionic mechanisms are described in detail in the Supporting Information (sections S1 and S2, Tables S1 and S2).

Hydroxide Ion/Water Ligands: Dianionic/Monoanionic Pathways. The monoanion and dianion reactants IwH and Iw have a similar geometry but the repulsion between the water ligands is increased due to the presence of the negative charge from the hydroxide ion. The coordination distances are increased by 0.038 Å to a mean value of 2.162 Å in Iw compared to IwH (Tables S1 and S2, Supporting Information). It is in agreement with previous findings on the correlation between the coordination distances and the ligand charges.³⁸ Coordination bonds with water ligands involved in internal H-bonding are generally stronger and even more perceptive to the charge of the ligands (increase by 0.071 Å to a mean coordination distance of 2.156 Å, Table S2, Supporting Information).

In the gas-phase DFT calculations, the presence of a hydroxide ligand in the first coordination sphere ion displaces the equilibrium in favor of the pentacoordinated $[\text{Mg}(\text{H}_2\text{O})_4 \cdot (\text{OH})]^+ \cdots (\text{H}_2\text{O})$ complex over the standard hexacoordinated $[\text{Mg}(\text{H}_2\text{O})_5 \cdot (\text{OH})]^+$ complex. It is noteworthy that no minimum can be found for the hexacoordinated $[\text{Mg}(\text{H}_2\text{O})_5(\text{OH})]^+$ complex in the gas phase (B3LYP/aug-cc-pVTZ).³⁹ In fact, the pentacoordinated complex is formed by a spontaneous migration of one of the water ligands from the first to the second coordination shell.³⁹ The decrease in the coordination number is driven by the repulsion

between the permanent and induced dipoles of the ligands and by Pauli repulsion,⁴⁰ but charge-transfer effects are not significant for the Mg^{2+} ion. A minor influence of charge-transfer effects for Mg^{2+} ion was also reported in the comparison of stabilities between octahedral and tetrahedral complexes of Mg^{2+} and Zn^{2+} .^{41,42}

However, it is difficult to extend the observations on simple solvated Mg^{2+} ions to more complex systems. In the Iw structure two charged ligands are present: a hydroxide ion and a charged RNA-like ligand (Figure 4). The pentacoordinated dianionic intermediate (IIIw) is less stable than the hexacoordinated dianion (Iw) reactant ($\Delta G_{\text{Iw-IIIw}} = 3.0$ kcal/mol, Table 3) whereas the monoanionic intermediate (IIIwH) is more stable than its corresponding hexacoordinated monoanion (IwH). The Gibbs free energy barrier associated with the formation of IIIw is 9.0 kcal/mol in DFT calculations (IIw) and even more pronounced in MP2 calculations (10.0 kcal/mol). By comparison, the Gibbs free energy barriers are at least 3 kcal/mol more favorable in the monoanionic mechanism (IwH to IIIwH, Table 2). Thus, the monoanionic preactivation is more favorable than the dianionic preactivation both from the kinetic and thermodynamic viewpoints (Tables 2 and 3).

In the monoanionic mechanism, a higher tendency to lower the coordination number of the Mg^{2+} ion can be explained in terms of reorganization energy (Figure S1, Supporting Information). The transition from a hexacoordinated to a pentacoordinated metal complex involves a rearrangement of four ligands from a square planar to a trigonal planar (three inner-sphere and one outer-sphere ligands) configuration, thus converting the octahedral into a trigonal bipyramidal geometry (Figure S1, Supporting Information). Both hexacoordinated metal complexes deviate from an ideal octahedral geometry: the distortion is located at the position of the hydroxide ligand and its neighbors for Iw and is more regularly distributed for IwH. One can expect that the reorganization energy is minimized when the coordination angles between the three ligands that are kept in the

Table 2. Relative Energies, Differences in Thermodynamic Corrections, and Relative Gibbs Free Energies (at 298 K) of the Stationary Points for the Monoanionic Activation Pathway and of Other Relevant Structures (Me-GB^{mono} Activation Modes)

structure ^a	ΔE (DFT) ^b	ΔE (MP2) ^c	ΔE_{ZPE}	ΔE_{TRV}	$-\Delta S$	$\Delta E_{solv-CPCM}$	$\Delta G_{tot-DFT/CPCM}^d$	$\Delta G_{tot-MP2/CPCM}^e$
IwH ^f	0.0	0.0	0.0	0.0	0.0	0.0	0.0	0.0
IIwH [†]	7.1	8.6	-0.5	-0.3	0.1	-1.2	5.1	6.7
IIIwH	-0.1	3.6	0.1	-0.0	-0.7	-1.8	-2.5	1.1
IIIH ^{g,h}	0.0	0.0	0.0	0.0	0.0	0.0	0.0	0.0
IVH [†]	4.2	2.3	0.2	-0.5	-1.7	1.7	7.2	5.3
VH	2.1	-1.8	0.4	-0.0	-1.0	1.5	4.9	1.0
VH-OR	14.1	12.7	-0.9	-0.4	-1.6	-7.2	7.1	5.6
VH-OS	4.3	-0.7	0.4	0.0	-1.1	2.3	8.1	3.1
VIH-OR [†]	18.9	16.8	-2.7	-0.5	-1.5	-3.5	13.7	11.7
VIH-OS [†]	13.2	7.6	-1.9	-0.3	-1.6	5.8	18.4	12.9
VIIH-OR	17.6	16.2	-0.1	-0.3	-1.1	-1.0	17.3	15.8
VIIH-OS	13.2	8.1	-0.6	0.2	-0.6	6.1	19.4	14.3
VIIH-O3	36.2	33.3	-1.1	0.6	1.7	6.9	41.0	38.1
TSH-O3 [†]	57.6	48.4	-2.5	-0.4	-1.7	3.0	59.5	50.3
TSH-OR [†]	48.6	39.8	-2.6	-0.4	-1.6	1.5	48.7	39.9
TSH-OS [†]	45.6	37.0	-2.4	-0.4	-1.8	2.8	47.3	38.8
INT	27.4	22.6	-0.5	0.5	-1.6	-0.3	25.6	20.7
TS-2 [†]	27.3	24.1	-1.0	0.2	1.1	-2.8	22.5	19.3
PROD	-2.6	-0.8	0.4	-0.0	1.2	2.7	-0.8	1.1

^a Structures marked with a † are transition states and the other states are minima on the potential energy surface. ^b B3LYP/6-311+G(2d,2p)//B3LYP/6-31+G* values in kcal/mol. ^c MP2(FC)/6-31+G**//B3LYP/6-31+G* values in kcal/mol. ^d B3LYP-CPCM/6-311+G(2d,2p)//B3LYP/6-31+G* values in kcal/mol. ^e B3LYP/6-31+G* ZPE, thermal, and Gibbs energy corrections and B3LYP-CPCM/6-311+G(2d,2p)//B3LYP/6-31+G* solvation corrections are considered. ^f The calculated values of energies for IwH are $E(\text{DFT}) = -1572.029354$ hartree, $E(\text{MP2}) = -1567.786332$ hartree, $ZPE = 0.296896$ hartree, $E_{TRV} + \Delta(pV) = 17.53$ kcal/mol, $S = 177.1$ cal/(mol·K), $E(\text{DFT-CPCM}) = -1572.108361$. ^g Structure IIIwH is considered to be equivalent to structure IIIH. In structure IIIH a water molecule in the second coordination shell of Mg^{2+} is missing as compared to structure IIIwH. The relative energy for structure IIIH is zeroed here. The relative energies of structures IIIH, IVH, VH, VIH-OR, VIH-OS, VIIH-O3, VIIH-OR, VIIH-OS, TSH-O3, TSH-OR, TSH-OS, INT, TS2 and PROD on Figure 3 are the sums of their relative energies with respect to the IIIwH structure and relative energy of the IIIH structure. ^h The calculated values of energies for IIIH are $E(\text{DFT}) = -1495.542982$ hartree, $E(\text{MP2}) = -1491.704672$ hartree, $ZPE = 0.271123$ hartree, $E_{TRV} + \Delta(pV) = 15.93$ kcal/mol, $S = 167.3$ cal/(mol·K), $E(\text{DFT-CPCM}) = -1495.630700$.

inner-coordination sphere in the trigonal plane (ligands labeled 1, 2, and 3; Figure S1, plane ((ligands labeled 1, 2, and 3; Figure S1, Supporting Information) are close to 120° as possible. The mean angle change between these ligands when going from IwH to IIIwH and from Iw to IIIw is 22.6° and 36.8°, respectively. So, the difference in energy barrier between the monoanion and the dianion for the transition from a hexacoordinated to a penta-coordinated metal complex can be explained in terms of reorganization of the metal ligands. It will depend on how close they are from the trigonal bipyramid and how easy they can be rearranged. Previous studies on hydrated Mg^{2+} complexes suggest the results obtained here using an explicit representation of the first hydration shell of the metal and an implicit representation (continuum model) for the other hydration shells gives a good description of the geometries and energetics.^{29,43–46}

1.2. Activation Paths: Disconnected or Coupled Proton Transfer with the In-Line Attack. Me-GB^{mono} Pathways with a Coupled Proton Transfer and Subsequent Reaction Steps. In the monoanionic mechanism, the proton transfer is intramolecular and the catalyst is an internal general base (Figure 1). Usually, it is one of the nonbridging oxygens (pro-R_P or pro-S_P) of the phosphate group as proposed in the uncatalyzed reaction¹⁴ or in the catalyzed reaction of the hairpin ribozyme.¹⁶ Alternatively, the 3′O bridging oxygen may be used as a general base as well but this reaction path was never described before (Figure 2B). The three Me-GB^{mono} pathways follow a preactivation as described above for the monoanionic mechanism (Figure 3).

The proton is transferred to the 3′-oxygen or either of the two nonbridging oxygens and leads to the formation of monoanionic intermediates; the reaction may then go forward with the in-line attack of the activated nucleophile on the phosphorus atom. In the Me-GB^{mono} pathways, this is the rate-limiting step of the reaction dissociated from the final step that corresponds to the departure of the leaving group (Figure 3). The more favorable energy barriers involve one of the two nonbridging oxygens as a general base (structures TSH-OS and TSH-OR); the less favorable pathway corresponds to the bridging 3′-oxygen as a general base with an energy barrier increased by 10 kcal/mol in the rate-limiting step (TSH-O3, Table 3). A more detailed description of the energetic and structural changes along the Me-GB^{mono} pathways can be found in the Supporting Information (section S3).

Me-GB^{di} Pathways: Inner/Outer-Sphere Coordination Spheres. In the dianionic mechanism, the preactivation has a higher energy barrier, as described previously. The activation per se involves the metal–hydroxide complex as a general base to activate the 2′OH nucleophile (Figure 4). This particular chemical step (V to VII) has a modest energy barrier; thus the activation is dominated by the energy cost of the preactivation (Table 3). A reaction pathway based on a Me-GB^{di} mode of activation has been proposed in a single-metal-ion model of catalysis for the hammerhead ribozyme.¹¹ In this model, the activation proceeds without preactivation because the 2′-oxygen remains in the outer-coordination sphere of the metal for the activation and the subsequent reaction

Table 3. Relative Energies, Differences in Thermodynamic Corrections, and Relative Gibbs Free Energies (at 298 K) of the Stationary Points for the Dianionic Activation Pathway and of Other Relevant Structures (Me-GB^{di} Activation Modes)

structure ^a	$\Delta E(\text{DFT})^b$	$\Delta E(\text{MP2})^c$	ΔE_{ZPE}	ΔE_{TRV}	$-T\Delta S$	$\Delta E_{\text{solv-CPCM}}$	$\Delta G_{\text{tot-DFT/CPCM}}^d$	$\Delta G_{\text{tot-MP2/CPCM}}^e$
Iw ^f	0.0	0.0	0.0	0.0	0.0	0.0	0.0	0.0
IIw [†]	5.3	6.3	-0.5	-0.0	-0.4	4.6	9.0	10.0
IIIw	-1.5	2.3	0.3	-0.1	-0.5	4.7	3.0	6.8
Vw	-1.7	-2.3	-0.9	-0.2	0.1	7.1	4.4	3.75
VHOH	-1.7	-2.3	-0.9	-0.2	0.1	7.1	4.4	3.75
VIw [†]	-1.1	-2.6	-2.4	-0.5	1.1	7.3	4.35	2.9
VIIw	-2.9	-4.5	-0.2	0.1	0.0	6.4	3.4	1.8
Vw2 [†]	-0.9	-1.2	-2.6	-0.4	0.4	7.6	4.2	4.0
Vw3	-1.6	-1.8	-0.8	0.2	-0.6	7.15	4.2	4.1
Iw2 ^g	10.0	7.5	0.1	0.3	-0.5	1.9	11.8	9.3
TS-Ow ^{†h}	38.9	28.3	-2.5	-0.9	3.0	-7.7	30.9	20.3
III ^{ij}	0.0	0.0	0.0	0.0	0.0	0.0	0.0	0.0
IV [†]	0.8	-0.6	-0.6	-0.3	0.8	2.5	3.2	1.8
V	0.7	-1.2	-0.5	0.2	-0.5	2.8	2.7	0.8
VI [†]	2.7	1.0	-2.35	-0.5	1.6	3.3	4.7	3.0
VII	-1.6	-4.6	-0.1	-0.1	0.8	3.0	1.9	-1.1
TS-OS [†]	36.9	29.0	-2.6	-0.7	2.2	6.5	39.1	31.2
III-2	-0.5	-0.2	0.2	-0.2	0.5	-1.3	-1.4	-1.1
IV-2 [†]	1.6	1.9	-0.8	-0.4	1.2	1.3	2.8	3.1
V-2	0.25	-0.7	-0.4	-0.1	0.7	3.0	3.4	2.5
VI-2 [†]	3.6	2.3	-2.8	-0.4	1.6	2.3	4.2	2.9

^a Structures marked with a † are transition states and the other states are minima on the potential energy surface. ^b B3LYP/6-311+G(2d,2p)//B3LYP/6-31+G* values in kcal/mol. ^c MP2(FC)/6-31+G**//B3LYP/6-31+G* values in kcal/mol. ^d B3LYP-CPCM/6-311+G(2d,2p)//B3LYP/6-31+G* values in kcal/mol. ^e B3LYP/6-31+G* ZPE, thermal, and Gibbs energy corrections and B3LYP-CPCM/6-311+G(2d,2p)//B3LYP/6-31+G* solvation corrections are considered. ^f The calculated values of energies for Iw are $E(\text{DFT}) = -1571.624349$ hartree, $E(\text{MP2}) = -1567.56780$ hartree, $\text{ZPE} = 0.286200$ hartree, $E_{\text{TRV}} + \Delta(\text{pV}) = 16.32$ kcal/mol, $S = 166.7$ cal/(mol·K), $E(\text{DFT-CPCM}) = -1571.651043$. ^g Iw2 structure corresponds to the reoptimized reactant I structure from ref 11. ^h TS-Ow[†] structure corresponds to the reoptimized TS2 structure from ref 11. ⁱ Structure IIIw is considered to be equivalent to structure III. In structure III a water molecule in the second coordination shell of Mg²⁺ is missing as compared to structure IIIw. The relative energy for structure III is zeroed here. The relative energies of structures III–VII, TS-OS and III-2, IV-2, V-2, and VI-2 in Figures 4 and S2 (Supporting Information) are the sums of the IIIw energy and the relative energy of the structure with respect to structure III. ^j The calculated values of energies for III are $E(\text{DFT}) = -1495.141387$ hartree, $E(\text{MP2}) = -1491.304434$ hartree, $\text{ZPE} = 0.260647$ hartree, $E_{\text{TRV}} + \Delta(\text{pV}) = 15.08$ kcal/mol, $S = 160.2$ cal/(mol·K), $E(\text{DFT-CPCM}) = -1495.162793$.

steps. Although the reaction follows a dianionic mechanism, the proton transfer and the in-line attack are coupled as proposed and reminiscent of monoanionic mechanisms. On the other hand, the proton transfer is disconnected from the in-line attack in the model proposed here.

To analyze the influence of the inner or outer-sphere coordinations on the respective activation modes Meⁱ-GB^{di} or Me^o-GB^{di}, the structure Iw was used as reference. A detailed comparison between Iw and the reactant Iw2 proposed in a previous study¹¹ is given in the Supporting Information (section S4, Table S3 and Figure S3). Iw is more stable than Iw2 in the Me^o-GB^{di} pathway.¹¹ Hence, Iw2 is not a global minimum and appears to be already in some “pre-activated” state (Figure 4). The metal ion is more tightly bound to the RNA-like ligand in Iw and would require a reorganization of its hydrogen bond network to be converted into Iw2 with a Gibbs free energy penalty of about 10 kcal/mol (Table 3).

In the Me-GB^{di} paths, the reaction requires at least two successive proton transfers: the first one for the 2'OH activation to proceed with the in-line attack, the second for the protonation on the 5'-oxygen to facilitate the departure of the leaving group. In the Me^o-GB^{di} mode, the hydroxide ion/metal complex activates the 2'OH before another proton from the hydrated metal is transferred to the 5' leaving group. Although the first

proton transfer has a high energy barrier (as shown previously¹¹) because it is coupled with the in-line attack, the rate-limiting step remains associated with the second proton transfer. So, taking into account the preactivation to go from Iw (stable hexacoordinated reactant) to Iw2 (predisposed for activation and in-line attack), the overall energy barrier rises to 31 kcal/mol (TS-Ow, Table 3, Figure 4) corresponding to an increase of about 10 kcal/mol with respect to the single-metal-ion model of catalysis.¹¹ In the Meⁱ-GB^{di} mode, the preactivation and activation have low energy barriers (9–10 kcal/mol). However, the subsequent reaction steps require one additional proton transfer to complete the reaction. With two inner-sphere coordinations to the RNA-like ligand, the hydrated Mg²⁺ ion has no direct interaction with the leaving group. Thus, the protonation of the leaving group has to proceed in two steps: a proton is first transferred from a water ligand to one the nonbridging oxygens and then it is transferred to the 5'-oxygen. The latter proton transfer is still the rate-limiting step (TS-OS, Figure 4) but the energy barrier is further increased, resulting in an overall energy barrier of 39 kcal/mol (Table 3) equivalent to the typical barrier estimated for the uncatalyzed reaction.⁴⁷

The catalytic power of the metal ion as the only catalyst in the reaction varies significantly depending on the coordinations with the RNA-like ligand (inner/outer-sphere coordinations) having

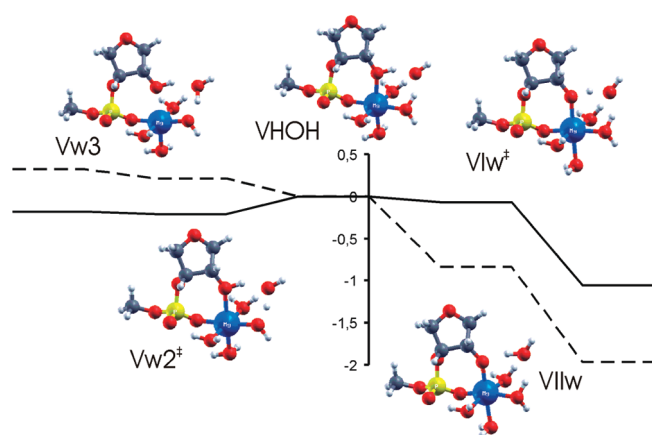


Figure 5. Gibbs free energy surface for the activation of the metal coordinated 2'OH group by a specific base (Me-SB activation mode). The competing deprotonation of a water ligand is shown for comparison (structures Vw2 and Vw3). Lines: full, DFT-PCM pathway; dashed, MP2-PCM pathway. Relative Gibbs energy (vertical axis) is in kcal/mol.

an impact on the stabilization of the negative charge on the nonbridging oxygens²⁴ and on the pK_a modulation of the coordinated proton donor. Although the monoanionic mechanisms exhibit a more favorable preactivation, the energy barrier of the cleavage reaction is significantly lower when a metal–hydroxide complex is involved, orienting the reaction toward the dianionic mechanism. The presence of a specific base (hydroxide OH^- anion) may decrease the barrier height of an equivalent cleavage pathway by about 4.5 kcal/mol (see relative energies of equivalent TSH-OS and TS-OS structures in Tables 2 and 3, respectively). In the dianionic mechanism, the existence of various concurrent paths may be detrimental to the catalytic efficiency of the metal ions as catalysts.

Me-SB Pathway: “Monoanionic” Preactivation and “Dianionic” Activation. The Me-SB path is a mix combining the more favorable paths from the monoanionic and dianionic mechanisms for the preactivation and the 2'OH activation, respectively. It follows the monoanionic preactivation (IwH to VH, Figure 3). Then, a hydroxide ion in the metal outer-sphere coordination (VHOH) acts as a specific base to activate the 2'OH nucleophile (Figure 5). A hydroxide ion was added to the second metal coordination shell in VH to obtain the VHOH structure (see Table 3 and Figure 5). Two concurrent processes are then possible depending on the proton donor: the 2'OH or an equatorial water ligand (for a more detailed description, see section S6 in the Supporting Information). In the first case, the reaction proceeds with the 2'OH activation without any apparent barrier. In the second case, the reaction leads to some intermediate (Vw3, Figure 5) equivalent to the preactivated metal–hydroxide complex in the dianionic mechanism (V, Figure 4). The reaction may further proceed as in the dianionic mechanism for the activation. In the Me-GB^{di} path, the proton transfer has a small activation barrier of 2 kcal/mol (V to VI, Table 3), which is eliminated in the Me-SB path.

2. Nucleobase-Dependent Activation. **2.1. Active Participation of Nucleobases as Catalysts: Monoanionic/Dianionic Mechanisms.** The participation of a nucleobase as a catalyst in the 2'OH activation has been addressed in the models of catalysis proposed for the hairpin ribozyme.^{16,24} Both the monoanionic and dianionic mechanisms have been studied where the nucleobase

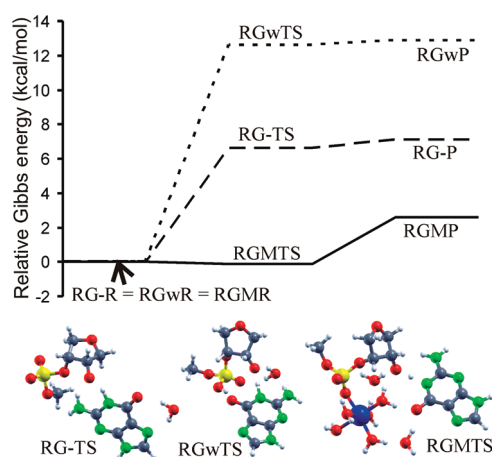


Figure 6. Gibbs free energy surfaces for activation of the 2'OH group by G_{DP} (dashed line), by G_{NE} (dotted line), and by G_{DP} (full line) in the presence of the hydrated Mg^{2+} ion (Nu-GB and Nu+Me-GB activation modes). Only structures of transition states are shown. Structures of reactants and products (Figure S4, Supporting Information) do not show significant changes of the positions of the atoms except for the transferred proton.

has a passive or active chemical role in the proton transfer, respectively. For the sake of comparison with those data, the same dianionic mechanism has been examined. On the other hand, an alternative pathway of activation corresponding to the monoanionic mechanism is also examined but where the nucleobase plays an active chemical role in the proton transfer. Moreover, a possible cooperative model based on the active participation of a nucleobase and the passive participation of a metal is also studied.

The 2'OH activation occurs through the proton transfer either to the anionic N1-deprotonated guanine (G_{DP}^{di}) (Nu-GB^{di} pathway) or to the neutral enol-tautomer of guanine (G_{NE}) (Nu-GB^{mono} pathway).⁴⁸ Indirect experimental evidence suggests the existence of G_{DP} in the active site of the hammerhead ribozyme.⁴⁹ In the cooperative model with a nucleobase and a metal catalyst (Nu+Me-GB^{di} pathway), the G_{DP} species is also involved in the activation of the 2'OH, which is facilitated by the outer-sphere coordinated metal. The initial structure of the RNA moieties (including the nucleobase) were taken from the in-line conformation in the crystal structure of the full-length hammerhead ribozyme.³⁴ The in-line conformation was preserved in the activation pathways except for Nu-GB^{di} where the substrate moiety flipped back to a more usual RNA conformation (the geometries of the reactants and products are provided in Figure S4, Supporting Information). In spite of this conformational difference for Nu-GB^{di}, the energy barriers between the three pathways can still be compared. In fact, recent evidence shows that the in-line conformation is not a decisive factor for the cleavage reaction⁵⁰ because it is responsible for a ~ 12 -fold increase of the cleavage rate. It corresponds to an activation barrier decrease of ~ 1.5 kcal/mol, which is insignificant in comparison to the overall $\sim 10^{12}$ increase due to the enzyme environment⁵⁰ (i.e., activation barrier decreased by ~ 16 kcal/mol). As shown in the three pathways (Figure 6), the proton transfer from the 2'OH group to the N1 imino nitrogen of guanine is always endergonic: the products are not stabilized with respect to the backward reaction when the thermochemical corrections are included (Table 4). Therefore, we will discuss only the

Table 4. Relative Energies and Gibbs Free Energies (at 298 K, in kcal/mol) of the Stationary Points for the Nucleobase-Dependent Activation Pathways^a (Nu-GB and Nu+Me-GB Activation Modes)

structure	$\Delta E(\text{DFT})$	$\Delta E(\text{MP2})$	ΔE_{ZPE}	ΔE_{TRV}	$-\Delta \Delta S$	$\Delta E_{\text{solv-CPCM}}$	$\Delta G_{\text{tot-DFT/CPCM}}$	$\Delta G_{\text{tot-MP2/CPCM}}$
RG-R	0.0 ^b	0.0 ^d	0.0	0.0	0.0	0.0	0.0 ^f	0.0 ^f
RG-TS	10.1 ^b	11.4 ^d	-2.7	-0.5	-1.4	-1.6	6.6 ^f	8.0 ^f
RG-P	9.9 ^b	13.5 ^d	-1.1	-0.2	-0.1	-1.6	7.1 ^f	10.6 ^f
RGwR	0.0 ^b	0.0 ^d	0.0	0.0	0.0	0.0	0.0 ^f	0.0 ^f
RGwTS	11.7 ^b	10.9 ^d	-2.7	-0.6	-3.0	1.2	12.6 ^f	11.8 ^f
RGwP	12.0	11.7 ^d	-1.7	-0.2	-1.6	1.1	12.9 ^f	12.5 ^f
RGMR	0.0 ^c	0.0 ^e	0.0	0.0	0.0	0.0	0.0 ^g	0.0 ^g
RGMTS	1.7 ^c	1.4 ^e	-2.5	-0.3	-0.6	0.4	-0.1 ^g	-0.4 ^g
RGMP	-0.9 ^c	1.3 ^e	3.0	-0.1	0.5	1.1	2.6 ^g	4.8 ^g

^a See the text for the description. ^b Relative energies are based on B3LYP/6-311+G(2d,2p)//B3LYP/6-31+G*. ^c Relative energies are based on B3LYP/6-311+G(2d,2p)//HF/3-21+G*. ^d Relative energies are based on MP2(FC)/6-31+G**//B3LYP/6-31+G*. ^e Relative energies are based on MP2(FC)/6-31+G**//HF/3-21+G* values. ^f B3LYP-CPCM/6-311+G(2d,2p)//B3LYP/6-31+G* relative solvation energies with B3LYP/6-31+G* ZPE, thermal, and Gibbs energy corrections are considered. ^g B3LYP-CPCM/6-311+G(2d,2p)//HF/3-21+G* relative solvation energies with HF/3-21+G* ZPE, thermal, and Gibbs energy corrections are considered.

changes in reaction Gibbs energy (endergonicity) rather than Gibbs energy barriers.

The Nu-GB^{mono} reaction pathway is more endergonic than the two other reaction pathways: Nu-GB^{di} and Nu+Me-GB^{di}, which involve a single proton-transfer event. On the other hand, the Nu-GB^{mono} activation mode requires two concerted proton transfers for the 2'OH activation and the conversion of the enol to keto tautomer. In this second event, the proton donor is the O6-enol group and the proton acceptor the pro-S_p nonbridging oxygen. As a result, G_{NE} is converted into its standard tautomeric form and the overall change on the RNA-like substrate is equivalent to a GB^{mono} activation mode in the uncatalyzed reaction. The reaction path is similar when the stationary points are optimized using an implicit solvent model (CPCM/B3LYP/6-31+G* level), suggesting that the two concerted proton transfers can take place in solution as described in the activation model. The reaction is strongly endothermic: $\Delta G_r^0 = 12.9$ kcal/mol (Figure 6) but the energy barrier can be considered slightly underestimated because the reactant is taken in a minor tautomeric form. An energy correction of 1.1 kcal/mol may be applied to account for the energy barrier to displace the guanine into its enol tautomeric form,¹⁶ raising the overall Gibbs energy difference to $\Delta G_r^0 \approx 14$ kcal/mol. The reaction path is somehow similar to the Nu-GB^{mono} activation mode described for the hairpin ribozyme^{16,24} where the proton is transferred to one of the two nonbridging oxygens (Nu-GB^{mono}-OR or Nu-GB^{mono}-OS). Here, the proton is transferred specifically to the pro-S_p oxygen but no significant difference is expected for the transfer to the pro-R_p oxygen. Although the nucleobase does play an active chemical role in this case, the Gibbs energy difference associated with the formation of the activated intermediate (RGwP, Figure 6) is equivalent to that calculated for an endothermic reaction following the Nu-GB^{mono}-OR or Nu-GB^{mono}-OS mode of activation: 14 and 11 kcal/mol, respectively.^{16,24}

The activation Gibbs energy and the endergonicity of the reaction are strongly lowered when the catalyst is an anionic guanine (G_{DP}) and further if a metal catalyst is also present. The endergonicity is reduced by about half with a Gibbs energy difference of 7.1 kcal/mol in the presence of an anionic nucleobase (Nu-GB^{di}) and yet lowered to 2.6 kcal/mol in the presence of a metal (Nu+Me-GB^{di}). In the Nu+Me-GB^{di} pathway, the metal is directly coordinated to pro-R_p oxygen in the reactant

(RGMR, Figure S4, Supporting Information). The 2'OH group lies in the second coordination sphere of the metal, which is hexacoordinated and includes two additional water molecules in the second hydration shell. One of the water molecules solvates the 2'OH group, the other one the O6-keto group from G_{DP}. The explicit solvation of the 2'OH group is ensured by two water molecules from the first and second hydration shells of the metal. In this model, the reaction has a well-balanced transition state where the proton is halfway from the proton donor and acceptor (Table 4).

2.2. Metal Ion as a Cocatalyst: pK_a Shift of the 2'OH Group. The comparison of the Nu+Me-GB^{di} and Nu-GB^{di} pathways suggests that the metal ion plays a major role in the decrease of the activation energy and endergonicity of the 2'OH activation by the nucleobase. The endergonicity of the process is lowered by 4.5 kcal/mol, which corresponds to a decrease in pK_a by 3.3 log units. The presence of several water molecules in the first or second coordination spheres of the metal makes the 2'OH group more explicitly solvated in Nu+Me-GB^{di} compared to Nu-GB^{di}.

To determine more precisely the role of the metal and the solvation of the 2'OH on the activation, complementary calculations were performed on the reactant and products (RGM-R and RGM-P, Figure S4, Supporting Information). In the first series of calculations, the Mg²⁺ ion was replaced by point charges on a scale between 0.0e and +3.0e; the difference in electronic energy between the two structures was calculated by single point energy calculations without optimization. In the second series of calculations, the Mg²⁺ ion was first replaced by a monovalent Li⁺ ion (metal charge reduction) and then removed (metal charge cancellation). The resulting structures were fully optimized but preserved the interactions between the water molecules in the initial structures in the presence of a divalent ion.

Either way, the endergonicity of the proton transfer is linearly dependent on the charge obeying Coulomb's law (Figure 7). The slope of the energy/charge variation is much higher for the point charges because here a reorganization of the solvent molecules and charge-transfer effects are not allowed. The increasing charge on the 2'O atom polarizes the first coordination shell of the metal. However, no change in charge transfer between the solvated metal and the 2'-oxygen was observed. Thus, the activated 2'O⁽⁻⁾ group is stabilized purely by electrostatic forces. The results are consistent for both ways to vary the metal charge: whether the

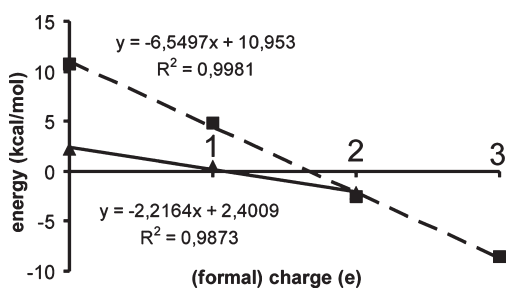


Figure 7. Endergonicity versus charge in the Nu+Me-GB activation mode. Gibbs free energies are calculated on the B3LYP-CPCM/6-311+G(2d,2p)//B3LYP/6-31+G* level. Dashed line: the point charges are placed on the Mg²⁺ positions in the RGMR and RGMP structures, no optimizations were performed, and only the change in electronic energy between the reactant and product structures is considered. Full line: formal charges +2 and +1 are represented by the optimized structures with Mg²⁺ and Li⁺ ions. The metal ion was taken out to represent +0 formal charge. The structures were fully optimized and thermal corrections to energy were considered.

Gibbs energy is calculated for a divalent ion or extrapolated from the calculations on the monovalent ion. The Li⁺ and Mg²⁺ ions lower the endergonicity of the proton transfer by 1.78 and 4.43 kcal/mol, respectively. The pK_a value is decreased accordingly by 1.31 and 3.25 log units. The endergonicities of the 2′OH activation, as calculated above for the end points of the charge scale (corresponding to the absence or presence of a divalent ion: 0.0 and +2.0e), correlate very well with the reaction free energies in the Nu+Me-GB^{di} or Nu-GB^{di} pathways. It suggests that the metal acts via nonspecific electrostatic interactions⁵¹ as a cocatalyst to increase the acidity of the proton and facilitate the 2′OH activation by a nucleobase.

DISCUSSION

The roles of the metal and nucleobase catalysts can be inferred from the comparison between the catalyzed and uncatalyzed reactions. For each reaction mechanism, the catalysts can also be evaluated with respect to the activation step for their catalytic efficiency and for their influence on the reaction pathway. Finally, some insights may be gathered on the influence of the active site environment by the comparison between QM and QM/MM models, whether the active site is represented only by the catalyst(s) or by the catalysts included in the full ribozyme, respectively. However, the comparison between different studies on a given activation mode can be tricky because the 2′OH activation may be concerted or not with the in-line attack (monoanionic mechanism). Thus, the Gibbs energy differences to compare are those of the in-line attack, which include the 2′OH activation. On the other hand, the preactivation is not included in the previous studies, as described above. So, energy corrections are applied when necessary for a fair comparison.

In the monoanionic mechanism, both the metal and the nucleobase catalysts facilitate the 2′OH activation with respect to the uncatalyzed reaction. The nucleobase catalyst can lower the energy barrier by 7 kcal/mol for two variants of the Nu-GB^{mono} activation mode: Nu-GB^{mono}-OR/GB^{mono}-OR or Nu-GB^{mono}-OS/GB^{mono}-OS (Table 5). In the current study, only the Nu-GB^{mono}-OS mode has been evaluated; the catalytic efficiency is slightly weaker: 5 kcal/mol (Nu-GB^{mono}-OS/GB^{mono}-OS). As for the metal catalysts, the different Me-GB^{mono} modes (-O3, -OR, -OS)

require some rearrangements for the proton to be transferred on any of the three proton acceptors: the 3′O bridging or pro-R_p or pro-S_p nonbridging oxygens (Figure 3). These rearrangements may include coordination changes such as the loss of the inner-sphere coordination with the nonbridging oxygen and the formation of a pentacoordinated metal (VIII-OR). The metal catalysts lower the energy barrier but by 5 kcal/mol in the most favorable case (Me-GB^{mono}-OR/GB^{mono}-OR, Table 5). Taken together, the data suggest a nucleobase is slightly more efficient for the 2′OH activation.

The Nu-GB^{mono}-OS examined here does involve an active chemical role of the nucleobase, but the corresponding energy barrier is a bit higher (2 kcal/mol) than what has been reported previously in a QM/MM model.¹⁶ Half of the energy difference between the two models is due to the energy cost for converting the guanine to its active tautomeric form (1.1 kcal/mol). The other half is probably due to the difference in the reaction path. A single internal proton transfer is involved from the 2′OH to one of the two nonbridging oxygens (with no chemical role of the nucleobase) in Nu-GB^{mono}-OS. Two concerted proton transfers are involved from the 2′OH to the N1-imino of guanine and from the O6-enol group and to the nonbridging oxygen in Nu-GB^{mono}. In this latter case, the nucleobase has an active chemical role as a general acid/base (Figures 6 and S4, Supporting Information). The similar energy barrier between the two models (Nu-GB^{mono}/Nu-GB^{mono}-OS: 14 kcal/mol vs 12 kcal/mol) suggests that the nucleobase can still have a chemical role in the proton transfer in the monoanionic mechanism. The presence of the nucleobase alone, whether it has a chemical role or not (QM model vs QM/MM model, Table 5), is sufficient to lower significantly the energy barrier of the uncatalyzed reaction. Thus, the nucleobase environment should provide a proper arrangement of the catalyst in the active site for the 2′OH activation and the following chemical steps, but it may not have any additional positive contribution, at least in the case of the hairpin ribozyme. We may expect a different trend in the case of metal catalysts, which are very dependent on the environment for binding.

Putting in perspective the 2′OH activation with the RNA catalysis, one may compare the energy barriers for the rate-limiting step depending on the catalytic strategy. The 2′OH activation represents an energy cost important with respect to the energy barrier of the rate-limiting step in the nucleobase catalysis (Nu-GB^{mono}), as shown in previous studies (Table 5). The nucleobase catalysis (Nu-GB^{mono}: -OR, -OS) appears to be generally more efficient than the metal ion catalysis, which cannot match the same efficiency (Me-GB^{mono}: -OR, -OS, -O3). However, such comparison is partly biased by the fact that what is attributed to the nucleobase catalysis includes the whole contribution from the active site, which may or may not be significant to facilitate the catalysis depending on the reaction step (see discussion above on 2′OH activation in the hairpin ribozyme). Besides, the presence of two metal catalysts appears to facilitate even more the 2′OH activation in a cooperative way (Me₂-GB^{mono}: 6.9 kcal/mol) but the energy barrier of the rate-limiting step in this reaction pathway is much larger (Table 5). The absence of the active site environment in this two-metal-ion model probably leads to an overestimation of the energy barrier. Although the nucleobase is more efficient as a single catalyst, the active site of self-cleaving ribozymes is likely evolutionary optimized to accommodate a specific catalyst.

In the dianionic mechanism, the 2′OH activation is generally omitted because it is not rate-controlling. The energy barrier was

Table 5. Comparison of the Relative Gibbs Free Energies for the Nucleophile Activation from Previous and Current Studies^a

activation mode	ΔG_{aq} (B3LYP)	ΔG_{aq} (CP)	stationary points in proton transfer	ΔG_{aq} rate-limiting step
Data on Uncatalyzed Reaction in Solution				
GB ^{mono} -TS-OR [¶]	21–22 ^b (25–26)*		PROD to TS2 ^{exo/endo} ^b (a) to (b) (Figure 7) ^c	44 ^b
		17 ^c		58 ^c
GB ^{mono} -TS-OS [¶]	19 ^d	NA	R to TS _{PT1}	38 ^d
Published Data on Different Mechanisms and Activation Modes				
Me-GB ^{mono}	NA	NS	NA	56 ^e
Me ^o -GB ^{di}	19* ^f (≥28) ^{§,†}		reactant to TS1	21 (31) ^g
		13 ^c	(a) to (b) (Figure 9)	49 ^e
Me ₂ -GB ^{mono}	NA	6.9 ^e	(a) to (b) (Figure 3)	45 ^e
Me ₂ -GB ^{di}	2.6 ^h (≥13) [†]		I to II [†] ^h	11 (≥20) ^g
		5.4 ^c	(a) to (b) (Figure 7) ^e	42
Nu-GB ^{mono} -TS-OR [¶]	15 ⁱ (15)*	NA	R to TS _{PT1} (O1P path)	25
Nu-GB ^{mono} -TS-OS [¶]	12 ⁱ (14)*	NA	R to TS _{PT1} (O2P path)	21
Nu-GB ^{di} *	15* ⁱ	NA	R to TS _{PT1} (N1 path)	27
Data from the Current Study				
Me-GB ^{mono} -TSH-OR	17	NA	VIIIH-OR	49
Me-GB ^{mono} -TSH-OS	19	NA	VIIIH-OS	47
Me-GB ^{mono} -TSH-O3	41	NA	VIIIH-O3	60
Me ⁱ -GB ^{di}	9.0 (39) ^{§,†}	NA	Iw to IIw	39
Me ⁱ -SB	5.1 (39) ^{§,†}	NA	IwH to IIwH	39
Nu-GB ^{mono}	14 ^j	NA	RGwR to RGw-TS	NA
Nu-GB ^{di}	7.1 ^k (11) [◇]	NA	RG to RG-TS to RG-P	NA
Nu+Me-GB ^{di}	2.6	NA	RGMR to RGMTS	NA

^a The values in parentheses indicate a correction of the energy barrier: (*) energy barrier including the 2'OH activation and the in-line attack; (†) energy barrier including the 2'OH activation and the preactivation steps; (§) energy barrier including the 2'OH activation and the in-line attack and the departure of the leaving group; (¶) QM/MM calculations including the full ribozyme structure; (◇) energy barrier including the conformational rearrangement for the in-line attack. NA: not available. NS: not specified. All energies are in kcal/mol. ^b B3LYP/6-311++G(3df,2p)//B3LYP/6-31++G(d,p). ^c CP (HCTH); ^d B3LYP/6-31++G(d,p)//B3LYP/6-31+G(d). ^e CP (HCTH). ^f B3LYP/6-311+G(2d,2p)//B3LYP/6-31G(d,p). ^g The Gibbs energy barrier for the nucleophile activation¹¹ can be corrected by including the contributions from the metal binding and conformational rearrangements (Table 3: 11.8 kcal/mol for Iw-2). ^h B3LYP/6-31+G**//HF/3-21+G*. ⁱ B3LYP/6-311++G(3df,2p)//B3LYP/6-31++G(d,p). ^j B3LYP/6-311+G(2d,2p)//B3LYP/6-31+G*: the Gibbs energy barrier corresponds to the 2'OH activation by a nucleobase as catalyst (RGwR to RGwP via RGwTS: Table 4) including an energy correction for converting the standard guanine tautomer into its enol tautomer (1.1 kcal/mol¹⁶).

^k B3LYP/6-311+G(2d,2p)//B3LYP/6-31+G*: the Gibbs energy barrier corresponds to the 2'OH activation by a nucleobase as catalyst (RG-R to RG-P via RG-TS: Table 4). Calculated energy correction for the conversion of phospho-ribose units in RG-R and RG-P into an in-line conformation is 4.2 kcal/mol. The geometry of the phospho-ribose moiety of the residue C17 as found in the crystal structure (PDB ID: 2GOZ)³⁴ were taken as a reference in-line conformation.

estimated computationally to be around 21 kcal/mol for the reaction in solution.⁵² Only the more recent studies, involving a nucleobase catalyst, treat explicitly this reaction step in a QM/MM model of the hairpin ribozyme.¹⁶ On the basis of the estimation given above and the available data, the nucleobase catalyst would lower the energy barrier for the 2'OH activation by 7 kcal/mol (Nu-GB^{di}, Table 5). In the single-metal-ion models, the 2'OH activation may be coupled to the in-line attack when the 2'-oxygen is in the outer-sphere coordination of the metal (Me^o-GB^{di}, Table 5). Moreover, the classical DFT methods used for Me^o-GB^{di} did not take into account the preactivation steps.

Thus, the activation barrier for Me^o-GB^{di} (B3LYP) is largely underestimated, as described above. On the other hand, the 2'OH activation is independent from the in-line attack in Car–Parrinello studies (CP: 13 kcal/mol, Table 5): the metal catalyst would then lower the activation barrier by 8 kcal/mol. The presence of the 2'-oxygen in the inner-sphere coordination (Meⁱ-GB^{di}) would make the 2'OH activation even more favorable with an energy barrier lowered by 12 kcal/mol. When the general base is replaced by a specific base, the energy barrier can still be reduced with respect to the uncatalyzed reaction by almost 16 kcal/mol (Meⁱ-SB, Table 5). In the two-metal-ion

models, the energy barrier for the 2′OH activation (including the preactivation steps for the DFT study) is between 5 and 13 kcal/mol, which is not very different from that calculated for the single-metal-ion model corresponding to $\text{Me}^{\text{i}}\text{-GB}^{\text{di}}$ (9 kcal/mol) despite subtle differences in conformations and metal coordinations between the models (Table S5). Nevertheless, a single metal catalyst involved in the first steps of the reaction (2′OH activation and in-line attack) cannot play any significant role in the rate-limiting step of the reaction: the departure of the leaving group. The energy barrier for the subsequent rate-limiting step with a single metal catalyst are thus significantly larger than those calculated in the presence of two catalysts a fortiori when the models also include the active site environment (Nu-GB modes for the hairpin ribozyme).

In the presence of two distinct catalysts, the metal catalysts are expected to be more efficient than the nucleobase catalysts in the dianionic mechanism by facilitating the 2′OH activation and the in-line attack. Alternatively, both metals and nucleobases may act in concert in the 2′OH activation as shown in the Nu+Me-GB^{di} mode (Figure 6) where the energy barrier is even more favorable and 18 kcal/mol lower than that of the uncatalyzed reaction. In the hammerhead ribozyme, the current models largely support a catalytic strategy based on nucleobases as the main and essential catalysts for both the 2′OH activation/in-line attack and the departure of the leaving group. However, both computational and experimental studies suggested recently an active participation of metal catalysts either in the departure of the leaving group²³ or in the 2′OH activation/in-line attack,⁵³ respectively. A Nu+Me-GB mode may be involved where the nucleobase is a general base and the metal a Lewis acid and/or where the metal is a cocatalyst activating the nucleobase.⁵ Other recent experimental data on the HDV ribozyme strongly support a role as a Lewis acid for the metal catalyst and a hydroxide ion as a specific base (Me-SB mode) for the 2′OH activation.⁵⁴ A nucleobase (G25) is also involved in this model as a cofactor for binding the metal catalyst on its hoogsteen face. In the hairpin ribozyme, two nucleobases act as catalysts, but it is not clear yet whether they have an active chemical role in the 2′-hydroxyl deprotonation or the 5′-oxygen protonation. This study does not provide any further argument because the Nu-GB^{mono} modes are equivalent whether the nucleobase has a chemical role as an enol tautomer or just facilitates the 2′OH activation through solvation and specific hydrogen-bonding interactions.¹⁶

CONCLUSIONS

The nucleophile activation is the first chemical step of the transphosphorylation. Although it is not the rate-determining step in the overall reaction in any of these ribozymes, it represents a significant energy cost with respect to the overall energy barrier, especially in the monoanionic mechanism. In the dianionic mechanism, the nucleophile activation is generally examined starting from a preactivated conformational or chemical state for the catalysts. So, the metal and nucleobase catalysts are available as general bases (metal–hydroxide complex or anionic guanine). Thus, the energy barrier of activation has generally been underestimated by not taking into account some nonchemical steps involved in the prior activation of the catalyst responsible for the 2′OH activation.

The 2′OH activation can involve different catalysts and follow different pathways, which can be combined into different modes of activation (Figure 1 and Table 1). A representative number of

them has been explored in this study on the basis of the different models proposed for the catalytic strategies of self-cleaving ribozymes. Although most of the metal activation modes presented here have been previously evaluated using different methods (DFT or CP), the energy barriers calculated for the preactivation steps allow to reconsider the corresponding models of catalysis. The results on the activation by a metal catalyst suggest that a single catalyst is not efficient enough to lower the overall activation barrier as expected from the experimental data, even if the barriers are likely overestimated (due to the absence of the active site environment that may contribute to lower the energy barrier). The Me-SB activation mode appears to be the more favorable way to activate the 2′OH nucleophile and is probably effective in the HDV ribozyme.

The nucleobase catalysts are generally more efficient than the metal catalysts in the monoanionic mechanism, but their exact role in the catalysis is still unclear. The activation modes, evaluated in a previous study on the hairpin ribozyme,²⁴ suggested the nucleobase may contribute to lower the energy barrier just by providing a favorable charge environment in the active site. In this study, an additional activation mode involving an enol tautomer of guanine with an active chemical role in the catalysis has been identified. However, the energy barrier for this activation mode is equivalent to that of the other three activation modes already proposed. Finally, the endergonic activation modes also suggest a single nucleobase catalyst is not efficient enough for the reaction to proceed, unless it is pushed due to the participation of another catalyst and/or the active site environment in the following exergonic reaction steps (online attack and departure of the leaving group).

The 2′OH activation can be potentiated using both kinds of catalysts: metals and nucleobases. The specific case presented here involves a nucleobase as a general base and a metal that promotes the activation through nonspecific long-range electrostatic forces.⁵¹ Thus, the metal may be distant from the 2′OH group but effective on the 2′OH activation and may also act as a Lewis acid in the departure of the leaving group. Some recent data suggest this activation mode may be effective in the hammerhead ribozyme. Beyond the static picture given by this model, the metal may also contribute to rearrange the active site to orient and/or activate the nucleobase to act as a general base. Vice versa, the nucleobase may contribute to create a favorable binding site where the metal can act as a Lewis acid.

ASSOCIATED CONTENT

S Supporting Information. Details on (1) the geometries of the stationary points (Tables S1, S2 and Figures S1, S2, S4), structures, and potential energy surfaces, especially on the structures Iw and Iw2 and of those related to the $\text{Me}^{\text{i}}\text{-GB}^{\text{di}}$ and $\text{Me}^{\text{o}}\text{-GB}^{\text{di}}$ mechanisms (section S4, Figure S3, Table S3); (2) the energy decomposition analysis (sections S1–S7 and Table S4), a detailed description of the monoanionic (section S1), dianionic (section S2), Me-GB^{mono} (section S3), Me-SB (section S6), and Nu-SB and Nu-GB (section S7) pathways. This material is available free of charge via Internet at <http://pubs.acs.org>

AUTHOR INFORMATION

Corresponding Authors

*E-mail: Z.C., chval@jcu.cz; F.L., fabrice.leclerc@maem.uhp-nancy.fr.

ACKNOWLEDGMENT

This project was supported by grants from the Czech Science Foundation (204/09/J010) and from the Ministry of Education, Youth and Sports of the Czech Republic (grants ME09062 and CZ.1.07/2.3.00/09.0076: to Z.C. and D.C., respectively) and by CNRS funding for young investigators (ATIP, France) (to F.L.). The calculations were performed partly at the Metacentrum (Czech Republic, project MSM6383917201), partly at the "Centre Informatique National de l'Enseignement Supérieur" (CINES, France) and the "Institut du Développement et des Ressources en Informatique Scientifique" (IDRIS, France: Project IDRIS 061413). Access to these supercomputing centers is highly acknowledged.

REFERENCES

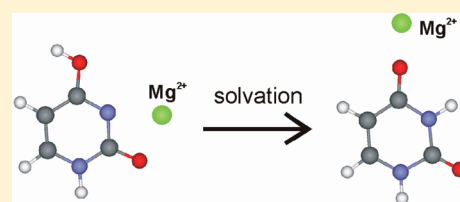
- (1) Gordon, P. M.; Fong, R.; Piccirilli, J. A. *Chem. Biol.* **2007**, *14*, 607–612.
- (2) Fedor, M. J.; Williamson, J. R. *Nat. Rev. Mol. Cell Biol.* **2005**, *6*, 399–412.
- (3) Bevilacqua, P. C.; Yajima, R. *Curr. Opin. Chem. Biol.* **2006**, *10*, 455–464.
- (4) Stahley, M. R.; Strobel, S. A. *Science* **2005**, *309*, 1587–1590.
- (5) Leclerc, F. *Molecules* **2010**, *15*, 5389–5407.
- (6) Fedor, M. J. *Annu. Rev. Biophys.* **2009**, *38*, 271–299.
- (7) Cochrane, J. C.; Strobel, S. A. *Acc. Chem. Res.* **2008**, *41*, 1027–1035.
- (8) Murray, J. B.; Dunham, C. M.; Scott, W. G. *J. Mol. Biol.* **2002**, *315*, 121–130.
- (9) Hampel, K. J.; Burke, J. M. *Biochemistry* **2003**, *42*, 4421–4429.
- (10) Martick, M.; Lee, T. S.; York, D. M.; Scott, W. G. *Chem. Biol.* **2008**, *15*, 332–342.
- (11) Torres, R. A.; Himo, F.; Bruice, T. C.; Noodleman, L.; Lovell, T. *J. Am. Chem. Soc.* **2003**, *125*, 9861–9867.
- (12) Boero, M.; Terakura, K.; Tateno, M. *J. Am. Chem. Soc.* **2002**, *124*, 8949–8957.
- (13) Boero, M.; Tateno, M.; Terakura, K.; Oshiyama, A. *J. Chem. Theory Comput.* **2005**, *1*, 925–934.
- (14) Lopez, X.; Dejaegere, A.; Leclerc, F.; York, D. M.; Karplus, M. *J. Phys. Chem. B* **2006**, *110*, 11525–11539.
- (15) Leclerc, F.; Karplus, M. *J. Phys. Chem. B* **2006**, *110*, 3395–3409.
- (16) Nam, K.; Gao, J.; York, D. M. *J. Am. Chem. Soc.* **2008**, *130*, 4680–4691.
- (17) Mlýnský, V.; Banáš, P.; Hollas, D.; Réblová, K.; Walter, N. G.; Šponer, J.; Otyepka, M. *J. Phys. Chem. B* **2010**, *114*, 6642–6652.
- (18) Lee, T. S.; Lopez, C. S.; Giambasu, G. M.; Martick, M.; Scott, W. G.; York, D. M. *J. Am. Chem. Soc.* **2008**, *130*, 3053–3064.
- (19) Lee, T. S.; York, D. M. *J. Am. Chem. Soc.* **2008**, *130*, 7168–7169.
- (20) Lee, T. S.; Giambasu, G. M.; Sosa, C. P.; Martick, M.; Scott, W. G.; York, D. M. *J. Mol. Biol.* **2009**, *388*, 195–206.
- (21) Wei, K.; Liu, L.; Cheng, Y. H.; Fu, Y.; Guo, Q. X. *J. Phys. Chem. B* **2007**, *111*, 1514–1516.
- (22) Banáš, P.; Rulíšek, L.; Hánošová, V.; Svozil, D.; Walter, N. G.; Šponer, J.; Otyepka, M. *J. Phys. Chem. B* **2008**, *112*, 11177–11187.
- (23) Wong, K. Y.; Lee, T. S.; York, D. M. *J. Chem. Theory Comput.* **2011**, *7*, 1–3.
- (24) Nam, K.; Gao, J.; York, D. M. *RNA* **2008**, *14*, 1501–1507.
- (25) Frisch, M. J.; Trucks, G. W.; Schlegel, H. B.; Scuseria, G. E.; Robb, M. A.; Cheeseman, J. R.; Montgomery, J. A., Jr.; Vreven, T.; Kudin, K. N.; Burant, J. C. et al. *Gaussian 03*, Revision E.01; Gaussian, Inc.: Pittsburgh, PA, 2003.
- (26) Schaftenaar, G.; Noordik, J. H. *J. Comput.-Aided Mol. Des.* **2000**, *14*, 123–134.
- (27) Kokalj, A. *Comput. Mater. Sci.* **2003**, *28*, 155–168.
- (28) Caminiti, R.; Licheri, G.; Piccaluga, G.; Pinna, G. *Chem. Phys. Lett.* **1979**, *61*, 45–49.
- (29) Markham, G. D.; Glusker, J. P.; Bock, C. W. *J. Phys. Chem. B* **2002**, *106*, 5118–5134.
- (30) Velde, G. T.; Bickelhaupt, F. M.; Baerends, E. J.; Guerra, C. F.; Van Ginsbergen, S. J. A.; Snijders, J. G.; Ziegler, T. *J. Comput. Chem.* **2001**, *22*, 931–967.
- (31) Ziegler, T.; Rauk, A. *Theor. Chim. Acta* **1977**, *46*, 1–10.
- (32) Schneider, B.; Kabeláč, M.; Hobza, P. *J. Am. Chem. Soc.* **1996**, *118*, 12207–12217.
- (33) Schneider, B.; Kabeláč, M. *J. Am. Chem. Soc.* **1998**, *120*, 161–165.
- (34) Martick, M.; Scott, W. G. *Cell* **2006**, *126*, 309–320.
- (35) Lee, T. S.; York, D. M. *J. Am. Chem. Soc.* **2010**, *132*, 13505–13518.
- (36) Klein, D. J.; Been, M. D.; Ferre-D'Amare, A. R. *J. Am. Chem. Soc.* **2007**, *129*, 14858–14859.
- (37) Klein, D. J.; Ferre-D'Amare, A. R. *Science* **2006**, *313*, 1752–1756.
- (38) Mayaan, E.; Range, K.; York, D. M. *J. Biol. Inorg. Chem.* **2004**, *9*, 807–817.
- (39) Kluge, S.; Weston, J. *Biochemistry* **2005**, *44*, 4877–4885.
- (40) Katz, A. K.; Glusker, J. P.; Beebe, S. A.; Bock, C. W. *J. Am. Chem. Soc.* **1996**, *118*, 5752–5763.
- (41) Dudev, T.; Lim, C. *J. Am. Chem. Soc.* **2000**, *122*, 11146–11153.
- (42) Dudev, T.; Lim, C. *Chem. Rev.* **2003**, *103*, 773–788.
- (43) Pavlov, M.; Siegbahn, P. E. M.; Sandstrom, M. *J. Phys. Chem. A* **1998**, *102*, 219–228.
- (44) Pye, C. C.; Rudolph, W. W. *J. Phys. Chem. A* **1998**, *102*, 9933–9943.
- (45) Šponer, J. E.; Sychrovský, V.; Hobza, P.; Šponer, J. *Phys. Chem. Chem. Phys.* **2004**, *6*, 2772–2780.
- (46) Šponer, J.; Burda, J. V.; Leszczynski, J.; Hobza, P. *J. Biomol. Struct. Dynam.* **1999**, *17*, 61–77.
- (47) Nam, K.; Cui, Q.; Gao, J. L.; York, D. M. *J. Chem. Theory Comput.* **2007**, *3*, 486–504.
- (48) Lippert, B. *Chem. Biodiversity* **2008**, *5*, 1455–1474.
- (49) Thomas, J. M.; Perrin, D. M. *J. Am. Chem. Soc.* **2008**, *130*, 15467–15475.
- (50) Min, D. H.; Xue, S.; Li, H.; Yang, W. *Nucleic Acids Res.* **2007**, *35*, 4001–4006.
- (51) Sigel, R. K. O.; Pyle, A. M. *Chem. Rev.* **2007**, *107*, 97–113.
- (52) Glennon, T. M.; Warshel, A. *J. Am. Chem. Soc.* **1998**, *120*, 10234–10247.
- (53) Osborne, E. M.; Ward, W. L.; Ruehle, M. Z.; DeRose, V. J. *Biochemistry* **2009**, *48*, 10654–10664.
- (54) Chen, J. H.; Yajima, R.; Chadalavada, D. M.; Chase, E.; Bevilacqua, P. C.; Golden, B. L. *Biochemistry* **2010**, *49*, 6508–6518.
- (55) Pontius, B. W.; Lott, W. B.; von Hippel, P. H. *Proc. Natl. Acad. Sci. U. S. A.* **1997**, *94*, 2290–2294.
- (56) Rupert, P. B.; Ferre-D'Amare, A. R. *Nature* **2001**, *410*, 780–786.
- (57) Nesbitt, S.; Hegg, L. A.; Fedor, M. J. *Chem. Biol.* **1997**, *4*, 619–630.
- (58) Pinard, R.; Hampel, K. J.; Heckman, J. E.; Lambert, D.; Chan, P. A.; Major, F.; Burke, J. M. *EMBO J.* **2001**, *20*, 6434–6442.
- (59) Park, H.; Lee, S. J. *J. Chem. Theory Comput.* **2006**, *2*, 858–862.
- (60) Rhodes, M. M.; Réblová, K.; Šponer, J.; Walter, N. G. *Proc. Natl. Acad. Sci. U. S. A.* **2006**, *103*, 13380–13385.
- (61) Ke, A. L.; Zhou, K. H.; Ding, F.; Cate, J. H. D.; Doudna, J. A. *Nature* **2004**, *429*, 201–205.
- (62) Das, S. R.; Piccirilli, J. A. *Nat. Chem. Biol.* **2005**, *1*, 45–52.
- (63) Nakano, S.; Chadalavada, D. M.; Bevilacqua, P. C. *Science* **2000**, *287*, 1493–1497.
- (64) Nakano, S.; Proctor, D. J.; Bevilacqua, P. C. *Biochemistry* **2001**, *40*, 12022–12038.
- (65) Wilson, T. J.; McLeod, A. C.; Lilley, D. M. J. *EMBO J.* **2007**, *26*, 2489–2500.
- (66) Wilson, T. J.; Li, N. S.; Lu, J.; Frederiksen, J. K.; Piccirilli, J. A.; Lilley, D. M. J. *Proc. Natl. Acad. Sci. U. S. A.* **2010**, *107*, 11751–11756.
- (67) Cochrane, J. C.; Lipchick, S. V.; Strobel, S. A. *Chem. Biol.* **2007**, *14*, 97–105.

Influence of the Environment on the Specificity of the Mg(II) Binding to Uracil

Ingrid Romancová,[†] Zdeněk Chval,^{*,‡} and Milan Předota[†][†]Institute of Physics and Biophysics, Faculty of Science, University of South Bohemia, Branišovská 31, CZ-370 05 České Budějovice, Czech Republic[‡]Department of Laboratory Methods and Information Systems, Faculty of Health and Social Studies, University of South Bohemia, J. Boreckého 27, CZ-370 11 České Budějovice, Czech Republic

Supporting Information

ABSTRACT: Interactions of uracil with the Mg^{2+} ion were studied theoretically in the gas phase and in solution. The bare Mg^{2+} prefers bidentate N–C=O binding sites stabilizing rare keto–enol forms of the base. Hydration and/or phosphate binding of the Mg^{2+} ion shield its positive charge, which leads to preference of monodentate binding to the oxygen keto atoms, shifting fully the equilibrium between the tautomers back toward the canonical diketo tautomer. In solution, a direct inner-sphere metal binding to uracil is not clearly advantageous compared to the outer-sphere metal binding. Similar trends were also obtained for the Ca^{2+} ion. Results are supported by the natural bond orbital (NBO) and atoms in molecule (AIM) analyses and the combined extended transition-state energy decomposition analysis and natural orbitals for chemical valence (ETS-NOCV).



INTRODUCTION

Metal ion–nucleobase interactions are recognized as fundamental with respect to changes in the nucleic acid structure stabilizing a number of local motifs. This is especially important for complicated RNA structures in which metal ions ensure their proper folding. Uracil is a specific base for RNA in which it pairs up with adenine. All nucleobases including uracil may exist in different tautomeric forms, and this behavior may have important biological consequences, such as point mutations^{1,2} because the mismatches of DNA bases can be stabilized by metalation.^{3–6} In case of RNA, the rare tautomers may be stabilized by specific tertiary interactions, and they may take part in ribozyme catalysis. Tautomeric equilibria of the nucleobases were studied in a number of previous studies in the gas phase and in aqueous solution.^{7–12} The metal ions may shift the tautomeric equilibria toward to rare enol tautomers mainly in the case of isolated adenine and thymine, while for cytosine, this event is not probable.¹³ In the case of guanine, the rare tautomers can coexist when the base is isolated; however, their formation is suppressed in the case of strong interactions between the metal ion and the phosphate group.¹⁴

The other factor that affects the chemical equilibrium between tautomers is the surrounding environment.¹⁵ Water molecules may significantly change the relative stabilities of tautomers compared to the gas phase and nonpolar solvents. For example, the enol form of cytosine is the most stable tautomer in the gas phase, but its canonical form is more stable in water because it is much better stabilized; hydration by just two water molecules is sufficient for this stabilization.¹⁶ Water as a polar solvent better stabilizes the tautomers with a larger

dipole moment and may shield unfavorable electrostatic interactions.¹⁷

Beside the phosphate oxygens, the main metal binding sites of the metals on nucleobases are N7 and N3 atoms of purines, O6 of guanine, and oxo groups of pyrimidines. Stabilization of rare nucleobase tautomers by metal ions was studied extensively^{13,18–23} as well as the influence of the metal ions on the base pairing.^{24–29} For a complex of the Mg^{2+} ion with uracil, the most favored binding motif in the gas phase is $N\cdots Mg^{2+}\cdots O$.²¹ Because the canonical form of uracil offers only the monodentate binding motif, the rare enol tautomers, which offer bidentate binding sites, are expected to be stabilized in the presence of a metal ion. For example Wang et al.³⁰ studied uracil interactions with the Zn^{2+} ion. In the most stable structure, the Zn^{2+} ion binds in the bidentate manner to N1 and O2 atoms. The canonical tautomer with the metal bound to O4 is by 22.4 kcal/mol less stable. Monohydration of the Zn^{2+} ion decreases the difference between the two binding modes by one-third to the value of 15.0 kcal/mol.³⁰ In the gas phase, a monodentate Mg^{2+} binding to thymine may at first activate the 1,3 hydrogen transfer, which is followed by the metal cation migration to form a bidentate complex,³¹ stabilizing a rare tautomer. The speed of the hydrogen transfer can be substantially increased if at least one water molecule is involved in the reaction mechanism.^{32,33}

On the other hand, monovalent metal ions probably are not able to stabilize the rare tautomers. For example, adducts of the

Received: September 13, 2011

Revised: January 13, 2012

Published: January 20, 2012

Li^+ ion with the uke2 keto–enol tautomer (equivalent to uke2–O+w and uke2–ON+w (Figure 1)) were, respectively,

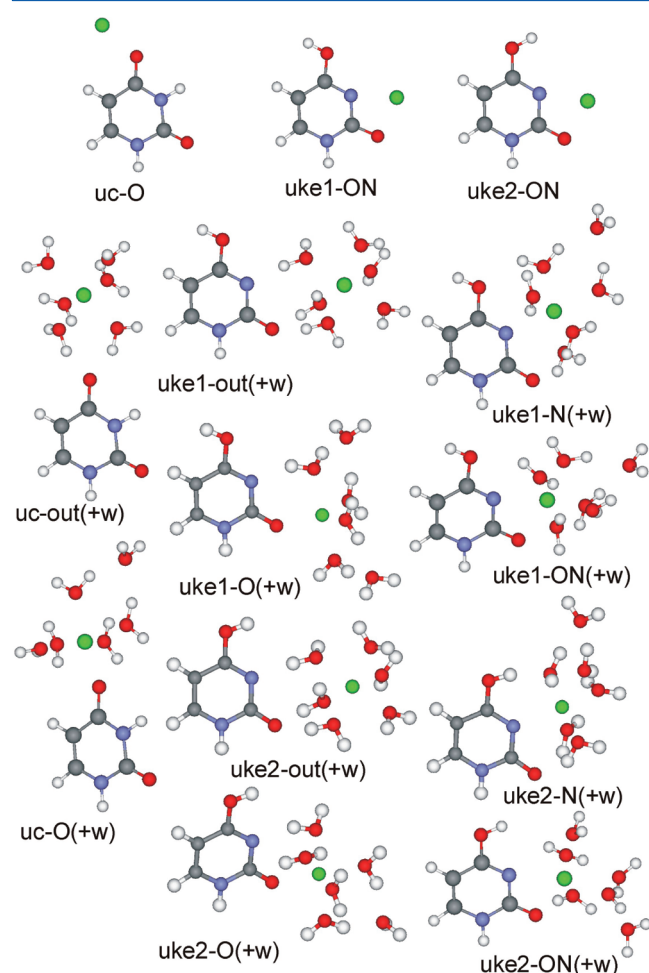


Figure 1. Optimized complexes of the Mg^{2+} ion that belong to the $\text{U} + \text{M}$ (the upper part) and $\text{U} + \text{M} + 6\text{W}$ systems (the lower part). Structures are designated according to the uracil tautomer (uc = diketo canonical tautomer; uke1 and uke2 = keto–enol rare tautomers) and a metal's binding mode (out = outer-sphere binding of uracil; O = binding to the keto oxygen (O2 or O4); N = binding to the N3; ON = bidentate binding to O2 and N3). The part of the name in parentheses is used in the text and Table 4, but not in Tables 1–3, where the name of the system is used to distinguish between the same structures that belong to different systems. Only the most stable conformer of each structure is shown.

by 12.8 and 15.2 kcal/mol less stable than the complex with the canonical uc tautomer (equivalent to uc–O+w (Figure 1) in the gas phase and when only one water ligand from the metal coordination shell was considered.³⁴

In case of the Cu^{2+} ion, the interaction with uracil is more complex than that for the divalent ions studied here. The rare tautomers will not be stabilized in the $(\text{Cu} - \text{uracil})^{2+}$ system as the most stable adduct is formed with the canonical forms of uracil and thymine even for the bare Cu^{2+} ion in the gas phase.^{19,35} However, Cu^{2+} is a strong oxidizing agent^{36–39} forming a $\text{Cu}^+ - \text{U}^+$ type of complex.³⁷ It promotes a deprotonation of the N3 nitrogen and stabilization of the bidentate N3 and carbonyl oxygen adduct (at least in the gas phase).⁴⁰

Description of the binding of the metal ions in solution is more complicated because an establishing a direct coordination bond of the nucleobase to the metal is connected with the exchange for one (monodentate binding) or two (bidentate binding) water ligands. When calculating energetic feasibility of this process, one should consider the specific environment of the metal ion because it influences the strengths of metal ions' coordination bonds. In the case of nucleobases, the metal ion binding to a negatively charged backbone phosphate group can be expected.⁴¹ This interaction may suppress the likelihood of the rare tautomer formation.¹⁴

The importance of the solvent effects on the relative stability of the uracil tautomers complexed with Pt(II) compounds was already stressed by Lippert and co-workers.⁴² Although the Pt(II) complexes with uracil are also usually deprotonated to U^- , forming the Pt–N3 bond,^{42,43} it was shown that stabilization of rare tautomers of uracil in Pt(II) complexes may occur even for neutral uracil in solution and it is caused by a preferential binding to the N3 atom over O2 and O4.⁴²

Metal interactions with uracil and its derivatives were studied in a number of theoretical and experimental studies.^{22,30,32,40,44–53} However, to the best of our knowledge, there is not any systematic study dealing with uracil interactions with the Mg^{2+} ion, which is the most relevant divalent metal cation in vivo. The current paper extends the study of Russo et al.²¹ in which three possible complexes of uracil tautomers with the bare Mg^{2+} ion were compared and the study of Kabeláč and Hobza, where interactions of bare metal ions Na^+ and Mg^{2+} with DNA nucleobases were studied systematically.¹³ Unlike the cited studies, we also study in detail the influence of environmental effects, such as the presence of the metal ion's hydration shell, of bulk water, and of the phosphate group, on the specificity of the binding of the metal ion. For the sake of simplicity, these effects are usually neglected in most theoretical studies.

Finally, the relevant complexes of the bare/hydrated Mg^{2+} ion with uracil were reoptimized also for the Ca^{2+} ion, and differences resulting from the different behavior of the two ions were discussed.

■ COMPUTATIONAL METHODS

Starting geometries of all structures were generated with the MOLDEN program,⁵⁴ and calculations were performed with the Gaussian 09 (G09) program package.⁵⁵ The DFT/B3LYP method was used for both geometry optimizations and single-point calculations. Calculation of each structure was done in three steps: (i) every structure was preliminarily optimized with the 6-31+G* basis set and also the nature of the obtained stationary points was checked by a vibrational analysis. Thermal contributions to the energetic properties were calculated using the canonical ensemble of statistical mechanics at standard conditions ($T = 298 \text{ K}$, $p = 101.325 \text{ kPa}$). (ii) Final geometry optimizations were performed with the more flexible 6-311++G** basis set in both the gas phase and in solution. (iii) Single-point energy evaluations on the final optimized geometries were carried out with the 6-311++G(2df,2pd) basis set. Default PCM parametrization as implemented for water in G09 was used in all solution-phase calculations. The calculated electron densities on this level of theory were used for natural bond order (NBO) and atoms in molecule (AIM) analyses. AIM analyses were performed by the AIMALL program.⁵⁶

Structures with one or two H_2O ligands in the second coordination shell have more possible conformers, differing in

the position of the outer-sphere ligand(s). Because we are interested in the changes of relative energies upon different modes of Mg^{2+} ion binding, we considered only structures in which the outer-sphere water ligand(s) interacted only with the inner-sphere water or phosphate ligands, while structures with direct contacts of the outer-sphere water ligand(s) with uracil were discarded. It decreased the number of possible conformers.

Interaction energies were computed as the differences between the total energies of the complexes and the energies of the isolated monomers and have been corrected for deformation energies and the basis set superposition error (BSSE) using the standard counterpoise method.⁵⁷ In the calculations of BSSE corrections within the PCM regime, the ghost atomic orbital functions were localized inside of the cavity, which has the same size as the whole complex, as was described previously by Zimmermann and Burda.⁵⁸

Additional single-point calculations on selected G09-optimized structures were conducted using the Amsterdam density functional 2010.01 package (ADF)⁵⁹ to calculate fragment energy decompositions according to the extended transition-state theory^{60,61} and to perform bond analysis using the combined extended transition-state energy decomposition analysis and natural orbitals for chemical valence (ETS-NOCV).^{62–64} In these calculations, a triple- ζ STO basis set was used, with two sets of polarization functions as provided in the ADF.

RESULTS AND DISCUSSION

We compared relative energies of uracil tautomers (U) in the presence of (1) a bare Mg^{2+} cation in the gas phase (the system U+M), (2) the hexahydrated Mg^{2+} cation (the system U+M+6W) in both the gas phase and continuum water environment (Figure 1), and (3) the hydrated Mg^{2+} ion with a coordinated phosphate anion (the system U+M+5W+P) in both the gas phase and continuum water environment (Figure 2). By this, we were able to evaluate quantitatively the influence of the ion coordination (inner and outer) and of the environment on the equilibrium between the tautomers.

1. Gas-Phase Environment. U+M System. Interaction and relative energies of structures of the U+M system are depicted in Table S1 (Supporting Information) and are compared with interaction energies for the thymine– Mg^{2+} system. Interaction energies for the uracil are systematically by about 4–5 kcal/mol less negative than those for thymine.

The most favorable structures are formed by the Mg^{2+} interactions with keto–enol uracil (uke) tautomer(s) that exhibit a bidentate $\text{N}\cdots\text{Mg}^{2+}\cdots\text{O}(\text{keto})$ binding motif, the $\text{N3}\cdots\text{Mg}^{2+}\cdots\text{O2}(\text{keto})$ motif being the most stable (structure uke1–ON; see Figure 1 and Table S1, Supporting Information). The metal complex with the canonical form of uracil (uc) enables only monodentate $\text{Mg}^{2+}\cdots\text{O}(\text{keto})$ binding motifs. The one with the $\text{Mg}^{2+}\cdots\text{O4}(\text{keto})$ binding motif (structure uc–O) represents energetically the seventh structure, being less stable by 22.1 kcal/mol than the uke1–ON structure. This is in reasonable agreement with the study of Russo et al.²¹ considering that uc–O, uke2–ON, and uke5–ON structures (Table 1 and Table S1, Supporting Information) were compared in the cited study. Note that in the absence of the metal ion, the canonical diketo uc tautomer is by at least 10 kcal/mol more stable than any other possible isomer (cf. Table 1).^{15,42,65,66}

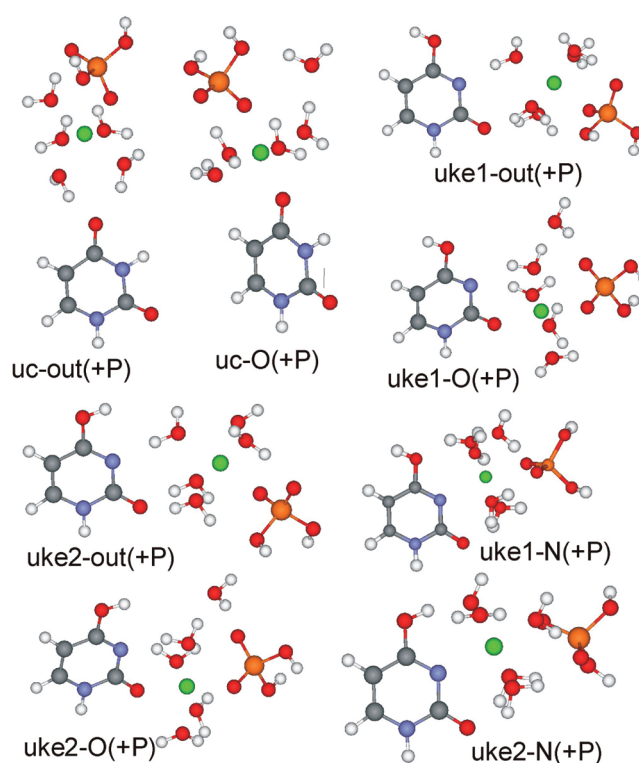


Figure 2. Optimized complexes of the Mg^{2+} ion that belong to U+M+5W+P system. See Figure 1 for further description.

Table 1. Dependence of Relative Free Energies (in kcal/mol) of the uc, uke1, and uke2 Tautomers on the Surroundings of the Bound Mg^{2+} Ion^a

structure/ system	U		U+M		U+M+6W		U+M+5W+P	
	gas phase	PCM	gas phase	gas phase	PCM	gas phase	PCM	
uc–out	0.0	0.0	n.a.	3.3	1.6	1.5	2.0	
uc–O			0.0	0.0	0.0	0.0	0.0	
uke1–out	17.7	12.7	n.a.	2.9	11.0	11.5	12.9	
uke1–O			n.a.	–3.2	8.4	6.9	9.9	
uke1–N			n.a.	7.8	14.2	13.3	14.9	
uke1–ON			–22.1	0.4	11.9	n.s.	n.s.	
uke2–out	11.6	10.9	n.a.	5.4	10.5	10.5	12.2	
uke2–O			n.a.	–2.2	7.4	4.3	8.4	
uke2–N			n.a.	10.7	12.9	11.7	15.6	
uke2–ON			–16.5 ^b	3.9	11.2	n.c.	n.c.	

^an.s. = not stable structure, see the text; n.a. = structure is not available; n.c. = not considered, see the text. ^bA relative energy ΔE_{ZPE} of –17.4 kcal/mol was calculated in ref 21.

U+M+6W System. In the water environment, the Mg^{2+} ion is surrounded by water ligands, which can be exchanged for electronegative groups of biomolecules if it is energetically feasible. Water ligands on the one hand screen the charge of the Mg^{2+} ion, decreasing electrostatic forces between the metal and uracil; on the other hand, additional H-bond interactions between the water molecules and uracil may be formed. Thus, interaction of uracil with the hydrated Mg^{2+} ion is a more complex event than uracil interaction with the bare Mg^{2+} ion.

The goal of this study is to show dependence of the specificity of the Mg^{2+} ion's binding to uracil on its environment, especially with respect to the monodentate/bidentate binding because it is directly related to the

tautomerism of uracil. Therefore, we have not calculated relative stabilities of all possible metal binding sites with all uracil tautomers as was done for the bare Mg^{2+} ion. For the U+M+6W system, the seven most stable structures of the U+M system (Table S1, Supporting Information) were hydrated by six water molecules⁶⁷ considering the following types of structures: (1) structures in which the hydrated Mg^{2+} ion interacts with the uracil isomer only via hydrogen bonds, that is, the uracil molecule is in the second coordination shell of the Mg^{2+} ion (structures uc-out+w and uken-out+w, $n = 1-6$) and (2) structures with a monodentate Mg^{2+} coordination to the keto-oxygen (structures uc-O+w and uken-O+w, $n = 1-6$). Two other types of complexes are possible for the uken enol-keto tautomers: (3) monodentate Mg^{2+} coordinated structures and (4) bidentate Mg^{2+} coordinated structures, wherein the metal is coordinated only to the N3 atom of uracil (structures uken-N+w) and to O2 and N3 atoms (structures uken-ON+w). The most stable complexes with the metal are formed by the uke1 and uke2 keto-enol tautomers and by the canonical uc tautomer (Table 1). In the subsequent text, we will concentrate on the description of the energy changes between the complexes of these three tautomers. Relative energies of metal complexes of uke3-6 tautomers are shown in Table S2 (Supporting Information).

In the gas phase, the energy gap of 22.1 kcal/mol calculated between the most stable uke1-ON structure (within the U+M system) and the canonical uc-O structure almost fully diminished in the U+M+6W system. The most stable uke1-O+w structure is only lower than the uc-O+w canonical structure by 3.2 kcal/mol (Table 1). The former structure is stabilized mainly by electrostatic interactions (-84.6 kcal/mol, Table S3, Supporting Information). Orbital interactions can be decomposed to (1) σ -electron polarization, which strongly contributes to Mg-O2 bonding (-15.7 kcal/mol, Table S3, Supporting Information) and H-bonding (-10.0 kcal/mol) and (2) π -electron polarization (-11.2 kcal/mol). The most important deformation density contributions belonging to these effects are shown in Figure 3. In the gas phase, the strength of these interactions compensates for the penalty of 17.7 kcal/mol needed for the diketo \rightarrow keto-enol tautomerization. An exchange of a water ligand for the N3 nitrogen is not energetically feasible due to the well-known magnesium preference for oxygen over nitrogen binding.⁶⁸

Explicit inclusion of the first metal's coordination shell relatively destabilizes the bidentate uke1-ON+w structure (with the N3-Mg-O2 binding motif). Formation of the Mg-N3 bond at the expense of breaking of the O4...HOH(Mg) H-bond is connected with an energy gain of only 0.4 kcal/mol (Figure 1, Table S3, Supporting Information); however, the change in the π -electron polarization contribution makes the uke1-ON+w structure less stable by 3.6 kcal/mol than the monodentate structure uke1-O+w (with the Mg-O2 bond). Therefore, the bidentate structures should not be detected in solution, and a hydrogen transfer from the N3 to O4 keto group, which leads to formation of the keto-enol tautomer (and which might be facilitated in the presence of water molecules^{47,69-72}), cannot be expected to activate the metal chelation process, as was observed for the bare metal ion in the gas phase.⁷³

Electron densities at bond critical points (BCPs) between the metal and uracil are decreased by 45 and 40% when the metal ion in the uco-O and uke-ON structures is hydrated to form the uc-O+w and uke-ON+w structures, respectively (Table

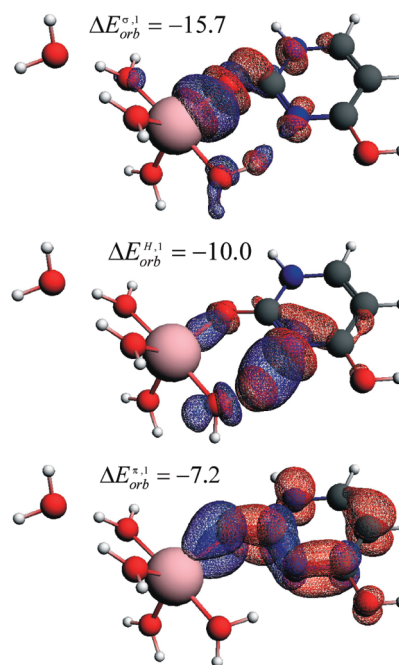


Figure 3. The contours of three most important deformation density contributions $\Delta\rho_{\sigma,1}$, $\Delta\rho_{\pi,1}$, and $\Delta\rho_{\text{H},1}$ describing the interaction of the uracil fragment with the hydrated Mg^{2+} ion in the uke1-O+w structure. In addition, the corresponding ETS-NOCV-based energies (in kcal/mol) are shown. Total interaction energies assigned to σ -bonding, π -electron polarization and to H-bonding are shown for selected structures in Table S3 (Supporting Information). The contour values are ± 0.001 au. The blue/red contours correspond to accumulation/depletion of electron density.

S4, Supporting Information). However, the interaction energies are decreased more than three times for both systems after inclusion of the first hydration shell (Table 2). It refers to a

Table 2. Gas-Phase and Solvent-Phase Interaction Energies (in kcal/mol, Corrected for the Deformation Energies and BSSE Error) of the Uracil Tautomers with the Mg^{2+} Ion and Its Environment (Explicit Water Molecules and the Phosphate)

structure/system	U+M		U+M+6W		U+M+5W+P	
	gas phase	gas phase	PCM	gas phase	PCM	
uc-out	n.a.	-36.3	-9.4	-21.1	-9.4	
uc-O	-130.47	-38.5	-9.9	-20.4	-9.2	
uke1-out	n.a.	-57.4	-15.5	-32.1	-14.5	
uke1-O	n.a.	-63.1	-19.3	-34.6	-15.4	
uke1-N	n.a.	-51.4	-11.5	-29.0	-11.1	
uke1-ON	-170.95	-55.5	-10.5	n.s.	n.s.	
uke2-out	n.a.	-48.3	-13.8	-26.6	-13.1	
uke2-O	n.a.	-57.0	-15.5	-30.6	-14.6	
uke2-N	n.a.	-43.8	-13.9	-26.0	-10.3	
uke2-ON	-158.4	-48.9	-12.0	n.c.	n.c.	

basically electrostatic nature of the Mg-O and Mg-N bonds in the uco-O and uke-ON structures with an unscreened Mg^{2+} charge. Moreover, it has to be stressed that the Laplacian of the electron density at BCP $\nabla^2\rho_{\text{BCP}}$ is positive for all M^{2+} -uracil interactions in all structures discussed in this study, which refers to ionic nature of M^{2+} -uracil bonds.

Table 3. Bond Distances (in Å) of Structures Optimized in the Gas Phase (Upper Values) and in the Solvent (Lower Values)^a

structure/bond	Mg–O2	Mg–N3	Mg–O4	H-bonds	Mg–O2	Mg–N3	Mg–O4	H-bonds
U+M+6W				U+M+5W+P				
uc–out				1.675 ^d ; 1.695 ^d 1.754 ^d ; 1.782 ^d				1.764 ^d ; 1.872 ^d 1.771 ^d ; 1.803 ^d
uc–O			2.013 2.038				2.069 2.073	
uke1–out				1.797 ^b ; 1.800 ^b ; 1.777 ^c 1.821 ^b ; 1.826 ^b ; 1.796 ^c				1.950 ^b ; 1.958 ^b ; 1.852 ^c 1.833 ^b ; 1.881 ^b ; 1.806 ^c
uke1–O	2.012 2.036			1.873 ^c 1.868 ^c	2.106 2.089			2.010 ^c 1.903 ^c
uke1–N		2.352 2.309		1.855 ^b ; 1.899 ^b ; 2.205 ^d 2.073 ^b ; 2.033 ^b ; 2.152		2.414 2.378		1.892 ^b ; 2.185 ^d 1.792 ^b ; 2.070 ^d
uke1–ON	2.142 2.262	2.343 2.245		2.893 ^d 2.397 ^d				
uke2–out				1.765 ^b ; 1.784 ^b ; 1.869 ^c 1.807 ^b ; 1.834 ^b ; 1.863 ^c				1.897 ^b ; 1.987 ^b ; 1.887 ^c 1.840 ^b ; 1.868 ^b ; 1.867 ^c
uke2–O	1.999 2.029			1.928 ^c 1.936 ^c	2.095 2.085			2.034 ^c 1.955 ^c
uke2–N		2.186 2.269		2.158 ^b ; 2.319 ^b ; 2.054 ^e 1.854 ^b ; 2.317 ^b ; 1.779 ^e		2.263 2.294		2.062 ^b ; 2.363 ^b ; 1.830 ^e 1.950 ^b ; 2.130 ^b ; 1.778 ^e
uke2–ON	2.297 2.301	2.400 2.190		– 1.971 ^e				

^aSee Table S4 (Supporting Information) for electron densities at BCPs. In the U+M system, the bonding distance Mg–O4 is 1.795 Å for the uc–O structure. Mg–O2 and Mg–N3 distances are 1.967 and 2.089 Å and 1.945 and 2.135 Å for the uke1–ON and uke2–ON structures, respectively. ^bO2...HOH hydrogen bond. ^cN3...HOH hydrogen bond. ^dO4...HOH hydrogen bond. ^eO4H...OH₂ hydrogen bond

NBO analysis shows that a mean transferred charge to Mg²⁺ is about –0.1 e per ligand for the U+M+6W system in the gas phase. This value is almost independent of the number and the size of the ligands, being roughly the same for all structures in both the U+M and U+M+6W systems with the same coordination number, that is, magnesium has NPA charges of ~1.5 and ~1.4 e when it is, respectively, penta- and hexa-coordinated (Table S5, Supporting Information). Looking at the charges of the uc–out and uke1(2)–out structures in Table S5 (Supporting Information), one can also see an indirect charge flow from uracil to the metal ion via H-bonded water ligands (cf. Figure 3).

U+M+5W+P System. In nucleic acids, the sugar–phosphate backbone is the main target of the Mg²⁺ ions. Direct phosphate–uracil contacts cannot be observed in nucleic acids (at least at physiological pH) but have to be mediated by metal ions and/or water molecules. To study the influence of electrostatic screening of the phosphates on the specificity of the metal ion binding to uracil, the inner-sphere water ligand, which is in the trans position with respect to the bound uracil, was replaced by the phosphate H₂PO₄[–] anion. This arrangement ensured that no direct contacts between the phosphate and uracil groups might be established during optimizations. Of course, this arrangement does not represent a realistic model of uridine monophosphate (or an intranucleotide macrochelate) because we completely neglected the sugar linkage. However, in a real RNA environment, the uracil base and the phosphate group bound by the same metal do not need to belong to the same nucleotide, forming an internucleotide macrochelate.⁷⁴ Note that the Mg²⁺ ion may also bind the phosphate anion in the outer-sphere manner. This situation is not described in this study due to a large number of possible energetically close conformers, but its influence on tautomer stabilization can be estimated considering U+M+6W and U+M+5W+P as the boundary systems.

The presence of the phosphate anion in the metal's first coordination shell further destabilizes the bidentate uke–ON +P structure, which does not exist as a minimum always being transferred to the monodentate uke–O+P structure upon optimization. On the other hand, the uke2–ON+P structure is stable but only due to a direct phosphate–uracil O4H...OP interaction. Therefore, the stability of uke2–ON+P is overestimated with respect to the other structures (where the direct phosphate–uracil interactions are avoided; see above), and therefore, we do not consider this structure here.

In the U+M+5W+P system, the gas-phase results already predict a higher stability of the uc complexes than of the rare tautomer uke1 and uke2 complexes but still overestimates the stability of the latter complexes with respect to the results for the solvent environment (Table 1). In the gas phase, the presence of a negatively charged phosphate decreases the values of interaction energies to less than two-thirds (by 37 ± 2%) with respect to the values calculated for the U+M+6W system (Table 2). Note that the same effect was already observed in the inverse sense; the inner-shell binding of the metal to guanine substantially reduced the strength of the (outer-shell) metal binding to the phosphate group.⁷⁵

Because the metal–uracil interactions are governed mainly by electrostatics, we decided to analyze the changes in the interaction energies upon phosphate binding (i.e., when reducing the charge of the metal fragment from +2 to +1 e). According to the energy decomposition analysis, a drop of energies of orbital interactions covers more than 50% of the total decrease of interaction energies caused by a phosphate binding because a decrease of the electrostatic energy is partly compensated for by a decrease of the Pauli repulsion (Table S3, Supporting Information). ETS-NOCV analysis of orbital interactions shows that the presence of the phosphate decreases mainly energy contributions connected with a polarization of π -electrons of the uracil aromatic ring (by ~70%), the energy of

H-bonds (by $\sim 40\%$), and, to the least extent, the energy of the direct Mg^{2+} –uracil interactions (by $\sim 20\%$) connected with the redistribution of the σ -electrons (Figure 3 and Table S3, Supporting Information).

These results are in agreement with the AIM analysis (Table S4, Supporting Information); the phosphate binding does not change the strengths of Mg – OH_2 interactions but decreases the strength of H-bond interactions between uracil and water ligands (by at least 25%) and also slightly that of direct Mg –uracil interactions (by at least 10%).

Substitution of one water ligand in the first coordination shell for the phosphate group lowers the metal's charge only by about 0.03e. The phosphate group has the total charge of about -0.79e (Table S3, Supporting Information). The transferred negative charge is uniformly spread over the system, and the total charges of the other metal's ligands (including uracil) are decreased also by about 0.03 e per ligand (i.e., by the same value as the metal). A water environment decreases the charge transfer from the phosphate group by about 10% (cf. results in the next section).

2. Water (Solvent-Phase) Environment. The water environment affects the geometries of the optimized structures to some extent; it especially tends to shorten the H-bonds (Table 3). The electron densities at BCPs of these H-bonds are increased accordingly, which may increase their relative strengths with respect to the direct Mg – O/Mg – N interactions in solution. However, the nature of all H-bond interactions remains strongly ionic ($\nabla^2\rho_{\text{BCP}} > 0$); therefore, their real absolute strengths are governed by electrostatics. For example, in uc-O+w , the metal fragment interacts with uracil only via two H-bonds, which are shortened by about 0.08 Å in solution (Table 3), but at the same time, the interaction energy between the fragments is decreased almost four times (Table 2).

The water environment has a profound effect on the relative energies of the complexes. The canonical uc-O+w structure is by 8.4 and 7.4 kcal/mol more stable than the uke-O+w and uke2-O+w structures, respectively (Table 1). The uke2 tautomer complexes are systematically more stable by about 1–2 kcal/mol than the uke1 ones. Inclusion of the implicit solvent leads to even larger destabilization of the complexes with the bidentate bonding of the metal represented by the uke-ON+w and uke2-ON+w structures; they are by 11.9 and 11.2 kcal/mol, respectively, less stable than the uc-O+w structure. Therefore, in solution, the formation of the rare tautomers of uracil with a bound Mg^{2+} ion should be completely suppressed.

There is only a slight free-energy gain upon the direct metal coordination to uracil with respect to the outer-sphere binding because the difference between the uc-O+w and uc-out+w structures is only 1.6 kcal/mol. The O4 atom of the canonical form is the main metal's binding site in uracil. In solution, one can expect a similar probability for its inner- and outer-sphere binding by the Mg^{2+} ion. This finding is in accord with experimental observations.⁷⁴

The solvation diminishes differences in interaction energies between the uracil and metal fragments in the structures of the U+M+6W and U+M+5W+P systems. Compared to the gas phase, the lowering of the interaction energies in the +2 charged structures of the U+M+6W system is more than two times higher than that in the +1 charged structures of the U+M+5W+P system. It refers to the importance of the electrostatic stabilization of the gas-phase structures.

In solvent, the relative energies of the U+M+5W+P structures are in qualitative agreement with the results for the U+M+6W system, but still, the presence of the phosphate in the first coordination shell destabilizes systematically the keto–enol tautomers by about 2 kcal/mol (Table 1). Therefore, the phosphate group enhances the protective and shielding effects of the water environment against the possible shifts of tautomeric equilibria caused by metal ions, as suggested already for the metal binding to guanine.¹⁴

The water environment decreases the polarization of the uracil and also very slightly the charge transfer from the uracil fragment toward the hydrated metal fragment. The changes of the NPA charges of the atoms on the uracil fragment can be up to the order of several tenths of the elementary charge (e) decreasing the polarization of uracil by more than 50% for all the structures. The changes in the transferred charges are on the order of 0.01 e, reducing the charge transfer but only by less than 10% for most of the structures.

3. Comparison with the Ca^{2+} Ion. We performed optimizations of the structures in the U+M and U+M+6W systems also with the Ca^{2+} ion. The Ca^{2+} ion forms weaker interactions with uracil than the Mg^{2+} ion. For structures in the U+M system, interaction energies with uracil are smaller for the Ca^{2+} ion than for the Mg^{2+} ion by about 20%. The water ligands (U+M+6W system) decrease this relative difference down to $\sim 10\%$ mainly due to a higher flexibility of the Ca^{2+} hydration shell (cf. gas-phase interaction energies corrected for deformation energies in Tables 2 and 4 with the uncorrected

Table 4. Relative Gibbs Free Energies (in kcal/mol) of the Structures in the U+M , U+M+6W Systems Stabilized by the Ca^{2+} Ion Together with Interaction Energies (Corrected for the Deformation Energies and BSSE) between the Uracil and Metal Fragments^a

	ΔG		ΔE_{int}	
	gas phase	PCM	gas phase	PCM
uc–O	0.0		–106.9	
uke1–ON	–10.6		–136.5	
uke2–ON	–5.5 ^b		–124.8	
uc–out+w	3.3	–0.6	–34.2	–9.0
uc–O+w	0.0	0.0	–38.3	–9.2
uke1–out+w	4.8	10.0	–53.7	–14.5
uke1–O+w	0.3	8.9	–57.5	–16.1
uke1–N+w	n.s.	11.9	n.s.	–13.2
uke1–ON+w	3.3	10.2	–55.5	–12.7
uke2–out+w	7.1	9.4	–45.0	–12.9
uke2–O+w	1.4	7.6	–51.0	–15.1
uke2–N+w	n.s.	12.0	n.s.	–9.1
uke2–ON+w	6.8	7.6	–48.3	–16.5

^an.s. not stable structure (see the text). ^bRelative energy ΔE_{ZPE} of -6.3 kcal/mol was calculated for the U-Ca^{2+} complex (ref 21).

ones in Table S3, Supporting Information). Surprisingly, the larger differences between the metals are in electrostatic rather than in orbital interactions (Table S3, Supporting Information). In solution, interaction energies of some structures with a highly distorted hydration shell are even higher for Ca^{2+} than those for Mg^{2+} .

In the U+M system, the complexes of the rare keto–enol tautomers uke1(2)-ON are much less stabilized by the Ca^{2+} ion than by the Mg^{2+} ion. After inclusion of the first hydration shell (U+M+6W system), all Ca^{2+} complexes of the rare keto–

enol uke1(2) tautomers are less stable than the canonical uc-O+w structure. In the gas phase, we were not able to optimize stable uke1(2)-N+w^{Ca} structures, which were converted spontaneously to uke1(2)-ON+w^{Ca} structures. This refers to a low affinity of Ca²⁺ for N3.

CONCLUSIONS

In this contribution, the influence of the environment of the Mg²⁺ ion on the specificity of its binding to uracil is discussed and evaluated. On the basis of the gas-phase and solvent-phase results, we have chosen three structures for a detailed analysis, (1) the diketo tautomer with the O4 metal's binding site and (2 and 3) the two keto-enol tautomers with the N3-O2(keto) bidentate metal's binding site as the representatives of the canonical and rare tautomers, respectively. An explicit inclusion of the first coordination shell and implicit description of the bulk environment is necessary to obtain biologically relevant results. In the gas phase, the bidentate N3-Mg-O(keto) binding motif is strongly preferred, stabilizing the rare keto-enol tautomers. On the other hand, the water environment and/or presence of the phosphate group clearly stabilize the canonical diketo tautomer with oxygen atoms as the only metal's binding targets. Thus, the environment has a protective function against point mutations.

Keto oxygens in uracil are weak nucleophiles because a substitution of a water ligand for the O2/O4 keto oxygen is connected with an exergonicity of max. 2.0 kcal/mol (Tables 1 and 4). Therefore, a similar probability of the inner- and outer-sphere binding by the Mg²⁺ ion can be expected.

ASSOCIATED CONTENT

Supporting Information

Table S1 with schematic drawings of the optimized complexes of uracil with the bare Mg²⁺ ion. Their relative and interaction energies are also given and compared with energies of corresponding structures of the thymine-bare Mg²⁺ ion system. Relative energies of the Mg²⁺ complexes of uken ($n = 3-6$) tautomers are given in Table S2. For the Mg²⁺ complexes, the energy decomposition analysis of gas-phase optimized structures of the U+M+6W and U+M+5W+P systems, electron densities at BCPs of gas-phase and solvent-phase optimized structures, and NBO charges of the fragments in gas-phase and solvent-phase optimized structures are shown in Tables S3-S5. For the Ca²⁺ complexes, the energy decomposition analysis of the gas-phase optimized structures of the metal complexes of the U+M+6W system are given in Table S3. This material is available free of charge via the Internet at <http://pubs.acs.org>.

AUTHOR INFORMATION

Corresponding Author

*E-mail: chval@jcu.cz.

Notes

The authors declare no competing financial interest.

ACKNOWLEDGMENTS

This project was supported by grants from the Czech Science Foundation (204/09/J010) and from the Ministry of Education, Youth and Sports of the Czech Republic (ME09062). The access to the MetaCentrum supercomputing facilities (Grant LM2010005) is highly appreciated.

REFERENCES

- (1) Florián, J.; Leszczynski, J. *J. Am. Chem. Soc.* **1996**, *118*, 3010–3017.
- (2) Bregadze, V. G.; Gelagutashvili, E. S.; Tsakadze, K. J.; Melikishvili, S. Z. *Chem. Biodiversity* **2008**, *5*, 1980–1989.
- (3) Šponer, J.; Šponer, J. E.; Gorb, L.; Leszczynski, J.; Lippert, B. *J. Phys. Chem. A* **1999**, *103*, 11406–11413.
- (4) Torigoe, H.; Ono, A.; Kozasa, T. *Chem.—Eur. J.* **2010**, *16*, 13218–13225.
- (5) Benda, L.; Straka, M.; Tanaka, Y.; Sychrovský, V. *Phys. Chem. Chem. Phys.* **2011**, *13*, 100–103.
- (6) Miyachi, H.; Matsui, T.; Shigeta, Y.; Yamashita, K.; Hirao, K. *Chem. Phys. Lett.* **2010**, *495*, 125–130.
- (7) Hanus, M.; Kabeláč, M.; Rejnek, M.; Ryjáček, F.; Hobza, P. *J. Phys. Chem. B* **2004**, *108*, 2087–2097.
- (8) Kwiatkowski, J. S.; Bartlett, R. J.; Person, W. B. *J. Am. Chem. Soc.* **1988**, *110*, 2353–2358.
- (9) Colominas, C.; Luque, F. J.; Orozco, M. *J. Am. Chem. Soc.* **1996**, *118*, 6811–6821.
- (10) Kabeláč, M.; Hobza, P. *Phys. Chem. Chem. Phys.* **2007**, *9*, 903.
- (11) Kryachko, E. S.; Nguyen, M. T.; Zeegers-Huyskens, T. *J. Phys. Chem. A* **2001**, *105*, 1288–1295.
- (12) Leszczynski, J. *J. Phys. Chem.* **1992**, *96*, 1649–1653.
- (13) Kabeláč, M.; Hobza, P. *J. Phys. Chem. B* **2006**, *110*, 14515–14523.
- (14) Kosenkov, D.; Gorb, L.; Shishkin, O. V.; Šponer, J.; Leszczynski, J. *J. Phys. Chem. B* **2008**, *112*, 150–157.
- (15) Rejnek, J.; Hanus, M.; Kabeláč, M.; Ryjáček, F.; Hobza, P. *Phys. Chem. Chem. Phys.* **2005**, *7*, 2006.
- (16) Trygubenko, S. A.; Bogdan, T. V.; Rueda, M.; Orozco, M.; Luque, F. J.; Šponer, J.; Slaviček, P.; Hobza, P. *Phys. Chem. Chem. Phys.* **2002**, *4*, 4192–4203.
- (17) Jang, Y. H.; Goddard, W. A.; Noyes, K. T.; Sowers, L. C.; Hwang, S.; Chung, D. S. *J. Phys. Chem. B* **2003**, *107*, 344–357.
- (18) Burda, J. V.; Šponer, J.; Leszczynski, J. *J. Biol. Inorg. Chem.* **2000**, *5*, 178–188.
- (19) Rincón, E.; Yáñez, M.; Toro-Labbé, A.; Mó, O. *Phys. Chem. Chem. Phys.* **2007**, *9*, 2531–2537.
- (20) Marino, T.; Mazzuca, D.; Toscano, M.; Russo, N.; Grand, A. *Int. J. Quantum Chem.* **2007**, *107*, 311–317.
- (21) Russo, N.; Toscano, M.; Grand, A. *J. Phys. Chem. A* **2003**, *107*, 11533–11538.
- (22) Lamsabhi, A. M.; Mó, O.; Yáñez, M.; Boyd, R. J. *J. Chem. Theory Comput.* **2008**, *4*, 1002–1011.
- (23) Lippert, B.; Gupta, D. *Dalton Trans.* **2009**, 4619.
- (24) Burda, J. V.; Šponer, J.; Leszczynski, J.; Hobza, P. *J. Phys. Chem. B* **1997**, *101*, 9670–9677.
- (25) Šponer, J.; Sabat, M.; Burda, J. V.; Leszczynski, J.; Hobza, P. *J. Phys. Chem. B* **1999**, *103*, 2528–2534.
- (26) Poater, J.; Sodupe, M.; Bertran, J.; Solà, M. *Mol. Phys.* **2005**, *103*, 163–173.
- (27) Cerón-Carrasco, J. P.; Jacquemin, D. *ChemPhysChem* **2011**, *12*, 2615–2623.
- (28) Ono, A.; Torigoe, H.; Tanaka, Y.; Okamoto, I. *Chem. Soc. Rev.* **2011**, *40*, 5855–5866.
- (29) Martínez, A. *J. Phys. Chem. A* **2009**, *113*, 1134–1140.
- (30) Wang, N.; Li, P.; Hu, Y.; Bu, Y.; Wang, W.; Xie, X. *J. Theor. Comput. Chem.* **2007**, *06*, 197.
- (31) Rincón, E.; Jaque, P.; Toro-Labbé, A. *J. Phys. Chem. A* **2006**, *110*, 9478–9485.
- (32) Gutlé, Salpin, J.; Cartailier, T.; Tortajada, J.; Gaigeot, M. *J. Phys. Chem. A* **2006**, *110*, 11684–11694.
- (33) Li, D.; Ai, H. *J. Phys. Chem. B* **2009**, *113*, 11732–11742.
- (34) Gillis, E. A. L.; Rajabi, K.; Fridgen, T. D. *J. Phys. Chem. A* **2009**, *113*, 824–832.
- (35) Marino, T.; Toscano, M.; Russo, N.; Grand, A. *Int. J. Quantum Chem.* **2004**, *98*, 347–354.
- (36) Noguera, M.; Bertran, J.; Sodupe, M. *J. Phys. Chem. A* **2004**, *108*, 333–341.

- (37) Pavelka, M.; Shukla, M. K.; Leszczynski, J.; Burda, J. V. *J. Phys. Chem. A* **2008**, *112*, 256–267.
- (38) Pavelka, M.; Šimánek, M.; Šponer, J.; Burda, J. V. *J. Phys. Chem. A* **2006**, *110*, 4795–4809.
- (39) Noguera, M.; Bertran, J.; Sodupe, M. *J. Phys. Chem. B* **2008**, *112*, 4817–4825.
- (40) Lamsabhi, A. M.; Alcamí, M.; Mó, O.; Yáñez, M.; Tortajada, J. *J. Phys. Chem. A* **2006**, *110*, 1943–1950.
- (41) Sigel, R.; Sigel, H. *Acc. Chem. Res.* **2010**, *43*, 974–984.
- (42) van der Wijst, T.; Fonseca Guerra, C.; Swart, M.; Bickelhaupt, F. M.; Lippert, B. *Chem.—Eur. J.* **2009**, *15*, 209–218.
- (43) Lippert, B. *Prog. Inorg. Chem.* **1989**, *37*, 1–97.
- (44) Lamsabhi, A. M.; Alcamí, M.; Mó, O.; Yáñez, M.; Tortajada, J. *ChemPhysChem* **2004**, *5*, 1871–1878.
- (45) Lamsabhi, A. M.; Alcamí, M.; Mó, O.; Yáñez, M.; Tortajada, J.; Salpin, J. Y. *ChemPhysChem* **2007**, *8*, 181–187.
- (46) Odani, A.; Kozłowski, H.; Swiatek-Kozłowska, J.; Brasun, J.; Operschall, B. P.; Sigel, H. *J. Inorg. Biochem.* **2007**, *101*, 727–735.
- (47) Hu, X. B.; Li, H. R.; Zhang, L.; Han, S. J. *J. Phys. Chem. B* **2007**, *111*, 9347–9354.
- (48) Schoellhorn, H.; Thewalt, U.; Lippert, B. *J. Am. Chem. Soc.* **1989**, *111*, 7213–7221.
- (49) Eizaguirre, A.; Lamsabhi, A. M.; Mó, O.; Yáñez, M. *Theor. Chem. Acc.* **2010**, *128*, 457–464.
- (50) Russo, N.; Sicilia, E.; Toscano, M.; Grand, A. *Int. J. Quantum Chem.* **2002**, *90*, 903–909.
- (51) Trujillo, C.; Lamsabhi, A. M.; Mó, O.; Yáñez, M.; Salpin, J.-Y. *Org. Biomol. Chem.* **2008**, *6*, 3695–3702.
- (52) Eizaguirre, A.; Mó, O.; Yáñez, M.; Boyd, R. J. *Org. Biomol. Chem.* **2010**, *9*, 423–431.
- (53) Salpin, J.-Y.; Guillaumont, S.; Ortiz, D.; Tortajada, J.; Maitre, P. *Inorg. Chem.* **2011**, *50*, 7769–7778.
- (54) Schaftenaar, G.; Noordik, J. *J. Comput.-Aided Mol. Des.* **2000**, *14*, 123–134.
- (55) Frisch, M. J. et al. *Gaussian 09*, revision A.01; Gaussian, Inc.: Pittsburgh, PA, 2009.
- (56) Keith, T. A. *AIMAll*, version 10.11.24. <http://aim.tkgristmill.com> (2010).
- (57) Boys, S. F.; Bernardi, F. *Mol. Phys.* **1970**, *19*, 553–566.
- (58) Zimmermann, T.; Chval, Z.; Burda, J. V. *J. Phys. Chem. B* **2009**, *113*, 3139–3150.
- (59) ADF2010, *SCM, Theoretical Chemistry*; Vrije Universiteit: Amsterdam, The Netherlands, 2010.
- (60) Ziegler, T.; Rauk, A. *Theor. Chim. Acta* **1977**, *46*, 1–10.
- (61) Ziegler, T.; Rauk, A. *Inorg. Chem.* **1979**, *18*, 1755–1759.
- (62) Mitoraj, M.; Michalak, A.; Ziegler, T. *J. Chem. Theory Comput.* **2009**, *5*, 962–975.
- (63) Mitoraj, M. P.; Michalak, A.; Ziegler, T. *Organometallics* **2009**, *28*, 3727–3733.
- (64) Mitoraj, M. P.; Kurczab, R.; Boczar, M.; Michalak, A. *J. Mol. Model.* **2010**, *16*, 1789–1795.
- (65) Wu, R.; McMahon, T. B. *J. Am. Chem. Soc.* **2006**, *129*, 569–580.
- (66) Millefiori, S.; Alparone, A. *Chem. Phys.* **2004**, *303*, 27–36.
- (67) As a minimal model for a solvated ion, see: Deerfield, D. W.; Fox, D. J.; Head-Gordon, M.; Hiskey, R. G.; Pedersen, L. G. *J. Am. Chem. Soc.* **1991**, *113*, 1892–1899.
- (68) Šponer, J. E.; Sychrovský, V.; Hobza, P.; Šponer, J. *Phys. Chem. Chem. Phys.* **2004**, *6*, 2772–2780.
- (69) Hu, X.; Li, H.; Liang, W.; Han, S. *J. Phys. Chem. B* **2004**, *108*, 12999–13007.
- (70) Hu, X.; Li, H.; Liang, W.; Han, S. *J. Phys. Chem. B* **2005**, *109*, 5935.
- (71) Fan, J.; Shang, Z.; Liang, J.; Liu, X.; Jin, H. *J. Mol. Struct.: THEOCHEM* **2010**, *939*, 106–111.
- (72) Kryachko, E. S.; Nguyen, M. T.; Zeegers-Huyskens, T. *J. Phys. Chem. A* **2001**, *105*, 1934.
- (73) Rincón, E.; Toro-Labbé, A. *Chem. Phys. Lett.* **2007**, *438*, 93–98.
- (74) Freisinger, E.; Sigel, R. K. O. *Coord. Chem. Rev.* **2007**, *251*, 1834–1851.
- (75) Rulíšek, L.; Šponer, J. *J. Phys. Chem. B* **2003**, *107*, 1913–1923.

Mechanism of the *cis*-[Pt(1*R*,2*R*-DACH)(H₂O)₂]²⁺ Intrastrand Binding to the Double-Stranded (pGpG)·(CpC) Dinucleotide in Aqueous Solution: A Computational DFT Study

Zdeněk Chval,^{*,†} Martin Kabeláč,[‡] and Jaroslav V. Burda^{*,§}

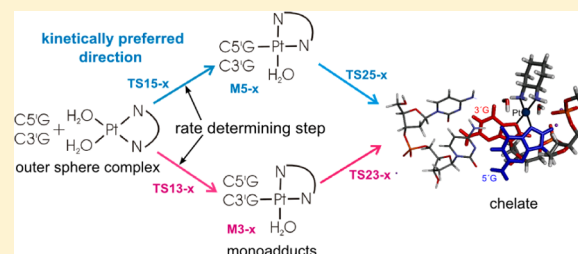
[†]Department of Laboratory Methods and Information Systems, Faculty of Health and Social Studies, University of South Bohemia, J. Boreckého 27, 370 11 České Budějovice, Czech Republic

[‡]Department of Chemistry, Faculty of Science, University of South Bohemia, Branišovská 31, 37005 České Budějovice, Czech Republic

[§]Department of Chemical Physics and Optics, Faculty of Mathematics and Physics, Charles University, Ke Karlovu 3, 121 16 Prague 2, Czech Republic

Supporting Information

ABSTRACT: A mechanism of the intrastrand 1,2-cross-link formation between the double-stranded pGpG·CpC dinucleotide (ds(pGpG)) and fully aquated oxaliplatin *cis*-[Pt(DACH)(H₂O)₂]²⁺ (DACH = cyclohexane-1*R*,2*R*-diamine) is presented. All structures of the reaction pathways including the transition states (TSs) were fully optimized in water solvent using DFT methodology with dispersion corrections. Both 5' → 3' and 3' → 5' binding directions were considered. In the first step there is a slight kinetic preference for 5'-guanine (5'G) monoadduct formation with an activation Gibbs free energy of 18.7 kcal/mol since the N7 center of the 5'G base is fully exposed to the solvent. On the other hand, the N7 atom of 3'-guanine (3'G) is sterically shielded by 5'G. The lowest energy path for formation of the 3'G monoadduct with an activation barrier of 19.3 kcal/mol is connected with a disruption of the 'DNA-like' structure of ds(pGpG). Monoadduct formation is the rate-determining process. The second step, chelate formation, is kinetically preferred in the 3' → 5' direction. The whole process of the platination is exergonic by up to -18.8 kcal/mol. Structural changes of ds(pGpG), charge transfer effects, and the influence of platination on the G·C base pair interaction strengths are also discussed in detail.



INTRODUCTION

Discovery of antitumor activity of cisplatin by Rosenberg more than 40 years ago¹ started an extended study of the chemical and biological properties of platinum compounds. Cisplatin is a very efficient drug against ovarian, bladder, head, neck, as well as nonsmall lung and cervical cancers. However, its use has several limitations such as severe side effects and the possibility of intrinsic and acquired resistance promoting the search for new, less toxic, and more efficient drugs.

Oxaliplatin [(cyclohexane-1*R*,2*R*-diammine)oxalatoplatinum(II)] is a third-generation platinum drug,² which is active against some cisplatin-resistant tumors³ and has a lower overall toxicity than cisplatin. In oxaliplatin, the two ammine and chloro ligands of cisplatin are replaced by the bidentate DACH and oxalate group ligands (Figure 1). Oxaliplatin forms similar adducts with DNA as cisplatin; however, adduct affinity toward proteins may be different for the two drugs.⁴ On the other hand, the oxalate leaving group changes the rate of aquation⁵ and cellular uptake of the drug.⁶ Biotransformation of oxaliplatin was recently reviewed by Jerremalm et al.⁷ In the blood oxaliplatin reacts rapidly with proteins and sulfur-containing compounds like methionine and glutathione, but

the resulting adducts are probably noncytotoxic. Oxaliplatin can be also rapidly hydrolyzed, establishing an equilibrium between intact oxaliplatin and the highly reactive oxalato monodentate [Pt(DACH)(oxalate)(H₂O)]⁺ complex.⁸ However, whether this complex represents the active form of oxaliplatin which reacts with DNA is to the best of our knowledge unknown.

In the simpler case of cisplatin there is a general agreement that the partially aquated [Pt(NH₃)₂Cl(H₂O)]⁺ complex is the active form of the drug which interacts with DNA.^{9–11} However, it is still not clear to what extent [Pt(NH₃)₂Cl(H₂O)]⁺ reacts with DNA forming covalently bound monoadducts since according to an alternative mechanism [Pt(NH₃)₂Cl(H₂O)]⁺ forms an outer-sphere complex with DNA.¹² Then a specific local DNA microenvironment may speed up substantially the second aquation step and suppress formation of [Pt(NH₃)₂(OH)(H₂O)]⁺ from [Pt(NH₃)₂(H₂O)₂]²⁺ (its p*K*_a value is ca. 5.5^{13,14} in the 'bulk' water solution). Thus, the most reactive and fully aquated [Pt(NH₃)₂(H₂O)₂]²⁺ complex could be the species that forms a

Received: December 4, 2012

Published: May 8, 2013

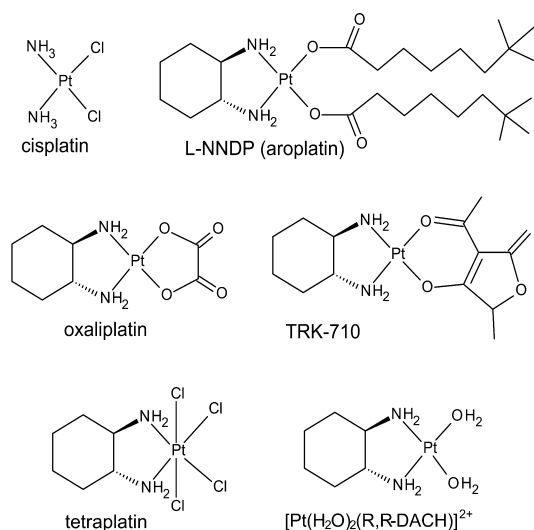


Figure 1. Structures of cisplatin, oxaliplatin, some other DACH-containing drugs which entered to clinical trials,¹⁵ and the fully aquated form $[\text{Pt}(\text{H}_2\text{O})_2(\text{R,R-DACH})]^{2+}$ that is considered in this study.

covalent bond with the N7 atom of guanine.¹² According to the cited paper the hydrogen bond (H-bond) interactions play an important role in stabilization of the transition state for monoadduct formation, and the rate of platination is given by the H-bond donor ability of the ligands of the Pt(II) drug.¹² If these assumptions are correct then the diaqua $[\text{Pt}(\text{R,R-DACH})(\text{H}_2\text{O})_2]^{2+}$ complex may have an even more important impact on the reactivity of Pt(DACH) complexes than the $[\text{Pt}(\text{NH}_3)_2(\text{H}_2\text{O})_2]^{2+}$ hydrated form for cisplatin since some H-bond acceptor centers on DNA may be inaccessible for the bulkier DACH ligand. This increases the relative importance of the leaving group ligands as H-bond donors. Thus, we believe that our model represented by the fully aquated $[\text{Pt}(\text{R,R-DACH})(\text{H}_2\text{O})_2]^{2+}$ complex, and the ds(pGpG) dinucleotide may offer useful insight into the DNA binding mechanism of oxaliplatin and other DACH-containing drugs (Figure 1).

It is known that 60–65% of cisplatin is bound to GpG sites.¹⁶ Experimental results show that the rate of platination is higher for double-stranded oligonucleotides than for single-stranded ones,^{3,17,18} and it increases with the length of the oligonucleotide.¹⁹ This is probably caused by an enhanced diffusion due to electrostatic attraction between a higher number of the negatively charged phosphate groups and the positively charged (aquated) Pt(II) drug.¹⁷

Monofunctional adducts are formed faster with 5'G than 3'G in the GG sequences.^{3,4,6} On the other hand, in the AG/GA sequence context intrastrand 1,2-AG cross-links are formed (representing 20–25% of all platinum adducts), while 1,2-GA chelates are hardly detectable despite very similar binding energies.²⁰ It suggests that cross-link formation should start uniquely on 3'G since the first platinum attack occurs always at a guanine base. Therefore, the exact place of the first platinum attack is clearly sequence dependent. Baik et al.²¹ used pApG and pGpA single strands to model the AG and GA chelate formations, respectively. The AG chelate was formed preferably compared to the GA one due to transition state stabilization by an H-bond between the ammine and the 5'-phosphate (5'P) groups.²¹ A detailed discussion about the mechanistic aspects of the platinum drugs' binding to DNA is presented in a review by Kozelka.²²

There are a number of studies dealing with the mechanisms of the substitutions of aqua ligand(s) by one or two isolated guanine nucleobases in various activated (aquated) platinum square planar compounds.^{23–30} Three basic conformations of the two guanine ligands have been recognized in product structures: one head-to-head (HH) and two head-to-tail conformations ($\Delta\text{HT}, \Lambda\text{HT}$).³¹ The HT conformations are energetically more feasible than the HH conformation.^{26,31} However, only the HH conformation can be regarded for the intrastrand cross-link in double-stranded DNA (ds-DNA).

In this contribution the fully optimized stationary points for monoadduct formation of the $[\text{Pt}(\text{H}_2\text{O})_2(\text{R,R-DACH})]^{2+}$ complex (labeled as PtDACH hereafter) with ds(pGpG) and for subsequent formation of the 1,2-GG chelate are presented. Both possible 5' → 3' and 3' → 5' binding directions (Figure 2) are considered. While structures of the stable monoadducts

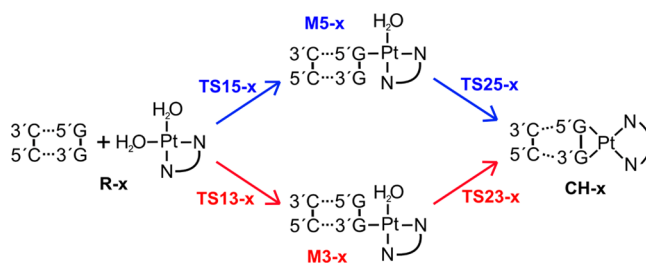


Figure 2. Platinum cross-linked structure with the GG sequence may be formed either via a 5'G-monoadduct (5'G → 3'G direction, blue) or via a 3'G-monoadduct (3'G → 5'G direction, red).

and chelates of the Pt(II) compounds with DNA have been studied in many theoretical as well as experimental studies,^{4,32–48} fully optimized structures of all important structures (including the transition states) along both possible reaction pathways are published for the first time. Since the DACH amine groups have neither strong σ -donation nor strong π -back-donation ability it can be expected that substitution in both directions will follow an associative interchange mechanism⁴⁹ with elongated bonds to the entering and leaving ligands.⁵⁰ It is shown that steric hindrance and nonbonding interactions affect the structures of transition states and monoadducts, and in this way, they influence the energetics and specificity of the binding.

COMPUTATIONAL DETAILS

All geometries were fully optimized using the RI-TPSS-D/COSMO method, which comprises the TPSS functional⁵¹ including the resolution of identity (RI) approximation of the Coulomb integrals, the empirical dispersion term for the main group elements,⁵² and the COSMO continuum solvation model with the cavities constructed based on the Klamt's atomic radii⁵³ and water as the medium. The Coulomb potentials of all elements were approximated by auxiliary basis sets developed by Weigend.⁵⁴

The TPSS-D functional is able to reproduce well the conformational changes and stacking interactions in nucleic acids and related systems.^{55–57} Recently, a similar methodology was used also for description of transition metal compounds.^{58,59} In the optimization model used in this study, the main group elements are described by a split valence def2-SV(P) basis set. The platinum atom was treated using Dresden–Stuttgart quazirelativistic energy-averaged effective pseudopotentials⁶⁰ with a pseudo-orbital basis set augmented by the set of diffuse ($\alpha_s = 0.0075$, $\alpha_p = 0.013$, $\alpha_d = 0.025$) and polarization ($\alpha_f = 0.98$) functions.⁶¹ These calculations were performed by the Turbomole 6.1 program⁶² and labeled as RI-TPSS-D/BSI/COSMO in

further text. Despite the fact that it is known⁶³ that combination of TPSS-D with a DZ basis set generally leads to slightly underestimated H-bond distances, we found that the RI-TPSS-D/BSI/COSMO method offers very good geometries of Pt(II) complexes and a reasonable description of the dispersion interactions (cf. below). Since the main structural changes during the PtDACH binding are connected with ligand substitutions on the Pt(II) center and unstacking of both guanines, this method represents in our opinion a reasonable compromise between applicability and accuracy.

All geometries were fully optimized with a tight converge maximum norm of the Cartesian gradient of 10^{-4} au and the DFT energy convergence criterion of 10^{-8} hartree. The nature of the obtained stationary points was always checked by a numeric evaluation of the Hessian matrix. Calculated frequencies were corrected by a default scaling factor of 0.9914. Thermal contributions to the energetic properties were calculated using the canonical ensemble at standard gas-phase conditions ($T = 298$ K, $p = 101.325$ kPa). We are aware of the fact that this approach is not completely consistent for the solvent-optimized structures,⁶⁴ but optimizations in the gas phase and subsequent Hessian evaluations would almost double the needed computational time.

Wave function properties and relative energies of the optimized structures were obtained by the ω B97XD/MWB-60(2f)/6-311+G-(2d,2p)/IEFPCM/UFF single-point calculations. The platinum atom was augmented by the set of diffuse functions in analogy to BSI and by the set of polarization functions ($\alpha_f = 1.419$; 0.466). The main group elements were described by the 6-311G(2d,2p) basis set, and electronegative N, O elements were furthermore augmented by a set of diffuse functions (6-311+G(2d,2p) basis set). This basis set is designated as BSII in further text. These calculations were carried out by the Gaussian 09 (G09) program package⁶⁵ with the Integral Equation Formalism-PCM solvent model (IEFPCM and UFF scaled radii for cavity construction). Atoms in molecules (AIM) topological analysis of the electron density in bond critical points was performed by the AIMAll program,⁶⁶ and natural population analysis (NPA) partial charges were determined by the NBO 3.1 program.⁶⁷ Structures were visualized, and structural properties were analyzed using the Molden, Gabedit, X3DNA, and Olex2 programs.^{68–71}

In order to facilitate a comparison with the previous quantum chemical studies on guanine binding to platinum complexes calculated almost exclusively with the B3LYP functional,^{21,23–26,29,30,72,73} single-point energy calculations were also performed at the B3LYP-D/MWB-60(2f)/def2-TVPZVPP/COSMO level by the Turbomole 6.1 program. This basis set is labeled as BSIII in further text.

Solvent-phase interaction energies $\Delta E_{\text{INT}}^{\text{wat}}$ were calculated at the ω B97XD/BSII/IEFPCM level for two different sets of fragments: [pGpG(PtDACH) = pGpG(Pt) and CpC] and [ds(pGpG) and PtDACH] as the differences between the total energies of the complexes and the energies of the given fragment sets. Obtained values have been corrected for the basis set superposition error (BSSE) using the standard counterpoise method.⁷⁴ In calculations of BSSE corrections within the PCM regime, the ghost atomic orbital functions were localized inside the cavity, which has the same size as the whole complex. Such a model was described in our previous study.⁷⁵

For the interaction of the pGpG(Pt) and CpC fragments in the minimum structures also solvent-phase pairing energies $\Delta E_{\text{PAIR}}^{\text{wat}}$ were calculated from $\Delta E_{\text{INT}}^{\text{wat}}$ considering deformation energies ΔE_{def}^i of the fragments

$$\Delta E_{\text{PAIR}}^{\text{wat}} = \Delta E_{\text{INT}}^{\text{wat}} + \sum_i \Delta E_{\text{def}}^i \quad (1)$$

Additional single-point calculations on selected optimized structures were conducted using the Amsterdam Density Functional 2008.1 package (ADF)⁶⁴ to calculate fragment energy decompositions according to the extended transition state theory^{76,77} combined with natural orbitals for chemical valence (ETS-NOCV).^{78–80} Gas-phase interaction energies $\Delta E_{\text{INT}}^{\text{gas}}$ (not corrected for the BSSE error) were decomposed to Pauli (ΔE_{Pauli}), electrostatic (ΔE_{elstat}), orbital (ΔE_{orb}), and dispersion (ΔE_{disp}) energy contributions

$$\Delta E_{\text{INT}}^{\text{gas}} = \Delta E_{\text{Pauli}} + \Delta E_{\text{elstat}} + \Delta E_{\text{orb}} + \Delta E_{\text{disp}} \quad (2)$$

In these calculations, scalar relativistic effects were treated within the zeroth-order regular approximation (ZORA).^{81,82} The TPSS-D functional was used with the all-electron TZ2P (ZORA) basis set for all atoms.

RESULTS AND DISCUSSION

Model Preparation. ds-DNA was simulated by the double-stranded pGpG-CpC dinucleotide (ds(pGpG)). The initial structure was generated in the ideal B-DNA conformation by the NAB program, which is a part of the AmberTools package. The negative charge of the phosphate groups was compensated by three Na^+ ions. The terminal 5'-phosphate group (5'P) on the pGpG strand stabilizes the DNA adducts with cisplatin-like drugs.^{21,83} In the first step the 5'P group was kept fixed when optimizing the rest of the system to ensure a reasonable starting conformation of 5'P for a structural alignment of ds(pGpG) with the PtDACH complex.

Different starting conformations between the ds(pGpG) and the PtDACH subunits were considered where the two subunits were associated by the H-bonds to each other. The N7 and O6 atoms of 5'G and 3'G together with 5'-phosphate oxygens O(5'P) of the pGpG strand were considered as H-bond acceptors. The two H_2O ligands and two H_2N - groups of PtDACH were involved as H-bond donors. Resulting structures were fully optimized to obtain "reactant" structures. The two lowest reactants R-1 and R-2 (Figures 3 and 4) were chosen for exploration of the reaction mechanism.

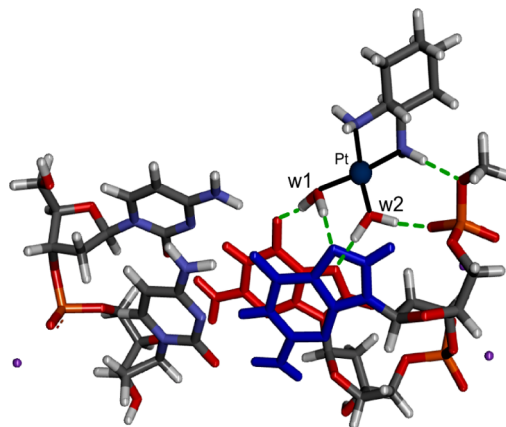


Figure 3. Structure of R-1 with the designation of water ligands w1 and w2. 5'G and 3'G are colored in blue and red, respectively. Coordination bonds of the Pt atom and selected H-bonds are represented by the solid black and dashed green lines, respectively.

Structures with the H-bonds between the N7(3'G, 5'G) atoms and the H_2N - groups of DACH were not energetically feasible due to close contacts between ds(pGpG) and the bulky DACH ligand, which lead to severe deformations of the pGpG strand. All structures were by at least 7.6 kcal/mol higher in energy than the most stable reactant structure R-1 and therefore are not considered in this study. Clearly, more H-bond patterns would be possible for cisplatin with much smaller ammine ligands than for oxaliplatin with the bidentate DACH ligand. Structural parameters of R-1 are summarized in Tables 1, 2, and S1, Supporting Information. R-1 is stabilized by five strong H-bonds (Figure 3) with a total interaction energy of -65.9 kcal/mol between the ds(pGpG) and the PtDACH

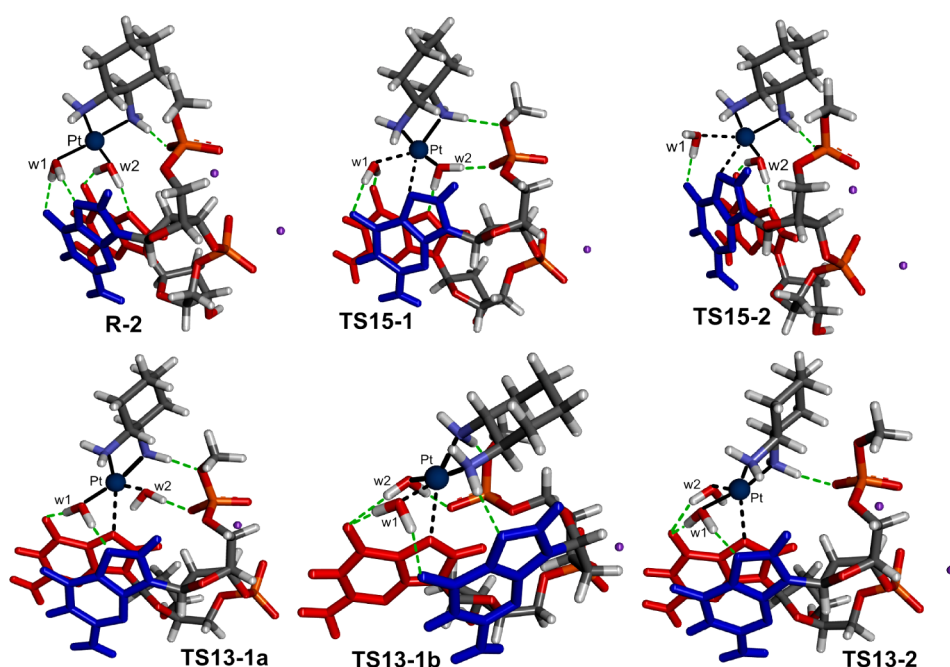


Figure 4. Structures of R-2 and transition states for monoadduct formation. CpC strand is not shown for clarity. Pt–entering ligand and Pt–leaving ligand bonds are shown by the black dashed lines. 5'G and 3'G are colored in blue and red, respectively. Coordination bonds of the Pt(II) atom and selected H-bonds are represented by the solid black and dashed green lines, respectively.

Table 1. Main Bonding Distances for Selected Structures and Geometric Parameters That Describe the Mutual Position of the Pt(II) Complex with the Planes of 5'G and 3'G^a

structure	Pt–N7(5'G)	Pt–N7(3'G)	Pt–O(w1)	Pt–O(w2)	Pt–5'G distance ^b	Pt–3'G distance ^b	PtDACH–5'G angle ^c	PtDACH–3'G angle ^c
R-1	3.844	4.206	2.059	2.043	3.455	0.338	39.7	38.4
R-2	3.457	4.345	2.085	2.044	2.978	0.431	62.6	68.0
TS15-1	2.468	4.139	2.366	2.057	1.896	1.323	60.3	60.0
TS15-2	2.391	4.283	2.456	2.050	1.901	1.082	74.1	76.2
TS13-1a	3.765	2.855	2.063	2.739	3.090	0.432	54.4	49.8
TS13-2	3.561	2.610	2.074	2.349	3.458	0.355	61.4	58.7
TS13-1b	4.170	2.440	2.455	2.087	3.997	1.157	74.5	81.1
M5	2.019	4.083	3.273	2.061	0.664	1.677	77.7	65.5
M5-w	2.021	3.985	n.a.	2.054	0.791	1.898	79.9	76.8
M3-1a	3.658	2.037	2.070	4.244	3.628	0.462	56.9	50.7
M3-2	3.404	2.035	2.066	3.165	3.176	0.337	47.2	45.6
M3-2-w	3.457	2.034	2.068	n.a.	3.226	0.338	45.9	49.5
TS25	2.040	2.581	3.465	2.403	1.012	1.339	80.0	87.5
TS25-w	2.025	2.405	n.a.	2.491	1.001	1.549	78.8	90.0
TS23	2.419	2.026	2.421	4.119	2.057	0.203	74.4	67.0
TS23-w	2.400	2.022	2.427	n.a.	2.044	0.262	74.3	65.4
CH5	2.058	2.032	3.095	3.658	1.398	0.599	69.9	71.1
CH5-w	2.062	2.048	n.a.	3.436	1.284	0.375	54.4	49.8
CH3	2.058	2.028	3.109	3.499	1.407	0.499	64.3	66.5
CH3-w	2.043	2.031	3.165	n.a.	1.125	0.658	70.5	69.8
OX-DNA (X-ray) ^d	1.98	1.94	n.a.	n.a.	1.37	0.83	68.4	67.2

^aDistances are in Angstroms and angles in degrees. ^bDistance between the Pt atom and the mean plane of guanine (5'G or 3'G). ^cAngle between the mean planes of guanine (5'G or 3'G) and the Pt(II) complex. ^dData based on analysis of the PDB structure 1IHH⁴⁵ by the Olex2 program.⁷¹

fragments (Table 3). Pt–N7(5'G) and Pt–N7(3'G) distances are 3.844 and 4.206 Å, respectively (Table 1). The two water ligands w1 and w2 have H-bond contacts with N7(5'G), O6(3'G) and N7(3'G), O(5'P), respectively. The flexible 5'P group is distorted having the β (C4'–C5'–O5'–P) dihedral angle of $\sim 100^\circ$, while in the native B-DNA the values of this angle are about 143° and 180° for the BII and BI forms,

respectively.^{84,85} Note, however, that the distribution of the β torsion values is significantly broadened in the DNA complexes, and values even below 80° are possible.⁸⁵ Besides formation of the H-bond between the NH₂ group and 5'P, the distortion of the β dihedral angle enables establishment of an additional strong H-bond interaction between w2 and 5'P (Figure 3).

Table 2. Changes of the DNA Parameters During Pt–DACH Binding

structure	shift	slide	rise	tilt	roll	twist	5'G–3'G angle
DNA (NMR) ⁹³	0.24	–1.55 ^a			1.12	30.29	
DNA (QM/MM) ⁹⁵	0.87	–1.73	3.83	2.27	–1.02	36.16	
<i>d</i> (pGpG)	–0.08	–0.82	3.62	4.86	3.81	45.48	1.7
R-1	0.23	–0.94	3.56	7.47	6.66	46.24	1.9
R-2	0.26	–1.84	3.70	7.39	5.34	41.36	5.6
TS15-1	0.40	–1.42	3.65	8.76	6.76	42.02	0.3
TS15-2	0.15	–1.49	3.60	6.29	6.03	42.88	3.3
TS13-1a	1.15	–1.27	3.70	10.46	12.16	37.81	8.9
TS13-2	0.70	–1.22	3.56	8.42	7.79	40.25	2.8
TS13-1b	0.77	–2.77	4.29	12.46	11.73	39.86	10.9
M5	0.83	–2.57	4.20	11.06	14.73	38.28	12.3
M5-w	0.85	–2.14	3.71	10.21	11.98	38.1	5.4
M3-1a	0.88	–1.26	3.50	10.35	8.91	39.47	7.4
M3-2	1.09	–1.17	3.63	8.81	10.36	36.65	7.0
M3-2-w	1.07	–1.17	3.63	9.63	10.97	36.98	7.9
TS25	1.39	–1.59	3.88	10.22	15.06	34.41	11.8
TS25-w	1.45	–1.66	3.97	8.39	13.16	32.64	11.5
TS23	1.14	–1.68	3.72	9.69	17.83	35.99	18.8
TS23-w	1.10	–1.62	3.67	9.41	17.39	35.2	19.0
CH5	1.27	–1.66	3.80	10.84	20.94	36.28	24.0
CH5-w	1.45	–2.19	4.21	12.04	23.89	38.88	24.6
CH3	1.33	–1.81	3.85	11.75	22.02	37.57	24.3
CH3-w	1.26	–1.62	3.80	11.40	23.85	34.69	30.4
OX-DNA (X-ray) ^b	1.05	–1.73	3.44	1.43	21.89	34.59	25.0
OX-DNA (NMR) ⁹³	0.84	–1.36			28.30	25.20	35.6
OX-DNA(QM/MM) ⁹⁵	0.95	–1.60	3.34	–5.50	25.51	23.88	

^aThis value of the slide is typical for A-DNA rather than for B-DNA for which it should be much less negative. ^bData based on analysis of the PDB structure 1IHH⁴⁵ by the X3DNA program.⁷⁰

Table 3. Gas-Phase $\Delta E_{\text{IE}}^{\text{gas}}$ and Solvent-Phase $\Delta E_{\text{IE}}^{\text{wat}}$ Interaction Energies between the pGpG-CpC and the Pt(DACH) Fragments^a

structure	ΔE_{Pauli}	ΔE_{elstat}	ΔE_{orb}	$\Delta E_{\text{IE}}^{\text{gas}}$	$\Delta E_{\text{IE}}^{\text{wat}}$	$\Delta E_{\text{def}}^{\text{DNA}}$
R-1	90.7	–168.6	–103.1	–199.0	–65.9	1.0
R-2	96.0	–176.2	–95.2	–194.7	–59.0	2.6
TS15-1	116.8	–198.9	–99.5	–202.1	–59.2	1.0
TS15-2	126.8	–202.9	–95.4	–193.2	–51.8	2.5
TS13-1a	83.0	–164.53	–88.34	–190.0	–49.4	1.9
TS13-2	93.2	–176.4	–85.0	–191.5	–50.6	0.9
TS13-1b	122.7	–206.0	–101.4	–211.8	–59.0	5.3
M5	169.7	–261.2	–132.8	–241.4	–78.4	4.8
M3-1a	163.0	–254.5	–132.6	–245.4	–80.6	4.8
M3-2	183.3	–262.4	–138.3	–241.1	–80.0	2.6
TS25	158.8	–251.6	–125.9	–237.6	–67.0	7.0
TS23	188.0	–279.1	–140.1	–254.2	–75.8	8.4
TS23-w	188.9	–278.6	–138.2	–249.9	–74.5	7.9
CH5	204.7	–311.4	–171.9	–299.7	–94.2 ^b	11.7
CH3	204.1	–309.3	–169.0	–299.1	–95.2 ^b	10.7
CH3-w	204.3	–304.7	–171.4	–288.8	–91.6 ^b	14.4

^aGas-phase interaction energies are decomposed to Pauli ΔE_{Pauli} , electrostatic ΔE_{elstat} and orbital ΔE_{orb} energy contributions (eq 2). Deformation energies of the pGpG-CpC fragment $\Delta E_{\text{def}}^{\text{DNA}}$ are shown separately. Deformation energies of the Pt(DACH) fragment were not calculated since optimization of the metal complex without one or two ligands would lead to “imaginary” species with a substantially modified electronic configuration on the central cation, which is completely irrelevant to the original complex. All energies are in kcal/mol. ^bThe value of –109.2 kcal/mol was calculated by the RI-B97-D/def2-TZVP/COSMO method (BSSE not included) for a similar system in ref 95.

Since a strong w2...5'P H-bond may hamper binding of PtDACH to 3'G the R-2 structure was optimized where this H-bond was disrupted and replaced by the w2...O6(3'G) interaction. Nevertheless, the R-2 structure appeared to have a less advantageous network of H-bond interactions compared to R-1 (Figure 4, Table S2, Supporting Information, cf. the interaction and orbital interaction energies in Table 3), and consequently, the R-2 reactant is 6.0 kcal/mol less stable than R-1. It means that according to the Boltzmann equilibrium distribution the population of R-2 would be practically zero compared to R-1. For a longer DNA sequence the attainability of R-1 is unclear (see above) and therefore R-2 can be considered as the starting structure for alternative mechanisms of monoadduct formation in a more realistic model of natural ds-DNA. However, if not explicitly written, the relative energies of all structures described in this paper will be given with respect to R-1.

Monoadduct Formation. Mechanisms Starting from R-1. Nucleophilic attack of N7(5'G) on the Pt(II) center proceeds to the TS15-1 transition state with the standard geometry of a trigonal bipyramid (Figure 4). In TS15-1, the N7(5'G) center is not sterically shielded by the 3'G base. The two bonds toward the leaving and entering groups are elongated by 0.31 and 0.45 Å with respect to stable Pt–O and Pt–N bonds in the reactant and product structures, respectively (Table 1). The activation Gibbs free energy barrier is 18.7 kcal/mol (Table 4).

Reaction of the PtDACH complex with the N7(3'G) center is much more complicated. We considered both water ligands w2 and w1 as possible leaving groups with corresponding TS13-1a and TS13-1b transition states, respectively.

Table 4. Gibbs Free Energy Reaction Profile of the Binding Reactions of the $[\text{Pt}(\text{H}_2\text{O})_2(\text{DACH})]^{2+}$ Complex to $\text{ds}(\text{pGpG})$ in the $5' \rightarrow 3'$ and $3' \rightarrow 5'$ Directions Calculated at the $\omega\text{B97XD}/\text{IEFPCM}/\text{BSII}/\text{RI-TSSE-D}/\text{COSMO}/\text{BSI}$ Level (in kcal/mol)^a

$5' \rightarrow 3'$		$5' \rightarrow 3'$ (alternative)		$3' \rightarrow 5'$		$3' \rightarrow 5'$ (DNA deformed)		$3' \rightarrow 5'$ (alternative)	
R-1	0.0	R-2	6.0	R-1	0.0	R-1	0.0	R-2	6.0
TS15-1	18.7	TS15-2	23.2	TS13-1a	27.5	TS13-1b	19.3	TS13-2	24.7
M5-1	-7.7	M5-2	0.1	M3-1a	-4.5	M3-1b	-0.5	M3-2 = M3-2-w ^b	-8.8
TS25	16.4			TS23	12.4			TS23-w	13.6
CH5	-14.7			CH3	-18.8			CH3-w	-6.3

^aSee Table S6, Supporting Information, for B3LYP-D/BSIII/COSMO//RI-TSSE-D/BSI/COSMO energies. ^bThe structure M3-2-w is considered to be equivalent to the structure M3-2. In M3-2-w, the released water molecule w1 is missing as compared to M3-2 (see the text).

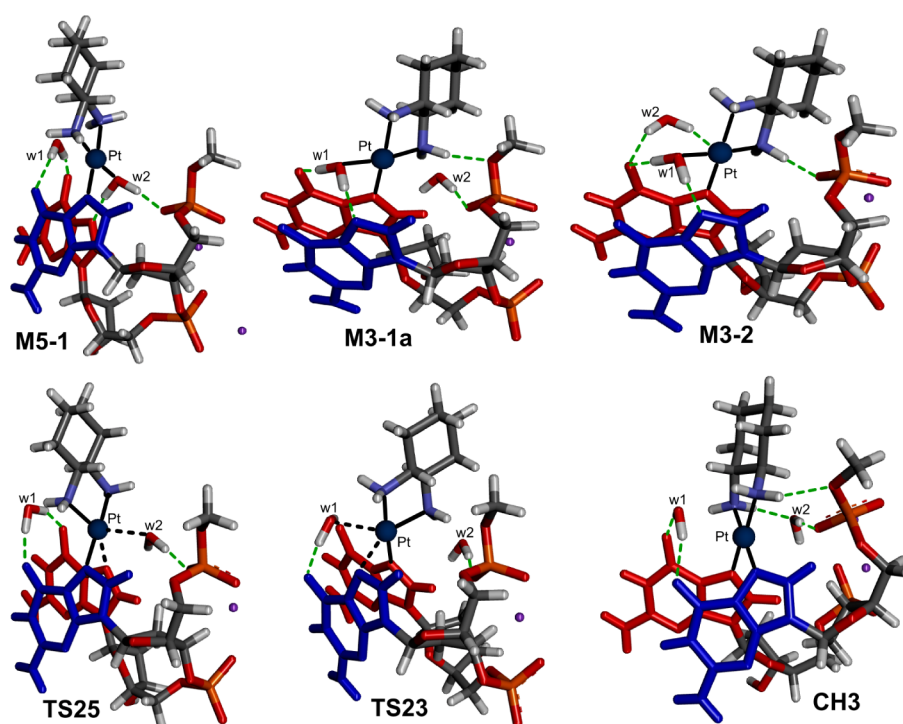


Figure 5. Geometries of monoadducts, TS structures for the chelate formation step, and CH3 chelate. CpC strand is not shown for clarity. Pt-entering ligand and Pt-leaving ligand bonds are shown by the black dashed lines. 5'G and 3'G are colored in blue and red, respectively. Coordination bonds of the Pt(II) atom and selected H-bonds are represented by the solid black and dashed green lines, respectively.

In the TS13-1a transition state structure, all H-bonding interactions described in the R-1 structure are preserved except the $w2 \cdots \text{N7}(3'G)$ interaction that is replaced by an incipient Pt–N7(3'G) covalent bond (Figure 4). Due to the spatial orientation of both nucleobases (steric shielding by 5'G) the structure of TS13-1a is almost planar, the angle between the plane [Pt, N7(3'G) atom from entering and O(w2) from leaving ligands] and the plane of the Pt(II) complex [Pt and N atoms of the ammine groups] is only 10.2° (cf. Figure 4). Also, 5'P forms a strong H-bond with w2, decreasing the conformational freedom of the PtDACH complex since the leaving w2 ligand is kept tightly bound to the phosphate oxygen (cf. Figure 4). The enforced planarity of all Pt bonds in TS13-1a increases the repulsion between the ligands, which causes leads to a more dissociative nature of the Pt–N7(3'G) and Pt–w2 bonds compared to the Pt–N7(5'G) and Pt–w1 bonds in TS15-1a (Table 1), respectively. It leads to the increase of activation free energy up to 27.5 kcal/mol.

The isolated $\text{ds}(\text{pGpG})$ dinucleotide is much more flexible than the corresponding segment incorporated in a longer DNA chain. This increased flexibility enables formation of TS13-1b, where the leaving water molecule w1 established the H-bond

with O6(5'G). The N7(5'G) site interacts with the H_2N group of DACH (see Figure 4). The Pt(II) coordination sphere of TS13-1b has almost an ideal geometry of a trigonal bipyramid with relatively short Pt–N7(3'G) and Pt–w1 distances of 2.440 and 2.455 Å, respectively. The PtDACH complex is nestled against the sugar–phosphate backbone of the pGpG strand, which is enabled by a strong bending of 5'P expressed by a very low value of the glycosyl bond torsion angle χ (89.1°). A normal conformation with χ between 200° and 300° ⁸⁴ would lead to a steric clash between 5'P and DACH. Therefore, we expect that the TS13-1b structure is not transferable to the real DNA environment. However, it represents kinetically the most advantageous pathway for N7(3'G) monoadduct formation with an activation free energy barrier of 19.3 kcal/mol. Note that this value is still 0.6 kcal/mol higher than for the platinum binding to N7(5'G) represented by TS15-1. The pathway over TS13-1b leads to the fairly distorted (and unstable) M3-1b monoadduct structure (cf. Figure S1, Supporting Information).

Monoadduct formations of M5-1, M3-1a, and M3-1b are exergonic by -7.7, -4.5, and -0.5 kcal/mol, respectively. Due to similar structural features as TS13-1b (see above) we assume that M3-1b is also not transferable to real DNA. Summing up

Table 5. Gas-Phase Interaction Energies $\Delta E_{\text{IE}}^{\text{gas}}$ (eq 2) and Solvent-Phase Interaction $\Delta E_{\text{IE}}^{\text{wat}}$ and Pairing Energies $\Delta E_{\text{PAIR}}^{\text{wat}}$ (eq 1) between the pGpG(Pt) and the CpC Fragments^a

structure	ΔE_{Pauli}	ΔE_{elstat}	ΔE_{orb}	$\Delta E_{\text{IE}}^{\text{gas}}$	$\Delta E_{\text{IE}}^{\text{wat}}$	$\Delta E_{\text{def}}^{\text{pGpG(Pt)}}$	$\Delta E_{\text{def}}^{\text{CC}}$	$\Delta E_{\text{PAIR}}^{\text{wat}}$
pGpG-CpC	89.6	-102.5	-47.1	-77.9 ^b	-43.7	7.9	3.2	-32.6
R-1	91.8	-117.5	-54.4	-99.1	-46.2	8.0	2.7	-35.5
R-2	88.9	-117.4	-50.5	-98.4	-47.1	7.0	2.6	-37.6
TS15-1	90.5	-117.2	-51.9	-98.2	-46.9		2.4	
TS15-2	89.8	-118.1	-53.5	-101.3	-47.2		2.6	
TS13-1a	92.7	-118.3	-53.0	-97.4	-46.6		2.9	
TS13-2	94.3	-122.0	-57.5	-104.4	-47.5		2.7	
TS13-1b	97.9	-125.4	-51.2	-102.9	-48.9		2.4	
M5	95.4	-121.9	-50.6	-101.1	-48.4	6.9	2.3	-39.2
M3-1a	94.4	-122.5	-55.8	-103.0	-47.7	7.5	2.8	-37.4
M3-2	94.4	-122.3	-57.4	-104.1	-48.3	8.4	3.0	-36.9
TS25	89.2	-116.5	-50.2	-98.3	-46.0		2.0	
TS23	91.5	-120.6	-53.9	-102.7	-48.0		2.4	
TS23-w	91.3	-120.8	-54.1	-102.9	-48.0		2.5	
CH5	91.8	-121.5	-54.4	-104.1	-48.4	14.8	2.4	-31.2
CH3	91.3	-121.4	-53.1	-103.5	-48.5	9.2	2.3	-37.0
CH3-w	90.8	-119.7	-52.8	-101.6	-48.1	18.1	2.4	-27.6

^aDeformation energies $\Delta E_{\text{def}}^{\text{pGpG(Pt)}}$ are calculated only for the stable minimum structures. All energies are in kcal/mol. ^bThis value is in a good accord with previous theoretical data, which show that the energy of one G–C Watson Crick H-bond pair is -32.1 kcal/mol,¹⁰⁷ and interstrand base-stacking energies are -4.2 and -3.1 kcal/mol for the methylated 5'C_3'-3'_G5' and 5'_C3'-3'_G_5' base pairs.¹⁰⁸

this fact and the low stability of this structure we did not consider it for the subsequent chelation step. Despite the structural complexity of all intermediates, interconversion of M3-1b into the more stable M3-1a structure can be expected to occur with a relatively low energy barrier.

M5-1 contains the stronger and shorter Pt–N7 bond of 2.019 Å compared to 2.037 Å in M3-1a (Tables 1 and S2, Supporting Information) as well as the larger bending of the planes of the two guanines (the GG angle) (Table 2). It is caused by the released w1 water molecule, which forms three H-bonds: two with the O6 atoms of the two guanines and one with the NH₂ group of DACH (the N–H...O distance is 1.867 Å) (Figure 5). If this water is removed from M5-1, the resulting M5-1-w structure (Figure S1, Supporting Information) is rather similar to M5-1 except the much smaller GG angle and roll values (Table 2). No H-bond contacts were established between the DACH amino group and the O6 atoms of G's in M5-1-w, which is in agreement with the experimental evidence that O6 is probably a worse H-bond acceptor than water when forming an H-bond with the Pt–NH groups.^{86,87}

Mechanisms Starting from R-2. The R-2 reactant structure was also considered for the monoadduct formation step in both 3'G and 5'G binding directions with corresponding TS13-2 and TS15-2 transition states, respectively. TS13-2 has a trigonal bipyramidal structure (Figure 4) with the Pt–N7(3'G) distance about 0.15 Å longer than the Pt–N7(5'G) bond in TS15-1. The reason is similar to that discussed in the case of TS13-1a but less pronounced. Again, the more dissociative character of TS13-2 is probably caused by the interplay between the shielding of the N7(3'G) site by the adjacent 5'G base and the H-bond network of platinum complex ligands with O6(3'G), N7(5'G), and 5'P (Figure 4). With respect to R-1, the activation barrier is 24.7 kcal/mol, i.e., TS13-2 is 2.8 kcal/mol lower than TS13-1a but lies 6.0 kcal/mol higher than TS15-1. Interestingly, with respect to R-2 the barrier is as high as the activation from R-1 to TS15-1 (18.7 kcal/mol). Nevertheless, N7(5'G) binding is kinetically preferred over N7(3'G) binding also in this case. Considering

R-2 as the reactant for N7(5'G) binding, the reaction proceeds over the TS15-2 structure (Figure 4) with an activation barrier (with respect to R2 reactant) of 17.2 kcal/mol. Thus, TS15-2 is 1.5 kcal/mol more stable than TS13-2. TS15-2 displays the shortest Pt–N7 distance for entering ligand (2.391 Å) from all TS structures (Table 1).

However, M5-2 represents a distorted monoadduct structure (Figure S1, Supporting Information) with an endergonicity of +0.1 kcal/mol. Therefore, rapid relaxation of this structure into the much more stable M5-1 structure can be expected. Furthermore, the H-bond pattern of the two structures differs only in the orientation of w2. In M5-2, both H-bonds between 3'G and w2 must be disrupted during the chelation step and then the reaction proceeds via the same (or very similar) TS structure as for M5-1. Thus, for subsequent chelate formation only the pathway starting from the M5-1 structure is assumed.

M3-2 is the most stable monoadduct structure with an exergonicity of -8.8 kcal/mol with respect to R-1. Note the presence of the stabilizing (w2)O–H...Pt interaction (Figure 5), which was already reported in previous studies.^{88–90} According to ETS-NOCV analysis this interaction contributes -6.9 kcal/mol to the orbital interaction energy of -138.3 kcal/mol between Pt(DACH) and ds(pGpG) fragments in the gas phase (Table 3). However, it was found that w2 is bound nonspecifically in M3-2. Therefore, w2 was removed and the M3-2-w structure (Figure S1, Supporting Information) used as the starting structure for the chelation step. The omitted w2 has a negligible influence on the structure of the monoadduct (cf. structural parameters of M3-2 and M3-2-w in Tables 1, 2, and S1, Supporting Information; the RMSD of the two structures (heavy atoms) is 0.121 Å).

Chelate Formation. M5-1, M3-1a, and M3-2-w monoadducts were used as starting structures for chelate formation with TS25, TS23-1, and TS23-2-w transition states in the corresponding pathways. TS25 has the highest activation free energy of 24.1 kcal/mol. It is caused by the more dissociative character of the incipient Pt–N7(3'G) bond (Figure 5), which is more than 0.15 Å longer than the Pt–N7(5'G) bond in

TS23-1 and **TS23-2-w** (Table 1). This results from the steric shielding of N7(3'G) by 5'G. Comparing **TS23-1** and **TS23-2-w** structures it can be seen (Table 4) that the former structure shows much lower activation energy (16.9 vs 22.4 kcal/mol), which is caused by the lower stability of the reference **M3-1a** structure compared to **M3-2-w**.

From the individual **TS25**, **TS23-1**, and **TS23-2-w** structures, the final chelates **CH5**, **CH3**, and **CH3-w** were obtained with reaction exergonicities of -14.7 , -18.8 , and -6.3 kcal/mol, respectively. The low stability of **CH3-w** is caused by the absence of any H-bond interactions between Pt(DACH) and 5'P (Figure S2, Supporting Information). **CH3-w** formation is in fact endergonic with respect to the corresponding monoadduct **M3-2-w** structure. On the other hand, the **CH5** and **CH3** chelates (Figures S2, Supporting Information, and 5, respectively) are significantly stabilized by several H-bonds: (1) between the NH_2 group of DACH and O6(3'G) and (2) involving 5'P: the weak direct $\text{NH}_2 \cdots \text{O}'3$ (5'P) interaction and the H-bonds mediated by the leaving water w2 molecule. This demonstrates an important role of 5'P in the thermodynamics of the chelation step.

CH5 and **CH3** differ mainly in the conformation of the pGpG sugar phosphate backbone, which is better relaxed in **CH3** than in **CH5** (cf. deformation energies $\Delta E_{\text{def}}^{\text{DNA}}$ and $\Delta E_{\text{def}}^{\text{pGpG(Pt)}}$ in Tables 3 and 5, respectively). Moreover, the Pt–N7(3'G) bond is slightly stronger in **CH3** (Tables 1 and S2, Supporting Information).

The geometry of the **CH3** chelate structure is very close to the crystallographic structure (PDB code 1IHH):⁴⁵ (1) The GG angle is 24.3° compared to 25° in the crystal (Table 2). The DNA environment and neighboring bases have probably only a small influence on the GG angle whose value is mainly a result of the interplay between the directionality of coordination covalent bonds in the Pt(II) cross-link and the Watson–Crick H-bonding with the complementary CpC strand. Note that the much higher GG angle value of 53.9° was found in the Pt(II) cross-link with the single-stranded pGpG sequence optimized by the RI-TPSS-D/BSI/COSMO method. Thus, the base pairing decreases the GG angle in the Pt(II) cross-links, and this decrease is accompanied by a distortion of the Pt atom from the 5'G plane (Table 1). (2) The NH_2 group also forms the H-bond to O6(3'G); the calculated distance is slightly longer compared to the crystal structure (3.2 vs 2.9 Å). The shortest distance between the nitrogen atom of the second DACH amino group and O6(5'G) is 4.7 Å, while in the crystal structure it is 4.4 Å.⁴⁵ This NH_2 group also forms a weak H-bond with water molecule w1, which spans the two O6 atoms. Such a water molecule was found in the high-resolution crystal structure of the cisplatin–DNA complex.⁴⁷ The displacement of the Pt atom from the 5'G and 3'G guanine planes is also rather similar for **CH3** and the crystal structure (see Table 1). The differences between the two structures can be mainly found in the puckering of sugar rings (Table S1, Supporting Information) and closer contacts of the DACH moiety with the 5'-phosphate in the **CH3** structure, which is caused by a larger conformational freedom of the terminal 5'P since it forms a free dangling end in our model.

In agreement with our previous study,²⁰ the Pt–N7(3'G) bond is stronger than Pt–N7(5'G) in all chelate structures (Table S2, Supporting Information), but unlike the cited study it is also shorter (Table 1). This is caused by geometric reasons since the Pt atom is much more displaced from the plane of 5'G than from the plane of 3'G (Table 1).

Energetics. Relative energies of all optimized structures calculated at the $\omega\text{B97XD}/\text{IEFPCM}/\text{BSII}$ and $\text{B3LYP-D}/\text{COSMO}/\text{BSIII}$ levels are collected in Tables 4 and S6, Supporting Information, and final energy profiles are drawn in Figure 6. The latter method gives systematically higher values of activation energies and underestimates the strengths of Pt–N7 coordination bonds compared to the former method.

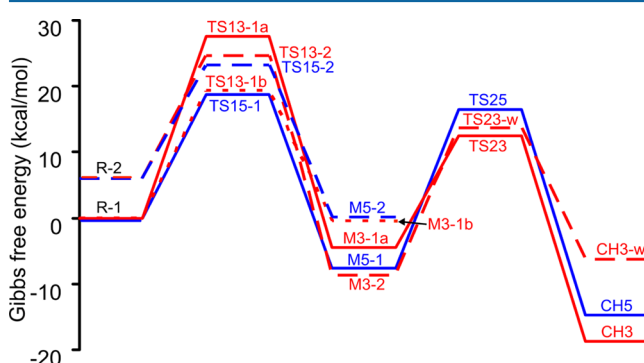


Figure 6. Gibbs free energy profiles of the binding reactions of the PtDACH complex to ds(pGpG) calculated at the $\omega\text{B97XD}/\text{PCM}/\text{BSII}/\text{RI-TPSS-D}/\text{COSMO}/\text{BSI}$ level (solid blue line, 5'G \rightarrow 3'G direction; solid red line, 3'G \rightarrow 5'G direction; long dashed blue line, an alternative mechanism for 5'G \rightarrow 3'G direction; long dashed red line, an alternative mechanism for 3'G \rightarrow 5'G direction; short dashed red line, a mechanism with a deformed dsDNA for 3'G \rightarrow 5'G direction).

PtDACH binding is kinetically controlled by the first binding step (the monoadduct formation step), in agreement with experimental data for fully aquated cisplatin.¹⁷ In the first step, N7(5'G) is slightly kinetically preferred over N7(3'G). The calculated B3LYP-D/BSIII activation barrier of 21.2 kcal/mol (TS15-1) is in a good agreement with the value of 21.4 kcal/mol published previously for binding of the fully aquated oxaliplatin with an isolated guanine.⁷² This preference can be explained by the fact that the N7(5'G) center is fully exposed to the solvent in ds(pGpG), and the 3'G neighboring base does not influence the energetics of platinum monoadduct formation on N7(5'G).

On the other hand, binding to N7(3'G) is sterically hindered by 5'G. The reactivity of the most stable reactant **R-1** toward N7(3'G) is further decreased due to the w2 \cdots 5'P H-bond stabilization. Thus, the conformational freedom of the entering and leaving ligands in the transition state region is decreased, leading to the almost planar **TS13-1a** structure. In this way, a disruption of either the 'DNA-like' structure of ds(pGpG) (as it occurs in **TS13-1b**) or the w2 \cdots 5'P H-bond (in **TS13-2**) substantially decreases the activation free energy barrier.

A larger model is needed for a more realistic comparison of the N7(5'G) and N7(3'G) reactivities since in a longer DNA chain the N7(5'G) center will be also shielded by a neighboring nucleotide on its 5'-side.⁹¹ The study with a larger model is currently under investigation.

Formation of the **M5**, **M3-1a**, and **M3-2** monoadducts is exergonic by -7.7 , -4.5 , and -8.8 kcal/mol, respectively. The latter two structures differ mainly in the position of the leaving water molecule w2. About 50% of the energy difference can be assigned to the larger deformation energy of the ds(pGpG) fragment in **M3-1a** compared to **M3-2** (Table 3).

In agreement with experimental data,¹⁹ the chelation step is more favorable in the 3'G \rightarrow 5'G direction overcoming a

barrier of 21.2 kcal/mol (TS23 vs M3-2) than in the 5'G → 3'G direction where the activation barrier is by 2.9 kcal/mol higher (but the relative energy of TS25 is 4.0 kcal/mol higher than TS23, Table 4). The whole process is exergonic but strongly dependent on established H-bond interactions. The most stable CH3 structure lies 18.8 kcal/mol below the reactant R-1 structure. More than 20% of this energy can be assigned to relaxation of the sugar phosphate backbone of the pGpG strand (the CH5 → CH3 transition, see above and Figure S2, Supporting Information).

Formation of one Pt–N7 dative bond increases the interaction energy between the ds(pGpG) and the Pt(DACH) fragments by about 15 kcal/mol in aqueous solution (Table 3), i.e., by about 30 kcal/mol in the chelates compared to R-1. In the gas phase this increase is about three times higher. Energy decomposition analysis in the gas phase shows that the difference is mainly caused by an increase of the orbital interaction energies since the change in the electrostatic contribution is to a large extent compensated by higher Pauli repulsion. Moreover, in water solvent the long-range electrostatic effects are essentially eliminated, while only the polarization part of the orbital interactions is affected to a larger extent compared to the gas phase.⁹²

Changes of the ds(pGpG) Structure during the Cross-Link Formation. The ribose rings on the 5'G–3'C base pair remain almost always on the starting C2'-endo puckering (Table S1, Supporting Information), which is typical for B-DNA. On the other hand, the 3'G–5'C nucleotides (and especially 3'G ribose) show more pronounced changes in the pucker (Table S1, Supporting Information) probably due to the increased strain during cross-link formation. All helical parameters except the tilt follow trends observed in experiments,^{45,47,93} molecular dynamics,⁹⁴ and QM/MM simulations.⁹⁵ The agreement with experimental results is good considering a large flexibility of the ds(pGpG) fragment. In comparison with ideal B-DNA, the two base pairs show increasing shift, negative slide, roll, and decreasing twist upon platinum binding (Table 2). The changes of these parameters are however not gradual for all structures along the reaction pathway, but local minima/maxima in their values may exist since these changes are driven by formation of the Pt–N7 bonds and H-bond interactions. For example, M5-1 shows the highest value of negative slide due to the existence of the number of interactions between the PtDACH, the w2, and the ds(pGpG) fragments. Although the X3DNA program was not able to determine the form of the duplex for all structures, the transition from the B-DNA form toward A-DNA is apparent (Tables 2 and S1, Supporting Information), in agreement with experiments.⁹⁶

Values of deformation energies for the ds(pGpG) fragment $\Delta E_{\text{def}}^{\text{DNA}}$ are shown in Table 3 and Figure 7. The ds(pGpG) fragment geometries in the reactant R-x and TS structures for the monoadduct formation step TS1a-x (a = 3, 5; x = 1a, 1b, 2) are only little affected by their interactions with the PtDACH complex. Starting from the monoadduct structures, the deformation energy $\Delta E_{\text{def}}^{\text{DNA}}$ gradually increases up to chelate values of ~11 kcal/mol (Figure 7), and it reflects the changes of the GG angle (Figure 7). All important conformational changes of ds(pGpG) occur on the pGpG strand since the complementary CpC strand structure is almost unaffected by platination (see below).

GG-CC Base Pair Interaction Strength. In agreement with previous theoretical studies,^{97,98} the strengths of the G–C

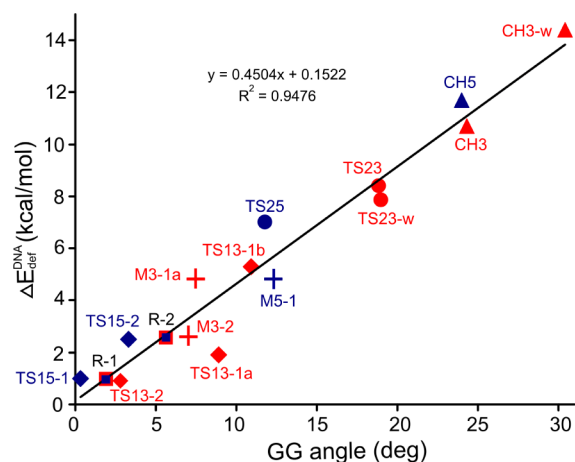


Figure 7. Roughly linear dependence of the ds(pGpG) deformation energy $\Delta E_{\text{def}}^{\text{DNA}}$ on the GG angle for the structures along the PtDACH binding pathways to ds(pGpG) (see Tables 2 and 3 for numeric values). Shapes of the points correspond to the positions of the structures on the reaction coordinate (■ → ◆ → + → ● → ▲), and color refers to the binding direction (blue, 5' → 3'; red, 3' → 5').

base pair interactions were tightened in the presence of the divalent platinum metal ion. Interaction and pairing energies between the platinated pGpG strand (pGpG(Pt)) and the CpC strand are shown in Table 5. The increase of the gas-phase interaction energies $\Delta E_{\text{PE}}^{\text{gas}}$ in R-1 and R-2 reactant structures with respect to the isolated ds(pGpG) complex is 21.2 and 20.5 kcal/mol, respectively. It is caused mainly by electrostatic interactions, which are however diminished to a large extent upon solvation. Thus, in aqueous solution the differences in pairing energies $\Delta E_{\text{PAIR}}^{\text{wat}}$ are lowered to 2.9 and 5.0 kcal/mol, respectively.

Formation of the covalent Pt–N7 bonds leads to additional enhancement of GG-CC interaction energies by up to 5% in both the gas phase and the water solvent as compared to R-1 and R-2 (Table 5). Thus, in the solvent enhancement is rather moderate and can be compensated by an increase of deformation energies of the pGpG(Pt) and CpC fragments in the platinated structures. The solvent-phase pairing energies $\Delta E_{\text{PAIR}}^{\text{wat}}$ range between –35.5 and –37.6 kcal/mol for most of the platinated structures, i.e., they are enlarged by about 10% with respect to the pGpG-CpC dinucleotide itself and do not visibly depend on the number of Pt–N7 bonds. The exceptions are M5, on the one hand, and the CH5, CH3-w structures, on the other, where lower and higher deformation energies of the pGpG(Pt) fragment affected the $\Delta E_{\text{PAIR}}^{\text{wat}}$ values being outside the above interval (Table 5). It should be stressed that the calculated deformation energies of the pGpG(Pt) fragment do not reflect the changes of DNA structure itself since they are calculated with respect to the minimized platinated single-stranded structures. Differences in deformation energies of the ds(pGpG) fragment itself are larger as follows from Table 3. The main structural changes occur only on the pGpG strand, and the deformation energies of the complementary CpC strand are very small and almost constant (Table 5).

Comparison of the H-bond strengths between the isolated GC pair and the different Pt(II) chelates was done by Robertazzi and Platts using AIM analyses.^{99,100} In our model we observe also changes which occur in the course of chelate formation. The changes of electron densities in BCP's show that platination primarily weakens the strength of O6···H4

interactions since the two O6 atoms are involved in a direct H-bonding with the platinum ligands (Figure 8, Table S3, Supporting Information), which is in accord with our previous results.¹⁰¹

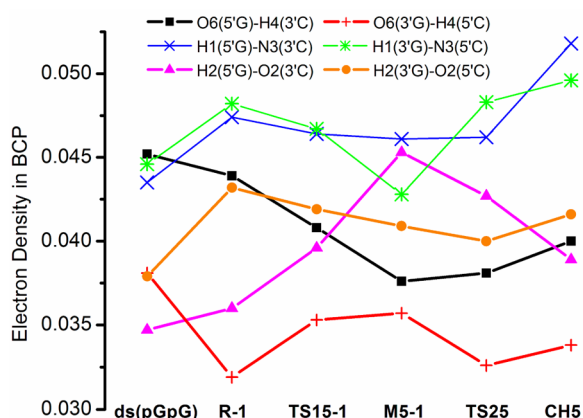


Figure 8. Electron densities in BCP's (in e/au^3) of the guanine–cytosine H-bonds for structures along the 5'G → 3'G direction of the PtDACH binding. See Table S3, Supporting Information, for values of other structures.

The changes in the BCP densities of the O6···H4 interactions can be used as an indirect measure of the strengths of the O6 interactions with PtDACH. For example in **R-1**, the O6(3'G) site serves as an H-bond acceptor in the strongest interaction with the w1 ligand of PtDACH compared to all other structures along the 5' → 3' pathway, which is demonstrated by the lowest electron density of $0.032 e/au^3$ in BCP of the O6(3'G)···H4(5'C) H-bond, while for ds(pGpG) the corresponding value is $0.038 e/au^3$ (Figure 8, Table S3, Supporting Information). On the other hand, the strength of the O6(5'G)···H4(3'C) H-bond is much less affected by the presence of PtDACH in **R-1**. Weakening of the O6···H4 interactions is compensated by the strengthening of the other two H1···N3 and H2···O2 H-bonds, where the platinated guanine serves as an H-bond donor. This effect was already reported in our previous studies.^{97,102} Mainly the strength of the H2···O2 interactions inversely correlates with the strength of O6···H4 (Figure 8).

Charge Transfer Between PtDACH, pGpG, and CpC Fragments. In this section the charge transfer between the three fragments upon platination is described. To offer a more detailed picture, the pGpG fragment is further divided into the 5'G, 3'G, and GG-backbone subunits (Figure 9, Table S3, Supporting Information).

The charge transfer between PtDACH and DNA can be formally divided into three basic steps: the first one involves formation of **R-1** from originally two isolated PtDACH and (pGpG)·(CpC) molecules, which are connected by five H-bonds; the other two steps involve formation of the two donor–acceptor Pt–N7 bonds. In the first step the charge of $-0.354 e$ is transferred from DNA to the drug; the net transferred charge is roughly proportional to a number of H-bonds, the charge of ca. $-0.06 e$ per one H-bond. Thus, the largest charge of ca. $-0.12 e$ is transferred from 3'G and GG-backbone subunits (Figure 9, Table S3, Supporting Information). Note that the charge transfer from the complementary CpC strand was enhanced by ca. $-0.05 e$ compared to bare ds(pGpG).

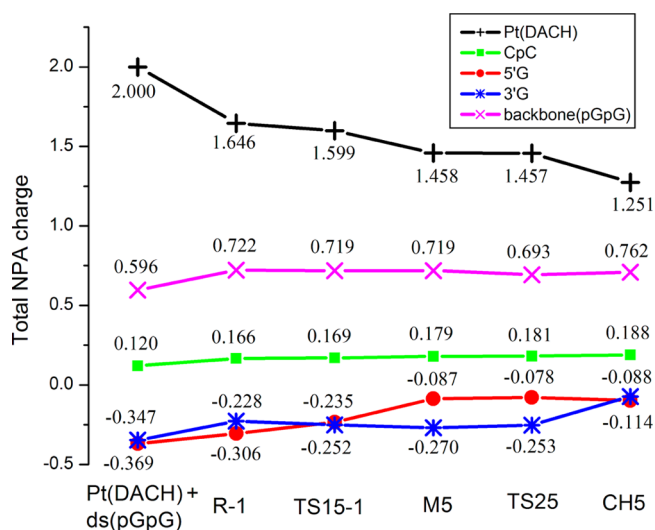


Figure 9. Changes of the NPA charges of the PtDACH, pGpG, and CpC fragments for structures along the 5'G → 3'G direction of the PtDACH binding. See Table S2, Supporting Information, for values of other structures.

Formation of the donor–acceptor Pt–N7 bonds is connected with the charge transfers of about $-0.2 e$ per one established bond, and charge transfer should occur in the late stage of the Pt–N7 bond formation (i.e., after the transition state). Electron density of the other parts of the system is almost unaffected (cf. Figure 9, Table S3, Supporting Information).

Transferability of the Model into Longer DNA Chains.

The ds(pGpG) structure represents a minimalistic model of DNA with the two guanine bases as reactive centers for platinum drug binding and the complementary CpC strand, which helps to keep the relative position of the two guanines close to that found in native DNA. Comparing experimental results for B-DNA and oxaliplatin–DNA chelates on one hand and our theoretical results for ds(pGpG) and CH3 structures on the other we can make the following assumptions about limitations of our model and its transferability into longer DNA chains.

- (1) The model is probably able to reproduce very well the changes in the GG angle upon platinum binding and reasonably well the changes in the helical parameters (except tilt), giving us confidence about a good description of the changes in the stacking interactions in the course of platinum binding (Table 2).
- (2) The Pt(DACH) fragment with the bidentate DACH ligand is a rigid structure. In the chelate structures the position of this fragment is determined by the positions of the covalently bound N7 atoms of guanine bases (and vice versa). Thus, the geometry of the chelates is the least dependent on the flanking bases, and the geometry of the optimized chelate structures is in very good agreement with the crystal structure⁴⁵ (Table 1). However, going back to the reactants the conformational freedom between the pGpG–CpC and the Pt(DACH) fragments gradually increases. Thus, the orientation of the Pt(DACH) fragment with respect to ds(pGpG) is the most dependent on the nonbonding interactions in the reactant structures **R-1** and **R-2** showing the highest possible variability in longer DNA chains. Consequently,

the monoadduct formation step can be expected to be more influenced by the flanking bases than the chelate formation step. Depending on the sequence context the flanking bases may partially influence geometries, relative energies of the structures (Tables 4 and S6, Supporting Information), and interaction energies between Pt-(DACH) and pGpG-CpC (or DNA) fragments (Table 3). Characteristics like, e.g., changes in interaction energies between the pGpG and the CpC fragments (Table 5) and charge transfer effects (Figure 9, Table S4, Supporting Information) will be affected only marginally. Deformation energies of the pGpG-CpC and pGpG(Pt) fragments (Tables 3 and 5) can be considered as the lower limit values for larger DNA fragments since deformation of DNA is not localized on the platinated GG sequence but also spread mainly to the 5' flanking base pair step.^{103,104} We believe that this study may provide useful reference data for more complex models, e.g., exploring the influence of flanking bases on both energetic and structural parameters connected with platinum drug binding.

- (3) Some weakness of our model represents the free dangling 5'P group, which always adopts a conformation to form most advantageous contacts with the platinum complex. In this way the absolute values of interaction energies between the Pt(DACH) and the pGpG-CpC fragments (Table 3) are systematically overestimated for the structures along the reaction pathway for the mechanisms starting from the R-1 structure. With this respect working with the relative energies of the structures we mostly relied on mutual cancellation of the errors. To overcome at least partially this problem the alternative mechanisms (starting from the R-2 reactant) for both binding directions were also proposed in which the number of the H-bond contacts between the platinum complex and 5'P were reduced.

CONCLUSIONS

The mechanism of the $[\text{Pt}(\text{H}_2\text{O})_2(\text{DACH})]^{2+}$ intrastrand binding to the ds(pGpG) sequence is presented with the fully optimized stationary points from the reaction coordinate. To the best of our knowledge, the results presented in this contribution offer the most realistic theoretical description of the course of the DNA platination available up to now. It enables us to describe not only the energetics of platinum binding but also the changes of the ds(pGpG) conformations, the influence of platination on the strengths of the G-C Watson-Crick base pairing, and the charge transfer effects. We show the importance of the transition state stabilization due to H-bond formation. The steric effects may also contribute to the transition state stabilization influencing mainly the strengths of the Pt-N7 bonds. A more dissociative nature of the incipient Pt-N7 bond in some TS structures is caused by close contacts between the Pt complex and the DNA molecule, distorting the trigonal bipyramidal geometry of the TS structure. In this way, the kinetics of platinum binding can be influenced by the flanking bases.¹⁰⁵ Our results support previous experimental evidence that Pt-N7 coordination is influenced mainly by the flanking bases from the 5' side.^{87,91,104,106} However, a larger model with more detailed insight into the structural relations between the stacked base pairs is necessary.

ASSOCIATED CONTENT

Supporting Information

Optimized structures of M3-1b, M5-2, M5-1-w, M3-2-w; optimized structures of TS23-2-w, CH3-w, CH5 and structural alignment of structures CH5 and CH3; sugar conformations of selected structures; values of electron densities in BCP's for the most important interactions between the Pt(DACH) and the ds(pGpG) fragments and H-bonds between pGpG(Pt) and CpC fragments; total NPA charges of fragments and selected atoms; base-pair parameters of selected structures; B3LYP-D/BSIII/COSMO//RI-TSSE-D/BSI/COSMO energies of the binding pathways; Cartesian coordinates of the optimized structures discussed in this paper. This material is available free of charge via the Internet at <http://pubs.acs.org>.

AUTHOR INFORMATION

Corresponding Author

*E-mail: chval@jcu.cz (Z.C.); burda@karlov.mff.cuni.cz (J.V.B.).

Notes

The authors declare no competing financial interest.

ACKNOWLEDGMENTS

This project was supported by grants from the Czech Science Foundation (project no. 208/12/0622) and from the Ministry of Education of the Czech Republic (MŠMT) (project ME 10149). Access to the MetaCentrum computing and storage facilities (grant LM2010005) is highly appreciated.

REFERENCES

- (1) Rosenberg, B.; van Camp, L.; Krigas, T. *Nature* **1965**, *205*, 698–699.
- (2) Mathe, G.; Kidani, Y.; Segiguchi, M.; Eriguchi, M.; Fredj, G.; Peytavin, G.; Misset, J.; Brienza, S.; Devassals, F.; Chenu, E.; Bourut, C. *Biomed. Pharmacother.* **1989**, *43*, 237–250.
- (3) Rixe, O.; Ortuzar, W.; Alvarez, M.; Parker, R.; Reed, E.; Paull, K.; Fojo, T. *Biochem. Pharmacol.* **1996**, *52*, 1855–1865.
- (4) Malina, J.; Novakova, O.; Vojtiskova, M.; Natile, G.; Brabec, V. *Biophys. J.* **2007**, *93*, 3950–3962.
- (5) Lucas, M.; Pavelka, M.; Alberto, M.; Russo, N. *J. Phys. Chem. B* **2009**, *113*, 831–838.
- (6) Zhang, S.; Lovejoy, K.; Shima, J.; Lagpacan, L.; Shu, Y.; Lapuk, A.; Chen, Y.; Komori, T.; Gray, J.; Chen, X.; Lippard, S.; Giacomini, K. *Cancer Res.* **2006**, *66*, 8847–8857.
- (7) Jerremalm, E.; Wallin, I.; Ehrsson, H. *J. Pharm. Sci.* **2009**, *98*, 3879–3885.
- (8) Jerremalm, E.; Eksborg, S.; Ehrsson, H. *J. Pharm. Sci.* **2003**, *92*, 436–438.
- (9) Bancroft, D. P.; Lepre, C. A.; Lippard, S. J. *J. Am. Chem. Soc.* **1990**, *112*, 6860–6871.
- (10) Davies, M. S.; Berners-Price, S. J.; Hambley, T. W. *J. Am. Chem. Soc.* **1998**, *120*, 11380–11390.
- (11) Davies, M. S.; Berners-Price, S. J.; Hambley, T. W. *Inorg. Chem.* **2000**, *39*, 5603–5613.
- (12) Legendre, F.; Bas, V.; Kozelka, J.; Chottard, J. C. *Chem.—Eur. J.* **2000**, *6*, 2002–2010.
- (13) Berners-Price, S. J.; Frenkiel, T. A.; Frey, U.; Ranford, J. D.; Sadler, P. J. *J. Chem. Soc., Chem. Commun.* **1992**, 789–791.
- (14) Zimmermann, T.; Leszczynski, J.; Burda, J. V. *J. Mol. Model.* **2011**, *17*, 2385–2393.
- (15) Wheate, N. J.; Walker, S.; Craig, G. E.; Oun, R. *Dalton Trans.* **2010**, *39*, 8113–8127.
- (16) Fichtinger-Schepman, A. M. J.; Van der Veer, J. L.; Den Hartog, J. H. J.; Lohman, P. H. M.; Reedijk, J. *Biochemistry* **1985**, *24*, 707–713.

- (17) Reeder, F.; Gonnet, F.; Kozelka, J.; Chottard, J.-C. *Chem.—Eur. J.* **1996**, *2*, 1068–1076.
- (18) Sadler, P. J.; Barnham, K. J.; Berners-Price, S. J.; Frey, U. *Chem.—Eur. J.* **1996**, *2*, 1283–1291.
- (19) Gonnet, F.; Reeder, F.; Kozelka, J.; Chottard, J.-C. *Inorg. Chem.* **1996**, *35*, 1653–1658.
- (20) Zeizinger, M.; Burda, J. V.; Leszczynski, J. *Phys. Chem. Chem. Phys.* **2004**, *6*, 3585–3590.
- (21) Mantri, Y.; Lippard, S. J.; Baik, M. H. *J. Am. Chem. Soc.* **2007**, *129*, 5023–5030.
- (22) Kozelka, J. *Inorg. Chim. Acta* **2009**, *362*, 651–668.
- (23) Chval, Z.; Šíp, M. *Collect. Czech. Chem. Commun.* **2003**, *68*, 1105–1118.
- (24) Baik, M. H.; Friesner, R. A.; Lippard, S. J. *J. Am. Chem. Soc.* **2003**, *125*, 14082–14092.
- (25) Costa, L. A. S.; Hambley, T. W.; Rocha, W. R.; De Almeida, W. B.; Dos Santos, H. F. *Int. J. Quantum Chem.* **2006**, *106*, 2129–2144.
- (26) Raber, J.; Zhu, C. B.; Eriksson, L. A. *J. Phys. Chem. B* **2005**, *109*, 11006–11015.
- (27) Pavelka, M.; Burda, J. V. *J. Mol. Model.* **2007**, *13*, 367–379.
- (28) Gao, Y.; Zhou, L. *Theor. Chem. Acc.* **2009**, *123*, 455–468.
- (29) Sarmah, P.; DeKa, R. C. *J. Mol. Struct. THEOCHEM* **2010**, *955*, 53–60.
- (30) Zhou, L. *Inorg. Chim. Acta* **2011**, *376*, 44–56.
- (31) Ranaldo, R.; Margiotta, N.; Intini, F.; Pacifico, C.; Natile, G. *Inorg. Chem.* **2008**, *47*, 2820–2830.
- (32) Yang, D.; van Boom, S.; Reedijk, J.; van Boom, J.; Wang, A. *Biochemistry* **1995**, *34*, 12912–12920.
- (33) Burda, J. V.; Leszczynski, J. *Inorg. Chem.* **2003**, *42*, 7162–7172.
- (34) Carloni, P.; Sprik, M.; Andreoni, W. *J. Phys. Chem. B* **2000**, *104*, 823–835.
- (35) Coste, F.; Malinge, J.; Serre, L.; Shepard, W.; Roth, M.; Leng, M.; Zelwer, C. *Nucleic Acids Res.* **1999**, *27*, 1837–1846.
- (36) Diakos, C.; Messerle, B.; Murdoch, P.; Parkinson, J.; Sadler, P.; Fenton, R.; Hambley, T. *Inorg. Chem.* **2009**, *48*, 3047–3056.
- (37) Elizondo-Riojas, M.; Kozelka, J. *J. Mol. Biol.* **2001**, *314*, 1227–1243.
- (38) Gelasco, A.; Lippard, S. *Biochemistry* **1998**, *37*, 9230–9239.
- (39) Gkionis, K.; Platts, J. *J. Biol. Inorg. Chem.* **2009**, *14*, 1165–1174.
- (40) Jamieson, E.; Lippard, S. *Chem. Rev.* **1999**, *99*, 2467–2498.
- (41) Natile, G.; Marzilli, L. G. *Coord. Chem. Rev.* **2006**, *250*, 1315–1331.
- (42) Robertazzi, A.; Platts, J. A. *Chem.—Eur. J.* **2006**, *12*, 5747–5756.
- (43) Saad, J.; Benedetti, M.; Natile, G.; Marzilli, L. *Inorg. Chem.* **2010**, *49*, 5573–5583.
- (44) Spiegel, K.; Magistrato, A. *Org. Biomol. Chem.* **2006**, *4*, 2507–2517.
- (45) Spingler, B.; Whittington, D.; Lippard, S. *Inorg. Chem.* **2001**, *40*, 5596–5602.
- (46) Teletchea, S.; Skauge, T.; Sletten, E.; Kozelka, J. *Chem.—Eur. J.* **2009**, *15*, 12320–12337.
- (47) Todd, R.; Lippard, S. *J. Inorg. Biochem.* **2010**, *104*, 902–908.
- (48) Zayed, A.; Jones, G. D. D.; Reid, H. J.; Shoeib, T.; Taylor, S. E.; Thomas, A. L.; Wood, J. P.; Sharp, B. L. *Metallomics* **2011**, *3*, 991–1000.
- (49) Chval, Z.; Šíp, M.; Burda, J. V. *J. Comput. Chem.* **2008**, *29*, 2370–2381.
- (50) Chval, Z.; Šíp, M. *J. Mol. Struct. THEOCHEM* **2000**, *532*, 59–68.
- (51) Tao, J.; Perdew, J.; Staroverov, V.; Scuseria, G. *Phys. Rev. Lett.* **2003**, *91*.
- (52) Grimme, S. *J. Comput. Chem.* **2006**, *27*, 1787–1799.
- (53) Klamt, A.; Schuurmann, G. *J. Chem. Soc., Perkin Trans. 2* **1993**, 799–805.
- (54) Weigend, F. *Phys. Chem. Chem. Phys.* **2006**, *8*, 1057–1065.
- (55) Kabeláč, M.; Valdes, H.; Sherer, E. C.; Cramer, C. J.; Hobza, P. *Phys. Chem. Chem. Phys.* **2007**, *9*, 5000–5008.
- (56) Šponer, J.; Riley, K. E.; Hobza, P. *Phys. Chem. Chem. Phys.* **2008**, *10*, 2595–2610.
- (57) Mládek, A.; Šponer, J. E.; Jurečka, P.; Banáš, P.; Otyepka, M.; Svozil, D.; Šponer, J. *J. Chem. Theory Comput.* **2010**, *6*, 3817–3835.
- (58) Grimme, S.; Djukic, J.-P. *Inorg. Chem.* **2011**, *50*, 2619–2628.
- (59) Mutter, S. T.; Platts, J. A. *J. Phys. Chem. A* **2011**, *115*, 11293–11302.
- (60) Andrae, D.; Häußermann, U.; Dolg, M.; Stoll, H.; Preuß, H. *Theor. Chem. Acc.* **1990**, *77*, 123–141.
- (61) Burda, J. V.; Zeizinger, M.; Šponer, J.; Leszczynski, J. *J. Chem. Phys.* **2000**, *113*, 2224–2232.
- (62) Ahlrichs, R.; Bar, M.; Haser, M.; Horn, H.; Kolmel, C. *Chem. Phys. Lett.* **1989**, *162*, 165–169.
- (63) Jurečka, P.; Černý, J.; Hobza, P.; Salahub, D. R. *J. Comput. Chem.* **2007**, *28*, 555–569.
- (64) Ho, J.; Klamt, A.; Coote, M. L. *J. Phys. Chem. A* **2010**, *114*, 13442–13444.
- (65) Frisch, M. J.; Trucks, G. W.; Schlegel, H. B.; Scuseria, G. E.; Robb, M. A.; Cheeseman, J. R.; Scalmani, G.; Barone, V.; Mennucci, B.; Petersson, G. A.; Nakatsuji, H.; Caricato, M.; Li, X.; Hratchian, H. P.; Izmaylov, A. F.; Bloino, J.; Zheng, G.; Sonnenberg, J. L.; Hada, M.; Ehara, M.; Toyota, K.; Fukuda, R.; Hasegawa, J.; Ishida, M.; Nakajima, T.; Honda, Y.; Kitao, O.; Nakai, H.; Vreven, T.; Montgomery, Jr., J. A.; Peralta, J. E.; Ogliaro, F.; Bearpark, M.; Heyd, J. J.; Brothers, E.; Kudin, K. N.; Staroverov, V. N.; Kobayashi, R.; Normand, J.; Raghavachari, K.; Rendell, A.; Burant, J. C.; Iyengar, S. S.; Tomasi, J.; Cossi, M.; Rega, N.; Millam, J. M.; Klene, M.; Knox, J. E.; Cross, J. B.; Bakken, V.; Adamo, C.; Jaramillo, J.; Gomperts, R.; Stratmann, R. E.; Yazyev, O.; Austin, A. J.; Cammi, R.; Pomelli, C.; Ochterski, J. W.; Martin, R. L.; Morokuma, K.; Zakrzewski, V. G.; Voth, G. A.; Salvador, P.; Dannenberg, J. J.; Dapprich, S.; Daniels, A. D.; Farkas, Ö.; Foresman, J. B.; Ortiz, J. V.; Cioslowski, J.; Fox, D. J. *Gaussian 09, Revision C.1*; Gaussian, Inc.: Wallingford, CT, 2009.
- (66) Keith, T. A. *AIMAll* (Version 10.11.24); TK Gristmill Software: Overland Park, KS, 2010; aim.tkgristmill.com.
- (67) Glendenning, E. D.; Reed, A. E.; Carpenter, J. E.; Weinhold F. *NBO 3.1*; Theoretical Chemistry Institute. University of Wisconsin: Madison, WI, 1996.
- (68) Schaftenaar, G.; Noordik, J. H. *J. Comput.-Aided Mol. Des.* **2000**, *14*, 123–134.
- (69) Allouche, A. *J. Comput. Chem.* **2011**, *32*, 174–182.
- (70) Lu, X.; Olson, W. *Nucleic Acids Res.* **2003**, *31*, S108–S121.
- (71) Dolomanov, O.; Bourhis, L.; Gildea, R.; Howard, J.; Puschmann, H. *J. Appl. Crystallogr.* **2009**, *42*, 339–341.
- (72) Alberto, M. E.; Butera, V.; Russo, N. *Inorg. Chem.* **2011**, *50*, 6965–6971.
- (73) Zhang, D.; Ren, X.; Zhou, L. *Can. J. Chem.* **2010**, *88*, 1240–1246.
- (74) Boys, S. F.; Bernardi, F. *Mol. Phys.* **1970**, *19*, 553–566.
- (75) Zimmermann, T.; Chval, Z.; Burda, J. V. *J. Phys. Chem. B* **2009**, *113*, 3139–3150.
- (76) Ziegler, T.; Rauk, A. *Theor. Chim. Acta* **1977**, *46*, 1–10.
- (77) Ziegler, T.; Rauk, A. *Inorg. Chem.* **1979**, *18*, 1558–1565.
- (78) Mitoraj, M.; Michalak, A.; Ziegler, T. *J. Chem. Theory Comput.* **2009**, *5*, 962–975.
- (79) Mitoraj, M. P.; Zhu, H.; Michalak, A.; Ziegler, T. *Int. J. Quantum Chem.* **2009**, *109*, 3379–3386.
- (80) Mitoraj, M. P.; Michalak, A.; Ziegler, T. *Organometallics* **2009**, *28*, 3727–3733.
- (81) van Lenthe, E.; Baerends, E. J.; Snijders, J. G. *J. Chem. Phys.* **1993**, *99*, 4597–4610.
- (82) van Lenthe, E.; van Leeuwen, R.; Baerends, E. J.; Snijders, J. G. *Int. J. Quantum Chem.* **1996**, *57*, 281–293.
- (83) Laoui, A.; Kozelka, J.; Chottard, J. *Inorg. Chem.* **1988**, *27*, 2751–2753.
- (84) Schneider, B.; Neidle, S.; Bertram, H. *Biopolymers* **1997**, *42*, 113–124.
- (85) Svozil, D.; Kalina, J.; Omelka, M.; Schneider, B. *Nucleic Acids Res.* **2008**, *36*, 3690–3706.
- (86) Carlone, M.; Marzilli, L. G.; Natile, G. *Inorg. Chem.* **2004**, *43*, 584–592.

- (87) Saad, J.; Natile, G.; Marzilli, L. *J. Am. Chem. Soc.* **2009**, *131*, 12314–12324.
- (88) Hambley, T. W. *Inorg. Chem.* **1998**, *37*, 3767–3774.
- (89) Rizzato, S.; Bergès, J.; Mason, S. A.; Albinati, A.; Kozelka, J. *Angew. Chem., Int. Ed.* **2010**, *49*, 7440–7443.
- (90) Truflandier, L. A.; Sutter, K.; Autschbach, J. *Inorg. Chem.* **2011**, *50*, 1723–1732.
- (91) Wu, B.; Davey, G. E.; Nazarov, A. A.; Dyson, P. J.; Davey, C. A. *Nucleic Acids Res.* **2011**, *39*, 8200–8212.
- (92) Romancová, I.; Chval, Z.; Předota, M. *J. Phys. Chem. A* **2012**, *116*, 1786–1793.
- (93) Wu, Y.; Bhattacharyya, D.; King, C. L.; Baskerville-Abraham, I.; Huh, S.-H.; Boysen, G.; Swenberg, J. A.; Temple, B.; Campbell, S. L.; Chaney, S. G. *Biochemistry* **2007**, *46*, 6477–6487.
- (94) Sharma, S.; Gong, P.; Temple, B.; Bhattacharyya, D.; Dokholyan, N. V.; Chaney, S. G. *J. Mol. Biol.* **2007**, *373*, 1123–1140.
- (95) Margiotta, N.; Marzano, C.; Gandin, V.; Osella, D.; Ravera, M.; Gabano, E.; Platts, J. A.; Petruzzella, E.; Hoeschele, J. D.; Natile, G. *J. Med. Chem.* **2012**, *55*, 7182–7192.
- (96) Vrána, O.; Mašek, V.; Dražan, V.; Brabec, V. *J. Struct. Biol.* **2007**, *159*, 1–8.
- (97) Šponer, J.; Sabat, M.; Gorb, L.; Leszczynski, J.; Lippert, B.; Hobza, P. *J. Phys. Chem. B* **2000**, *104*, 7535–7544.
- (98) Burda, J. V.; Šponer, J.; Hrabakova, J.; Zeizinger, M.; Leszczynski, J. *J. Phys. Chem. B* **2003**, *107*, 5349–5356.
- (99) Robertazzi, A.; Platts, J. *J. Biol. Inorg. Chem.* **2005**, *10*, 854–866.
- (100) Robertazzi, A.; Platts, J. *Inorg. Chem.* **2005**, *44*, 267–274.
- (101) Burda, J. V.; Šponer, J.; Leszczynski, J.; Hobza, P. *J. Phys. Chem. B* **1997**, *101*, 9670–9677.
- (102) Burda, J. V.; Šponer, J.; Leszczynski, J. *Phys. Chem. Chem. Phys.* **2001**, *3*, 4404–4411.
- (103) Ohndorf, U.-M.; Rould, M. A.; He, Q.; Pabo, C. O.; Lippard, S. *J. Nature* **1999**, *399*, 708–712.
- (104) Sullivan, S. T.; Saad, J. S.; Fanizzi, F. P.; Marzilli, L. G. *J. Am. Chem. Soc.* **2002**, *124*, 1558–1559.
- (105) Delalande, O.; Malina, J.; Brabec, V.; Kozelka, J. *Biophys. J.* **2005**, *88*, 4159–4169.
- (106) Florian, J.; Brabec, V. *Chem.—Eur. J.* **2012**, *18*, 1634–1639.
- (107) Jurečka, P.; Šponer, J.; Černý, J.; Hobza, P. *Phys. Chem. Chem. Phys.* **2006**, *8*, 1985–1993.
- (108) Johnson, C. A.; Bloomingdale, R. J.; Ponnusamy, V. E.; Tillinghast, C. A.; Znosko, B. M.; Lewis, M. *J. Phys. Chem. B* **2011**, *115*, 9244–9251.

Exploration of various electronic properties along the reaction coordinate for hydration of Pt(II) and Ru(II) complexes; the CCSD, MP_x, and DFT computational study

Jaroslav V. Burda · Zdeněk Futera · Zdeněk Chval

Received: 2 December 2012 / Accepted: 30 August 2013 / Published online: 15 October 2013
© Springer-Verlag Berlin Heidelberg 2013

Abstract In the study behavior of molecular electrostatic potential, averaged local ionization energy, and reaction electronic flux along the reaction coordinate of hydration process of three representative Ru(II) and Pt(II) complexes were explored using both post-HF and DFT quantum chemical approximations. Previously determined reaction mechanisms were explored by more detailed insight into changes of electronic properties using ω B97XD functional and MP2 method with 6–311++G(2df,2pd) basis set and CCSD/6–31(+G(d,p)) approach. The dependences of all examined properties on reaction coordinate give more detailed understanding of the hydration process.

Keywords Ab initio calculations · Average local ionization energy · DFT · Reaction electronic flux · Electrostatic potential · Metallodrugs

Introduction

Organometallic complexes, which are important in anticancer treatment and contain chloro-ligand, are in cellular environment activated by hydration reaction (i.e., substitution reaction

where chloro ligand is replaced by water molecule). This process is usually endothermic but its occurrence is enforced by very low concentration of chloride anions in cytoplasm of the cells [1, 2]. This process has to pass with appropriate rate constant since too slow a process is inefficient and too fast a reaction leads to activation out of cell or immediately after passing through cellular membrane. This enables the drug to bind to any ‘appropriate’ site of the closest biomolecule, e.g., to side-chains of amino acids, which are on the protein surface, and to form (often) irreversible coordination. Here it may not block any basic life functions and can be finally replace by expressing new unharmed biomolecule. Therefore tuning the drug activation, in the case of chloro-complexes, e.g., by the hydration reaction, is one of the key steps in successful design of new metallodrug. The activation of Pt(II) and other metallocomplexes was explored computationally by several groups recently,[3–10].

Also, the Ru(II) ‘piano-stool’ complexes attract a lot of attention due to their promising properties and their activation mechanism was examined in many theoretical papers, e.g., [11–19].

For the given chemical reaction a potential energy curve along the reaction coordinate (ϑ) can be determined, e.g., by the intrinsic reaction coordinate (IRC) method. Then, a reaction force F in each point of the coordinate ϑ can be defined [20] as:

$$F(\vartheta) = -\frac{\partial V(\vartheta)}{\partial \vartheta}. \quad (1)$$

Several critical points occur on the reaction force curve $F(\vartheta)$, which can divide the reaction into several areas: where a) mainly structural changes take place—from reactants to force minimum (alpha-point), b) electronic changes predominates—from force minimum to force maximum (gamma-point) and c) final structural reorganization finishes the process—from force maximum to product [21–23]. These points are shown in Fig. 1b.

J. V. Burda (✉) · Z. Futera
Department of Chemical Physics and Optics,
Faculty of Mathematics and Physics, Charles University,
Ke Karlovu 3, 121 16 Prague 2, Czech Republic
e-mail: Jaroslav.Burda@mff.cuni.cz

Z. Futera
Keio University, 3-14-1 Hiyoshi, Kohoku-Ku, Yokohama 223-8522,
Japan

Z. Chval
Department of Laboratory Methods and Information Systems,
Faculty of Health and Social Studies, University of South Bohemia,
J. Boreckého 27, 370 11 České Budějovice, Czech Republic

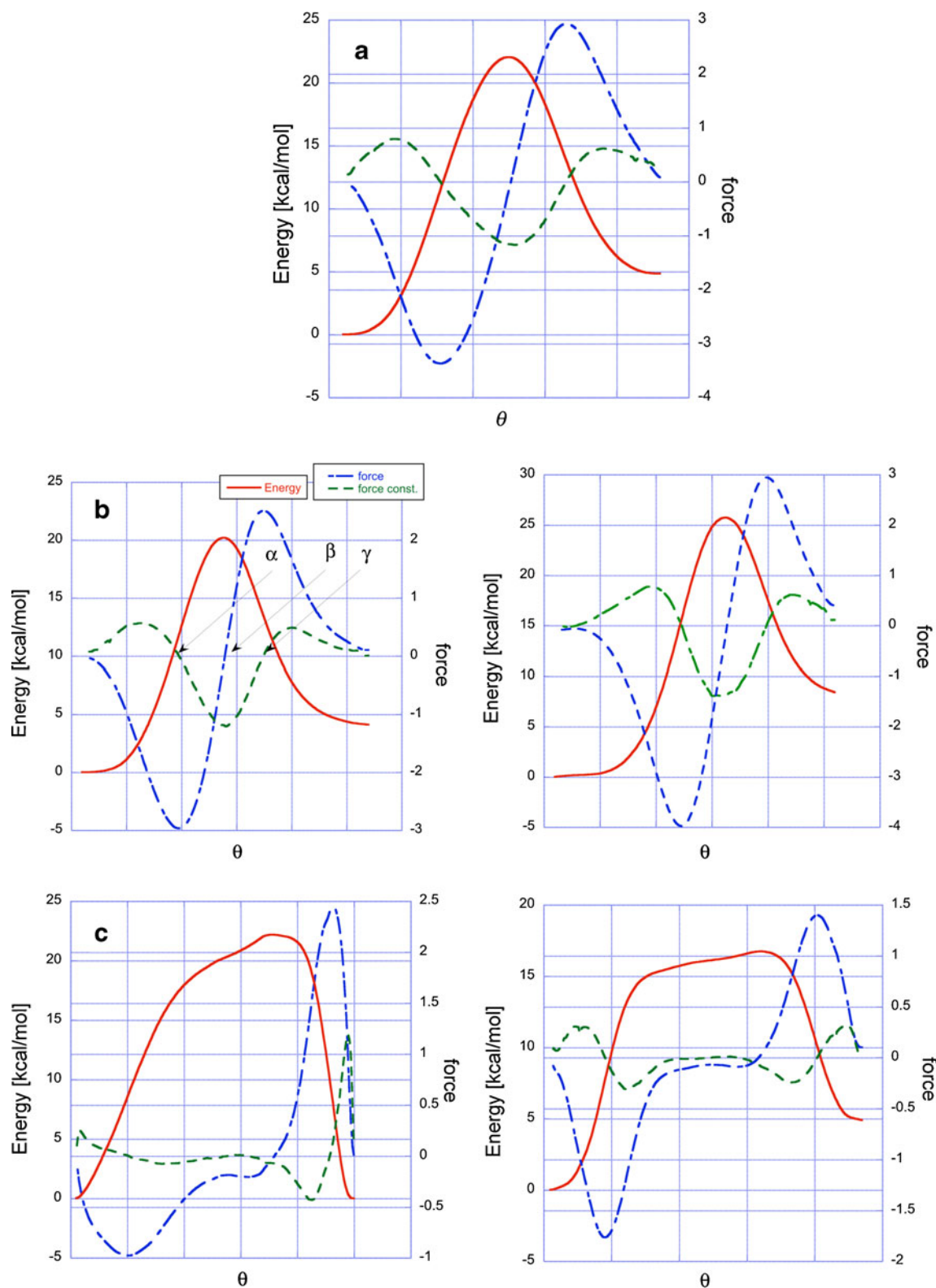


Fig. 1 PEC (red solid line), force (blue dot-dashed line) and force constant (green dashed line) for hydration process of: **a**) $[\text{Ru}(\text{en})\text{Cl}(\text{benzene})]^+$ **b**) cisplatin, and **c**) RAPTA-B complexes (by dissociative mechanism). Both

dechlorination steps were considered in the cisplatin and RAPTA cases (first step left)

In a similar way to reaction force also a concept of reaction electronic flux (REF) along ϑ was introduced [24] as:

$$J(\vartheta) = -\frac{\partial\mu(\vartheta)}{\partial\vartheta}, \quad (2)$$

where $\mu(\vartheta)$ means chemical potential, which can be roughly estimated from energy of HOMO and LUMO orbitals in the individual point of IRC:

$$\mu \approx \frac{1}{2}(\varepsilon_{HOMO} + \varepsilon_{LUMO}). \quad (3)$$

It was found [25] that areas with $J(\vartheta) > 0$ are connected with spontaneous electronic rearrangement indicating formation of covalent bond while $J(\vartheta) < 0$ corresponds to weakening of a bond.

Important property for recognition and interaction of the given molecule in any biosystem is molecular electrostatic potential (MEP), for very instructive introduction see ref [26]. It can be defined as force acting on a positive (unit) charge located at some point in the space through the electronic charge cloud generated by the electron density and nuclei positions:

$$V(\mathbf{r}) = \sum_A \frac{z_A}{|\mathbf{R}_A - \mathbf{r}|} - \int \frac{\rho(\mathbf{r}') d\mathbf{r}'}{|\mathbf{r}' - \mathbf{r}|}. \quad (4)$$

Another tool for reactivity description of the given molecule is Average Local Ionization Energy (ALIE). It was introduced by Politzer, e.g., in refs [27, 28]

$$\bar{I}(\mathbf{r}) = \sum_i \frac{\rho_i(\mathbf{r})|\varepsilon_i|}{\rho(\mathbf{r})} \quad (5)$$

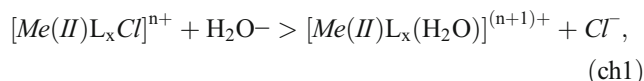
in order to shed light into the location of the most reactive (easily removable) electrons. Both $V(\mathbf{r})$ and $\bar{I}(\mathbf{r})$ are local, site-specific, properties that require the determination of electron density.

In this study we concentrate on the comparison of several different kinds of electron densities (HF, MP2, CCSD, and ω B97XD) for these descriptors evaluated along the reaction coordinate of the hydration process from the reactant system: chloro-complex + water to product state: aqua-complex + chloride. Recently we have compared the thermodynamic and kinetic parameters for hydration of [Pt(NH₃)₂Cl₂] (cisplatin), [Ru(η^6 -benzene)(en)Cl]⁺ (en = ethylenediamine, further abbreviated as Ru_en [29, 30]), and [Ru(η^6 -benzene)(pta)Cl₂] complexes (labeled as RAPTA complex with pta ligand: pta=1.3.5-triaza-7-phosphatocyclo[3.3.1.1] decane [31, 32]) [33]; their structures are drawn in Scheme 1. We reexamined the

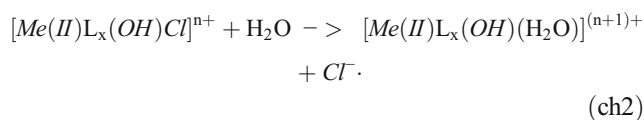
hydration process using the above-mentioned reaction descriptors for a detailed insight into the reaction mechanism.

Computational details

Since $V(\mathbf{r})$ and $\bar{I}(\mathbf{r})$ are local properties, for which determination of an electron density is necessary, we have chosen several levels of computation for possible comparison: the MP2/6-311++G(2df,2pd), ω B97XD/6-311++G(2df,2pd) [34], and CCSD/6-31(+G(d) methods. The (+) acronym labels a set of diffuse functions on oxygen and chlorine atoms only. The corresponding extensions for Pt and Ru pseudoorbitals by polarization and diffuse functions are taken from refs [35, 36]. For simulation of water solution the implicit solvation model (PCM) was used with cavities constructed using AU0 atomic radii. Hereafter the 6-31(+G(d) basis set will be signed as BSOpt and the 6-311++G(2df,2pd) set as BSSP. The intrinsic reaction coordinate (IRC) calculations and optimizations were performed at B3LYP/6-31(+G(d) level. The evaluation of MEP, ALIE, REF and some other electronic properties was done in the selected IRC points and stationary structures of the considered hydration based on the chemical reaction:



where $n=0$ for cisplatin and RAPTA complexes and $n=1$ for Ru_en complex. For the second hydration step the first aqua ligand is replaced by (OH)⁻ ligand in order to keep the complex during both steps electroneutral. Also, the hydroxo-aqua-cisplatin form corresponds more closely to the situation in real neutral (pH=7) solution:

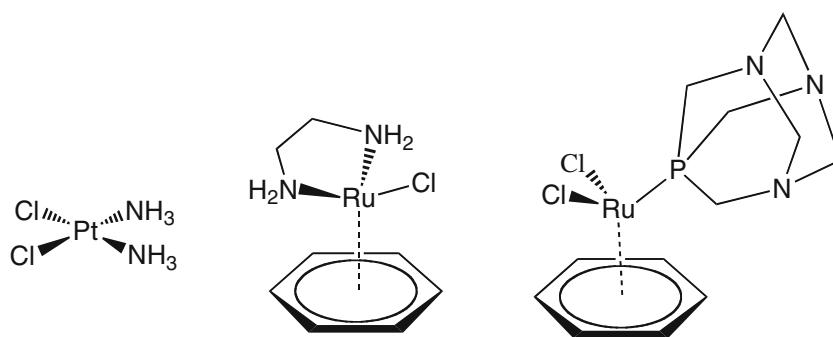


Results and discussion

Potential energy curves

For all the hydration processes the reactants and products were considered in supermolecular form. Their structures were optimized at B3LYP/BSOpt level and a correct character of minima was confirmed by diagonalization of the Hessian matrix. The same procedure was also used for determination of the TS structure and finding the appropriate vibration mode. While in the case of cisplatin and Ru_en complexes the associative interchange mechanism was considered with

Scheme 1 Structural formulas of a) cisplatin, b) Ru_en, and c) RAPTA-B complexes



prolonged bonds to the entering and leaving ligands [37] in the case of RAPTA complex the dissociative mechanism was considered as kinetically preferable over associative one [33].

From optimized TS structures, the IRC points were obtained and potential energy curves (PEC) were constructed using the chosen computational levels. These potential curves are plotted in Figs. 1 and 2. The thermodynamic data, activation energies and rate constants were already discussed in our previous study [33]. In this contribution we will concentrate on the changes in electron densities and other above-mentioned descriptors along the reaction coordinate.

Reaction force and force constant for the CCSD/BSOpt results are plotted in Fig. 1. The alpha, beta = TS, and gamma points are marked only in Fig. 1b for clarity. It can be seen that relatively simple (textbook) behavior is displayed for the Ru_en and cisplatin complexes where activation barrier is connected with typical force shape describing single-step process and an area of negative force constant—negative eigenvalue of one vibrational mode (of antisymmetric stretching O-Me-Cl character) defines the reaction coordinate. In the case of dissociative mechanism of RAPTA, the activation exhibits a more complex course of reaction force and force constants giving the evidence of multi-step behavior. It is worth mentioning that in the RAPTA dissociative mechanism, two TS structures were localized with a stable intermediate in-between. However, none of the post-Hartree-Fock methods reproduce this picture and no stable intermediate is predicted. Instead of the first TS (TS1) maximum only a change of slope occurs leaving TS2 as a single ‘true’ TS structure. The existence of a stable intermediate is noticeable only at the HF and DFT levels. This can be demonstrated in Fig. 2c where PECs for the RAPTA complex are plotted. In Table 1 the activation barrier and reaction energies are collected. As compared with our previous papers [7, 33, 35] the heights of activation barriers at various computational levels can differ quite significantly. It can be noticed that HF results are quite close to CCSD values in the case of cisplatin while for Ru(II)-complexes it fails completely especially in the case of RAPTA activation energies. This is mainly due to missing description of the interaction between metal and arene [35]. The MP2/BSSP results overestimate both activation and

reaction energies quite substantially in comparison with CCSD results up to 5 kcal mol⁻¹. Using smaller basis set gives much closer agreement (as is known from literature, too). As can be expected from the perturbation theory, MP3 values always improve the MP2 profile leading to usually better accord with CC method. The DFT levels (as already mentioned previously) match relatively very well the CCSD calculations with exception of the RAPTA case.

The complexity of dechlorination processes in the RAPTA complex is clearly demonstrated by more complicated shapes of force and force constant. Nevertheless, the force curves resemble, at least partially, a ‘standard’ behavior with both accelerating and decelerating areas separated on the reaction coordinate. From the REF values it follows that from the very beginning large decrease of bonding occurs connected with Ru-Cl bond breaking practically without any preparation phase where structural reorientation is necessary (cf. below). This is actually easy to understand since the dechlorination does not require any basic geometry changes or relaxations. The only (marginal) structural change is connected with stabilization of intermediate structure, which is represented by placing the pta and remaining chloro ligand (in first hydration step) so that the Cl-Ru-P atoms form plane perpendicular to benzene plane minimizing the steric repulsion (as already described as a necessary condition for dissociative mechanism of these complexes [33]). The RAPTA energy profiles display the highest variation of energies. While in the case of Ru_en and cisplatin all the TS energies vary within ca 6–8 kcal mol⁻¹ (even including HF energies in Ru_en complex) in the RAPTA case they vary in the range of 14 kcal mol⁻¹ in second dechlorination and even 17 kcal mol⁻¹ in the first hydration step. Omitting HF level, the variation is still in range of 10 kcal mol⁻¹ clearly pointing to high accuracy required for the proper description of these reactions.

Chemical potential and reaction electronic flux curves

For the reaction pathways the changes of chemical potential and REF are summarized in plots in Fig. 3. From the course of REF in Fig. 3 it follows that all the explored reactions start by weakening M-Cl bond. Just after the TS point, the REF curve

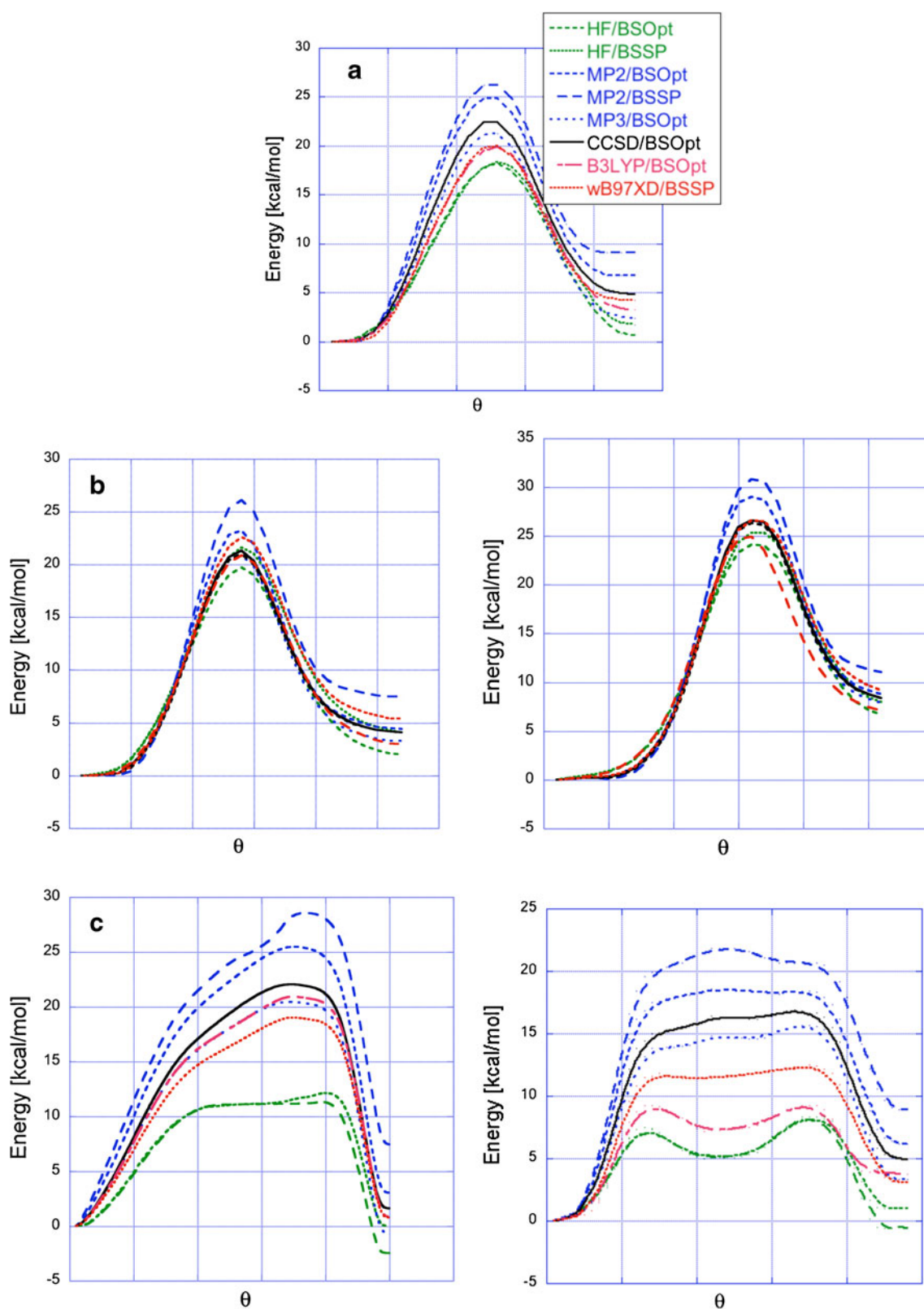


Fig. 2 Hydration energy profiles along the reaction coordinate for all the chosen computational levels. **a)** $[\text{Ru}(\text{en})\text{Cl}(\text{benzene})]^+$. **b)** cisplatin, and **c)** RAPTA-B complexes (by dissociative mechanism)

of the Ru_{en} complex already achieves maximum demonstrating that a new $\text{Ru}-\text{O}(\text{aqua})$ bond is being formed. The partially

released chlorine is H-bonded simultaneously to water and en ligand. The negative area of $J(\vartheta)$ at the end of reaction is

Table 1 The height of activation barriers and reaction energies at chosen computational levels (in kcal mol⁻¹)

	Ru_en		cisPt_I		cisPt_II		RAPTA_I			RAPTA_II		
	ΔE_a	ΔE_r	ΔE_a	ΔE_r	ΔE_a	ΔE_r	ΔE_{a1}	ΔE_{a2}	ΔE_r	ΔE_{a1}	ΔE_{a2}	ΔE_r
HF/BSOpt	18.2	0.6	19.7	2.0	24.1	6.7	11.0	11.6	-2.5	7.5	8.3	-0.6
HF/BSSP	18.4	1.7	21.6	4.1	25.3	8.0	11.1	12.6	0.0	7.5	8.3	1.0
MP2/BSOpt	24.8	4.8	23.2	4.4	29.0	8.8	20.5	24.1	3.0	16.8	18.4	6.2
MP2/BSSP	26.3	6.8	26.1	7.5	30.8	11.0	21.9	28.0	7.4	19.9	20.7	8.9
MP3/BSOpt	21.2	9.7	20.9	3.3	26.4	7.9	16.5	19.5	-0.7	13.8	15.7	3.3
B3LYP/BSOpt	20.0	2.8	20.9	5.2	25.9	10.5	18.7	20.6	4.1	11.9	12.6	4.6
ω B97XD/BSSP	20.1	4.3	22.6	5.4	26.6	9.2	15.1	18.4	0.8	13.4	13.6	3.1
CCSD/BSOpt	22.4	2.4	21.3	4.1	26.6	8.4	17.6	20.9	1.6	15.0	16.7	4.9
CCSD(T)/BSOpt			21.0	4.1	26.3	8.4						

connected with breaking of Cl...H(en) H-bond since the optimally coordinated aqua ligand is positioned so that it is not possible for chlorine to keep both H-bond. This relatively marginal process is clearly visible thanks to the REF behavior.

In the hydration of cisplatin the shape of chemical potential in the TS area resemble behavior of energy profile being shifted slightly toward product region clearly pointing where the largest changes of chemical potential occur. The electronic flux curves in the range of TS exhibit still weakening of bonding. This is in accord with the previously described fact that despite an associative mechanism, in the TS structures (for both first and second dechlorination) Cl and water are only very weakly bonded to central Pt atom [8] and only after TS positive area of $J(\vartheta)$ can be seen where Pt-O bond is formed.

In the RAPTA hydrations the shape of chemical potential (in accord with course of reaction force) speaks about complex course. Similarly like the energy profiles they do not reflect existence of stable intermediate that should separate two TS points. The $\mu(\vartheta)$ curves exhibit one minimum. In the first dechlorination step, it is localized in the area of the TS2 structure, after which a positive area of $J(\vartheta)$ starts. It is connected with formation of Ru-O(aqua) bond. Similar conclusions hold also for the second hydration step. The most striking difference is in much narrower but substantially deeper negative course of $J(\vartheta)$ curve and much broader and lower area of positive values. Also the minimum of chemical potentials changes is 'more central' and can correspond to flatter area between both TS structures in the case of second dechlorination.

MEP and ALIE

Molecular electrostatic potential and average local ionization energy were examined on the $0.001\text{e}/\text{\AA}^3$ isodensity surface [38] of the individual structures. Several maxima and minima were localized on the isodensity surface of each structure. The CCSD/BSOpt level was used for further discussion. The

differences of global maxima and minima (relative to corresponding absolute minimal value from the whole reaction coordinate) are plotted in Fig. 4. The absolute minima and maxima together with their relative positions on ϑ (between 0 and 1) are collected in Table 2 for the CCSD electron density. These absolute minima are localized on the released chloride anion (for MEP and ALIE of Ru_en, MEP of cisplatin, MEP and ALIE of RAPTA I and II). The only exception is the ALIE minimum in the case of cisplatin, which is located on Pt atom (cf. discussion below). Absolute maxima are located on amino groups—either of en (in Ru_en) or ammine (of cisplatin). In the RAPTA case, the MEP and ALIE maxima are localized on hydrogens of benzene ring.

Despite a 'smooth' behavior of MEP minima (MEP_min hereafter) along ϑ , the position of global minimum is relocated from water oxygen to chloro-ligand (as follows from Fig. 5a and b) in the area where ALIE_min exhibit maximal value ($\vartheta \approx 0.22$ – in relative values). For the same ϑ , also the first minimum occurs on REF curve demonstrating the decrease of Ru-Cl bonding is connected with switching the MEP_min from oxygen to chlorine region. The MEP_min becomes mildly negative before the TS is achieved clearly showing the reduction of the Cl lone-pair donation to Ru (also visible in maximal NPA partial charge $\delta(\text{Ru})=0.26\text{ e}$, which occurs in TS). With the consequent releasing of Cl⁻ from Ru(II) complex, the MEP_min value further decreases till the final value -24 kcal mol^{-1} (-1.05 eV), which is taken as relative zero. The MEP maximum (MEP_max) curve shows how the Ru(II) complex becomes 'more attractive' for nucleofiles—increasing MEP_max values in amino hydrogen area (up to 155 kcal mol^{-1}). This is a very important feature for further reactivity of these hydrated complexes. Also, the acidity of aqua proton is quite high—exhibiting the second (local) maximum in the product area of ϑ —about 144 kcal mol^{-1} . This high acidity correlates well with partial charge $\delta(\text{H-aq})=0.56\text{ e}$ in NBO analysis; partial charges of amino hydrogens are $0.46\text{--}0.47\text{ e}$.

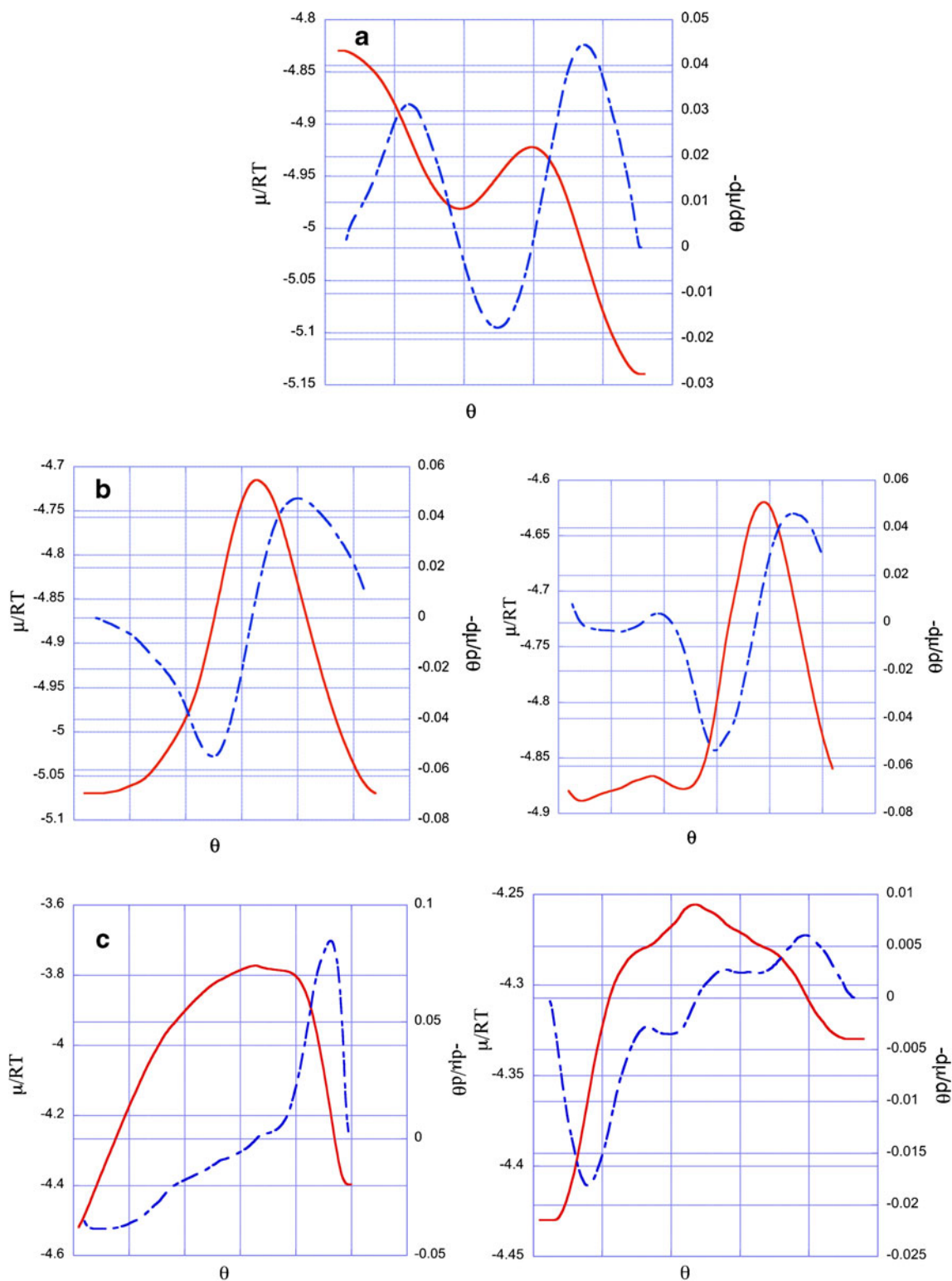
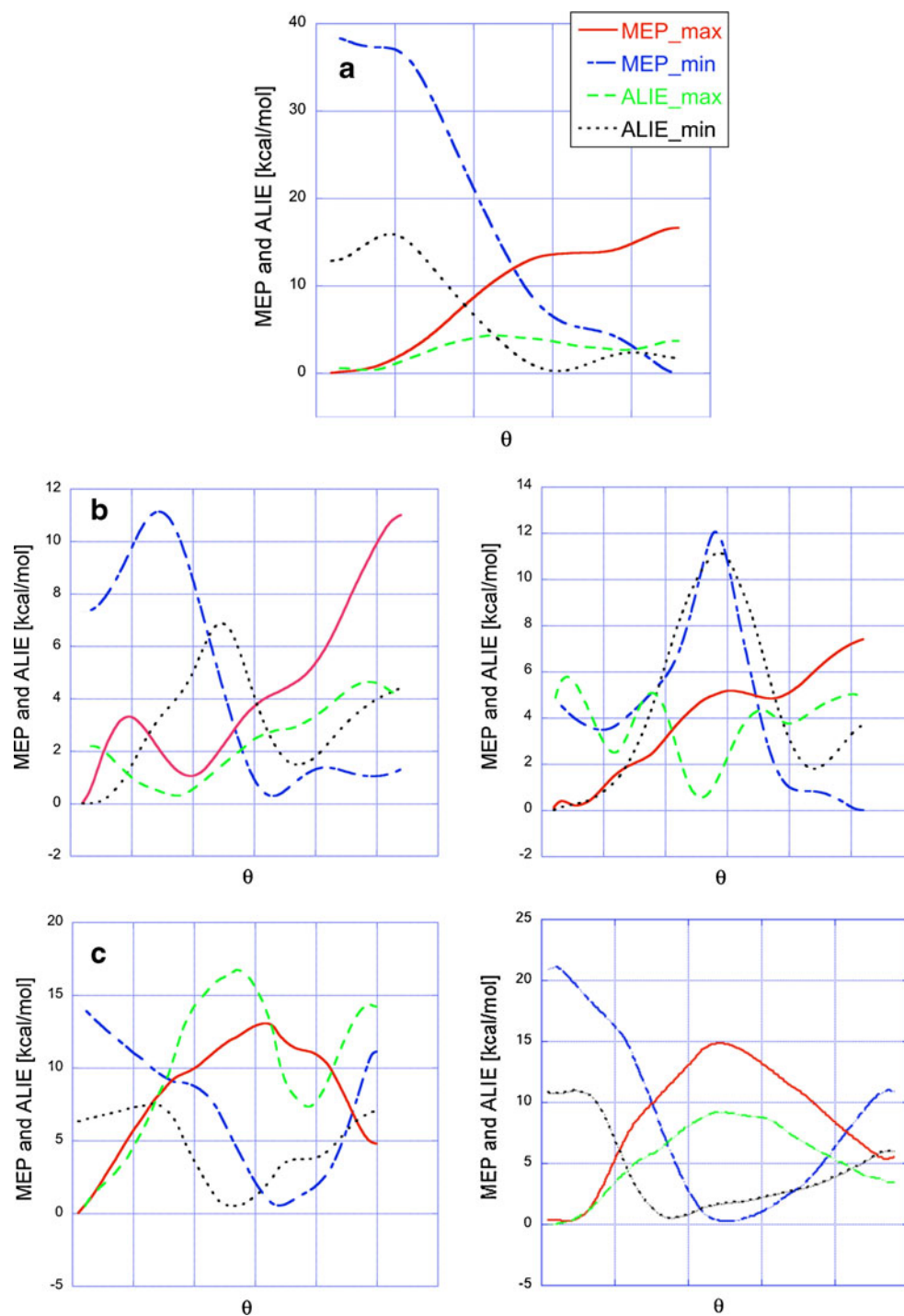


Fig. 3 Variation of chemical potential (μ/RT ... red solid line) and $REF(-\frac{d\mu}{d\theta})$... blue dot-dashed line) along ϑ for the complexes of: **a)** $[Ru(en)Cl(benzene)]^+$ **b)** cisplatin, and **c)** RAPTA-B

As mentioned above, in Fig. 4a there is a maximum of ALIE_min value of Ru_en complex at ca 1/4 of ϑ . From a closer inspection of localization of individual minima on ALIE surface along the reaction coordinate, it was found that

this change is connected with relocation of maximum point localized on chlorine from the vicinity of benzene ring to the top of the complex close to approaching water molecule (cf. Fig. 6a and b). In the second part of ϑ , a minimum on the

Fig. 4 Relative MEP and ALIE profiles along the reaction coordinate. MEP_max values are solid red, MEP_min blue dash-dotted, ALIE_max green dashed, and ALIE_min black dotted lines **a**) $[\text{Ru}(\text{en})\text{Cl}(\text{benzene})]^+$ **b**) cisplatin, and **c**) RAPTA-B complexes



ALIE curve occurs. In this case the chloride anion, where the minimum point is localized, is already relatively far from the Ru(II) complex so that minima connected with non-bonding lone pairs are practically degenerate ('averaged') without any preferred (lower) value and therefore MEP_min increases a little afterward.

In the case of cisplatin, the 1st step hydration MEP_min curve displays quite complicated character. In reactant area of

θ the MEP_min is localized in conjunction of both chlorine atoms ca $-76 \text{ kcal mol}^{-1}$ (cf. Fig. 5c) and the second minimum on the oxygen atom is about 20 kcal mol^{-1} higher.

The ALIE_min of isolated cisplatin is connected with electron density of d_{z^2} occupied AO and it is degenerated below and above the square-planar complex as corresponds to the d_{z^2} symmetry. Due to remote water/chloride particle the symmetry of this minimum is removed and the lowest ALIE

Table 2 Absolute maxima and minima of MEP and ALIE (in eV) on the $0.001 \text{ e}/\text{\AA}^3$ isodensity surface of the supermolecular complex and their relative position on the reaction coordinate (from 0 to 1)

		MEP		ALIE	
		min	max	min	max
Ru_en	ϑ	1.00	1.00	0.65	0.47
	energy	-1.05	6.74	11.28	20.43
cisPt_I	ϑ	0.63	0.00	0.00	0.33
	energy	-3.34	4.63	10.81	20.97
cisPt_II	ϑ	1.00	0.00	0.00	0.54
	energy	-3.18	3.93	10.36	20.70
RAPTA_I	ϑ	0.68	0.68	0.25	0.55
	energy	-3.69	3.26	9.63	18.43
RAPTA_II	ϑ	0.46	0.46	0.35	0.50
	energy	-4.06	3.24	10.82	20.38

value is 'below' square-planar complex—connected with 'bottom' d_{z^2} lobe (if water is approaching from above – cf. Fig. 6c). After TS, when the chloro-ligand is changing to chloride anion and being released under the complex plane, the global minimum is switched to 'upper' d_{z^2} lobe, cf. Fig. 6d. From this discussion follows one very remarkable fact namely that the lowest ALIE values, e.g., the place where an electron density could be the most easily removed is not chloro-ligand but the Pt(II) orbital, which is a slightly surprising result especially because the most electronegative negative area (MEP minimum) is localized on Cl-(ligand - > anion). In the case of ALIE only the higher local minima are localized on Cl surface. This conclusion is valid for all kinds of explored electron densities - HF, MP2, DFT, and CCSD.

Actually, this situation can be explained by the fact that cisplatin, and Pt(II) complexes generally, can be easily oxidized to Pt(III) and Pt(IV) more stable complexes [39]. Interestingly, MEP_min and ALIE_min maxima occur before TS, maximum of MEP_min already after α -point. From closer inspection of the electrostatic maps, it can be found that the MEP_min region starts to move from conjunction of both Cl spheres (Fig. 5c) to the top of released Cl (top in sense of continuation of Pt-Cl bond – Fig. 5d) and reaching this area after the γ -point. It should be mentioned that the MEP_min and MEP_max (in both hydration steps) remain connected with the same atom (chlorine and hydrogen of ammine group, respectively) through the whole ϑ , similarly to ALIE_min (which is localized on Pt).

Fig. 5 MEP of **a**) Ru_en hydration process: IRC point from $\vartheta = 0.20$ **b**) IRC point from $\vartheta = 0.30$ **c**) cisplatin: $\vartheta = 0.01$ **d**) $\vartheta = 0.97$. All extremes are displayed in a.u.

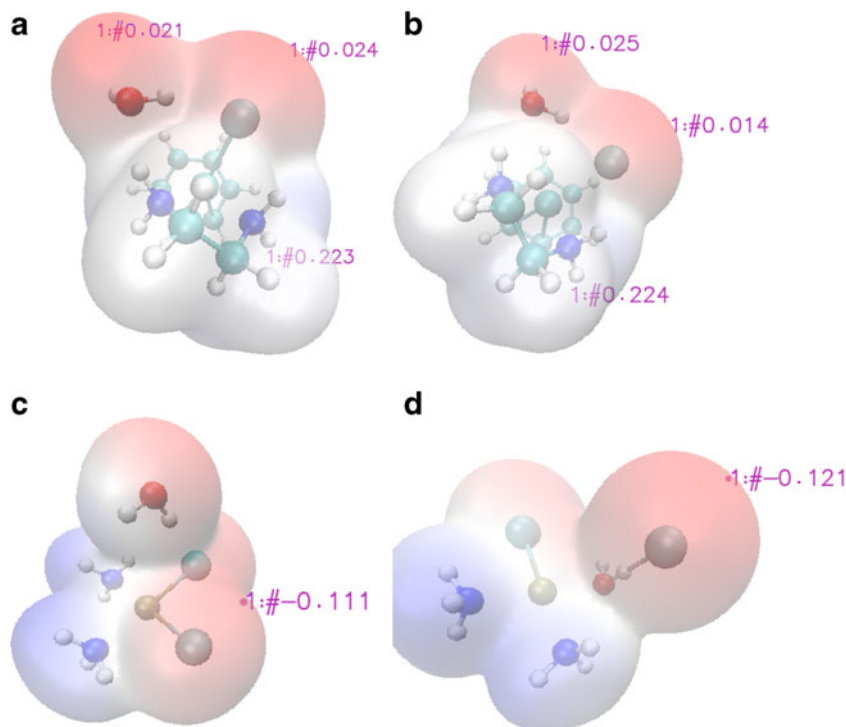
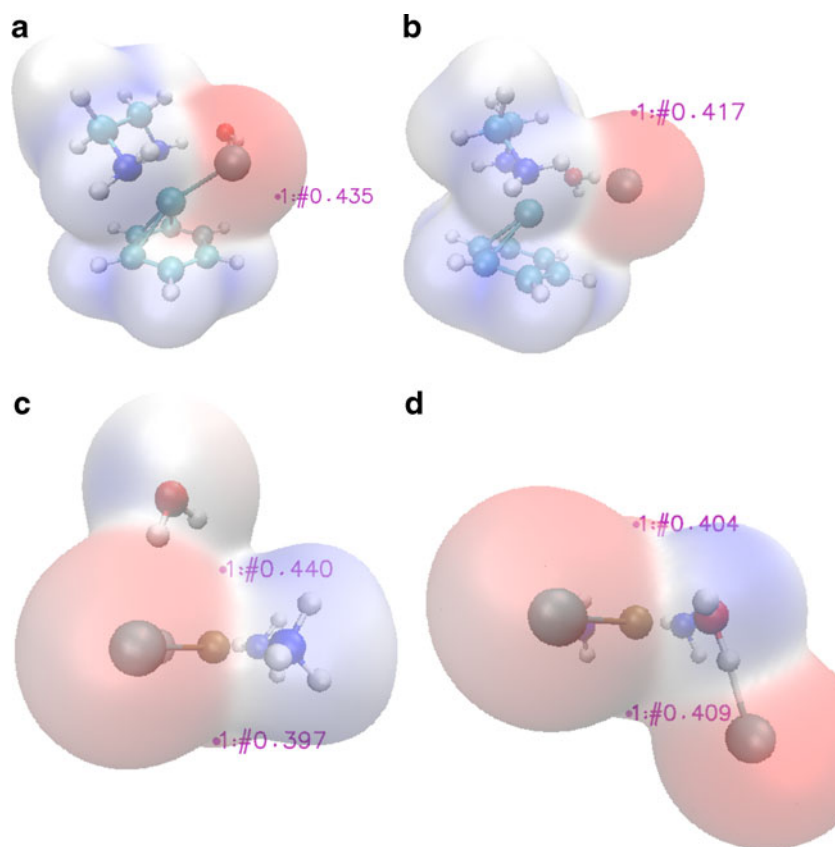


Fig. 6 ALIE surface of **a**) Ru_{en} hydration process: $\vartheta = 0.01$ **b**) $\vartheta = 0.55$ **c**) cisplatin hydration: $\vartheta = 0.05$ **d**) $\vartheta = 0.95$. All extremes are displayed in a.u.



The second hydration step has slightly different MEP_{min} preference. The global minimum is first localized on approaching water and only in the close vicinity of TS the minimum connected with chlorine starts to dominate. Similar behavior was discussed also in the Ru_{en} complex. As to the position on ϑ , this switching point can be roughly associated with force maximum or maximum of chemical potential. Just after TS, the (second) MEP minimum localized on water becomes finally higher than the one of hydroxyl ligand (aqua ligand from the first step). Simultaneously also the ALIE_{min} reaches its highest values in this region, which corresponds to the same switching of global minimum from one plane of Pt complex to the opposite one as discussed in the first hydration step. The small fluctuations of ALIE_{max} are basically irrelevant (this is valid for all studied reactions). They are usually caused by various polarization effects due to H-bond formation and annihilation of approaching/released water/chloride particles.

In the first hydration process of RAPTA complex, the MEP_{min} is, similarly to Ru_{en} case, localized first on oxygen of the water molecule and only after the ‘TS1’ structure, it is relocalized to the released chlorine. In the water coordination part of ϑ , the values of MEP_{min} are increasing as Ru–O bond is formed. As concerns the ALIE surfaces, one remarkable fact is that the lowest values are connected with lone pairs of one of the nitrogen atoms of PTA-ligand and only higher local minima can be associated with Cl lone pairs. This order

is changed in the TS1 area and released Cl exhibits (also like in MEP) ALIE absolute minimum on the whole ϑ . The existence of both MEP_{min} and ALIE_{min} minimum inside the reaction intermediate can be explained by temporarily existence of the ‘isolated’ Cl...H₂O associate. When water coordinates to Ru complex it becomes much more polarized, which also increases the strength of Cl...H(aq) H-bond and in this way also the amount of Cl electron density involved in this bonding. This causes the observed increase of both MEP_{min} and ALIE_{min} values in the later parts of ϑ . However, it can be expected that this effect is model dependent and in real sample chloride will migrate to solvent, which will recover the absolute MEP_{min} and ALIE_{min} values.

Comparing both plots of Fig. 4c, it can be seen that practically the same profiles were obtained for the second hydration. In this way the discussion can be repeated also for this reaction step and it concerns not only the curve shapes but also the location of individual maxima and minima of MEP and ALIE on the isodensity surfaces.

The direct comparison of changes of chemical potential and REF along the reaction coordinate with analogous changes of MEP and ALIE is not straightforward. The main reason is that while REF and chemical potential are connected with changes of electron density during the reaction the MEP and ALIE analyses point to the places on chosen molecular surface where some ‘virtual’ interaction can occur—a place for possible attack by

some other species. And, of course, these places change with changing character of the complex—as a consequence of substitution reaction (hydration in these cases). In this way, the MEP and ALIE analyses of isolated reactant must be considered.

Conclusions

In this contribution we give more detailed insight into reaction mechanism of hydration/dechlorination reactions of platinum(II) and ruthenium(II) complexes studied recently. Since cisplatin and RAPTA complexes contains two chloro-ligands both dechlorination steps were considered. In RAPTA complex the dissociative mechanism is assumed as preferable where after dechlorination a stable intermediate is expected, followed by water coordination. From obtained energy profiles it is revealed that the existence of stable intermediate is not predicted at all computational levels but only at the HF (both basis sets) and B3LYP/BSOpt level used for optimization and IRC construction. From the MEP and ALIE shapes it can be found that changes occur either by switching location of global minima from one atom to another (when different ‘local’ minimum starts to dominate) or by shifting these locations on the surface from one part (close to some ligands) to another. All these changes occur or start and end in the region of specific key points of $\vartheta - \alpha$, β =TS or γ -point.

Acknowledgments Authors are grateful to Grant Agency of Czech Republic (GAČR) project No P205/10/0228 for supporting this study. Also, the access to the MetaCentrum computing and storage facilities (grant LM2010005) is highly appreciated.

References

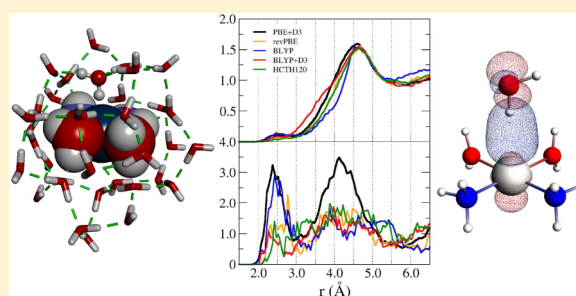
- Lippert B (1999) Cisplatin, Wiley-VCH, Weinheim, 1999
- Zimmermann T, Leszczynski J, Burda JV (2011) *J Mol Model* 17: 2385–2393
- Zeizinger M, Burda JV, Šponer J, Kapsa V, Leszczynski J (2001) *J Phys Chem A* 105:8086–8092
- Raber J, Zhu C, Eriksson LA (2005) *J Phys Chem* 109:11006–11015
- Robertazzi A, Platts JA (2004) *J Comput Chem* 25:1060–1067
- Zhang Y, Guo Z, You X-Z (2001) *J Am Chem Soc* 123:9378–9387
- Burda JV, Zeizinger M, Leszczynski J (2005) *J Comput Chem* 26: 907–914
- Burda JV, Zeizinger M, Leszczynski J (2004) *J Chem Phys* 120: 1253–1262
- Schroeder G, Kozelka J, Sabat M, Fouchet M-H, Beyerle-Pfnur R, Lippert B (1996) *Inorg Chem* 35:1647–1652
- Lopes JF, Menezes VSD, Duarte HA, Rocha WR, De Almeida WB, Dos Santos HF (2006) *J Phys Chem B* 110:12047–12054
- Gossens C, Tavernelli I, Rothlisberger U (2005) *Chimia* 59:81–84
- Deubel DV, Lau JKC (2006) *Chem Commun* 2451–2453
- Wang F, Chen HM, Parsons S, Oswald LDH, Davidson JE, Sadler PJ (2003) *Chem Eur J* 9:5810–5820
- Chen JC, Chen LM, Liao SY, Zheng K, Ji LN (2007) *Dalton Transact* 3507–3515
- Chen JC, Chen LM, Liao SY, Zheng KC, Ji LN (2009) *J Mol Struct -Theochem* 901:137–144
- Chen JC, Chen LM, Liao SY, Zheng KC, Ji LN (2009) *Phys Chem Chem Phys* 11:3401–3410
- Chen JC, Chen LM, Xu LC, Zheng KC, Ji LN (2008) *J Phys Chem B* 112:9966–9974
- Gossens C, Dorcier A, Dyson PJ, Rothlisberger U (2007) *Organomet* 26:3969–3975
- Gossens C, Tavernelli I, Rothlisberger U (2009) *J Phys Chem A* 113: 11888–11897
- Toro-Labbe A, Gutierrez-Oliva S, Concha MC, Murray JS, Politzer P (2004) *J Chem Phys* 121:4570–4576
- Burda JV, Toro-Labbe A, Gutierrez-Oliva S, Murray JS, Politzer PA (2007) *J Phys Chem A* 111:2455–2457
- Jaque P, Toro-Labbe A (2000) *J Phys Chem A* 104:995–1002
- Martinez J, Toro-Labbe A (2004) *Chem Phys Lett* 392:132–138
- Duarte F, Toro-Labbe A (2011) *J Phys Chem* 115:3050–3059
- Toro-Labbe A (1999) *J Phys Chem A* 103:4398–4401
- Politzer P, Laurence PR, Jayasuriya K (1985) *Environ Health Perspect* 61:191–202
- Sjoberg P, Murray JS, Brinck T, Politzer P (1990) *Can J Chem* 68: 1440–1446
- Murray JS, Brinck T, Grice ME, Politzer P (1992) *J Mol Struct - Theochem* 256:29–45
- Chen H, Parkinson JA, Parsons S, Coxal RA, Gould RO, Sadler P (2002) *J Am Chem Soc* 124:3064–3082
- Morris RE, Aird R, Murdoch PD, Chen H, Cummings J, Hughes ND, Parson S, Parkin A, Boyd G, Sadler P, Jodrell D (2001) *J Med Chem* 44:3616–3621
- Allardyce CS, Dyson PJ, Ellis DJ, Heath SL (2001) *Chem Commun* 1396–1402
- Allardyce CS, Dyson PJ, Ellis DJ, Salter PA, Scopelliti R (2003) *J Organomet Chem* 668:35–42
- Chval Z, Futera Z, Burda JV (2011) *J Chem Phys* 134:024520
- Chai J-D, Head-Gordon M (2008) *Phys Chem Chem Phys* 10:6615–6620
- Futera Z, Klenko J, Šponer JE, Šponer J, Burda JV (2009) *J Comput Chem* 30:1758–1770
- Burda JV, Zeizinger M, Šponer J, Leszczynski J (2000) *J Chem Phys* 113:2224–2232
- Chval Z, Sip M, Burda JV (2008) *J Comput Chem* 29:2370–2381
- Bader RFW, Carroll MT, Cheeseman JR, Chang C (1987) *J Am Chem Soc* 109:7968
- Bradáč O, Zimmermann T, Burda JV (2013) *J Mol Model* doi:10. 1007/s00894-012-1442-z

Pt⋯H Nonclassical Interaction in Water-Dissolved Pt(II) Complexes: Coaction of Electronic Effects with Solvent-Assisted Stabilization

Ondřej Kroutil,^{†,‡} Milan Předota,[‡] and Zdeněk Chval^{*,†}[†]Institute of Laboratory Diagnostics and Public Health, Faculty of Health and Social Studies, University of South Bohemia, J. Boreckého 27, 37011 České Budějovice, Czech Republic[‡]Institute of Physics and Biophysics, Faculty of Science, University of South Bohemia, Branišovská 1760, 37005 České Budějovice, Czech Republic

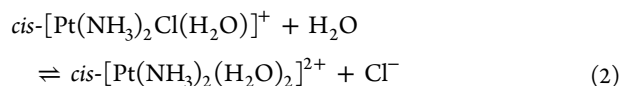
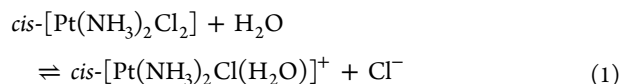
Supporting Information

ABSTRACT: The structure of the hydration shell of cisplatin, *cis*-[Pt(NH₃)₂Cl₂], and its aquated derivatives *cis*-[Pt(NH₃)₂Cl(H₂O)]⁺, *cis*-[Pt(NH₃)₂OH(H₂O)]⁺, and *cis*-[Pt(NH₃)₂(H₂O)₂]²⁺ were studied by a number of density functional molecular dynamics (DFT-MD) simulations (from 30 to 250 ps) in which Pt(II) complexes were immersed in a periodic box with 72 explicit water molecules. Furthermore, Pt(II) complex–water binding energy curves and full DFT optimizations of clusters derived from the lowest potential energy DFT-MD frames offered a deeper insight into the structure of the first hydration shell and electronic changes connected with the formation of a nonclassical Pt⋯H–O–H (Pt⋯Hw) hydrogen bond (inverse hydration). The probability of a Pt⋯Hw interaction decreases with increasing charge of the platinum complex due to disadvantageous electrostatics. The main stabilization comes from the charge transfer being followed by polarization and dispersion. Ligands form a framework for the network of H-bond interactions between the solvent molecules, which play an important role in the promotion/suppression of the formation of the Pt⋯Hw interactions. In the +2 charged diaqua complex the Pt⋯Hw interaction is still attractive but cannot compete with classical H bonds between solvent molecules. Thus, the formation of a Pt⋯Hw interaction is the result of a suitable solvent H-bonding network and the probability of its incidence decreases with increasing flexibility of the solvent.

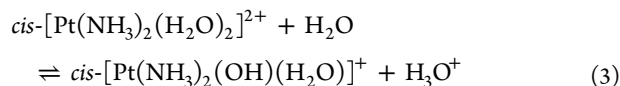


INTRODUCTION

Cisplatin and related compounds are currently the most frequently used anticancer drugs. Neutral cisplatin as a prodrug needs one or more aquation steps (reactions 1 and 2) prior to the binding to nucleic acids.



In the aquated complexes the water hydrogens are acidic and in pure water solution many possible acid–base equilibria exist. Except for the formation of inactive (with respect to DNA) neutral *cis*-[Pt(NH₃)₂(OH)₂] and *cis*-[Pt(NH₃)₂(OH)Cl] complexes, the aqua-hydroxo active complex arises.



The two possible aquation steps of cisplatin activation have been studied intensely during the past 15 years. The theoretical

studies have mostly relied on polarizable continuum models (PCM) on treatment of the solvent effects.^{2–7} Microscopic solvation structures of the points along the reaction pathway were described in Car–Parrinello molecular dynamics simulations (CPMD) using up to 50 water molecules in the periodic cubic box.^{8,9} Distribution of the explicit solvent molecules around the cisplatin complex has also been a subject of many previous studies which used molecular dynamics techniques.^{10–16} An interesting method capable of describing basic features of the solvent structure around the metal complex is the three-dimensional reference interaction site model self-consistent field (3D-RISM-SCF) method.¹⁷

Both aquation reactions (eqs 1 and 2) proceed by the associative interchange mechanism^{18,19} via pentacoordinated transition states,² but the direction of the attack of the entering water molecule is still a matter of debate. According to the study of Melchior et al.,²⁰ in which cisplatin was hydrated by 15 explicit water molecules, the “reactive” water molecule should be hydrogen-bonded to the leaving chloride but the reaction model still relied on a static description of the reaction. Therefore, a detailed understanding of the interactions of

Received: October 5, 2015

Published: March 14, 2016

cisplatin and its aquated derivatives with water solvent molecules and their dynamic behavior are of primary importance.

In addition to the articles cited above, the structure of the hydration shell of the square-planar Pt(II) complexes has been a subject of many previous studies and included a whole range of systems, from strongly negative complexes such as $[\text{PtCl}_4]^{2-}$ to strongly positive ones such as $[\text{Pt}(\text{H}_2\text{O})_4]^{2+}$.^{21–25}

While the hydration of ligands seems to be well understood and comes from their H-bond donor/acceptor abilities, the structure and existence of the so-called “meso-shell”²¹ are still a matter of debate. The meso-shell is represented by the water molecules which interact directly with the platinum center and may include Pt···H–O–H (Pt···Hw) “inverse hydration” interactions. While recent quantum mechanical calculations^{26–28} together with NMR¹² and neutron diffraction experiments^{29,30} supported this phenomenon, classical molecular dynamics simulations provided inconsistent results even when elaborate force fields were used.^{15,31}

Inverse hydration was observed also in e.g. Pd(II) square-planar complexes.^{22,25,32,33}

Generally, a Pt···H–X H-bond interaction (X = nonmetal) is the result of favorable dispersion^{27,30,34} and/or orbital³⁵ energies, while electrostatic attraction is very weak.²⁷ For neutral systems this kind of interaction was also proved in solid-state experiments^{29,30,36,37} as well as observed in theoretical studies.^{12,13,24,26,27,35,38}

On the other hand, for a highly charged +2 complex this interaction has been observed only theoretically for the $[\text{Pt}(\text{H}_2\text{O})_4]^{2+}$ complex.^{22,25} Very recently, a comprehensive review of agostic and hydrogen-bonding M···H interactions (M = d⁸ metal center) was given by Kozelka.³⁹

Truflandier et al.¹² also studied dynamic properties connected with the Pt···Hw interaction in hydrated cisplatin, and they found that the distribution of N–Pt···Hw was asymmetric with a significant probability of angles above 110°. This asymmetry was correlated to transient departures of the axial water molecule from the meso-shell to the first solvation shell, with the conclusion that inverse hydration is solvent-assisted.

Our goal was to show how the Pt···Hw interaction and the solvation shell structure of the Pt(II) complexes are affected by the increasing positive charge of the complex and the change in chemical composition during the platinum hydrolysis. We studied the structure and dynamics of the hydration shell of cisplatin, *cis*- $[\text{Pt}(\text{NH}_3)_2\text{Cl}_2]$ (Pt+0), and its positively charged and hydrolyzed forms *cis*- $[\text{Pt}(\text{NH}_3)_2\text{Cl}(\text{H}_2\text{O})]^+$ (Pt+1-Cl), *cis*- $[\text{Pt}(\text{NH}_3)_2(\text{OH})(\text{H}_2\text{O})]^+$ (Pt+1-OH), and *cis*- $[\text{Pt}(\text{NH}_3)_2(\text{H}_2\text{O})_2]^{2+}$ (Pt+2). Pt+0, Pt+1-Cl, and Pt+2 structures were studied by Lau and Ensing using CPMD⁹ and also in recent studies of Melchior et al.^{15,31} using classical MD simulations. Here we also included Pt+1-OH, which was shown to be the most abundant active form of the hydrolyzed cisplatin complex in solution under physiological conditions if equilibrium is reached.^{1,40}

The first part of this study is based on various DFT-MD simulations (from 30 ps up to 250 ps) with 72 explicit water molecules which describe the structure of at least the first solvation shell of the Pt(II) complexes with rigorous description of the polarization and charge-transfer effects and at the same time already offer a reasonable sampling. In the second part a small system composed of the Pt(II) complex and the interacting water molecule was studied using ab initio

and DFT methods to obtain a better insight into the nature of the Pt···Hw interaction. Furthermore, clusters of the complexes with 36 nearest-neighbor water molecules were taken from the DFT-MD frames and fully optimized. These calculations enabled us to evaluate the influence of surrounding explicit water molecules on the Pt···Hw interaction and the electronic structure of Pt(II) complexes.

The paper is organized as follows: the **Computational Methods** and **Results** are divided into two sections separately describing DFT-MD simulations and static ab initio and DFT results. The **Discussion** deals mainly with the precision of our results, the sampling, and a comparison with previous studies. Finally, the paper is summarized in **Conclusions**.

■ COMPUTATIONAL METHODS

DFT-MD. Born–Oppenheimer based ab initio MD simulations with periodic boundary conditions were carried out using a hybrid Gaussian and plane-wave method (GPW) as implemented in the CP2K software.⁴¹ A charge density cutoff of 400 Ry with NN50 smoothing has been used in all simulations in conjunction with double- ξ molecularly optimized basis functions augmented with a polarization function (DZVP)⁴² and the appropriate pseudopotentials of Goedecker, Teter, and Hutter (GTH).⁴³ All hydrogen atoms in the systems were represented by the deuterium isotope to reduce quantum effects of the hydrogen nuclei and to increase the time step up to 1 fs.

Each simulation box was composed of the Pt(II) complex and 72 water D₂O molecules (in the text deuterium and light hydrogen atoms are not distinguished and are treated simply as water hydrogen Hw atoms; water oxygen atoms are designated as Ow atoms). The box dimensions were adjusted to match a density of 1.12 g cm⁻³ (equal to 1.01 g cm⁻³ for light water), resulting in a cubic box of length ~1.36 nm (Figure S1 in the Supporting Information). The net charge of the Pt(II) complexes has been compensated by the neutralizing background charge.

A number of functionals, including PBE-D3,⁴⁴ BLYP,^{45,46} BLYP-D3, HCTH120,⁴⁷ and revPBE,⁴⁸ were tested. PBE-D3 and BLYP-D3 functionals include the empirical dispersion term for the main-group elements.⁴⁹ All simulations have been carried out in the NVT ensemble with the Nosé–Hoover thermostat (the time constant 500 fs) and temperatures of 323 K (PBE-D3) and 350 K (BLYP, BLYP-D3, HCTH120, revPBE) to avoid nonergodic behavior.⁵⁰ Lengths of trajectories ranged between 35 and 255 ps. The first 5 ps of every trajectory was considered as the equilibration phase and was not included in the analyses of the results. Structures were saved every 1 fs, analyzed using Gromacs analysis tools,⁵¹ and visualized by VMD.⁵²

Ab Initio and DFT. Pt(II) Complex–Water Systems. Restricted optimizations were performed using the MP2/MWB-60(f)/6-311++G(d,p) method. The main-group elements were described by the all-electron 6-311++G(d,p) basis set. Platinum atoms were treated using Dresden–Stuttgart quasi-relativistic energy-averaged effective pseudopotentials⁵³ with a pseudo-orbital basis set augmented by a set of diffuse ($\alpha_s = 0.0075$, $\alpha_p = 0.013$, $\alpha_d = 0.025$) and polarization ($\alpha_f = 0.98$) functions.⁵⁴ This basis set is designated as BSI in the text. Wavefunction properties and relative energies of the optimized structures were obtained by M06-2X-D3/def2-QZVPPD single-point calculations.^{53,55,56} This basis set is denoted as BSII. Binding energies included interaction energies and deformation energies of the fragments.

Reference CCSD(T)/BSIII binding energies were obtained using the formula⁵⁷ $E_{\text{int}}^{\text{CCSD(T)/BSIII}} = E_{\text{int}}^{\text{MP2/BSIII}} + E_{\text{int}}^{\text{CCSD(T)/BSI}} - E_{\text{int}}^{\text{MP2/BSI}}$, where BSIII corresponds to the def2-TZVPPD basis set, and these energies included interaction energies, deformation energies of the fragments, and counterpoise correction⁵⁸ of the basis set superposition error.

Additional single-point calculations on selected optimized structures were conducted using the Amsterdam Density Functional 2014.05 package (ADF)⁵⁹ to calculate fragment energy decompositions according to the extended transition state theory^{60,61} combined with

natural orbitals for chemical valence (ETS-NOCV).^{62–64} Gas phase interaction energies $\Delta E_{\text{INT}}^{\text{gas}}$ were decomposed into Pauli (ΔE_{Pauli}), electrostatic (ΔE_{elstat}), orbital (ΔE_{orb}), and dispersion (ΔE_{disp}) energy contributions:

$$\Delta E_{\text{INT}}^{\text{gas}} = \Delta E_{\text{Pauli}} + \Delta E_{\text{elstat}} + \Delta E_{\text{orb}} + \Delta E_{\text{disp}} \quad (4)$$

In these calculations, scalar relativistic effects were treated within the zeroth order regular approximation (ZORA).^{65,66} The M06-2X functional was used with the all-electron QZ4P (ZORA) basis set for all atoms.

Cluster Calculations. Twenty-five frames with the lowest potential energy were selected from each DFT-MD simulation for full cluster optimizations. To prevent the optimization of structurally similar clusters, the minimum time span between two selected frames was 1 ps. The clusters were represented by the structure of the complex hydrated by 36 explicit water molecules which were selected by a simple Pt–Ow distance criterion. This number roughly corresponded to the number of water molecules inside the inscribed sphere of the DFT-MD cubic box (unit cell; Figure S1 in the Supporting Information).

The clusters were optimized using the B3LYP-D3/MWB-60(f)/6-311+G** method^{67,68} being immersed in the implicit water environment described by the integral equation formalism-PCM methodology and UFF scaled radii for cavity construction.⁶⁹ Since the basis set used is the same as BSI but lacks diffuse functions on hydrogen atoms, it is designated as BSI- in the text.

The B3LYP-D3 geometries of the most stable clusters were used for the evaluation of charge transfer and polarization effects in the mixed discrete-continuum solvation model (further referred to as the cluster model) and their comparison with simpler Pt(II) complex–water systems. These calculations were performed by the B97D3/MWB-60(2fg)/6-311++G(2df,2pd) method.^{68,70} The platinum atom was augmented by a set of diffuse functions in analogy to BSI and by a set of polarization functions ($\alpha_f = 1.419$, 0.466 ; $\alpha_g = 1.208$).⁵⁴ The main-group elements were described by the 6-311++G(2df,2pd) basis set. This basis set is designated as BSIV in the text.

All static DFT-D calculations were carried out with the Gaussian 09 (G09) program package.⁷¹

RESULTS

DFT-MD. Sensitivity of Results to the Choice of DFT Functionals. For all systems studied, 30 ps runs were performed using BLYP-D3 and HCTH120. With the PBE-D3 functional, 250 ps simulations were carried out. In addition, 30 ps simulations with the BLYP and revPBE functionals were used for the most controversial Pt+2 system. The choice of a functional affects the observed structural results and the dynamics of water ranging from understructured to overstructured water. However, as detailed below, the key results are captured by all functionals studied. Values of water diffusion coefficients for all simulations are shown in Table 1 and Pt–Hw radial distribution functions (RDFs) for the Pt+2 system in Figure 1. PBE-D3 and BLYP gave overstructured water with the lowest self-diffusion coefficients and the highest probabilities of a Pt–Hw interaction. HCTH120, revPBE, and BLYP-D3 functionals resulted in understructured water showing similar

Table 1. Self-Diffusion Coefficients of Water ($D/10^{-9} \text{ m}^2 \text{ s}^{-1}$) Calculated for 30 ps (a), 60 ps (b), and 250 ps (c) Runs

	Pt+0	Pt+1-Cl	Pt+1-OH	Pt+2
PBE-D3	0.3 ± 0.1^c	0.5 ± 0.1^c	0.4 ± 0.1^c	0.2 ± 0.2^c
BLYP-D3	2.9 ± 0.3^b	2.6 ± 0.6^a	2.8 ± 0.4^a	2.8 ± 0.1^b
HCTH120	4.2 ± 0.4^b	4.2 ± 0.3^a	3.3 ± 0.4^a	4.4 ± 0.7^b
revPBE				3.5 ± 0.1^a
BLYP				0.8 ± 0.1^a

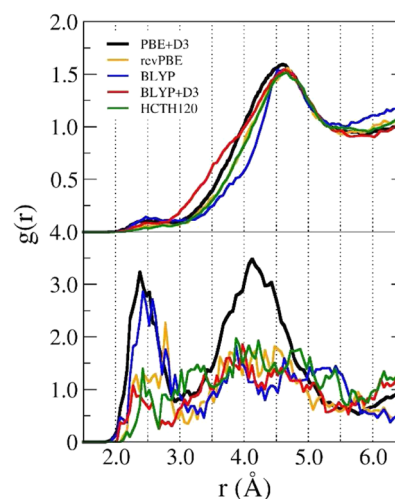


Figure 1. Total RDFs (upper panel) and angle-solved RDFs (lower panel; for the conical region 10° see Scheme 1) of Pt–Hw distances for the Pt+2 system calculated by different functionals.

probabilities of a Pt–Hw interaction. The BLYP-D3 water self-diffusion coefficient is closest to the experimental value of $2.3 \times 10^{-9} \text{ m}^2 \text{ s}^{-1}$.⁷² Simulations of Pt+0 and Pt+2 systems with the BLYP-D3 and HCTH120 functionals were prolonged to 60 ps to ensure better sampling with respect to orientation of the NH_3 ligands and the water molecules bound by inverse hydration (see below). In cases where the results from all functionals are similar, PBE-D3 results are presented, since they are most straightforwardly interpretable and were obtained from the longest runs. Results for HCTH120 and BLYP-D3 functionals are given in the Supporting Information. In other cases, results for PBE-D3, BLYP-D3, and HCTH120 functionals will be presented in the main text.

RDFs. RDFs show the distribution of water oxygen and hydrogen atoms around the Pt(II) center of the complexes (Figure 2 and Figure S2 in the Supporting Information). The size of our system enabled a good description of the first hydration shell, while the second shell is included only partially within the periodic box. Absolute maxima at ca. 4.5 and 4.0 Å

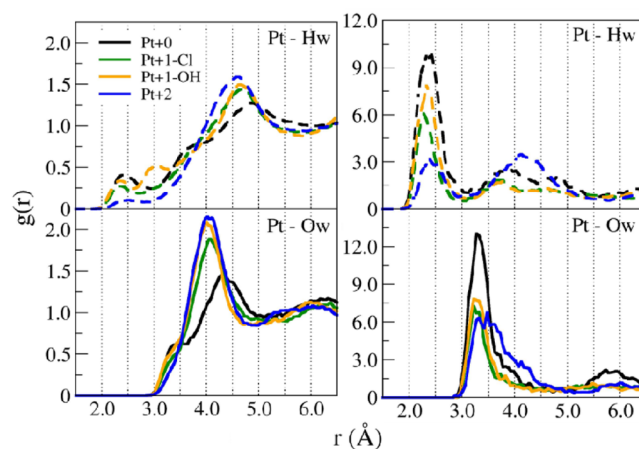


Figure 2. PBE-D3 total RDFs (left panels) and angle-solved RDFs (right panels; conical region 10° ; Scheme 1) of Pt–Ow (solid lines) and Pt–Hw (dashed lines) distances. More detailed total RDFs for Pt+1-OH resolved according to the orientation of the OH group are given in Figure 4.

for hydrogen and oxygen atoms, respectively, correspond to the water molecules from the first hydration shell of the complex. The height of the absolute maxima decreases following the sequence $\text{Pt}+2 > \text{Pt}+1\text{-OH} > \text{Pt}+1\text{-Cl} > \text{Pt}+0$, which is caused mainly by a change in the nature of the ligands. This conclusion results from the following: (1) RDFs of the specific ligands do not depend on the charge of the complex (Figure 3), (2) the

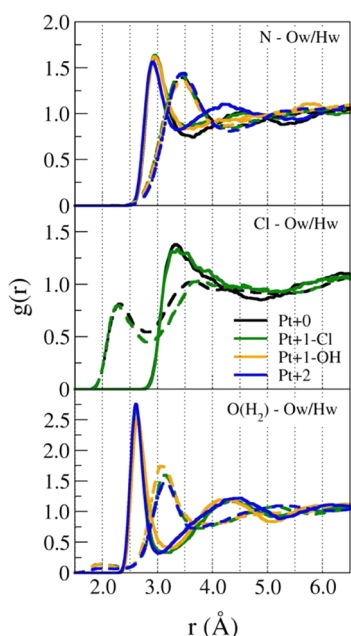


Figure 3. PBE-D3 RDFs of Ow and Hw atoms around the ligands of the Pt(II) complex (solid and dashed lines, respectively): NH_3 (top panel); Cl^- (middle panel); H_2O (bottom panel). See Figure S4 in the Supporting Information for BLYP-D3 and HCTH120 results.

chloro ligand shows the least specific and the most diffusive first hydration shell (Table 2 and Figure 3), and (3) the angle-solved RDFs which include only interactions with the central Pt(II) atom show just the opposite trend (Figure 2). Note that for the angle-solved RDFs we used the smaller value for the azimuthal angle of 10° , since for the value of 30° (Scheme 1) used in previous studies^{15,31} the influence of the ligands is already visible mainly for $\text{Pt}+2$ (Figure S3 in the Supporting Information).

The meso-shell is represented by up to two solvent molecules which may directly interact with the central Pt(II) atom, each from one side of the square-planar complex. The $\text{Pt}\cdots\text{OH}_2$ ($\text{Pt}\cdots\text{Ow}$) interaction was repulsive for neutral $[\text{Pt}(\text{NH}_3)_2(\text{OH})_2]$ at all distances in the gas phase.²⁶ We showed before that for a cisplatin–water system the structures with $\text{Pt}\cdots\text{Ow}$ interactions may correspond to true transition states between the structures with different H-bonding patterns of the weakly bound water and ligands.² Thus, water molecules should interact with the central Pt(II) atom directly only via a hydrogen atom. In our simulations the inversely bound water molecules identified themselves by small peaks observed in the $\text{Pt}\text{--}\text{Hw}$ RDFs at ca. 2.4 Å and accompanied by weak shoulders at ca. 3.3 Å in the $\text{Pt}\text{--}\text{Ow}$ RDFs (Figure 2). The Hw coordination number decreases linearly with increasing positive charge of the complex, giving the values ca. 1.1, 0.7, 0.5, and 0.2 for $\text{Pt}+0$, $\text{Pt}+1\text{-Cl}$, $\text{Pt}+1\text{-OH}$, and $\text{Pt}+2$ complexes, respectively (Table 2).

H-Bonding Network of the Solvent Molecules around the Pt(II) Complex. The inverse hydration on one side of the complex lowers the probability of inverse hydration from the other side (Table 3). For PBE-D3 and HCTH120 this effect is negligible for $\text{Pt}+2$ but significant for $\text{Pt}+0$ and $\text{Pt}+1\text{-Cl}$ and especially for $\text{Pt}+1\text{-OH}$. The minor reason might be electronic effects on the Pt(II) center caused by the first incoming water molecule (see below). More importantly, a specific rotation of the ligands with respect to each other may form a “proper” network of the H-bonded water molecules which stabilizes the inverse hydrated water molecule and increases the probability of this binding.

For PBE-D3 and HCTH120 functionals and the $\text{Pt}+1\text{-OH}$ system the probability of inverse hydration strongly depends on the orientation of the OH group being approximately 4 times more probable from the side to which the OH group is oriented than from the opposite side (Figure 4). The oxygen of the OH group is hydrated by strong H bonds with ca. two water molecules, which are represented by the peaks at 2.97 and 1.67 Å on the $\text{Pt}\text{--}\text{Hw}$ and $\text{O}(\text{H})\text{--}\text{Hw}$ PBE-D3 RDFs, respectively (Figure 4A and Figure S5 in the Supporting Information). The orientation of these strongly bound water molecules determined to a large extent the positions of the neighboring more flexible water molecules, and these did not fit well with the establishment of the $\text{Pt}\cdots\text{Hw}$ interaction. On the other hand, the orientation of water molecules which interact with the hydrogen atom of the OH group was much more suitable for inverse hydration (Figure 4B).

For the BLYP-D3 functional the above dependence of inverse hydration probability on the orientation of the OH group was almost negligible. A distribution analysis of $\text{N}\text{--}\text{Pt}\text{--}\text{O}\text{--}\text{H}$ angle values indicated that this functional gave a completely different structure of the $\text{Pt}+1\text{-OH}$ complex. While in PBE-D3 and HCTH120 simulations the OH group was preferably oriented toward the NH_3 group, for BLYP-D3 its orientation was opposite: toward the H_2O group (Figure 4C). BLYP-D3 simulations showed extremely low probabilities of inverse hydration binding from both sides of the complex for $\text{Pt}+1\text{-Cl}$ and $\text{Pt}+2$ systems (Table 3), but we have not found any reason for this.

The orientation of other ligands also had an influence on the probability of inverse hydration binding at least in overstructured water from PBE-D3 simulations. Figure 5 and Figure S6 in the Supporting Information show that the probability of inverse hydration was much lower when both NH_3 groups pointed toward the bound water by one of their H atoms (i.e., for dihedral angles -90 and $+90^\circ$). The influence of NH_3 groups was most distinctive for +1 charged complexes (especially for $\text{Pt}+1\text{-OH}$). $\text{Pt}+0$ showed the combination of dihedrals with the highest probability of binding (0.97) but the minimum probability still remained at a decent value of 0.25, while for the other complexes it reached 0.0.

Moreover, we found striking similarity in the orientation of the two NH_3 groups for all four complexes in PBE-D3 simulations (Figure S7 in the Supporting Information). In overstructured water the (mutual) orientation of ligands is strongly influenced by the solvent structure.

In understructured water (BLYP-D3 and HCTH120 simulations) we did not find any clear dependence of the probability of inverse hydration on the orientation of the two NH_3 groups.

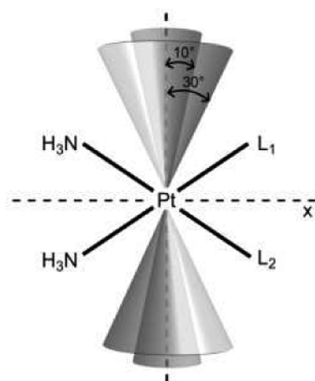
Orientation of the Inversely Bound Water Molecules. The inversely bound water molecule should not be oriented

Table 2. Positions of the First Peak of RDFs (in Å) for PBE-D3 and Corresponding Running Coordination Numbers (CN) for (a) PBE-D3, (b) BLYP-D3, and (c) HCTH120^a and (d) with Respect to the Two Semispaces Divided by the Plane of the Complex^b

	Pt–Ow					Pt–Hw				
	1st max	1st min	CN ^a	CN ^b	CN ^c	1st max	1st min	CN ^a	CN ^b	CN ^c
Pt+0	4.30	5.23	13.7	14.6	16.5	2.43	2.95	1.2	1.0	1.2
Pt+1-Cl	4.07	5.24	15.0	15.8	9.9	2.34	2.73	0.6	0.6	0.8
Pt+1-OH	4.00	4.97	13.2	14.4	11.3	2.36	2.60	0.6	0.4	0.4
Pt+2	4.06	4.90	13.2	13.7	14.5	2.52	2.91	0.3	0.2	0.1
	N–Ow					N–Hw				
	1st max	1st min	CN ^a	CN ^b	CN ^c	1st max	1st min	CN ^a	CN ^b	CN ^c
Pt+0	2.98	3.65	3.6	5.2	3.3	3.46	4.34	14.3	16.7	14.1
Pt+1-Cl	2.96	3.55	3.5	5.1	3.7	3.43	4.34	14.5	14.6	14.2
Pt+1-OH	2.96	3.55	3.5	5.3	3.2	3.46	4.34	14.4	14.2	13.9
Pt+2	2.91	3.34	2.5	4.8	3.0	3.47	4.34	14.4	17.3	14.0
	O(H ₂)–Ow					O(H ₂)–Hw				
	1st max	1st min	CN ^a	CN ^b	CN ^c	1st max	1st min	CN ^a	CN ^b	CN ^c
Pt+1-Cl	2.61	3.16	2.3	2.3	2.0	3.14	3.77	8.7	9.8	7.8
Pt+1-OH	2.64	3.23	2.6	2.4	2.1	3.09	3.88	10.9	11.3	8.5
Pt+2	2.61	3.02	2.1	2.3	2.2	3.15	3.65	7.4	9.3	7.5
	Cl–Ow					Cl–Hw				
	1st max	1st min	CN ^a	CN ^b	CN ^c	1st max	1st min	CN ^a	CN ^b	CN ^c
Pt+0	3.33	4.85	10.7	11.2	8.1	2.31	2.82	2.2	1.8	2.8
Pt+1-Cl	3.42	5.00	12.4	12.4	9.1	2.28	2.88	2.2	1.7	2.6
	O(H)–Ow					O(H)–Hw				
	1st max	1st min	CN ^a	CN ^b	CN ^c	1st max	1st min	CN ^a	CN ^b	CN ^c
Pt+1-OH (opposite) ^d	2.66	3.43	1.48	0.9	1.1	1.67	2.46	1.28	1.1	1.0
Pt+1-OH (same) ^d	2.66	3.22	1.57	1.5	1.7	1.67	2.46	0.59	1.0	1.0

^aPositions of the first peak of RDFs for BLYP-D3 and HCTH120 are presented in Table S1 in the Supporting Information. ^bThe semispaces which contains the H atom from the OH group is designated as “same” and the other as “opposite” (see text).

Scheme 1. Conical Regions Perpendicular to the Plane of the Pt(II) Complex and Defined by Azimuthal Angles 10° and 30°^a



^aThese help to define axial water molecules which interact only with the central Pt(II) atom and not with ligands.

accidentally as the part of the H-bonding network formed by solvent molecules. To analyze orientation preferences, two angles φ and ω were defined: the angle φ is formed by the dipole moment of the water molecule and the normal to the plane of the complex (denoted as z axis in Scheme 2); the angle ω is given by the projection of the dipole moment into the plane of the complex and the axis bisecting the N–Pt–N angle (x axis in Scheme 2).

Figure 6 shows the angular distribution of dipole moments of water molecules in the first coordination shell (Pt–Ow < 5 Å)

Table 3. Probabilities (in Percent) of the Occurrence of the Pt···Hw Binding from Just One Side or from Both Sides of the Pt(II) Complexes

no. of Pt–Hw contacts	functional	Pt+0	Pt+1-Cl	Pt+1-OH	Pt+2
0	PBE-D3	10.1	45.1	43.4	69.8
	BLYP-D3	27.8	49.1	71.0	80.5
	HCTH120	25.6	38.4	65.4	93.1
1	PBE-D3	56.7	50.9	55.8	28.6
	BLYP-D3	54.1	49.4	27.6	19.4
	HCTH120	43.9	52.4	34.2	6.9
2	PBE-D3	33.2	4.0	0.8	1.6
	BLYP-D3	18.2	1.5	1.4	0.1
	HCTH120	30.5	9.2	0.4	0.6

and the conical region 10° (Scheme 1) for PBE-D3 simulations. Water molecules pointing by Hw and Ow atoms toward the Pt(II) atom of the complex represent inversely bound and nonspecifically bound (see below) water molecules and can be roughly distinguished by the value of $\cos \varphi$ being negative and positive, respectively (the border value of $\cos \varphi = 0$ is marked by a dashed line in Figure 6 and Figure S8 in the Supporting Information). Figure S8 presents the angular distribution for the conical region 30°. The orientation of water molecules depends on the nature of the ligands and on the nature of their binding interactions with the complex. For the Pt+0 complexes the dipole moments of inversely bound water molecules are oriented along the $-x$ axis toward the two NH₃ ligands, while for nonspecifically bound molecules they are oriented toward

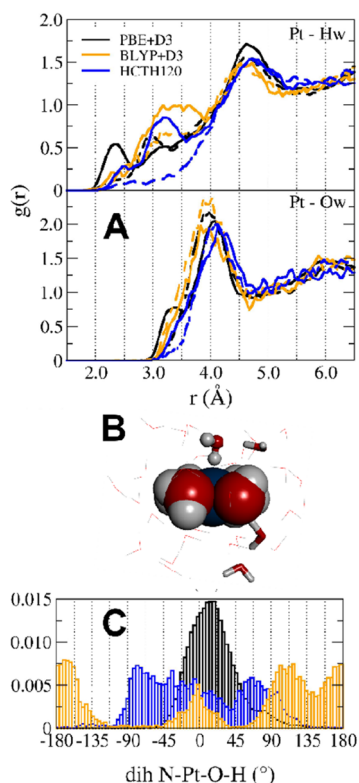


Figure 4. (A) Pt–Hw and Pt–Ow RDFs for the semispaces defined by the plane of the complex and the orientation of the OH group. RDFs for the semispace opposite to the position of the H atom from the OH group are drawn with dashed lines. RDFs for the semispace to which the H atom of the OH group is oriented are drawn with solid lines. (B) Snapshot of Pt-1-OH from a PBE-D3 simulation showing the difference in the H-bond pattern of bridge water molecules interacting with H and O atoms of the OH group (above and below the complex, respectively, highlighted by a stick model). The water molecule involved in the Pt···Hw bonding is shown by a ball-and-stick model. (C) Distribution of the values of N–Pt–O–H dihedral angles for the three functionals. The coloring is the same as in panel A. O(H)–Hw and O(H)–Ow RDFs are shown in Figure S5 in the Supporting Information.

the chloro ligands. For Pt+2 the water dipole moments of nonspecifically bound molecules point toward the two NH₃ ligands, while inversely bound molecules have only a slight preference for one of the water ligands. For Pt+1-Cl and Pt+1-OH the preferred orientation of the dipole moment of inversely bound molecules is toward Cl[−] and OH[−] ligands, respectively.

Orientation of water molecules in the first coordination shell (Pt–Ow < 5 Å) and the conical region 10° (Scheme 1) was almost the same in the BLYP-D3 simulation as in PBE-D3 (Figure S9 in the Supporting Information). HCTH120 did not show any directional preference for Pt+0. In Pt+1-Cl and Pt+1-OH the water dipole was oriented along the *x* axis away from the two NH₃ ligands (Figure S10 in the Supporting Information).

Spatial Distribution Functions (SDFs). Square-planar Pt(II) complexes are strongly anisotropic with respect to the structural arrangement of the solvent molecules, and thus, one-dimensional RDFs cannot describe all important features of the solvation shell(s).^{15,31} SDFs providing three-dimensional information about the solvation structure and the isosurfaces for all four complexes on the basis of PBE-D3 simulations are shown in Figure 7. We do not present results for BLYP-D3 and

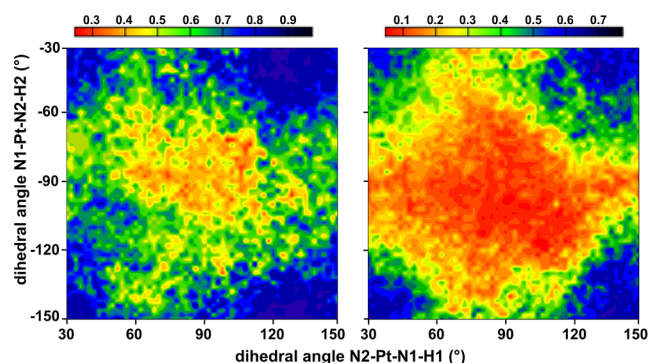
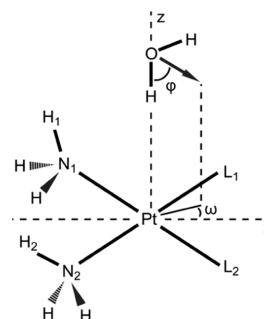


Figure 5. PBE-D3: Bivariate distribution of the normalized probability of the inverse hydration as a function of N1–Pt–N2–H2 and N2–Pt–N1–H1 dihedral angles for Pt+0 (left) and Pt+1-OH (right) (see Figure S6 in the Supporting Information for Pt+1-Cl and Pt+2). The orientation of the NH₃ groups was characterized by the positions of the H atoms which pointed toward the interacting water. The numbering of the atoms which pointed toward the interacting water corresponds to the situation in Scheme 2 (bound water “above” the complex). For water binding “below” the complex the numbering of N1/N2 and H1/H2 atoms had to be formally interchanged to obtain a pair of values for the two dihedral angles in the ranges <+30, +150> and <−150, −30>.

Scheme 2. Definition of φ and ω Angles, the Direction of the Dipole Moment of the Interacting Water Molecule, and the Numbering of Ligands and Key Atoms^a



^aFor Pt+1-OH and Pt+1-Cl complexes the L₁ ligand is water while L₂ is OH[−] and Cl[−], respectively.

HCTH120, since they are very fragmented due to the short simulation time and understructured water.

Basic features of SDFs are similar to the MD results of Melchior et al.^{15,31} The preferred positions of water binding form lobelike structures in the intersections of the range of neighbor ligands. The chloride ligands have the least defined hydration structure, while the OH ligand shows the tightest contacts with the solvent (cf. for example differences in the solvation of the NH₃, H₂O, and OH ligands in Figure 7C, left: the OH ligand is on the right down side of the complex). The inversely hydrated water molecules are represented by yellow “sandwich structures” just above and below the central Pt(II) atom.

Ab Initio and DFT. Binding Energies for the Isolated Pt(II) Complex–H₂O Systems. We performed a number of restricted MP2/BSI optimizations in which a water molecule was forced to approach the Pt(II) complex from the perpendicular direction with either a H–O bond (cf. Scheme 2) or the Ow atom oriented toward the Pt(II) atom to obtain a closer insight into Pt···Hw or Pt···Ow interactions, respectively. Binding energy curves for similar systems in the gas phase have already

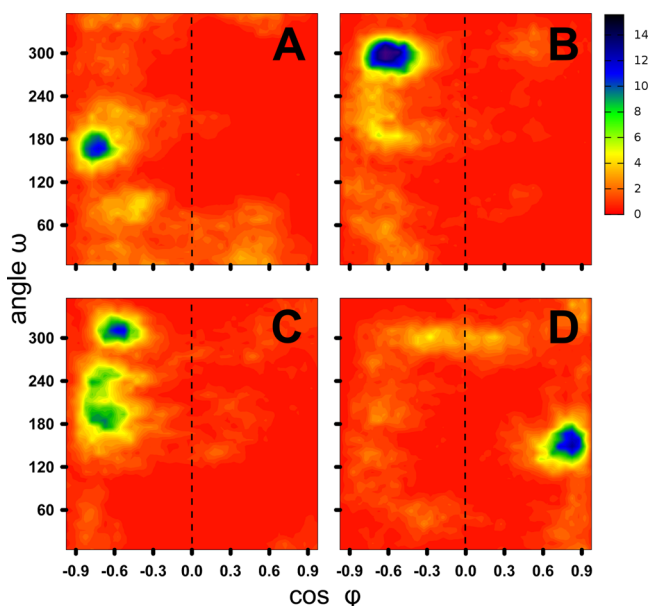


Figure 6. PBE-D3: probability density function of ω and φ angles for dipole moments (Scheme 2) of all water molecules from the first coordination shell ($\text{Pt}-\text{Ow} \lesssim 5 \text{ \AA}$) and the conical region 10° (Scheme 1) for (A) Pt+0, (B) Pt+1-Cl, (C) Pt+1-OH, and (D) Pt+2.

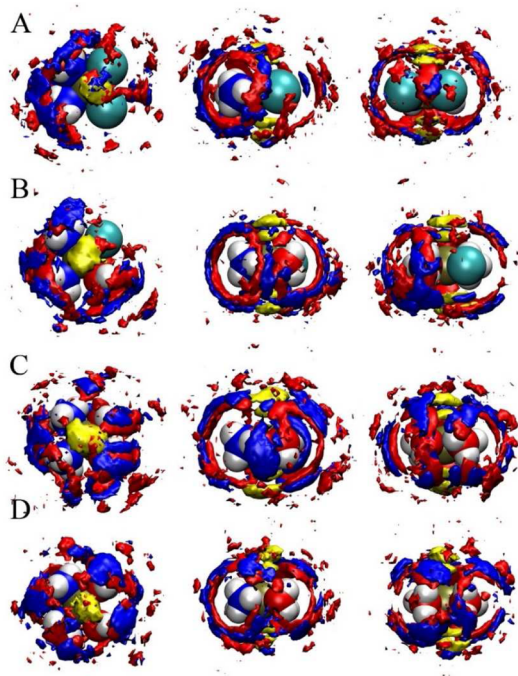


Figure 7. Top view (left) and two side views (middle and right) of SDFs of the Pt(II) complexes: (A) Pt+0; (B) Pt+1-Cl; (C) Pt+1-OH; (D) Pt+2. The isosurfaces for oxygen (red) and hydrogen (blue) atoms correspond to 2.5 times greater probability in comparison to pure solvent density (cf. refs 15 and 31). The inversely bound water molecules are shown in yellow.

been studied, and for Pt+0 a binding energy of ~ -6 kcal/mol (Figure 8) agrees with published data.^{12,26,27,73} Further in the text we will focus in more detail mainly on Pt \cdots Hw interaction energies of the Pt+2 complex since, in agreement with previous evidence,^{25,26} they were positive for all interatomic distances in the gas phase and the basic features of the binding energy curve

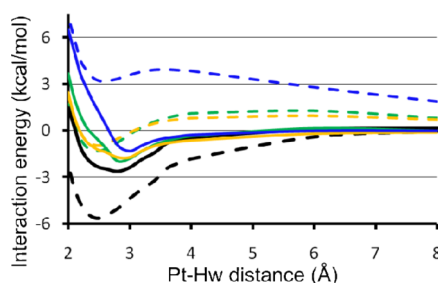


Figure 8. Pt \cdots Hw binding energies calculated on the M06-2X-D3/BSII/MP2/BSI level for the systems of one water molecule and Pt+0 (black), Pt+1-Cl (green), Pt+1-OH (ocher), and Pt+2 (blue) complexes in the gas phase (dashed lines) and in the PCM water solvent (solid lines).

are also valid for +1 charged complexes but are less distinctive (Figure 8).

At first, we tested the performance of different DFT functionals in combination with the BSII basis set. With the exception of PBE all dispersion-uncorrected DFT functionals underestimated the strength of the Pt \cdots Hw interaction in the gas phase in comparison to CCSD(T) (Table S2 in the Supporting Information). On the other hand, dispersion-corrected functionals tend to overbind the Pt \cdots Hw interaction. The best agreement with CCSD(T) results was obtained with the M06-2X-D3 functional, which we used for the calculation of P \cdots Hw binding energy curves for the other systems. The TPSS functional was used for ETS-NOCV analyses. In ETS-NOCV analyses the dispersion energy calculated by the TPSS-D3 functional will be also shown for a comparison but not included in total binding energies.

We also tested the performance of DFT in combination with GTH pseudopotentials and the GPW method as implemented in the CP2K program. With the exception of revPBE all functionals overestimated the strength of the Pt \cdots Hw interaction (Table S3 in the Supporting Information).

The Pt \cdots Hw gas phase binding energy curve for Pt+2 has a nontrivial course (Figure 8): after overcoming a local maximum at ca. 3.6 Å, the further shortening of Pt–Hw distance leads to a stabilization with a local minimum at ~ 2.6 Å. ETS energy decomposition analysis showed that it was caused by ΔE_{elstat} which reached a maximum at ca. 3.3 Å (Figure 9B) and then decreased to less positive values mainly due to reorganization of the electron density, whose contribution can be quantified by ΔE_{orb} . ETS-NOCV analysis enables decomposition of ΔE_{orb} into contributions which correspond to different electron-transfer channels. In our case the two dominating channels are (1) the charge transfer from the d_z^2 orbital of the Pt(II) atom and the p orbital of the Ow atom ($\Delta E_{\text{orb}}^{\text{CT}}$) and (2) internal polarization of the two interacting species ($\Delta E_{\text{orb}}^{\text{IP}}$) (Figure 9C). The major stabilization comes from $\Delta E_{\text{orb}}^{\text{CT}}$, accounting for 60–70% of ΔE_{orb} (Figure 9B), while $\Delta E_{\text{orb}}^{\text{IP}}$ contributes by about 20%. Thus, the Pt \cdots Hw interaction is stabilized mainly by ΔE_{orb} (cf. ref 35) but dispersion is also very important, since it contributes 1.9–2.7 kcal/mol depending on the DFT functional. At a Pt \cdots Hw distance of ~ 3 Å or longer the importance of dispersion is comparable with ΔE_{orb} or even slightly higher. In any event, in the gas phase the Pt \cdots Ow interaction is strongly preferred over Pt \cdots Hw by about 13 kcal/mol and the reason lies purely in electrostatics (Figure S11 in the Supporting Information).

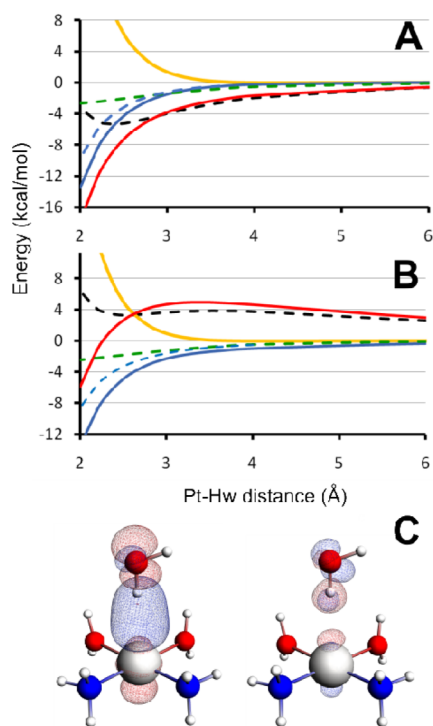


Figure 9. Energy decomposition analysis of the Pt...Hw interaction of Pt+0 (A) and Pt+2 (B) in the gas phase: ΔE_{elstat} red; ΔE_{paulij} ochre; ΔE_{orb} blue; ΔE_{disp} green; ΔE_{INT}^{RAS} black dashed line; ΔE_{orb}^{CT} blue dashed line. (C) Contours of the two most important deformation density contributions describing Pt...Hw interactions: ΔE_{orb}^{CT} (left) and ΔE_{orb}^{IP} (right). The contour values are ± 0.0005 au. The blue/red contours correspond to accumulation/depletion of electron density.

ETS-NOCV analysis of Pt+0 shows similar values of all contributions in comparison to Pt+2, except for ΔE_{elstat} which is negative for all distances and is responsible for the large difference of ~ 8.6 kcal/mol in the stabilization of the Pt...Hw interaction. An advantageous ΔE_{elstat} also enables a higher proportion of ΔE_{orb}^{CT} in comparison to ΔE_{orb}^{IP} (Figure 9A).

In an implicit water environment the ETS-NOCV analysis cannot be performed and, thus, we rely on relative changes of the NBO charges when discussing the relative importance of charge transfer and polarization effects (Figure 10). ΔE_{elstat} is essentially eliminated in a water environment, which enables (analogously to the Pt+2 vs Pt+0 comparison above) much higher electron transfer toward the water molecule and therefore smaller polarization of fragments is needed (Figure 10). As a result, Pt...Hw binding energies are negative with a minimum of -1.3 kcal/mol at ca. 3.0 Å on the M06-2X/BSII//MP2/BSI level (Figure 8) and the Pt...Hw interaction is more advantageous than Pt...Ow by ca. 0.7 kcal/mol even for Pt+2 (Figure S11 in the Supporting Information).

Similar trends, but to a smaller extent, can be observed also for Pt...Hw interactions of the other complexes with the water molecule. The lower the charge of the complex, the lower the relative importance of internal polarization and the higher the charge transfer from the platinum to the water molecule (Figure 10). These differences almost diminish in the water environment, but electrostatics still plays some role, stabilizing more strongly Pt...Hw interactions of Pt+0, Pt+1-Cl, and Pt+1-OH complexes by 1.3, 0.7, and 0.5 kcal/mol, respectively, in comparison to Pt+2 (Figure 8). For Pt+0 the stabilization was 2.6 kcal/mol, which is in fair agreement with the study of

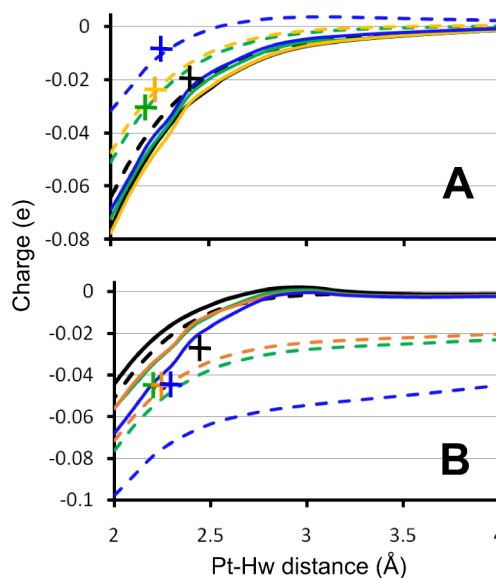


Figure 10. (A) Charge transfer from the Pt(II) complex to the inversely bound water molecule. (B) Polarization of the water molecule (estimated by the difference of the NBO charges of the interacting and noninteracting hydrogen atoms within the water molecule) obtained for the Pt...Hw interaction. Legend: Pt+0 (black), Pt+1-Cl (green), Pt+1-OH (ocher), and Pt+2 (blue) complexes in the gas phase (dashed line) and in the PCM water solvent (solid line). The values derived from the most stable structures obtained from cluster calculations (see below) are shown by crosses for a comparison.

Bergès et al.,²⁷ where stabilization by -4 kcal/mol was found for neutral Pt(II) complexes. More importantly, in vacuo differences between the studied complexes diminished in the continuum solvent model, which was explained by different electrostatics.²⁷ The amount of the charge transfer is slightly lower for Pt+0 in comparison to the average value of $-0.04e$ in the cited study, but this may reflect the difference in the charge assignment scheme (QTAIM vs NBO). Li et al.⁷⁴ calculated a 1 order of magnitude lower charge transfer (~ 0.002 – $0.003e$) in the crystallographic geometries³⁰ of the *trans*-[PtCl₂(NH₃)(N-glycine)]·H₂O complex, but this is in good agreement with our gas phase data considering a Pt–Hw distance of ca. 2.8 Å.

DFT Optimized Clusters and Effect of Environment. Twenty-five clusters composed of the Pt(II) complex and 32 nearest explicit water molecules were taken from the frames with the lowest potential energy from each DFT-MD trajectory, immersed in the implicit PCM solvent, and fully optimized using the B3LYP-D3/BSI-PCM method (the cluster model). For the Pt+2 system, the B3LYP-D3 method gives a Pt...Hw distance of 2.34 Å in the lowest energy optimized cluster. We tried also to reoptimize this structure with other functionals which overestimate the Pt...Hw interaction, B97D3 (2.250 Å), PBE0-D3 (2.294 Å), PBE (2.241 Å), PBE-D3 (2.198 Å), BLYP-D3 (2.251 Å), and TPSS-D3 (2.202 Å), or which underestimate the Pt...Hw interaction, B3LYP (2.61 Å), B3PW91 (2.367 Å), PBE0 (2.374 Å), PBEh1PBE (2.373 Å), tHCTH (2.287 Å), BLYP (2.393 Å), BHandHLYP (2.673 Å), LC-wPBE (2.500 Å), and TPSSh (2.315 Å). Optimizations of this structure with M06-2X and M06-2X-D3 functionals lead to disruption of the Pt...Hw interaction. We were able to optimize other +2 charged clusters with these functionals, but optimizations always led to very long Pt...Hw distances (>2.8 Å). There is no clear relationship between the binding energy and the interatomic

Table 4. Mean NBO Charges of the Pt(II) Atom and Ligands Calculated for the Isolated Complex in the Gas Phase, in the Continuum Solvent (PCM), and in the Cluster Model (Cluster)^a

	Pt+0			Pt+1-Cl			Pt+1-OH			Pt+2		
	gas	PCM	cluster	gas	PCM	cluster	gas	PCM	cluster	gas	PCM	cluster
Pt	0.460	0.503	0.470	0.569	0.636	0.586	0.674	0.709	0.681	0.710	0.768	0.682
NH ₃	0.261	0.335	0.321	0.316	0.357	0.332	0.304	0.338	0.322	0.407	0.394	0.340
Cl/OH	-0.491	-0.587	-0.575	-0.415	-0.567	-0.546	-0.483	-0.585	-0.558			
H ₂ O				0.215	0.215	0.138	0.201	0.201	0.126	0.238	0.222	0.132

^aAll calculations were performed for geometries in the most stable optimized clusters.

distances in clusters, but a rough correlation ($R^2 = 0.674$) between these distances and differences between Pt–Hw and water–water binding energies could be found. The B3LYP-D3 functional overestimates both water–water and Pt···Hw interactions by 0.7 and 1.4 kcal/mol, respectively (with the BSI basis set). Thus, for cluster calculations the charge transfer and polarization effects may be overestimated in absolute values but the trends should be correct.

The lowest energy structures of the four systems were analyzed by NBO and QTAIM methods (using B97D3/BSIV wavefunction). All of these four lowest energy structures had one inversely bound water molecule. However, among all the selected frames (100 in total) none showed two inversely bound water molecules. Thus, the hydration pattern of the central Pt(II) atom was not symmetrical with respect to the plane of the complex, showing a Pt···Hw interaction from one side while forming the cage of noninteracting or weakly interacting water molecules on the other side. AIM analysis showed a bond critical point for the Pt···Ow interaction only for the Pt+2 cluster. The Pt–Ow distance was 3.63 Å (electron density at BCP 0.005), which roughly corresponded to a minimum of the binding energy curve in Figure S11 in the Supporting Information. Thus, Pt···Ow interactions are energetically feasible for Pt+2 but are too weak in comparison to standard H bonding and the Ow atom still kept two H-bond interactions with neighboring water molecules. These interactions are probably common, since water molecules in the cage around the Pt(II) atom modified only slightly their H-bond network to enable some additional stabilization by weak Pt···Ow interactions.

We studied also the charge distribution in the Pt(II) complexes when changing the surrounding environment to higher complexity: i.e., isolated complexes either in the gas phase or in the implicit solvent represented by the PCM model and the cluster model. In comparison to the gas phase, dipole moments of the complexes and the positive charge on the central Pt(II) atom increase upon implicit PCM solvation, mainly due to reduced charge transfer from the chloro and hydroxo ligands (Table 4).

The charge transfer between the complex and the water molecules can be estimated from the differences in the atomic charges between the explicitly solvated complexes in clusters and implicitly solvated isolated complexes. The charge flow between the complex and the solvent depended on the charge of the complex and varied between -0.037 for neutral Pt+0 and 0.373 for Pt+2. The charge of the solvent molecules mostly depended on the specific H-bond contacts of the given molecule. Water molecules interacting with hydroxyl ligands were negatively charged ($-0.007e$ as H-bond donors and $-0.037e$ as an H-bond acceptor), while those with H-bond contacts to the H₂O ligand had the highest positive charge (between $0.016e$ and $0.020e$). Charge transfer from the chloro

and amino ligands was very small, and the interacting solvent molecules showed absolute charges lower than $0.01e$. Note that the charge is transferred also along the H-bond contacts of water molecules themselves, and thus, the charge of the specific water molecule depends on the number of H-bonds involved as the H-bond donor and acceptor. All interacting water molecules discussed above were involved in two H-bond donor and two H-bond acceptor bonds. Similarly saturated water molecules in the “bulk” (i.e., with four water molecule neighbors) had absolute charges lower than $0.01e$. On the other hand, water molecules with just two H-bond donor or just two H-bond acceptor bonds (molecules on the border of the cluster) had charges of at least $-0.038e$ or $+0.048e$, respectively. The inversely bound water molecules remained negatively charged (even for Pt+2) but to a smaller extent than if all other water molecules were modeled by implicit solvent (Figure 10). This was probably caused by a charge transfer to neighboring “bulk” water molecules. On the other hand, the inversely bound water molecules were more polarized in explicit solvent in comparison to implicit PCM solvent, and we may hypothesize that $\Delta E_{\text{orb}}^{\text{CT}}$ and $\Delta E_{\text{orb}}^{\text{IP}}$ complement each other to give ΔE_{orb} , which should be almost independent of the environment.

DISCUSSION

Comparison with Previous MD Studies. A comparison of RDFs for Pt+0 (cisplatin) with those of previous studies^{9,11,12,14,15,17} is given in Figure S12 in the Supporting Information. Positions of the absolute maxima and the general shape of the total RDF curves are mostly similar, but a few important differences can be found. (1) Classical MD simulations seem to have problems with correct description of the Cl···Hw H-bonding. The problem is probably in the orientation of interacting water molecules and the description of the directionality of the H bond, since all Cl–Ow RDFs are in good mutual agreement. (2) Pt···Hw bonding was observed only in the PBE-MD study of Truflandier et al.¹² In comparison to our results it showed exactly the same value of the Pt–Hw coordination number (1.2) but slightly longer Pt···Hw bond lengths. The position of the global Pt–Ow maxima was also shifted to a larger value in comparison to our study (Figure S12).

For Pt+2 the first maxima on the Pt–Hw RDF is in excellent agreement with a Car–Parrinello simulation using the PBE functional for the similar complex $[\text{Pt}(\text{H}_2\text{O})_4]^{2+}$ (2.52 Å vs 2.55 Å).²⁵ The other DFT-MD simulations as well as methods based on the electrostatic potential failed in a description of the inverse hydration.^{9,14,17} The latter methods are not able to predict Pt···Hw interactions if they reproduce exactly just electrostatic energy. The fact that some previous DFT-MD simulations⁹ did not reveal the existence of Pt···Hw interactions

may be a result of the combination of smaller box size, presence of counterions, the basis set, DFT functional, and short simulation time. Our results suggest that the Pt...Hw interaction is attractive even in the highly charged +2 complex on dissolution in a highly polar solvent such as water, although its strength cannot compete with classical H-bond interactions between two water molecules. The presence of counterions needs a larger simulation box size, since Pt–Hw is the weakest interaction in the system and close counterions affect the structure of the hydration shell around the Pt+2 complex. Lau and Ensing⁹ observed inverse hydration for Pt+0 and Pt+1-Cl complexes but not for Pt+2. We may hypothesize that a simulation box with ~50 water molecules, Pt+2 complex, and two Cl⁻ ions⁹ was too small for the detection of a Pt...Hw interaction. However, due to the low incidence and low stabilization effect of Pt...Hw in highly charged systems it could have only a negligible effect on the energetics of cisplatin hydrolysis studied in the cited report.

Neither our results nor previous theoretical studies^{9,22,23} confirmed the existence of one or two axial Pt–O bonds with distances of ~2.4 Å as suggested in experimental EXAFS⁷⁵ and vibrational spectroscopic⁶ studies for +2 charged Pt(II) complexes. These short bonds are highly improbable, since the Pt–Ow binding energy curve has a minimum at much greater Pt–O distance in both the gas phase and the solvent (Figure S11 in the Supporting Information). Moreover, such a close contact would probably require the disruption (at least partial) of both H bonds in which the axial water molecule acts as the H-bond acceptor. Instead, we propose just a slight deformation of the H-bond water network to enable a weak stabilization of Pt+2 by Pt...Ow interaction(s) at a Pt–Ow distance of ~3.5 Å. This distance roughly corresponds to the minima on the Pt–Ow binding energy curves (Figure S11) and to the position of the first maxima on the Pt–Ow angle-solved RDFs (Figure 2 and Figure S2 in the Supporting Information).

A comparison of our results with recent classical MD simulations of Melchior et al. for Pt+0, Pt+1-Cl, and Pt+2 complexes^{15,31} is shown in Figure S13 in the Supporting Information. Pt–Ow RDF absolute maxima are milder and are shifted toward longer distances in our DFT-MD simulations in comparison to classical MD. Opposite trends can be seen for Pt–Hw RDFs (Table 2 and Figure S13). For Pt–Ow RDFs the differences in the height and the position of the absolute maxima are increasing and decreasing, respectively, with the increasing charge of the complex. Thus, considering the water position as the result of a balance between the strengths of Pt...Ow and Pt...Hw interactions the classical MD seems to overestimate a relative strength of the Pt...Ow interaction in comparison to DFT-MD. The classical force fields are probably not able to cover all aspects of diverse systems, which consist of very distinct parts such as a transient metal Pt(II) center, H-bond donating NH₃ and H₂O ligands, and Cl⁻ ligands as weak H-bond acceptors. We may hypothesize that sometimes a small change in MD parameters could substantially improve agreement with our data. For example, neither Melchior's nor Lopes' force field was able to prove the existence of inverse hydration.^{10,15} However, the Lopes force field showed a shoulder in the Pt...Hw RDF and according to the Melchior force field some water molecules were in parallel orientation with respect to the plane of the complex. Thus, similarly to a Cl...H(w) interaction (see above), there seemed to be a problem with the orientation of the interacting water molecule and the description of the directionality of the Pt...Hw

interaction. Due to charge transfer and internal polarization the use of a polarizable force field is highly advisable. Considering the flexibility of the Pt(II) complex not only during simulation but also during parametrization of the force field may also improve the results in some applications.⁷⁷

Structure Sampling in DFT-MD. Basic structural parameters of DFT-MD runs are summarized in Table S4 in the Supporting Information, offering a reasonable agreement with previous calculations and experimental structures.^{2,4,54,78} Since all studied complexes are planar, the sampling of Pt–Ow and Pt–Hw distances can be checked by the comparison of RDFs taken separately for two semispaces designated arbitrarily as “up” and “down” with respect to the plane of the complex. Figure S14 in the Supporting Information shows that the PBE-D3 DFT-MD runs for Pt+0, Pt+1-Cl, and Pt+2 complexes are well sampled with respect to distances. BLYP-D3 and HCTH120 runs are much shorter, but we obtained similar results due to the much larger flexibility of these systems. In the case of Pt+1-OH, the limiting factor is the rotation of the OH group, since hydration of the complex is strongly dependent on the orientation of this group (as discussed above). For PBE-D3 the simulation time of 250 ps is still too short to reach an even distribution of the N–Pt–O–H dihedral angles with respect to the two semispaces. The other two functionals seem to work much better (cf. distributions in Figure 4C). The RDFs for Pt+1-OH which already took into account the orientation of the OH group (Figure 4A and Figure S5 in the Supporting Information) should not be affected.

To check an angular sampling, the C_{2v} symmetry of Pt+0 and Pt+2 complexes can be used. For these two systems the angular distributions of water dipole moments (Figure 6A,D) should be symmetric with respect to the angle ω value of 180°. One can see that this is not perfectly true, especially for Pt+2, showing still a limited sampling of our 250 ps DFT-MD run. Still, the presented angular distributions and SDFs provide useful information about the structure of the first hydration shell and cover the most important features of the interactions between the Pt(II) complex and water.

What We Have Learned from Our Calculations. A Pt...Hw interaction has a binding energy comparable with that of classical H bonds (ca. 5 kcal/mol) only for the neutral Pt+0 complex. For charged complexes the strength of the Pt...Hw interaction is much weaker (~1–2 kcal/mol). This may explain why probabilities of a Pt...Hw interaction for Pt+2 do not correlate either with binding energies calculated for different functionals (cf. Figure 1 with Tables S2 and S3 in the Supporting Information) or with any relationship which also includes water–water binding energies. An exact performance of the method with respect to binding energies between the Pt(II) complex and water seems to be not as important, since these are much lower than water–water binding energies in any event. For example, BLYP-D3 offers much stronger stabilization in comparison to BLYP (by 2.9 kcal/mol in the gas phase, 1.8 kcal/mol in PCM, and even 3.4 kcal/mol when GPW is used) but, surprisingly, a BLYP simulation shows a much higher probability of a Pt...Hw interaction for the Pt+2 system. According to our results the key parameter is flexibility of the water solvent, which can be quantified by a water self-diffusion coefficient (cf. Figure 1 and Table 1). Note that calculated values of water self-diffusion coefficients in Table 1 should be considered as indicative due to short trajectories, a low number of water molecules, and the presence of the Pt(II) complex in the system (although the calculated values are almost

independent of the nature of the ligands). Overstructured water is represented by PBE-D3 and BLYP functionals, and these simulations give a substantially higher incidence of a Pt...Hw interaction (Figure 1, lower panel) than the other three functionals (BLYP-D3, revPBE, and HCTH120) which represent understructured water. In our opinion in overstructured water the solvent molecules are more saturated with respect to the maximum number of H bonds. A water molecule for which the H-bond acceptor is missing accidentally settles for the Pt(II) atom to gain at least some small stabilization. In understructured water there is a larger probability that the missing H bond will be reestablished with another water molecule. In any case, the Pt...Hw interaction seems to have only a negligible influence on the structure of the solvent hydration shell around the charged complexes. The role of solvent flexibility seems to decrease with a decreasing charge of the complex (cf. Pt...Hw CN values in Table 2).

For cluster optimizations using static DFT we have only very limited experience with just one structure. The results may depend on the difference between water–water and Pt–Hw binding energies.

CONCLUSIONS

Our trajectories agree in basic features with previous DFT-MD simulations^{9,12} but provide extended information with respect to the number of complexes studied, the number of methods used, and the trajectory lengths. Nonclassical Pt...Hw interaction (inverse hydration) occurred in all systems studied, even for Pt+2. In the charged systems electrostatics has an unstabilizing effect, since the water dipole was oriented unfavorably with respect to the positively charged Pt(II) atom. However, orbital interactions stabilize inversely bound water molecules due to charge transfer and internal polarization of the fragments. Dispersion also contributes to the stability of the Pt...Hw interaction, but its inclusion by dispersion corrections to DFT functionals may lead to the overestimation of the strength of the Pt...Hw interaction.

The inversely bound water molecule takes part in the H-bond network comprised of all solvent molecules and the ligands of the complex. This was proven by two facts: (1) a specific orientation of the ligands suppresses/promotes the formation of the Pt...Hw bond and (2) the interacting water molecules have specific orientation with respect to the Pt(II) complex.

Our results show that for neutral and +1 charged complexes the most probable hydration pattern of the central Pt(II) atom is not symmetrical with respect to the plane of the complex showing a Pt...Hw interaction from one side while forming a cage of noninteracting water molecules on the other side. For +2 charged complexes the H-bond network of water molecules can be slightly deformed to enable a weak stabilization by a Pt...Ow interaction but the probability of Pt...Hw is still appreciable and this interaction is energetically feasible. However, for the charged complexes the Pt...Hw interaction cannot compete with classical H bonds between solvent molecules and, thus, the presence of a Pt...Hw interaction is the result of a suitable solvent structure but not vice versa: i.e., Pt...Hw is not an interaction whose formation is decisive for the solvent structure around a charged Pt(II) complex.

ASSOCIATED CONTENT

Supporting Information

The Supporting Information is available free of charge on the ACS Publications website at DOI: 10.1021/acs.inorgchem.5b02261.

Simulation box with the complex and water molecules, total and angle-resolved RDFs and RDF parameters for BLYP-D3 and HCTH120 functionals, PBE-D3 angle-resolved Pt–Ow and Pt–Hw RDFs for the axial region defined by the azimuthal angle $0^\circ < \theta < 30^\circ$, RDFs of Ow and Hw atoms around the ligands of the Pt(II) complex calculated by BLYP-D3 and HCTH120 functionals, O(H)–Hw and O(H)–Ow RDFs for the semispaces defined by the plane of the Pt+1–OH complex and the orientation of the OH group, bivariate distribution of the normalized probability of the inverse hydration as a function of N1–Pt–N2–H2 and N2–Pt–N1–H1 dihedral angles for Pt+1–Cl and Pt+2, bivariate distribution of the normalized occurrence of N1–Pt–N2–H2 and N2–Pt–N1–H1 dihedral angles for all complexes, probability density function of ω and φ angles for water molecules in the spatial region defined by the azimuthal angle $0^\circ < \theta < 30^\circ$ for PBE-D3 and the azimuthal angle $0^\circ < \theta < 10^\circ$ for BLYP-D3 and HCTH120, binding energy curves for Pt+2, comparison of RDFs with those of previous studies, comparison of RDFs for two subspaces “down” and “up” separated by the plane of the complex, geometrical parameters of the complexes, and Cartesian coordinates of the lowest energy clusters optimized by B3LYP-D3/BSI/PCM (PDF)

AUTHOR INFORMATION

Corresponding Author

*Z.C.: e-mail, chval@jcu.cz; tel, +420-389-037-612.

Notes

The authors declare no competing financial interest.

ACKNOWLEDGMENTS

This project was supported by the Czech Science Foundation: grants 208/12/0622 (O.K. and Z.C.) and 13-08651S (M.P.). Access to the MetaCentrum (grant LM2010005) and CERIT-SC (grant CZ.1.05/3.2.00/08.0144) computing and storage facilities is highly appreciated. We are very grateful to Ari Paavo Seitsonen for valuable help with the CP2K program. We are also grateful to anonymous reviewers for very valuable comments which helped us to substantially improve this contribution.

REFERENCES

- (1) Martin, R. B. In *Cisplatin: Chemistry and Biochemistry of a Leading Anticancer Drug*; Lippert, B., Ed.; Verlag Helvetica Chimica Acta: Zurich, Switzerland, 1999; pp 181–205.
- (2) Chval, Z.; Sip, M. *J. Mol. Struct.: THEOCHEM* **2000**, 532, 59–68.
- (3) Zhang, Y.; Guo, Z. J.; You, X. Z. *J. Am. Chem. Soc.* **2001**, 123, 9378–9387.
- (4) Burda, J. V.; Zeizinger, M.; Leszczynski, J. *J. Comput. Chem.* **2005**, 26, 907–914.
- (5) Burda, J. V.; Zeizinger, M.; Leszczynski, J. *J. Chem. Phys.* **2004**, 120, 1253–1262.
- (6) Costa, L. A. S.; Rocha, W. R.; De Almeida, W. B.; Dos Santos, H. F. *J. Chem. Phys.* **2003**, 118, 10584–10592.

- (7) Lau, J. K. C.; Deubel, D. V. *J. Chem. Theory Comput.* **2006**, *2*, 103–106.
- (8) Carloni, P.; Sprik, M.; Andreoni, W. *J. Phys. Chem. B* **2000**, *104*, 823–835.
- (9) Lau, J. K.-C.; Ensing, B. *Phys. Chem. Chem. Phys.* **2010**, *12*, 10348–10355.
- (10) Lopes, J. F.; Menezes, V. S. D.; Duarte, H. A.; Rocha, W. R.; De Almeida, W. B.; Dos Santos, H. F. *J. Phys. Chem. B* **2006**, *110*, 12047–12054.
- (11) Fu, C.-F.; Tian, S. X. *J. Chem. Phys.* **2010**, *132*, 174507.
- (12) Truflandier, L. A.; Sutter, K.; Autschbach, J. *Inorg. Chem.* **2011**, *50*, 1723–1732.
- (13) Sutter, K.; Truflandier, L. A.; Autschbach, J. *ChemPhysChem* **2011**, *12*, 1448–1455.
- (14) Mori, H.; Hirayama, N.; Komeiji, Y.; Mochizuki, Y. *Comput. Theor. Chem.* **2012**, *986*, 30–34.
- (15) Melchior, A.; Martínez, J. M.; Pappalardo, R. R.; Sánchez Marcos, E. *J. Chem. Theory Comput.* **2013**, *9*, 4562–4573.
- (16) Zhang, C.; Naziga, E. B.; Guidoni, L. *J. Phys. Chem. B* **2014**, *118*, 11487–11495.
- (17) Aono, S.; Sakaki, S. *J. Phys. Chem. B* **2012**, *116*, 13045–13062.
- (18) Miller, S. E.; House, D. A. *Inorg. Chim. Acta* **1989**, *161*, 131–137.
- (19) Chval, Z.; Sip, M.; Burda, J. V. *J. Comput. Chem.* **2008**, *29*, 2370–2381.
- (20) Melchior, A.; Marcos, E. S.; Pappalardo, R. R.; Martínez, J. M. *Theor. Chem. Acc.* **2011**, *128*, 627–638.
- (21) Martínez, J. M.; Torrico, F.; Pappalardo, R. R.; Sánchez Marcos, E. *J. Phys. Chem. B* **2004**, *108*, 15851–15855.
- (22) Beret, E. C.; Martínez, J. M.; Pappalardo, R. R.; Marcos, E. S.; Doltsinis, N. L.; Marx, D. *J. Chem. Theory Comput.* **2008**, *4*, 2108–2121.
- (23) Stirling, A.; Bakó, I.; Kocsis, L.; Hajba, L.; Mink, J. *Int. J. Quantum Chem.* **2009**, *109*, 2591–2598.
- (24) Truflandier, L. A.; Autschbach, J. *J. Am. Chem. Soc.* **2010**, *132*, 3472–3483.
- (25) Beret, E. C.; Pappalardo, R. R.; Doltsinis, N. L.; Marx, D.; Sánchez Marcos, E. *ChemPhysChem* **2008**, *9*, 237–240.
- (26) Berges, J.; Caillet, J.; Langlet, J.; Kozelka, J. *Chem. Phys. Lett.* **2001**, *344*, 573–577.
- (27) Bergès, J.; Fourré, I.; Pilmé, J.; Kozelka, J. *Inorg. Chem.* **2013**, *52*, 1217–1227.
- (28) Chval, Z.; Kabeláč, M.; Burda, J. V. *Inorg. Chem.* **2013**, *52*, 5801–5813.
- (29) Brammer, L.; Charnock, J. M.; Goggin, P. L.; Goodfellow, R. J.; Koetzle, T. F.; Orpen, A. G. *J. Chem. Soc., Chem. Commun.* **1987**, 443–445.
- (30) Rizzato, S.; Bergès, J.; Mason, S. A.; Albinati, A.; Kozelka, J. *Angew. Chem., Int. Ed.* **2010**, *49*, 7440–7443.
- (31) Melchior, A.; Tolazzi, M.; Martínez, J. M.; Pappalardo, R. R.; Sánchez Marcos, E. *J. Chem. Theory Comput.* **2015**, *11*, 1735–1744.
- (32) Purans, J.; Fourest, B.; Cannes, C.; Sladkov, V.; David, F.; Venault, L.; Lecomte, M. *J. Phys. Chem. B* **2005**, *109*, 11074–11082.
- (33) Hofer, T. S.; Randolf, B. R.; Adnan Ali Shah, S.; Rode, B. M.; Persson, I. *Chem. Phys. Lett.* **2007**, *445*, 193–197.
- (34) Kozelka, J.; Bergès, J.; Attias, R.; Fraitag, J. *Angew. Chem., Int. Ed.* **2000**, *39*, 198–201.
- (35) Sánchez-de-Armas, R.; Ahlquist, M. S. G. *Phys. Chem. Chem. Phys.* **2015**, *17*, 812–816.
- (36) Braga, D.; Grepioni, F.; Tedesco, E.; Biradha, K.; Desiraju, G. R. *Organometallics* **1997**, *16*, 1846–1856.
- (37) Baya, M.; Belío, Ú.; Martín, A. *Inorg. Chem.* **2014**, *53*, 189–200.
- (38) Vidossich, P.; Ortuño, M. Á.; Ujaque, G.; Lledós, A. *ChemPhysChem* **2011**, *12*, 1666–1668.
- (39) Kozelka, J. In *Noncovalent Forces, Challenges and Advances in Computational Chemistry and Physics*; Scheiner, S., Ed.; Springer International: Berlin, 2015; Vol. 19, pp 129–158.
- (40) Zimmermann, T.; Leszczynski, J.; Burda, J. V. *J. Mol. Model.* **2011**, *17*, 2385–2393.
- (41) Hutter, J.; Iannuzzi, M.; Schiffmann, F.; VandeVondele, J. *Wiley Interdiscip. Rev. Comput. Mol. Sci.* **2014**, *4*, 15–25.
- (42) VandeVondele, J.; Hutter, J. *J. Chem. Phys.* **2007**, *127*, 114105.
- (43) Goedecker, S.; Teter, M.; Hutter, J. *Phys. Rev. B: Condens. Matter Mater. Phys.* **1996**, *54*, 1703–1710.
- (44) Ahlrichs, R.; Bar, M.; Haser, M.; Horn, H.; Kolmel, C. *Chem. Phys. Lett.* **1989**, *162*, 165–169.
- (45) Becke, A. D. *Phys. Rev. A: At., Mol., Opt. Phys.* **1988**, *38*, 3098.
- (46) Lee, C.; Yang, W.; Parr, R. G. *Phys. Rev. B: Condens. Matter Mater. Phys.* **1988**, *37*, 785.
- (47) Boese, A. D.; Doltsinis, N. L.; Handy, N. C.; Sprik, M. *J. Chem. Phys.* **2000**, *112*, 1670–1678.
- (48) Zhang, Y.; Yang, W. *Phys. Rev. Lett.* **1998**, *80*, 890–890.
- (49) Grimme, S.; Antony, J.; Ehrlich, S.; Krieg, H. *J. Chem. Phys.* **2010**, *132*, 154104.
- (50) VandeVondele, J.; Mohamed, F.; Krack, M.; Hutter, J.; Sprik, M.; Parrinello, M. *J. Chem. Phys.* **2005**, *122*, 014515.
- (51) Hess, B.; Kutzner, C.; van der Spoel, D.; Lindahl, E. *J. Chem. Theory Comput.* **2008**, *4*, 435–447.
- (52) Humphrey, W.; Dalke, A.; Schulten, K. *J. Mol. Graphics* **1996**, *14*, 33–38.
- (53) Andrae, D.; Häußermann, U.; Dolg, M.; Stoll, H.; Preuß, H. *Theor. Chem. Acc. Theory Comput. Model. Theor. Chim. Acta* **1990**, *77*, 123–141.
- (54) Burda, J. V.; Zeizinger, M.; Sponer, J.; Leszczynski, J. *J. Chem. Phys.* **2000**, *113*, 2224–2232.
- (55) Zhao, Y.; Truhlar, D. G. *Theor. Chem. Acc.* **2008**, *120*, 215–241.
- (56) Schuchardt, K. L.; Didier, B. T.; Elsethagen, T.; Sun, L.; Gurumoorthi, V.; Chase, J.; Li, J.; Windus, T. L. *J. Chem. Inf. Model.* **2007**, *47*, 1045–1052.
- (57) Riley, K. E.; Pitoňák, M.; Jurečka, P.; Hobza, P. *Chem. Rev.* **2010**, *110*, 5023–5063.
- (58) Boys, S. F.; Bernardi, F. *Mol. Phys.* **1970**, *19*, 553–566.
- (59) te Velde, G.; Bickelhaupt, F. M.; Baerends, E. J.; Guerra, C. F.; Van Gisbergen, S. J. A.; Snijders, J. G.; Ziegler, T. *J. Comput. Chem.* **2001**, *22*, 931–967.
- (60) Ziegler, T.; Rauk, A. *Theor. Chim. Acta* **1977**, *46*, 1–10.
- (61) Ziegler, T.; Rauk, A. *Inorg. Chem.* **1979**, *18*, 1558–1565.
- (62) Mitoraj, M.; Michalak, A.; Ziegler, T. *J. Chem. Theory Comput.* **2009**, *5*, 962–975.
- (63) Mitoraj, M. P.; Kurczab, R.; Boczar, M.; Michalak, A. *J. Mol. Model.* **2010**, *16*, 1789–1795.
- (64) Mitoraj, M.; Michalak, A. *J. Mol. Model.* **2013**, *19*, 4681–4688.
- (65) van Lenthe, E.; Baerends, E. J.; Snijders, J. G. *J. Chem. Phys.* **1993**, *99*, 4597–4610.
- (66) van Lenthe, E.; van Leeuwen, R.; Baerends, E. J.; Snijders, J. G. *Int. J. Quantum Chem.* **1996**, *57*, 281–293.
- (67) Stephens, P. J.; Devlin, F. J.; Chabalowski, C. F.; Frisch, M. J. *J. Phys. Chem.* **1994**, *98*, 11623–11627.
- (68) Grimme, S.; Ehrlich, S.; Goerigk, L. *J. Comput. Chem.* **2011**, *32*, 1456–1465.
- (69) Tomasi, J.; Mennucci, B.; Cammi, R. *Chem. Rev.* **2005**, *105*, 2999–3094.
- (70) Grimme, S. *J. Comput. Chem.* **2006**, *27*, 1787–1799.
- (71) Frisch, M. J.; Trucks, G. W.; Schlegel, H. B.; Scuseria, G. E.; Robb, M. A.; Cheeseman, J. R.; Scalmani, G.; Barone, V.; Mennucci, B.; Petersson, G. A.; Nakatsuji, H.; Caricato, M.; Li, X.; Hratchian, H. P.; Izmaylov, A. F.; Bloino, J.; Zheng, G.; Sonnenberg, J. L.; Hada, M.; Ehara, M.; Toyota, K.; Fukuda, R.; Hasegawa, J.; Ishida, M.; Nakajima, T.; Honda, Y.; Kitao, O.; Nakai, H.; Vreven, T.; Montgomery, J. A., Jr.; Peralta, J. E.; Ogliaro, F.; Bearpark, M.; Heyd, J. J.; Brothers, E.; Kudin, K. N.; Staroverov, V. N.; Kobayashi, R.; Normand, J.; Raghavachari, K.; Rendell, A.; Burant, J. C.; Iyengar, S. S.; Tomasi, J.; Cossi, M.; Rega, N.; Millam, J. M.; Klene, M.; Knox, J. E.; Cross, J. B.; Bakken, V.; Adamo, C.; Jaramillo, J.; Gomperts, R.; Stratmann, R. E.; Yazyev, O.; Austin, A. J.; Cammi, R.; Pomelli, C.; Ochterski, J. W.; Martin, R. L.; Morokuma, K.; Zakrzewski, V. G.; Voth, G. A.; Salvador, P.; Dannenberg, J. J.; Dapprich, S.; Daniels, A. D.; Farkas, Ö;

Foresman, J. B.; Ortiz, J. V.; Cioslowski, J.; Fox, D. J. *Gaussian 09, Revision C.1*; Gaussian, Inc., Wallingford, CT, 2009.

(72) Holz, M.; Heil, S. R.; Sacco, A. *Phys. Chem. Chem. Phys.* **2000**, *2*, 4740–4742.

(73) Lopes, J. F.; Da Silva, J. C. S.; Rocha, W. R.; De Almeida, W. B.; Dos Santos, H. F. J. *J. Theor. Comput. Chem.* **2011**, *10*, 371–391.

(74) Li, Y.; Zhang, G.; Chen, D. *Mol. Phys.* **2012**, *110*, 179–184.

(75) Jalilehvand, F.; Laffin, L. J. *Inorg. Chem.* **2008**, *47*, 3248–3254.

(76) Kocsis, L.; Mink, J.; Jalilehvand, F.; Laffin, L. J.; Berkesi, O.; Hajba, L. *J. Raman Spectrosc.* **2009**, *40*, 481–490.

(77) Yesylevskyy, S.; Cardey, B.; Kraszewski, S.; Foley, S.; Enescu, M.; da Silva, A. M.; Santos, H. F. D.; Ramseyer, C. J. *Mol. Model.* **2015**, *21*, 1–9.

(78) Carloni, P.; Andreoni, W.; Hutter, J.; Curioni, A.; Giannozzi, P.; Parrinello, M. *Chem. Phys. Lett.* **1995**, *234*, 50–56.

Interactions of the “Piano-Stool” [Ruthenium(II)(η^6 -Arene)(Quinolone)Cl]⁺ Complexes with Water; DFT Computational Study

Tereza Zábajková,^[a] Radim Cajzl,^[a] Jakob Kljun,^[b] Zdeněk Chval,^[c] Iztok Turel,^[b] and Jaroslav V. Burda*^[a]

Full optimizations of stationary points along the reaction coordinate for the hydration of several quinolone Ru(II) half-sandwich complexes were performed in water environment using the B3PW91/6-31+G(d)/PCM/UAKS method. The role of diffuse functions (especially on oxygen) was found crucial for correct geometries along the reaction coordinate. Single-point (SP) calculations were performed at the B3LYP/6-311++G(2df,2pd)/DPCM/scaled-UAKS level. In the first part, two possible reaction mechanisms—associative and dissociative were compared. It was found that the dissociative mechanism of the hydration process is kinetically slightly preferred. Another important conclusion concerns the reaction channels. It was found that substitution of chloride ligand (abbreviated in the text as dechlorination reaction) represents energetically and kinetically

the most feasible pathway. In the second part the same hydration reaction was explored for reactivity comparison of the Ru(II)-complexes with several derivatives of nalidixic acid: cinoxacin, ofloxacin, and (thio)nalidixic acid. The hydration process is about four orders of magnitude faster in a basic solution compared to neutral/acidic environment with cinoxacin and nalidixic acid as the most reactive complexes in the former and latter environments, respectively. The explored hydration reaction is in all cases endergonic; nevertheless the endergonicity is substantially lower (by ~6 kcal/mol) in basic environment. © 2016 Wiley Periodicals, Inc.

DOI: 10.1002/jcc.24373

Introduction

Since cisplatin was discovered as an effective anticancer drug by Rosenberg,^[1,2] an intense exploration of other metal complexes with reduced negative side-effects was started. The main reason can be seen in the fact that cisplatin is very toxic with many undesirable properties. Moreover, it is not active for all kinds of carcinomas. Nowadays many complexes of transition metals were found to be possible antitumor agents and some of them are in clinical testing. Many experimental studies appeared on complexes of rhodium,^[3–10] titanium,^[11–15] ruthenium,^[16–26] and other metals,^[27–30] which exhibit activity against cancer cells. These publications were usually followed by calculations at the molecular level to get a deeper insight into the curing process. A lot of effort was devoted to exploration of the most common metallodrug—cisplatin and its derivatives.^[31–38] Some studies concerned the activation of platinum complexes, which plays a crucial role in the process of apoptosis,^[39–45] interactions with nucleobases, and formation of crosslinked structures^[38,46–54] or other competitive reactions, for example, with side chains of amino acids.^[55–60]

Recently, a lot of attention has been devoted to ruthenium complexes, which represent another important family of explored substances.^[61–68] There are many interesting features concerning the hypotheses and conclusions made in the experimental works mainly from the Sadler,^[18,20,27,69–73] Dyson,^[24,74] and Turel^[77,78] laboratories, which deserve a deeper examination based on molecular approaches. The [Ru(η^6 -arene)(en)Cl]⁺ as well as [Ru(η^6 -arene)(quinolone)Cl]⁺ complexes^[26]

(en = ethylenediamine, arene = benzene, p-cymen, biphenyl or derivatives of anthracene) bind to the DNA helix in the form of monofunctional adducts (at least in the first step). However, there is some evidence that consequently the arene molecule is released and bidentate coordination becomes possible.^[63,75] Also, a pronounced selectivity to guanine was explained^[22,76] by formation of an additional H-bond between O6 and the amine group of the ethylenediamine ligand, which cannot stabilize neither adenine N7 nor cytosine N3 adducts.

In the present study we focus on basic quantum chemical characteristics of the Ru(II) “piano-stool” complexes containing the quinolone bidentate ligands. The hydration reaction of

[a] T. Zábajková, R. Cajzl, J. V. Burda

Department of Chemical Physics and Optics, Faculty of Mathematics and Physics, Charles University, Ke Karlovu 3, Prague 2, 121 16, Czech Republic
E-mail: burda@karlov.mff.cuni.cz

[b] J. Kljun, I. Turel

Faculty of Chemistry and Chemical Technology, University of Ljubljana, Večna pot 113, Ljubljana 1000, Slovenia

[c] Z. Chval

Department of Laboratory Methods and Information Systems, Faculty of Health and Social Studies, University of South Bohemia, J. Boreckého 27, České Budějovice, 370 11, Czech Republic

Contract grant sponsor: Grant Agency of Czech Republic; Contract grant number: 16-06240S; Contract grant sponsor: National Grid Infrastructure MetaCentrum; Contract grant number: LM2010005; Contract grant sponsor: Bilateral Slovenian-Czech project of the Slovenian Research Agency (ARRS) and Ministry of Education of Czech Republic; Contract grant number: MEB 09104; Contract grant sponsor: ARRS; Contract grant number: P1-0175

© 2016 Wiley Periodicals, Inc.

several related complexes (nalidixic acid, thionalidixic acid, ofloxacin, and cinoxacin), recently synthesized and characterized by us,^[26,77,78] is described from both thermodynamic and kinetic points of view. Also, some physico-chemical analyses based on the electron density distribution of reactants, products, and transition-state structures were performed to get a deeper insight into the reaction process.

Computational Details

The interaction of $[\text{Ru}(\eta^6\text{-arene})(\text{Qui})\text{Cl}]^+$ (arene is ben = benzene or p-cym = p-cymene molecule and Qui = derivatives of nalidixic acid—generally called quinolone ligand) with a water molecule and the subsequent replacement of the chloride ligand forming the aqua-complex $[\text{Ru}(\eta^6\text{-arene})(\text{Qui})\text{H}_2\text{O}]^{2+}$ were examined. To describe both the thermodynamics and kinetics of this hydration reaction, the supermolecular approach was considered with reactant molecules (Ru-complex and water) associated by H-bonding. All geometries were optimized at the DFT level with the hybrid B3PW91 functional^[79] and 6-31+G(d) basis set—further labeled as B1 computational level. The presence of a set of diffuse functions (especially on oxygen atoms) was found crucial for the determination of correct geometries and an appropriate shape of the reaction profile. The Stuttgart–Dresden pseudopotentials^[80,81] were chosen for the description of the Ru, S, and Cl atoms. The original pseudo-orbitals were extended with a set of diffuse and polarization functions (for Ru with exponents $\alpha_s = 0.008$, $\alpha_p = 0.011$, $\alpha_d = 0.025$, $\alpha_f = 1.29$, for S: $\alpha_s = 0.075$, $\alpha_p = 0.013$, $\alpha_d = 0.498$, and for Cl: $\alpha_s = 0.09$, $\alpha_p = 0.0075$, $\alpha_d = 0.618$) at the optimization level. The same level was used for the vibration analyses and determination of the thermal and entropy terms. These frequency-calculations also served as confirmation for the correct character of transition state (TS) structures as well as reactants, intermediates, and products. The B3LYP/6-311++G(2df,2pd) computational level^[82] (labeled as B2 level hereafter) was chosen for the single point (SP) energy determination and calculations of electronic properties. The same set of diffuse functions on the Ru atom, which was used in optimization calculations, was augmented by a more extended set of polarization functions 2fg at the B2 level ($\alpha_f = 2.233$, 0.650 , $\alpha_g = 1.422$ optimized for neutral Ru atom at CCSD level using the steepest descent method written in the MOLPRO “shell script”^[83]). In the SP calculations, the Cl and S atoms were also described with an all-electron basis set. Analyses of electron densities contained the determination of electrostatic potentials^[84] (MEP) and average local ionization energies^[85] (ALIE) using our program Potmin written by Futera,^[86] Natural Bond Orbital^[87–89] (NBO) using genNBO v.5.9 program,^[89] Bader’s Atoms in Molecules (AIM)^[90] using Keith’s program AIMAll v.14,^[91] ETS-NOCV^[92] (extended transition state for energy decomposition analysis combined with the natural orbitals for chemical valence analysis), and the Nalewajski–Mrozek bond order analysis^[93] as implemented in the ADF 2014 program. Gibbs free energies were obtained by summing energies at the B2 level with ΔG contributions from the B1 level of calculations.

Since we are studying reaction in a solution, the Integral Equation Formalism—Polarizable Continuum Model^[94,95] (IEF-PCM) was used with UAKS cavities^[96,97] for water solvent simu-

lation at the B1 optimization level and (Dielectric) DPCM/scaled-UAKS^[98] for SP calculations. Studied complexes are composed from three ligands and a Ru(II) cation and the total stabilization energy (ΔE^{Stab}) can be defined as:

$$\Delta E^{\text{Stab}} = - \left(E_{\text{compl}} - \sum_i E_{\text{Li}} - E_{\text{Ru}} \right) \quad (1a)$$

Here, E_{compl} is the total energy of the whole complex, E_{Li} and E_{Ru} are energies of a given ligand i (its geometry is taken from the whole complex) and Ru^{2+} cation (evaluated in the quintuplet electronic ground state), respectively. The BSSE corrections determined by counterpoise method within the PCM regime leads to some additional inaccuracies, as discussed previously.^[99] The ghost atomic orbital functions can be localized either inside the cavity of the whole complex, which however leads to incorrect cavity polarization from the given fragment, or outside the cavity of the given part but then these ghost orbitals cannot be appropriately used since the escaped charge from the cavity is corrected within the PCM framework. Therefore in this study, we decided to evaluate the BSSE correction in vacuum using PCM geometries. There is also another model for calculation of the stabilization energy where mutual repulsion of individual ligands is included in the $E_{\text{All-Ligands}}$ term. This energy can be determined according to the formula:

$$\Delta E^{\text{Stex}} = - (E_{\text{compl}} - E_{\text{All-Ligands}} - E_{\text{Ru}}); \quad (1b)$$

where the energy term $E_{\text{All-Ligands}}$ means energy of the whole system and only the central Ru(II) cation is removed. The difference between both stabilization energies: $\Delta E^{\text{Stab}} - \Delta E^{\text{Stex}}$ gives an estimation of the ligand–ligand repulsion. The ligand bonding and association energies (ΔE^{BE}) were evaluated according to the following equation:

$$\Delta E^{\text{BE}}(L) = (E_{\text{compl}} - E_{\text{L}} - E_{\text{res}}). \quad (2)$$

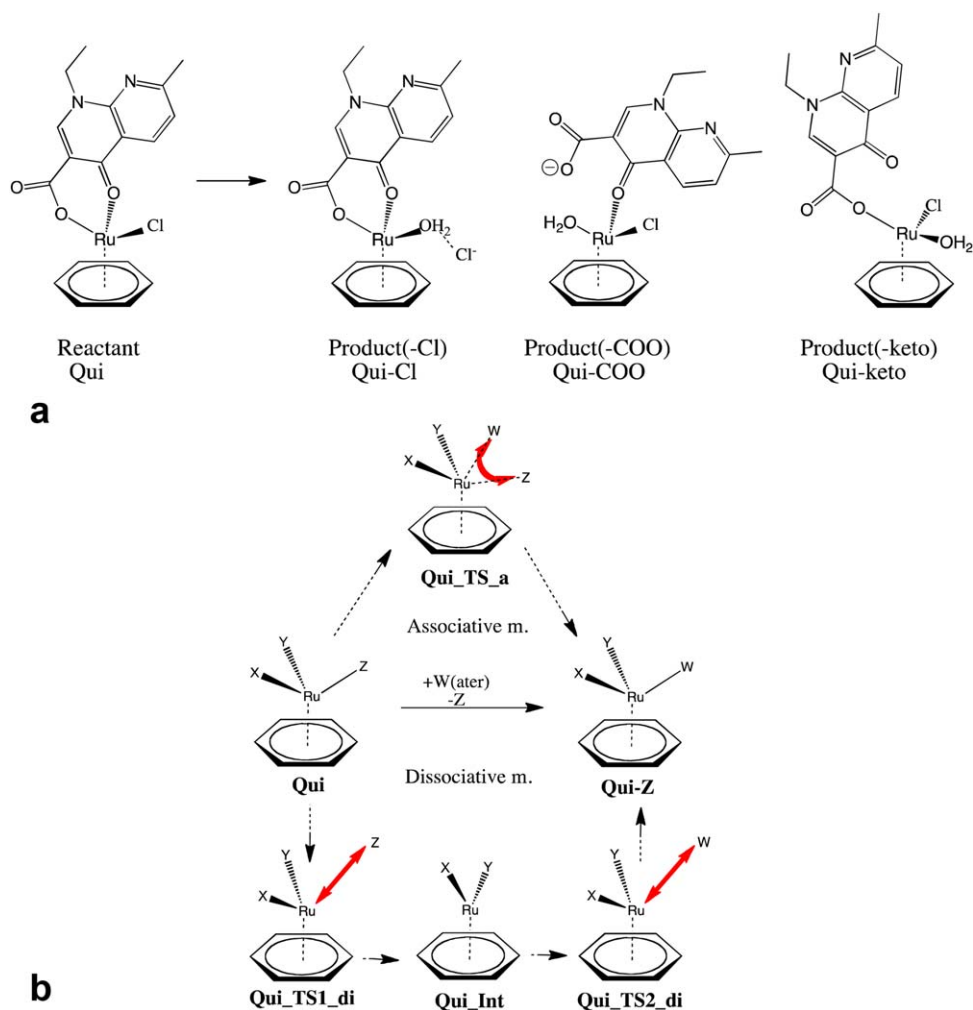
The E_{L} and E_{rest} label energies of the given ligand (or molecule) and the remaining part of the complex (both in the fixed geometry from the complex), respectively.

Kinetic parameters of the studied reactions were determined according to the Eyring’s Transition State Theory (TST). Since vibrational modes, energies, and geometries were obtained from the aforementioned calculations, the rate constants can be obtained from:

$$k^{\text{TST}}(T) = \frac{kT}{h} \cdot \exp(-\Delta G_0^\ddagger/kT) \quad (3)$$

where the ΔG_0^\ddagger is the Gibbs activation energy for the examined reaction coordinate.

In the following text, several abbreviations are used for structures on reaction coordinate: Qui means reactant $[\text{Ru}(\eta^6\text{-arene})(\text{Qui})\text{Cl}]^+$ complex; Qui-w stands for the same complex with an associated water molecule; Qui_w-Cl labels the product of the dechlorination reaction (with broken Ru–Cl bond) where



Scheme 1. a) Reactant complex and three possible products. b) Associative and dissociative mechanism for replacement of Z-ligand by W-ligand. [Color figure can be viewed in the online issue, which is available at wileyonlinelibrary.com]

chloride anion is associated to the Ru-complex (supermolecule of the product); Qui_w means the same product without the chloride anion; similarly -COO(H) labels a reaction where the Ru—O(COO) coordination is broken and -keto signs the reaction where the Ru—O(keto) bond is broken. Since both the protonated and deprotonated form of nalidixic acid (and its derivatives), a suffix *_d* is used for the deprotonated form of the given complex.

Determination of reaction mechanism

In the first part of the study, replacement of one of the Ru—Cl/O coordinations by water is explored in the model system with benzene as arene ligand and nalidixic acid as quinolone ligand. In this way, three different product complexes have to be expected as illustrated in Scheme 1a. Two possible pathways are considered in the reaction course – associative and/or dissociative mechanisms, cf. Scheme 1b. The associative mechanism is characterized by a single transition state (TS_a), which is connected with an imaginary vibration mode of the antisymmetric stretching character where simultaneously one coordination bond is broken and

another is formed (cf. red arrow in the upper part of Scheme 1b). The dissociative mechanism is linked with two transition states (TS1_{di}/TS2_{di}) and one intermediate structure (Int). Each of these two TS structures has an imaginary vibration mode associated with just a single bond stretching as depicted with red straight arrows in the lower part of the Scheme 1b. The intermediate lying between both TS's is a five-coordinated complex where two (Ru—Cl/O) dative bonds form a plane, which is approximately perpendicular to the arene ring as can be seen from Scheme 1b.

Figure 1 shows (in the upper part) the associative mechanism of the hydration process linked with release of the carboxyl group—structures of the reactant supermolecule with H-bonded water, TS, and product with broken Ru—O(COO) bond. In the lower part, the dechlorination process for complex with deprotonated thionalidixic acid (from the second part of the study) passing through the dissociative mechanism is depicted. The Gibbs free energy profile was determined for both reaction mechanisms and all three possible products. Since the nalidixic acid can exist in two forms (protonated and deprotonated) depending on the pH of the solution, both forms were explored in all the stationary points. The deprotonated form is common in solutions with

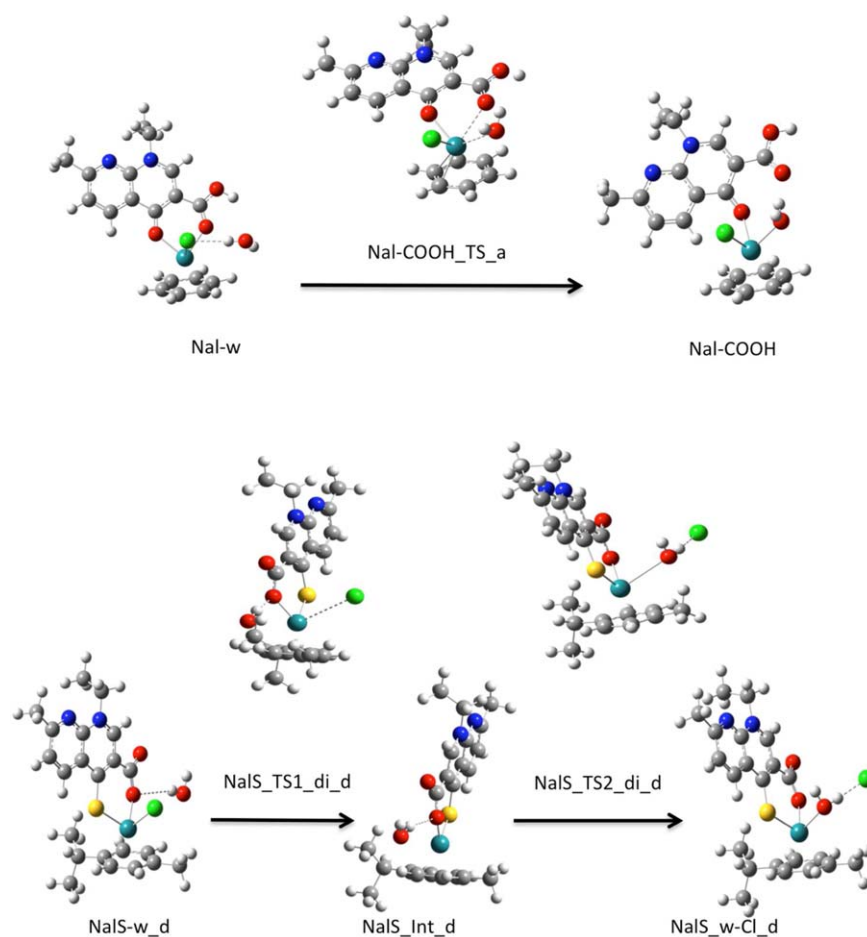


Figure 1. Associative mechanism of the protonated [Ru(ben)(Nal)Cl] complex and hydration process linked with release of the carboxyl group (in the upper part). Dissociative mechanism of the deprotonated [Ru(p-cym)(NalS)Cl] complex and dechlorination process (in the lower part). [Color figure can be viewed in the online issue, which is available at wileyonlinelibrary.com.]

higher pH (basic solutions). Experimentally determined pK_a value of Ru(Nal) complex is about 8.1–8.9^[77] and our computational pK_a estimation based on methodology from our previous study^[57] is 8.9.

Geometry optimization was performed for all structures within both associative and dissociative mechanisms. The distances of the Ru(II)-ligand bonds are collected in Table 1. As expected, the deprotonated complexes usually show shorter Ru–X distances than the protonated ones. The distance between metal and the arene ring decreases in all TS and intermediate structures due to a lower dative competition of smaller number of ligands. Nevertheless, the hapticity of the benzene ligand remains unchanged during the whole hydration process. In Table 1, experimental data are also included. Nevertheless, a comparison of the bonding distances is not straightforward mainly due to two facts: (i) the experimental data are based on X-ray measurement of crystals and (ii) different crystallization environment was used water in the case of ofloxacin and cinoxacin while toluene in the case of naldixic acid. It is also noticeable, that in a solution, slightly longer coordination distances are systematically obtained with usually small differences among individual structures (both in experimental and computational data). An interesting detail con-

cerns the optimizations of TS structures corresponding to the associative mechanism of the reaction where the Ru–O(keto) bond is broken and this released valence is used for water coordination. In this case another channel was found transforming the TS structures (both protonated and deprotonated) to the lower laying pathway, which corresponds to recoordination of O(keto) to Ru(II) cation, breaking of the Ru–O(COO) bond and replacing this released coordination by an aqua ligand. However, this TS lies ca 5 kcal/mol above the transition state, which corresponds to associative replacement of the carboxyl-group by water. Furthermore, another TS structure was found within the associative mechanism where the Ru(II) is coordinated to O(keto) and O(aq) oxygen atoms. This channel is connected with antisymmetric O(COO)–Ru–Cl vibration mode, which represents breaking of the Ru–O(COO) bond and reforming the Ru–Cl bond and vice versa. Nevertheless, also this TS lies slightly higher (ca 26.4 kcal/mol above reactants) than the channels for dechlorination as well as for the substitution of Ru–O(COO) bond by water (with activation energies of 23.9 and 25.6 kcal/mol, respectively).

Energies and rate constants. In Table 2, the electronic energies and Gibbs free energies for all the hydration reaction mechanisms

Table 1. Key coordination distances in the {Ru(Bez)(Nal)Cl}⁺ + H₂O complex. Ru-X(Ben) labels distance to the benzene ring center.

title:	Ru-O(keto)	Ru-O(COO)	Ru-Cl	Ru-O(aq)	Ru-X(Ben)
Nal ^[a]	2.099	2.125	2.442		1.648
Nal-w	2.093	2.121	2.451	4.494	1.649
Nal_d	2.091	2.089	2.461		1.650
Nal-w_d	2.088	2.087	2.462	5.135	1.651
Nal-Cl_TS_a	2.050	2.085	3.639	4.164	1.632
Nal-Cl_TS1_di	2.053	2.074	3.616	5.115	1.634
Nal-Cl_Int	2.042	2.063	5.943	5.135	1.648
Nal-Cl_TS2_di	2.053	2.082	4.973	3.220	1.633
Nal-Cl_TS_COOH_cl	2.171	2.491	2.979	2.242	1.616
Nal-Cl_TS_a_d	2.045	2.036	3.708	4.565	1.634
Nal-Cl_TS1_di_d	2.049	2.038	3.560	5.469	1.635
Nal-Cl_Int_d	2.036	2.025	5.393	3.493	1.638
Nal-Cl_TS2_di_d	2.044	2.037	5.143	3.267	1.635
Nal_w-Cl	2.088	2.116	4.410	2.153	1.645
Nal_w	2.084	2.116		2.171	1.644
Nal_w-Cl_d	2.073	2.070	4.431	2.181	1.649
Nal_w_d	2.078	2.075		2.182	1.646
Nal-COOH_TS_a	2.167	2.668	2.445	2.728	1.627
Nal-COOH_TS1_di	2.068	3.372	2.367	4.865	1.629
Nal-COOH_Int	2.048	3.691	2.376	5.595	1.630
Nal-COOH_TS2_di	2.077	4.220	2.388	3.160	1.630
Nal-COOH	2.141	4.104	2.425	2.182	1.641
Nal-COO_TS_a_d	2.168	2.595	2.484	2.608	1.625
Nal-COO_TS1_di_d	2.054	3.319	2.375	4.947	1.629
Nal-COO_Int_d	2.039	3.702	2.385	4.933	1.629
Nal-COO_TS2_di_d	2.062	4.079	2.400	3.090	1.630
Nal-COO_d	2.169	3.746	2.435	2.150	1.637
Nal-keto_TS1_di	2.938	2.356	2.592	5.325	1.612
Nal-keto_Int	4.447	2.099	2.363	3.407	1.629
Nal-keto_TS2_di	4.524	2.125	2.378	3.031	1.630
Nal-keto	4.150	2.135	2.422	2.183	1.640
Nal-keto_TS1_di_d	3.161	2.043	2.383	4.639	1.627
Nal-keto_Int_d	4.994	2.155	2.424	4.848	1.643
Nal-keto_TS2_di_d	4.692	2.091	2.397	3.059	1.633
Nal-keto_d	4.113	2.092	2.436	2.185	1.643

[a] Nal means complex with coordinated nalidixic acid; -w means with associated water; _w means coordinated aqua ligand; _d—deprotonated form of the complex; TS_a - TS of associative mechanism; TS_di - TS of dissociative mechanism; Int - intermediate structure with arene and two other coordinations to the Ru cation; -COOH labels reaction where the Ru—O(COO) coordination is broken; -keto - reaction where the Ru—O(keto) bond is broken; -Cl reaction where chloride anion is released; Nal_w-Cl means complex with coordinated water and associated Cl and Nal_w means complex with coordinated water (without Cl⁻ anion).

are displayed relatively to the reactant supermolecule. The dechlorination process has always the lowest activation barriers. In the protonated form, the remaining two processes: substitution of the Ru—O(keto) or Ru—O(COO) bond by water, exhibit practically the same reaction barriers of about 26 kcal/mol. On the contrary in the deprotonated form, breaking of the Ru—O(COO) bond requires a visibly higher amount of energy (27 vs. 23 kcal/mol for the Ru—O(keto) bond). This difference can be explained by an electrostatic enhancement of the Ru—O(COO) bond after deprotonation. These results are in fair accord with BCP's electron densities of Ru—O(keto) and Ru—O(COO) bonds in the corresponding (protonated/deprotonated) forms of reactant complex (cf. Table 5 and discussion below). In dissociative mechanism the deprotonated form of the intermediate complex with broken Ru—O(keto) bond lies visibly lower than the other intermediate

structures. The additional stabilization of this structure is connected with the reorientation of the Ru—O(COO) bond where partial rotation of the nalidixic acid above the Ru cation leads to the coordination of both oxygen atoms from carboxyl group to the Ru(II) cation. This coordination is also clearly visible in Tables 4 and 5 - footnote c) where additional BCP corresponding to Ru—O2(COO) was found. The Gibbs free energy profiles for the examined set of reactions are drawn in Figure 2. From this Figure, it can be noticed that the energies of two intermediate structures: (i) for keto-releasing reaction in protonated system and (ii) for dechlorination reaction in deprotonated system do not lie below the energies of both corresponding TS structures despite the correct energetical picture was obtained at the B1 level [cf. Table 2, *E*(B1) values]. It means that the energy profile in the area of TS structures is quite sensitive to computational levels and changing basis set and/or density functional to another (even to more accurate) one can lead to some deformation of the energy profile due to not completely optimal structures at those SP levels and should be taken with care. This fact can be demonstrated by re-optimization of the explored structures at the B2 level. We have performed such a re-optimization for the reaction coordinate of the dissociative mechanism in the case of the Ru—O(keto) bond breaking. This process has lower energy for TS2 structure than for Intermediate. The situation after re-optimization is displayed in Figure 2e and it can be seen that the energy of the intermediate structure was lowered (relatively to reactant) more (by ca 5 kcal/mol) than each of the two TS structures. In this way, the correct energy profile is again reconstructed.

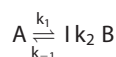
From Table 2 and Figure 2, it follows that the dissociative mechanism is kinetically slightly more preferable compared to the associative one in both neutral and basic solutions since the activation barriers for the associative mechanism are usually a little bit higher at all employed levels. All explored reactions are endergonic and endothermic with the only exception of the dechlorination reaction in a basic solution where an exothermicity of ca 1 kcal/mol is estimated. The association process (forming H-bond between both reactant molecules) is not a spontaneous reaction. Comparing individual reaction pathways, the dechlorination process is the dominant reaction channel from the thermodynamical and kinetical perspective in both acidic/neutral and basic solutions. The [Ru(η^6 -ben)(Nal)(OH)] complex can be considered as another possible product of dechlorination reaction. Nevertheless, this structure is not preferable from the thermodynamical point of view 8.4 vs. 13.0 kcal/mol. As follows from NBO and AIM analyses this product should be obtained through the same TS structure as [Ru(η^6 -ben)(Nal)(H₂O)]⁺ since aqua (or hydroxo) ligand coordinate only after passing the TS. Thus, it can be considered that formation of the Ru—O(hydroxyl) from water (simultaneously releasing proton to solution) occurs also in later reaction phase. The direct coordination of negatively charged OH⁻ to the Ru complex seems to be substantially less probable since two negative particles (Cl⁻ and OH⁻) would have to come to proximity.

Rate constants were determined according to Eyring's transition state theory, formula (3) above. The dissociative reaction mechanism has two consecutive steps:

Table 2. Energies for chloride replacement by water molecule or for breaking one of the Ru-O bonds in the chelate structure and substituting the released valence by water (in kcal/mol).

Protonated	ΔE (B1)			ΔE (B2)			ΔG (B2)		
	Cl	COOH	Keto	Cl	COOH	Keto	Cl	COOH	Keto ^[a]
R0	-0.4			-0.6			-4.0		
R1	0.0	0.0	0.0	0.0	0.0	0.0	0.0	0.0	0.0
TS_a	13.6	17.4		23.1	26.2		23.1	25.6	
TS1_di	12.8	11.5	14.9	20.6	19.0	24.7	22.4	23.2	25.6/22.3
Int	12.7	11.0	13.5	16.6	18.8	22.4	19.1	21.4	25.1/21.3
TS2_di	13.6	13.8	14.9	22.5	22.3	18.5	22.9	25.6	21.2/22.7
P1	0.4	3.8	3.2	5.6	5.1	6.2	8.4	8.3	10.7/9.5
P1 (OH) ^[b]	6.7			12.7			13.0		
P0	-0.6			0.5			-3.8		
Deprotonated	Cl	COO	Keto	Cl	COO	Keto	Cl	COO	Keto
R0	0.3			-2.1			-5.4		
R1	0.0	0.0	0.0	0.0	0.0	0.0	0.0	0.0	0.0
TS_a	10.8	23.1		15.2	20.2		17.6	26.2	
TS1_di	10.7	18.6	14.9	15.1	23.9	18.8	17.3	25.3	22.5
Int	9.8	16.8	3.4	14.0	20.3	8.3	17.4	22.6	11.5
TS2_di	11.2	19.9	14.5	15.1	21.3	17.0	16.9	26.8	23.2
P1	0.0	9.9	4.2	-0.9	6.0	0.2	4.7	13.6	7.9
P0	-2.1			-4.6			-5.4		

R0 means noninteracting reactants, R1 supermolecule of water H-bonded to the Ru(II) complex, Int means intermediate with H-bonded water (and Cl⁻), P1 means product (supermolecule where Cl is H-bonded to Ru complex in dechlorination channel).
[a] P0 noninteracting product species (only in the dechlorination channel) Energies for optimized geometry at the B1 level/B2 level.
[b] For the dechlorination process, the [Ru(*η*⁶-ben)(Nal)(OH)] product was also considered.



where the first step is rate limiting and the following inequalities are valid: $k_1 \ll k_{-1}$ and $k_1 \ll k_2$. Thus, concentration of an intermediate [I] is low and a steady state condition can be applied:

$\frac{d[I]}{dt} \cong 0$. Within this assumption the final rate constant can be determined according to the equation:

$$k_d = \frac{k_1 k_2}{k_{-1} + k_2} \quad (4)$$

The obtained rate constants based on the Gibbs free energies from the last section of Table 2 are summarized in Table 3. From this table it can be concluded that the fastest reaction is dechlorination. This process will be very fast in a basic environment where both rate constants for associative and dissociative

Table 3. Rate constants determined for associative and dissociative mechanisms according to the formula (3).

Prot.	Cl	COO	Keto
k_a	7.09 E - 05	1.0 E - 06	
k_1	2.31 E - 04	5.9 E - 05	1.1 E - 06
k_{-1}	2.36 E + 10	2.9 E + 11	2.7 E + 12
k_2	1.01 E + 10	5.2 E + 09	4.4 E + 15
k_d	6.94 E - 05	1.0 E - 06	1.1 E - 06
Deprot.			
k_a	7.66 E - 01	3.7 E - 07	
k_1	1.27 E + 00	1.7 E - 06	1.9 E - 04
k_{-1}	7.35 E + 12	6.7 E + 10	5.3 E + 04
k_2	1.44 E + 13	5.6 E + 09	1.6 E + 04
k_d	8.43 E - 01	1.3 E - 07	4.6 E - 05

pathway are quite high (ca. $0.8 \text{ s}^{-[1]}$). As a consequence of the higher activation barrier of the Ru-O(COO) bond-breaking in deprotonated form, the rate constant of this process is about two orders of magnitude lower than rate constant for breaking of Ru-O(keto) bond despite essentially equal rate constants in a neutral solution. This low rate constant is a consequence of stronger Ru-O(COO) bond after deprotonation as already discussed above.

Electronic properties. The NBO and AIM analyses of the electron densities were performed at the B2 level. Based on partial charges of key atoms (Ru, O, Cl) and bond critical points of ruthenium coordination bonds, the extent of dative interactions or bond strengths can be estimated. In Table 4, the NBO partial charges of complexes from the examined reactions are displayed. In the protonated forms partial charges of both keto- and carboxylic oxygens are comparable, similarly to the charges in isolated nalidixic acid. In the deprotonated complexes, the NBO charges of both oxygens are decreased, nevertheless, a more remarkable change occurs on O(COO) due to the releasing proton from the carboxyl group. The partial charge of the Ru atom is systematically higher in deprotonated complexes than in protonated ones. Conclusion on stronger coordination of the keto- than carboxyl-group can follow from the Ru partial charges in the product state of the corresponding reaction channel. When releasing the keto-group, partial charge on the Ru is 0.483 e, while when the carboxyl-group is released, higher donation to Ru leads to a lower partial charge of 0.470 e. Therefore, a higher extent of donation can be assumed in the latter case leading to the stronger Ru-O(keto) bond. In the

Table 4. NBO partial charges of the key coordinated atoms (in e).

Title	O (keto)	O (COO)	O2 (COO)	O (aq)	Cl	Ru
Nal ^[a]	-0.592	-0.600	-0.688		-0.574	0.497
Nal-w	-0.591	-0.599	-0.687	-0.996	-0.573	0.495
Nal_d	-0.609	-0.715	-0.780		-0.599	0.512
Nal-w_d	-0.607	-0.714	-0.782	-0.976	-0.597	0.516
Nal-Cl_TS_a	-0.612	-0.627	-0.673	-0.998	-0.896	0.662
Nal-Cl_TS1_di	-0.616	-0.627	-0.682	-0.955	-0.930	0.666
Nal-Cl_Int	-0.630	-0.627	-0.682	-0.975	-0.920	0.691
Nal-Cl_TS2_di	-0.615	-0.617	-0.672	-0.993	-0.950	0.659
Nal-Cl_TS_COOH_cl	-0.661	-0.666	-0.699	-0.904	-0.803	0.629
Nal-Cl_TS_a_d	-0.628	-0.706	-0.725	-1.009	-0.920	0.673
Nal-Cl_TS1_di_d	-0.629	-0.689	-0.741	-1.011	-0.936	0.677
Nal-Cl_Int_d	-0.636	-0.695	-0.710	-0.976	-0.953	0.592 ^[b]
Nal-Cl_TS2_di_d	-0.632	-0.699	-0.723	-0.995	-0.953	0.669
Nal_w-Cl	-0.605	-0.609	-0.681	-0.892	-0.896	0.600
Nal_w	-0.615	-0.607	-0.679	-0.865		0.591
Nal_w-Cl_d	-0.608	-0.696	-0.749	-0.896	-0.907	0.611
Nal_w_d	-0.614	-0.724	-0.758	-0.865		0.598
Nal-COOH_TS_a	-0.657	-0.665	-0.710	-0.939	-0.574	0.566
Nal-COOH_TS1_di	-0.658	-0.643	-0.719	-0.968	-0.519	0.531
Nal-COOH_Int	-0.697	-0.633	-0.719	-0.963	-0.517	0.621
Nal-COOH_TS2_di	-0.667	-0.674	-0.718	-0.970	-0.529	0.524
Nal-COOH	-0.674	-0.681	-0.709	-0.874	-0.556	0.483
Nal-COO_TS_a_d	-0.634	-0.804	-0.791	-0.938	-0.604	0.574
Nal-COO_TS1_di_d	-0.704	-0.838	-0.865	-0.982	-0.539	0.651
Nal-COO_Int_d	-0.678	-0.800	-0.785	-1.012	-0.533	0.539
Nal-COO_TS2_di_d	-0.690	-0.817	-0.785	-0.977	-0.549	0.546
Nal-COO_d	-0.688	-0.815	-0.792	-0.885	-0.572	0.510
Nal-keto_TS1_di	-0.671	-0.668	-0.707	-0.967	-0.616	0.626
Nal-keto_Int	-0.658	-0.632	-0.696	-0.938	-0.490	0.470 ^[b]
Nal-keto_TS2_di	-0.658	-0.627	-0.695	-0.961	-0.516	0.499
Nal-keto	-0.696	-0.636	-0.667	-0.880	-0.555	0.470
Nal-keto_TS1_di_d	-0.674	-0.727	-0.744	-1.007	-0.541	0.556
Nal-keto_Int_d	-0.683	-0.633 ^[c]	-0.669 ^[c]	-0.973	-0.574	0.483
Nal-keto_TS2_di_d	-0.689	-0.704	-0.797	-0.986	-0.550	0.538
Nal-keto_d	-0.720	-0.717	-0.745	-0.884	-0.578	0.506

[a] the same abbreviation as in Table 1., [b] additional Ru...H(aq) interaction exists in this complex., [c] Ru is coordinated to both oxygens from carboxyl group.

deprotonated section of Table 4, much closer values for both kinds of complexes are noticeable ($\delta(\text{Ru}) = 0.510$ and 0.506 e). This conclusion is easy to understand since after the deprotonation a strengthening of the carboxyl-group coordination can be expected. The more profound answer can be received from AIM analysis, ETS-NOCV, and the Nalewajski-Mrozek bond order analysis,^[93] which were performed for the isolated reactant molecules in both protonated/deprotonated forms. In protonated systems, a higher bond order was obtained for Ru—O(keto) bond -0.48 vs. 0.42 for Ru—O(COO) bond. In the deprotonated complex, the corresponding bond orders are 0.51 for keto and 0.58 for carboxyl coordinations. This result is also in a fair accord with the AIM analysis. The electron densities of bond critical points (BCP) for all coordination bonds are collected in Table 5. Despite the similar partial charges of O(keto) and O(COO) atoms in protonated form, significantly higher BCP electron density occurs in the Ru—O(keto) bond. The BCP electron density of Ru—O(COO) coordination is in average by about 0.01 e lower (cf. the first two columns of Table 5). In deprotonated complexes, slightly higher BCP electron densities can be observed for the Ru—O(COO) than Ru—O(keto) bond.

Comparing the NBO charge of Ru cation, it follows that the chloro ligand in reactant has a higher dative affinity (reducing charge of the Ru cation to higher extent) than the aqua ligand in product. In all the reactions, the coordination of the aqua ligand occurs only after the corresponding transition state (after TS_a in associative and after TS2_di in dissociative mechanisms) since in all TS structures the partial charge of O(aq) is always lower than -0.97 e. It increases to ca -0.88 e only after the Ru—O(aqua) bond is fully established. As to the change of Cl partial charge, it can be noticed that chloride is released from the complex before the first TS structures (TS_a and TS1_di of dechlorination) since its partial charge in corresponding TS structure already approaches to -0.9 e, that is, the value of isolated chloride anion in the supermolecular model. These trends are also confirmed by the AIM analysis where the corresponding BCP for water coordination appears only in the very last part of reaction coordinate and BCP of the Ru—Cl bond disappears practically in the first TS structure.

When the interaction of a metal cation with arene ring is considered, Ru(II) is more weakly attached to the arene ring in reactant and product states while visibly stronger interaction occurs in TS and intermediate structures. This follows from the

Table 5. AIM electron densities (in $10^2 e/a_0^3$) in bond critical points (BCP) of the Ru coordination bonds.

Title/Ru-	O(keto)	O(COO)	O(aq)	Cl	X(Ben)	
Nal ^[a]	8.2	7.4		6.8	9.1	8.9
Nal-w	8.3	7.5		6.6	9.1	8.9
Nal_d	8.4	8.5		6.5	10.0	8.9
Nal-w_d	8.5	8.6		6.5	9.2	9.1
Nal-Cl_TS_a	9.5	8.4		0.7	10.0	10.0
Nal-Cl_TS1_di	9.4	8.7		0.8	9.9	9.8
Nal-Cl_Int	9.8	9.1			10.1	9.7
Nal-Cl_TS2_di	9.4	8.6	0.9		10.0	9.7
Nal-Cl_TS_a_d	9.7	0.1		0.7	10.1	9.7
Nal-Cl_TS1_di_d	9.6	9.9		0.8	10.1	9.7
Nal-Cl_Int_d	10.0	10.3	1.4 ^[b]		10.0	9.6
Nal-Cl_TS2_di_d	9.7	10.0	0.9		10.1	9.7
Nal_w-Cl	8.5	7.7	7.4		9.3	9.3
Nal_w	8.6	7.7	6.9		9.3	9.2
Nal_w-Cl_d	8.9	9.0	6.8		9.2	9.0
Nal_w_d	8.8	9.1	6.6		9.3	9.1
Nal-COOH_TS_a	6.7	2.4	2.3	6.8	10.2	10.1
Nal-COOH_TS1_di	8.7			8.1	10.1	9.7
Nal-COOH_Int	9.2			7.9	9.8	9.7
Nal-COOH_TS2_di	8.3		1.0	7.7	10.1	9.5
Nal-COOH	6.9		6.8	7.1	9.4	9.1
Nal-COO_TS_a_d	6.9	2.9	2.9	6.2	10.0	10.0
Nal-COO_TS1_di_d	9.2			7.9	9.9	9.6
Nal-COO_Int_d	9.6			7.8	9.7	9.5
Nal-COO_TS2_di_d	9.0		1.2	7.5	9.9	9.8
Nal-COO_d	6.4		7.5	6.9	9.4	9.4
Nal-keto_TS1_di	1.4	4.3		5.1	10.1	9.9
Nal-keto_Int		8.1	1.1 ^[b]	8.2	9.9	9.8
Nal-keto_TS2_di		7.6	1.3	7.9	10.1	9.8
Nal-keto		7.1	6.8	7.1	9.4	9.2
Nal-keto_TS1_di_d		9.5		7.8	10.1	9.7
Nal-keto_Int_d	7.7 ^[c]	7.8		7.1	9.5	9.4
Nal-keto_TS2_di_d		8.8	1.3	7.5	10.1	9.9
Nal-keto_d		8.5	6.7	6.8	9.3	9.2

[a] the same abbreviation as in **Table 1**. [b] Ru...H(aq) dispersion interaction. [c] Ru—O2(COO).

fact that higher electron densities in BCP's exist in these structures as shown in Table 5. The same conclusion holds for nalidixic acid as well and these stronger coordinations are simply a consequence of the lower donation competition since neither the chloro- nor aqua-ligand is bound.

In several intermediate structures, when an explicit water molecule is present, the dispersion interaction of water hydrogen with the Ru atom can be noticed. This interaction is demonstrated by the existence of BCP between these two atoms (cf. remark (b) in Table 5). The typical distance of Ru...H is 2.6 Å, which is slightly longer than Pt...H axial interaction described by Berges^[100] probably because of the higher number of surrounding ligands in comparison with cisplatin.

Comparison of selected derivatives of nalidixic acid

In the next part ruthenium(η^6 -*p*-cym) complexes with four different derivatives of nalidixic acid, synthesized recently,^[26,77] are compared: nalidixic (Nal) and thionalidixic (NalS) acids, cinoxacin (Cin), and the antibacterial agent ofloxacin (Ofi). Their structural formulas are drawn in Figure 3. Note that

structures of the Ru(II)-complexes in this part differ from the complexes explored in the previous section by the arene ligand. Here, *p*-cymene is used like in real experimental samples while a slightly smaller benzene molecule was employed in previous model calculations. Nevertheless, this change has only marginal influence on the obtained results (cf. the first line of Table 1 and second line of Table 6).

Only the dissociative mechanism of the hydration process is explored and only the dechlorination reaction channel is examined in this part. The other reaction channels (see above) are analyzed only with respect to the reactants and final products to make a mutual comparison of the thermodynamic behavior and to offer a deeper insight into the binding properties. We did not search for the corresponding TS structures since the kinetic preference for the dechlorination reaction was clearly demonstrated in the previous part. In the lower part of Figure 1 all the stationary points for Ru(II)-complex with deprotonated thionalidixic acid are displayed for the clarity.

Optimization of all the complexes was performed using the same computational model as in the previous part and the most important coordination parameters for isolated reactant complexes are summarized in Table 6. Remaining stationary points from the reaction coordinate are presented in the Supporting Information **Table S1**. Similarly to our previous calculations, both acidic/neutral and basic environments are considered using the protonated and deprotonated forms of the complexes. From Tables 6 and Supporting Information **Table S1**, basic differences in coordination are visible. For all the quinolones, the distances of Ru—O(keto) bonds are shorter than Ru—O(COO) one in protonated forms while in deprotonated forms both coordinations are quite similar, that is, the conclusion from the previous part about stronger keto-bonds remains valid. Some other bonding trends can be distinguished when individual quinolones are compared. For instance both Ru—O bonds for carboxyl and keto groups are (in average) slightly shortened, approximately in an order: cinoxacin (the longest) > nalidixic > ofloxacin > thionalidixic acid (for carboxyl group only) in both protonated/deprotonated isolated complexes. In supermolecular and TS structures, such a comparison is more difficult to observe due to additional effects caused by the associated water molecule. Also, the sulfur atom in the thionalidixic acid makes a mutual comparison of bonding relations more difficult. Nevertheless, in this system, coordination of the carboxyl group is also partially strengthened by deprotonation since the Ru—O bond is shortened (from 2.108 Å in protonated structure to 2.090 Å in deprotonated one, cf. Table 6). The same conclusion follows from increased BCP electron densities (Table 11). The Ru—NalS complexes show visibly longer Ru—X(arene), and Ru—Cl distances compared to the other structures (Table 6). This is also an indirect sign of a stronger dative interaction of the thionalidixic acid with the Ru(II) cation. Detailed insight into different Ru—O/S bonding can be found in the analysis of electron densities below.

Energy and kinetic characteristics. The most important part of the study deals with differences in reaction energy profiles of the hydration/dechlorination process and related quantities—

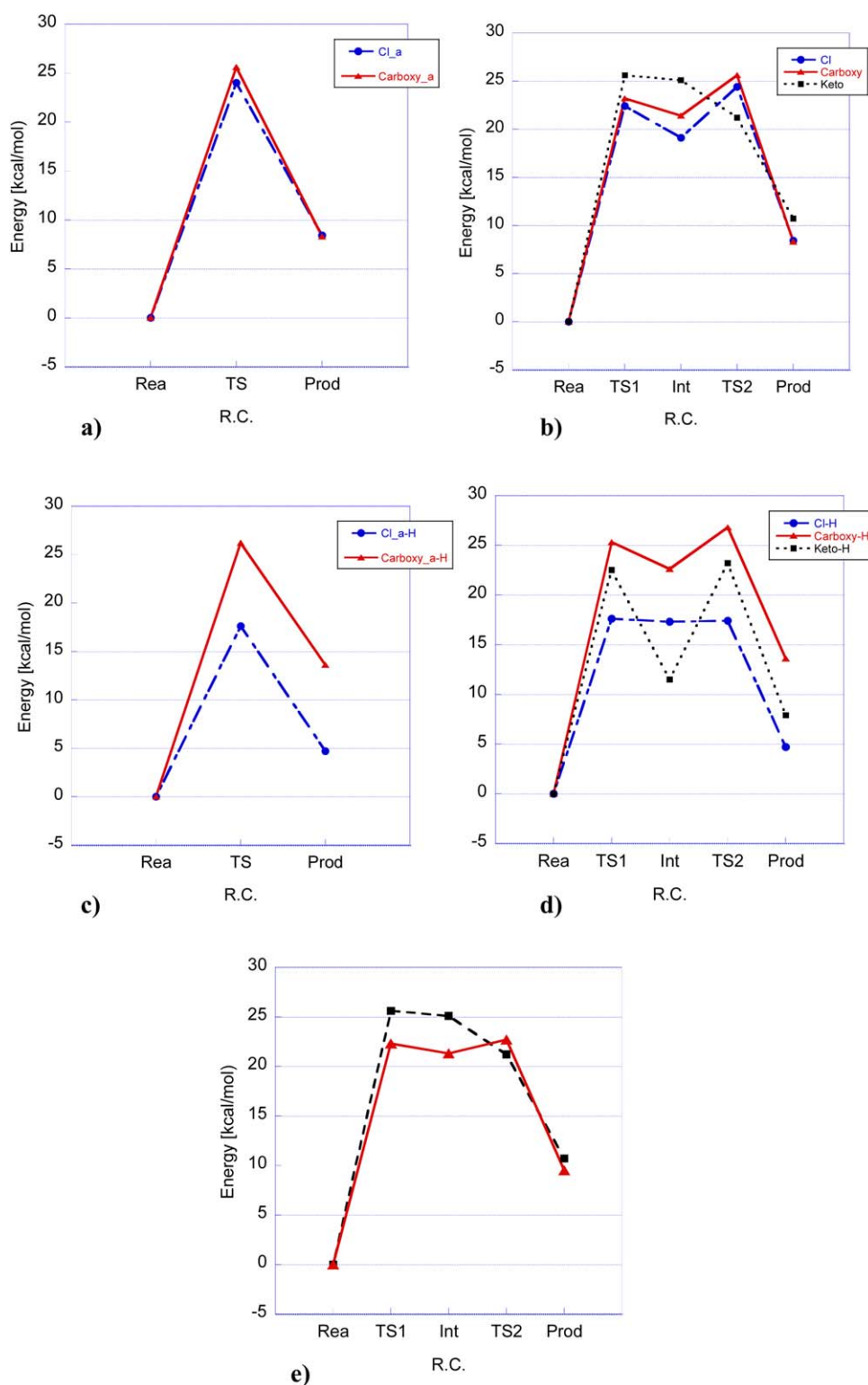


Figure 2. Associative (a and c) and dissociative (b and d) reaction pathways in neutral (a and b) and basic (c and d) solutions. Blue dashed line with circles signs dechlorination, solid red line with triangles hydrolysis of the Ru—O(COO) bond and black dotted line squares hydrolysis of the Ru—O(keto) bond. e) a comparison of energy profiles optimized at the both B1 (black dashed line) and B2 (red solid line) for hydrolysis of the Ru—O(keto) bond. [Color figure can be viewed in the online issue, which is available at wileyonlinelibrary.com.]

reaction energies and activation barriers. Stabilization energies and binding energies of individual ligands (arene, quinolone, aqua, and chloride) enable some further comparison with the AIM analysis of the corresponding BCP's. The reaction energy

profile (with the zero reference value taken for a supermolecule of the associated reactant complex) is summarized in Table 7. All the reactions are endergonic (comparing R1 and P1 states) and the dechlorination reaction is the least

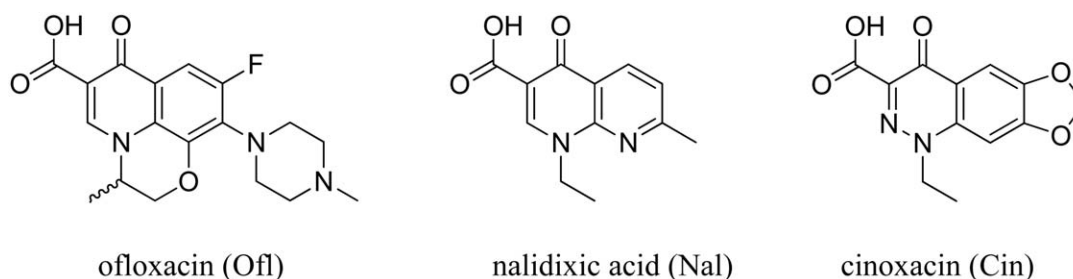


Figure 3. Chemical structures of the clinically applied quinolone antibacterials ofloxacin (OfI), nalidixic acid (Nal) and cinoxacin (Cin) used in this study.

endergonic reaction in comparison with the release of the other Ru—O/S coordinations for all quinolone ligands. (The only exception is releasing the Ru—O(COO) bond in a protonated complex with nalidixic acid). The equilibrium for dechlorination is shifted more distinctly towards product in basic solution (lower endergonicity in the deprotonated form of the complex). A similar conclusion holds also for the P1 Ru—keto product (where the Ru—O(keto) bond is broken) while in the case of the P1 Ru—COO product, the deprotonation leads to the stabilization of the reactant and thus, a higher ΔG for Ru—O(COO) bond-breaking is obtained. Also the stronger Ru—O(keto) bond correlates with higher endergonicity of the Ru—keto reaction in comparison with ΔG of the Ru—COO reaction in protonated complexes. When various quinolone ligands are compared, the least endergonic reaction occurs in the case of cinoxacin in neutral solutions; the free energy order is cinoxacin < thionalidixic \approx nalidixic acid < ofloxacin. In basic environment the ofloxacin has reaction free energy— ΔG practically equal to zero and is actually exothermic (by 3.1 kcal/mol - the only exothermic reaction). The order of ΔG is slightly different in basic solutions: ofloxacin < cinoxacin < thionalidixic \sim nalidixic acid. As to the reaction enthalpies (ΔH), hydration of complexes with nalidixic and thionalidixic acids is practically thermoneutral reaction ($\Delta H \approx 1$ –2 kcal/mol) in deprotonated forms. The same holds for complex with cinoxacin in the protonated form ($\Delta H = 2.2$ kcal/mol), which actually increases passing to basic solution by 1 kcal/mol.

Table 6. Coordination distances in the $\{\text{Ru}(\text{Cym})(\text{Quinolone})\text{Cl}\}^+ + \text{H}_2\text{O}$ reactant complex.

Title	Ru—O (keto/S)	Ru—O (COO)	Ru—Cl	Ru—X (Cym)
Cin	2.098	2.123	2.442	1.654
Cin(exp)	2.099	2.071	2.415	1.644
Nal	2.100	2.125	2.444	1.655
Nal(exp)	2.087	2.070	2.416	1.642
NalS	2.347	2.108	2.460	1.685
OfI	2.096	2.122	2.448	1.655
OfI(exp)	2.071	2.069	2.418	1.635
Cin_d	2.092	2.089	2.460	1.656
Nal_d	2.090	2.089	2.465	1.657
NalS_d	2.352	2.090	2.473	1.685
OfI_d	2.088	2.089	2.466	1.658

Ru—X(Cym) labels distance from Ru(II) to the p-cymene ring center (in Å). Exp values are taken from Ref. 77.

As to the reaction mechanism, it was already mentioned that only the dissociative pathway was explored, which means that two activation barriers and one intermediate structure were located on the reaction coordinate. Our data demonstrates much higher kinetic stability of the reactant complexes in acidic/neutral solutions than in basic ones since the activation barriers found in protonated forms are usually higher (by about 6 kcal/mol — cf. Fig. 4 and Table 7). The highest barrier

Table 7. Enthalpy and Gibbs free energy (in kcal/mol) for the hydration reaction.

Structure	Protonated form		Deprotonated form	
	H (SP)	G (SP)	H (SP)	G (SP)
Cin: R0	−3.4	−5.6	−2.4	−6.7
R1	0.0	0.0	0.0	0.0
TS1	19.0	23.0	17.2	15.4
Int	17.1	21.6	13.9	12.5
TS2	18.0	22.6	9.9	7.9
P1	2.2	6.9	3.2	3.2
P0	−2.7	−4.1	−3.7	−6.9
P1-keto	7.4	14.3	6.3	6.9
P1-COO	5.8	11.9	15.4	15.1
Nal: R0	1.5	−3.8	−3.2	−5.3
R1	0.0	0.0	0.0	0.0
TS1	22.9	22.5	15.1	16.9
Int	21.9	22.5	13.0	14.2
TS2	23.1	20.7	13.5	16.7
P1	10.5	10.8	1.7	7.0
P0	1.4	−2.4	−4.0	−4.8
P1-keto	9.8	11.4	0.1	7.6
P1-COO	5.3	6.4	5.4	12.8
NalS: R0	0.0	−4.5	−3.3	−5.0
R1	0.0	0.0	0.0	0.0
TS1	16.2	19.9	13.4	17.9
Int	23.9	19.6	10.0	12.1
TS2	24.5	24.0	12.3	14.7
P1	8.2	9.3	1.1	6.8
P0	2.2	−1.9	−3.9	−5.0
P1-keto	21.3	22.1	7.8	14.8
P1-COO	10.4	11.9	6.9	14.7
OfI: R0	2.8	−2.9	−2.6	−5.7
R1	0.0	0.0	0.0	0.0
TS1	23.2	23.5	20.8	19.5
Int	23.3	22.2	7.9	7.4
TS2	25.5	25.2	15.8	18.1
P1	12.4	13.7	−3.1	0.2
P0	−0.4	−3.3	−4.3	−6.1
P1-keto	17.0	16.6	3.0	6.3
P1-COO	12.0	13.8	8.1	13.7

Structure labels are taken from Table 2.

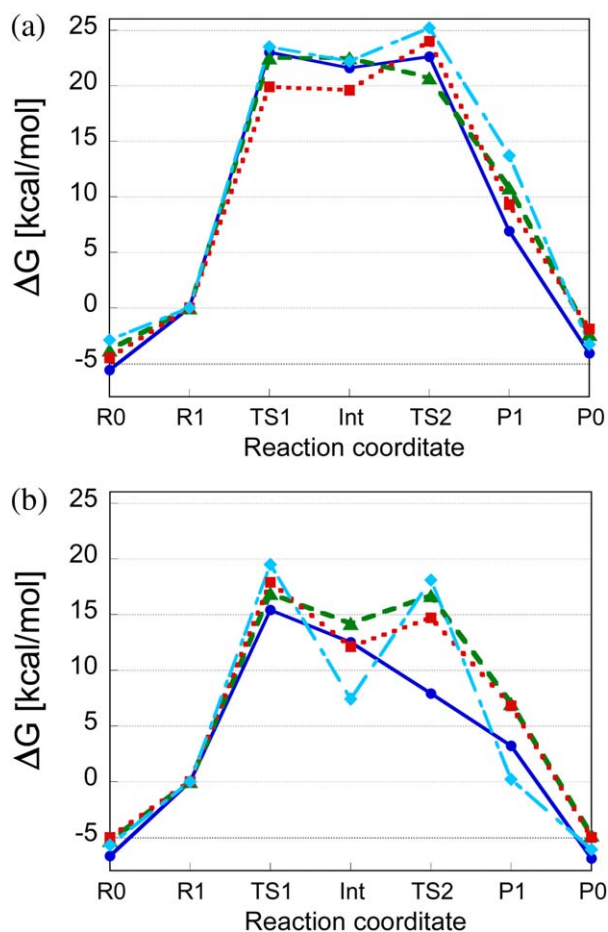


Figure 4. Dechlorination reaction profile for Ru(II) complexes with selected quinolone derivatives in a) neutral and b) basic solutions. Cin - blue solid line with circles, Nal - green dashed line with triangles, NalS red dotted line with squares, OfI - aqua blue dash-dotted line with diamonds. [Color figure can be viewed in the online issue, which is available at wileyonlinelibrary.com.]

occurs in the case of ofloxacin (ca 24 kcal/mol), the lowest one is in the complex with nalidixic acid. In a basic solution, the complex with cinoxacin has the lowest activation energy. This indirectly points to a slightly different chemical behavior of the individual derivatives. Intermediate structures (Int) represent very shallow minima enclosed by two close-in-energy TS1 and TS2 structures. Actually, all these structures (TS1, Int, and TS2) lie in the 2–3 kcal/mol energy range on the reaction coordinate at the B1 level. Considering thermal and entropy contributions to ΔH and ΔG energies, the intermediate structures of

Table 8. Rate constants for replacement of chloro ligand by water.

Neutral	Cin	Nal	NalS	OfI
k_1	9.0 E - 05	1.9 E - 04	1.6 E - 02	3.6 E - 05
k_{-1}	6.2 E + 11	6.6 E + 12	3.9 E + 12	6.9 E + 11
k_2	1.2 E + 12	1.3 E + 14	3.9 E + 09	3.9 E + 10
k_d	5.9 E - 05	1.8 E - 04	1.6 E - 05	1.9 E - 06
Basic				
k_1	3.1 E + 01	2.5 E + 00	4.7 E - 01	3.1 E - 02
k_{-1}	5.0 E + 10	6.5 E + 10	3.7 E + 08	8.2 E + 03
k_2	1.6 E + 16	9.9 E + 10	8.2 E + 10	8.3 E + 04
k_d	3.1 E + 01	1.5 E + 00	4.7 E - 01	2.8 E - 02

protonated nalidixic acid and deprotonated cinoxacin become higher in energy than the corresponding TS2 structure. Moreover, since SP electronic energies were obtained at the B2 level while optimized at the lower (B1) level, we can consider them as nonoptimal. Thus, they can cause some deformation of the reaction profiles since not all of these structures will be re-optimized to the same extent. So that some of the structures become higher in energy than the other. This occurred in the case of Intermediate structure, which got (relatively) slightly higher in energy than one of the surrounding TS's and thus, the reaction looks like a single-step process. The structural changes in this area of the potential energy surface are quite small, as it is shown in Supporting Information **Table S1**. The energy difference between the higher of the TS's and Intermediate structures often remains within 2 kcal/mol for protonated quinolones. Therefore, some small deformations can change the shape of the reaction profile. This was demonstrated in previous part, where the re-optimization at the B2 level can reconstruct the appropriate energy profile as corresponds to the standard dissociation mechanism, cf. Figure 2e. More pronounced energy differences occurs for deprotonated structures. In the case of deprotonated ofloxacin, the marked stabilization (more than 10 kcal/mol) of the intermediate structure is connected with symmetrical (bifurcated) H-bond of water hydrogen to both oxygens of the carboxyl group and simultaneous H-bond formation between water and chloride moved to the ofloxacin plane. These relatively large changes in structure of intermediate were not observed in any other quinolone system. Since two TS states appear on the reaction coordinate, it is interesting to compare their mutual energies. Generally the breaking of Ru—Cl bond (in the TS1) is connected with in average ca 2kcal/mol higher energy, cf. Figure 4.

According to Eyring's TST, the reaction rate constants are determined for all four quinolone derivatives. Table 8 shows, beside the final values of k_d , also 'partial' rate constants for both reaction steps. The reaction rate of the whole process decreases in order: nalidixic acid > cinoxacin > thionalidixic

Table 9. Stabilization (Stab and Stex) and bonding energies (in kcal/mol).

PCM	Stab	Stex	Qui	p-cym	Cl
Cin	182.0	232.0	41.0	62.8	16.8
Nal	179.0	227.9	38.3	60.7	19.1
NalS	188.4	235.2	50.2	55.4	15.2
OfI	183.3	236.7	42.3	62.9	15.6
Cin_d	194.4	254.2	54.4	59.6	10.7
Nal_d	193.9	254.2	53.9	60.2	11.9
NalS_d	203.1	236.2	78.1	58.2	9.6
OfI_d	195.1	260.0	55.2	58.8	9.4
g.p.	Stab	Stex	Qui	p-cym	Cl
Cin	601.2	624.8	75.3	80.1	183.6
Nal	602.6	625.5	82.5	75.7	186.2
NalS	604.8	625.8	81.8	70.5	179.2
OfI	606.6	629.2	79.8	79.5	181.2
Cin_d	696.3	780.6	171.9	67.1	112.8
Nal_d	694.7	780.5	170.7	66.8	112.4
NalS_d	696.6	780.8	175.0	58.3	108.5
OfI_d	696.9	781.2	172.9	66.7	110.0

Table 10. NBO partial charges of isolated complexes (in e).

structure	Ru	O (keto)/S	O (COO)	Cl/O
Cin ^[a]	0.492	-0.600	-0.597	-0.572
Cin_Int_isol ^[b]	0.783	-0.640	-0.647	
Cin_w	0.575	-0.604	-0.604	-0.869
Cin_d	0.508	-0.636	-0.698	-0.596
Cin_Int_isol_d	0.783	-0.658	-0.727	
Cin_w_d	0.600	-0.627	-0.703	-0.872
Nal	0.485	-0.613	-0.598	-0.569
Nal_Int_isol	0.799	-0.633	-0.645	
Nal_w	0.579	-0.598	-0.609	-0.872
Nal_d	0.685	-0.644	-0.714	-0.598
Nal_Int_isol_d	0.785	-0.654	-0.724	
Nal_w_d	0.736	-0.653	-0.722	-0.880
NalS	0.269	0.164	-0.587	-0.570
NalS_Int_isol	0.359	0.128	-0.614	
NalS_w	0.361	0.140	-0.598	-0.872
NalS_d	0.296	0.107	-0.686	-0.593
NalS_Int_isol_d	0.377	0.063	-0.696	
NalS_w_d	0.378	0.082	-0.690	-0.872
OfI	0.497	-0.602	-0.608	-0.580
OfI_Int_isol	0.637	-0.640	-0.636	
OfI_w	0.587	-0.609	-0.618	-0.879
OfI_d	0.523	-0.624	-0.696	-0.605
OfI_Int_isol_d	0.625	-0.653	-0.709	
OfI_w_d	0.600	-0.632	-0.707	-0.869

[a] Abbreviation analogous to Table 1. [b] isol means isolated molecule without Cl and H₂O associated (nonbonded) species.

acid > ofloxacin in neutral solution. In a basic solution the order of the first two derivatives is inverted. It is well known that rate constants are very sensitive to accuracy of determination of the activation barriers. In our study, two slightly different models were used for estimation of the rate constant of the Ru(II) complex with nalidixic acid with: (i) benzene and (ii) p-cymene ligands. If we assume a marginal influence of the nature of the arene ligand on the reaction profile (see above) we may compare the first column of Table 3 with the second column of Table 8. Deviation of both k_1 and k_d remains within an order of magnitude; individual values usually differ by a factor of two for both protonated and deprotonated forms. This corresponds to an error of ca. 2 kcal/mol in determination of relative free energies.

Analyses of Ru-quinolone complexes. Energy decomposition according to eqs. (1) and (2) was performed for all the studied complexes so that closer comparison with AIM electron densities would be available for the explored Ru coordination bonds. In Table 9, energy decomposition for isolated reactant complexes is displayed for both PCM and gas phase calculations (on the PCM optimized geometries). From the comparison of the first two columns the mutual repulsion of the ligands in the given Ru complex can be demonstrated. In protonated complexes these differences are surprisingly larger in the PCM model than in the gas phase model. This is a consequence of Cl...H(carboxyl) attraction in the gas phase. Such an attraction can be easily estimated according to Coulomb law using partial charges of Cl (-0.9e) and H (0.4e) atoms and their optimized distance of ca 8 a.u. giving roughly 0.045 hartree (28 kcal/mol). This value approximately agrees with the

differences ($\Delta E^{\text{Stab}} - \Delta E^{\text{Stex}}$) between gas phase and PCM models. Larger ligand repulsion in the gas phase of the deprotonated complexes is a consequence of effective electrostatic screening of negatively charged chloro-ligand and quinolone in the PCM model. Table 9 gives an important insight into the bonding strength of various quinolone molecules and p-cymene ligand. Similar insight is not possible within AIM electron densities of BCP's. The strongest quinolone coordination to the Ru(II) cation exhibits thionalidixic acid mainly due to the Ru-S interaction (see below) followed by ofloxacin > cinoxacin > nalidixic acid. The same order is valid for both protonated and deprotonated forms. The bonding energy (BE) of the p-cymene ligand is only slightly decreased after deprotonation; nevertheless, more distinct changes were observed in BE of the chloro-ligand, which are decreased by more than 5 kcal/mol. Decreased BE's of both p-cymene and Cl-ligand are a consequence of stronger Ru-O(COO) coordination after deprotonation of the carboxyl group.

The NBO partial charges are displayed in Table 10 for stable isolated molecules and in Supporting Information **Table S2** for supermolecules and TS structures. First of all, a much larger donation in complexes with thionalidixic acid is apparent due to stronger interaction of sulfur atom with Ru(II), cf. also in Table 9. Partial charge of the Ru(II) atom is reduced to one half compared to other structures. This fact correlates with higher electron density in Ru-S BCP (Table 11). Also, a positive partial charge appears on sulfur after its coordination to the metal. Nevertheless, Supporting Information **Table S2** shows, that breaking the Ru-S bond results in fairly negative charge on the sulfur atom—up to -0.7 e. Partial charges of

Table 11. AIM electron densities in BCP's for isolated stable complexes (in $10^2 e/a_0^3$).

structure	Ru-O (keto)/S	Ru-O (COO)	Ru-Cl/O (aqua)
Cin ^[a]	8.2	7.4	6.5
Cin_Int_isol ^[b]	9.8	8.8	
Cin_w	8.3	7.6	6.4
Cin_d	8.4	8.5	6.5
Cin_Int_isol_d	9.7	9.8	
Cin_w_d	8.9	9.0	6.3
Nal	8.1	7.4	6.8
Nal_Int_isol	9.7	8.9	
Nal_w	8.7	8.0	6.5
Nal_d	8.4	8.5	6.4
Nal_Int_isol_d	9.9	10.4	
Nal_w_d	8.8	9.0	6.3
NalS	9.1	7.6	6.5
NalS_Int_isol	10.4	9.0	
NalS_w	9.3	8.0	6.3
NalS_d	9.0	8.3	6.3
NalS_Int_isol_d	10.3	10.1	
NalS_w_d	9.2	8.8	6.1
OfI	8.3	7.5	6.7
OfI_Int_isol	9.8	8.8	
OfI_w	9.2	8.2	6.4
OfI_d	8.5	8.5	6.4
OfI_Int_isol_d	10.1	10.2	
OfI_w_d	8.9	9.0	6.4

[a] Abbreviation analogous to Table 1. [b] isol means isolated molecule without Cl and H₂O associated (nonbonded) species.

chloro and aqua ligands are practically as high as those of isolated water and chloride anion in both TS's and intermediate structures. Also very low BCP's electron densities of Ru—Cl and Ru—O(aq) bonds can be seen from Supporting Information **Table S3**, which proves a very loose coordination of the chloro and aqua ligands in TS structures. This fact was already discussed in the first part of this study.

Results of the AIM analysis are collected in Table 11 and Supporting Information **Table S3**, and they are in a good accord with conclusions of the NBO method and (for chloro-ligand) also with the energy decomposition analyses. The confirmation of stronger coordination of the carboxyl group in deprotonated complexes is clearly documented in Table 11. While in the case of protonated complexes electron densities at BCPs of Ru—O(keto) bonds are visibly higher (by about 0.01e), in deprotonated structures these values are nearly the same or even lower than corresponding values for the Ru—O(COO) bond. Similarly to the previously studied Ru(II) half-sandwich complexes^[86], the TS and intermediate structures have visibly stronger coordinations of quinolone and arene ligands to the Ru(II) cation than reactant or product complexes. This conclusion follows, for example, from Supporting Information **Table S3** where markedly higher electron densities in corresponding BCP's are apparent for any quinolone system. In Supporting Information **Table S3** also complexes are shown with only one of the Ru—O(S) coordination of quinolone ligand, either Ru—O(COO) (with released Ru—O(keto) bond, labeled Qui-keto) or Ru—O(keto) (with released carboxylic-bond, labeled Qui—COO(H)). In these complexes, the chloro-ligand remains coordinated and the structures represent the other hydration channels. Interestingly in both these cases, the electron densities in Ru—O BCP's are lower than in any Ru—O bond in reactant or in products of the dechlorination process, which means that non-negligible synergy effects are present in the chelate coordination. From BCPs densities of Ru—O(keto) and Ru—O(aq)/Ru—Cl bonds in Supporting Information **Table S3** it can be seen that when one of the Ru—O(quinolone) bond is broken the remaining coordination becomes even weaker than any of Ru—Cl or Ru—O(aq) bonds (with the only exception of cinoxacin).

Conclusions


In this study, we explored several quinolone Ru(II) half-sandwich complexes with benzene or p-cymene as the arene ligand. All structures were fully optimized using B3PW91/6-31 + G(d) in the polarizable continuum model. The role of diffuse functions especially on oxygen atoms was found crucial for obtaining appropriate geometries of all structures along the reaction coordinate and especially of all kinds of TS's. To achieve higher accuracy, SP calculations were performed at B3LYP/6-311++G(2df,2pd)/DPCM/scaled-UAKS level. Even though such a level is important for a better estimation of the activation barriers and reaction thermodynamics, we have also found several drawbacks caused by the effect of not relaxed structures on the reaction profile. On the SP level a few energies of the intermediate structure lay slightly higher than ener-

gies of one of the neighboring TS structures in the case of dissociative mechanism. Therefore, such energy profiles should be taken with caution. The size of the arene ligand has only marginal influence on the hydration reaction. In the first part of the study, two possible reaction mechanisms: associative and dissociative were compared and contrary to the hydration of the $[\text{Ru}(\eta^6\text{-p-cymene})(\text{en})\text{Cl}]^+$ complex studied previously,^[101,102] it was found that the examined process occurs with a higher probability via the dissociative mechanism in the Ru(II)-quinolone complexes. This mechanism is linked with two transition states and one intermediate structure. The first transition state (TS1) is linked to the dechlorination of the original Ru-complex (Ru—Cl bond breaking), the second TS to the formation of Ru—O(aqua) coordination bond. The other important conclusion from the first part of the study concerns the hydration channels, that is, an answer to the question, which of three different coordination-covalent bonds: Ru—Cl, Ru—O(keto), or Ru—O(COO) will be hydrolyzed first by the approaching water molecule. It was found that the dechlorination reaction is energetically and kinetically the most feasible channel.

In the second part, we focused only on the dissociative mechanism of the hydration reaction. The energy profile of this pathway was determined for several derivatives of nalidixic acid. As for thermodynamics, hydration of cinoxacin is the least endergonic while the reactant structure with ofloxacin is most stable and exhibits the highest endergonicity of 14 kcal/mol. Lower reaction Gibbs free energies were obtained for deprotonated forms with the order of quinolone ligands: ofloxacin < cinoxacin < nalidixic acid \approx thionalidixic acid. A slightly modified Gibbs energy picture is obtained if the whole reaction is considered in the model of isolated molecules (R0 and P0). Here, the complex with cinoxacin has the lowest Gibbs free energies (regardless acidity/basicity of the solution) while the least reactive complex will contain the thionalidixic acid in neutral solutions and nalidixic acid in basic solution. Nevertheless the energy differences are very small: up to 2 kcal/mol. The highest rate constants for the hydration reaction were calculated for the complexes of nalidixic acid and cinoxacin in neutral and basic environments, respectively. Basic environment promotes the hydration reaction by about four orders of magnitude compared to neutral/acidic ones.

Keywords: Ru(II) piano-stool complex · DFT method · thermodynamics · reaction mechanism · kinetics · rate constants

How to cite this article: T., Zájbojníková, R., Cajzl, J., Kljun, Z., Chval, I., Turel, J. V., Burda *J. Comput. Chem.* **2016**, *37*, 1766–1780. DOI: 10.1002/jcc.24373

 Additional Supporting Information may be found in the online version of this article.

[1] B. Rosenberg, L. Van Camp, T. Krigas, *Nature* **1965**, *205*, 698.

[2] B. Rosenberg, L. Van Camp, J. L. Trosko, V. H. Mansour, *Nature* **1969**, *222*, 385.

- [3] J. M. Asara, J. S. Hess, E. Lozada, K. R. Dunbar, J. Allison, *J. Am. Chem. Soc.* **2000**, 122, 8.
- [4] L. Oehninger, L. N. Kuster, C. Schmidt, A. Munoz-Castro, A. Prokop, I. Ott, *Chem. Eur. J.* **2013**, 19, 17871.
- [5] N. Katsaros, A. Anagnostopoulou, *Crit. Rev. Oncol. Hematol.* **2002**, 42, 297.
- [6] K. Sorasaene, J. R. Galan-Mascaros, K. R. Dunbar, *Inorg. Chem.* **2002**, 41, 433.
- [7] D. M. L. Goodgame, C. A. Omahoney, C. J. Page, D. J. Williams, *Inorg. Chim. Acta* **1990**, 175, 141.
- [8] G. Gupta, B. S. Murray, P. J. Dyson, B. Therrien, *J. Organomet. Chem.* **2014**, 767, 78.
- [9] S. J. Burya, A. M. Palmer, J. C. Gallucci, C. Turro, *Inorg. Chem.* **2012**, 51, 11882.
- [10] A. M. Palmer, S. J. Burya, J. C. Gallucci, C. Turro, *ChemMedChem* **2014**, 9, 1260.
- [11] F. Caruso, M. Rossi, *Mini Rev. Med. Chem.* **2004**, 4, 49.
- [12] M. Uudsemaa, T. Tamm, *Chem. Phys. Lett.* **2001**, 342, 667.
- [13] A. Deally, F. Hackenberg, G. Lally, H. Muller-Bunz, M. Tacke, *Organometallics* **2012**, 31, 5782.
- [14] B. M. zu Berstenhorst, G. Erker, G. Kehr, J. C. Wasilke, J. Muller, H. Redlich, J. Pyplo-Schnieders, *Eur. J. Inorg. Chem.* **2005**, 92.
- [15] S. Meker, K. Margulis-Goshen, E. Weiss, O. Braitbard, J. Hochman, S. Magdassi, E. Y. Tshuva, *ChemMedChem* **2014**, 9, 1294.
- [16] K. Gisselfaelt, P. Lincoln, B. Norden, M. Jonsson, *J. Phys. Chem. B* **2000**, 104, 3651.
- [17] V. G. Vaidyanathan, B. U. Nair, *J. Inorg. Biochem.* **2002**, 91, 405.
- [18] H. Chen, J. A. Parkinson, S. Parsons, R. A. Coxal, R. O. Gould, P. Sadler, *J. Am. Chem. Soc.* **2002**, 124, 3064.
- [19] A. Kueng, T. Pieper, R. Wissiack, E. Rosenberg, B. K. Keppler, *J. Biol. Inorg. Chem.* **2001**, 6, 292.
- [20] O. Novakova, H. Chen, O. Vrana, A. Rodger, P. J. Sadler, V. Brabec, *Biochemistry* **2003**, 42, 11544.
- [21] P. Lincoln, Norden, *B. J. Phys. Chem. B* **1998**, 102, 9583.
- [22] F. Wang, H. M. Chen, S. Parsons, L. D. H. Oswald, J. E. Davidson, P. Sadler, *J. Chem. Eur. J.* **2003**, 9, 5810.
- [23] R. Pettinari, F. Marchetti, F. Condello, C. Pettinari, G. Lupidi, R. Scopelliti, S. Mukhopadhyay, T. Riedel, P. Dyson, *Organometallics* **2014**, 33, 3709.
- [24] B. Serli, E. Zangrando, T. Gianferrara, C. Scolaro, P. J. Dyson, A. Bergamo, E. Alessio, *Eur. J. Inorg. Chem.* **2005**, 17, 3423.
- [25] C. Spoerlein-Guettler, K. Mahal, R. Schobert, B. Biersack, *J. Inorg. Chem.* **2014**, 138, 64.
- [26] J. Kljun, I. Bratsos, E. Alessio, G. Psomas, U. Repnik, M. Butinar, B. Turk, I. Turel, *Inorg. Chem.* **2013**, 52, 9039.
- [27] A. F. A. Peacock, A. Habtemariam, R. Fernandez, V. Walland, F. P. A. Fabbiani, S. Parsons, R. E. Aird, D. I. Jodrell, P. J. Sadler, *J. Am. Chem. Soc.* **2006**, 128, 1739.
- [28] A. Dorcier, P. J. Dyson, C. Gossens, U. Rothlisberger, R. Scopelliti, I. Tavernelli, *Organometallics* **2005**, 24, 2114.
- [29] S. S. Braga, A. M. S. Silva, *Organometallics* **2013**, 32, 5626.
- [30] I. Romero-Canelon, P. Sadler, *J. Inorg. Chem.* **2013**, 52, 12276.
- [31] P. N. Pavankumar, P. Seetharamulu, S. Yao, J. D. Saxe, D. G. Reddy, F. H. Hausheer, *J. Comput. Chem.* **1999**, 20, 365.
- [32] J. K. C. Lau, D. V. Deubel, *Chem. A Eur. J.* **2005**, 11, 2849.
- [33] D. V. Deubel, *J. Am. Chem. Soc.* **2006**, 128, 1654.
- [34] R. Wysockinski, D. Michalska, *J. Comput. Chem.* **2001**, 22, 901.
- [35] H. F. Dos Santos, B. L. Marcial, C. F. De Miranda, L. A. S. Costa, W. B. De Almeida, *J. Inorg. Biochem.* **2006**, 100, 1594.
- [36] L. A. S. Costa, W. R. Rocha, W. B. De Almeida, H. F. Dos Santos, *J. Inorg. Biochem.* **2005**, 99, 575.
- [37] P. Oliveira, L. Sartori, N. Rey, H. D. Dos Santos, M. Oliveira, L. Costa, *J. Brazilian Chem. Soc.* **2013**, 24, 1732.
- [38] K. Gkionis, S. T. Mutter, J. A. Platts, *RSC Adv.* **2014**, 3, 4066.
- [39] Y. Zhang, Z. Guo, X. Z. You, *J. Am. Chem. Soc.* **2001**, 123, 9378.
- [40] A. Robertazzi, J. A. Platts, *J. Comput. Chem.* **2004**, 25, 1060.
- [41] J. Raber, C. Zhu, L. A. Eriksson, *J. Phys. Chem.* **2005**, 109, 11006.
- [42] J. F. Lopes, V. S. D. Menezes, H. A. Duarte, W. R. Rocha, W. B. De Almeida, H. F. Dos Santos, *J. Phys. Chem. B* **2006**, 110, 12047.
- [43] J. V. Burda, M. Zeizinger, J. Leszczynski, *J. Comput. Chem.* **2005**, 26, 907.
- [44] J. V. Burda, M. Zeizinger, J. Leszczynski, *J. Chem. Phys.* **2004**, 120, 1253.
- [45] M. Zeizinger, J. V. Burda, J. Šponer, V. Kapsa, J. Leszczynski, *J. Phys. Chem. A* **2001**, 105, 8086.
- [46] M. H. Baik, R. A. Friesner, S. J. Lippard, *J. Am. Chem. Soc.* **2003**, 125, 14082.
- [47] K. Spiegel, U. Rothlisberger, P. Carloni, *J. Phys. Chem. B* **2004**, 108, 2699.
- [48] A. Robertazzi, J. A. Platts, *Inorg. Chem.* **2005**, 44, 267.
- [49] Z. Chval, M. Šíp, Collect. Czech. Chem. Commun. **2003**, 68, 1105.
- [50] J. V. Burda, J. Leszczynski, *Inorg. Chem.* **2003**, 42, 7162.
- [51] M. Zeizinger, J. V. Burda, J. Leszczynski, *Phys. Chem. Chem. Phys.* **2004**, 6, 3585.
- [52] M. Pavelka, M. Šimánek, J. Šponer, J. V. Burda, *J. Phys. Chem. A* **2006**, 110, 4795.
- [53] T. Li, Z. Xu, D. Zhang, L. Zhou, *J. Theor. Comput. Chem.* **2013**, 12, 1350020.
- [54] Z. Chval, M. Kabeláč, J. V. Burda, *Inorg. Chem.* **2013**, 52, 5801.
- [55] D. V. Deubel, *J. Am. Chem. Soc.* **2004**, 126, 5999.
- [56] T. Zimmermann, M. Zeizinger, J. V. Burda, *J. Inorg. Biochem.* **2005**, 99, 2184.
- [57] T. Zimmermann, J. V. Burda, *Dalton Trans.* **2010**, 39, 1295.
- [58] L. Michera, M. Nekardova, J. V. Burda, *Phys. Chem. Chem. Phys.* **2012**, 14, 12571.
- [59] V. Calandrini, F. Arnesano, A. Galliani, T. H. Nguyen, E. Lippoliti, P. Carloni, G. Natile, *Dalton Trans.* **2014**, 43, 12085.
- [60] T. Shoenib, B. L. Sharp, *Inorg. Chim. Acta* **2013**, 405, 258.
- [61] C. Gossens, I. Tavernelli, U. Rothlisberger, *Chimia* **2005**, 59, 81.
- [62] D. V. Deubel, J. K. C. Lau, *Chem. Commun.* **2006**, 2451.
- [63] Z. Futera, J. V. Burda, *J. Comput. Chem.* **2014**, 35, 1446.
- [64] Z. Futera, J. A. Platts, J. V. Burda, *J. Comput. Chem.* **2012**, 33, 2092.
- [65] M. Brindell, K. Dyduch, A. Adamowicz, E. Urbanowicz, M. Oszejka, A. Michalak, G. Stochel, R. van Eldik, *Eur. J. Inorg. Chem.* **2014**, 2014, 1333.
- [66] H. Wang, N. DeYonker, X. Zhang, C. Zhao, L. Ji, Z. Mao, *J. Mol. Model.* **2012**, 18, 4675.
- [67] H. Wang, N. DeYonker, H. Gao, C. Tan, X. Zhang, L. Ji, C. Zhao, Z. Mao, *RSC Adv.* **2012**, 2, 436.
- [68] S. T. Mutter, J. A. Platts, *J. Phys. Chem. A* **2011**, 115, 11293.
- [69] R. Aird, J. Cummings, A. Ritchie, M. Muir, R. Morris, H. Chen, P. Sadler, D. Jodrell, *Br. J. Cancer* **2002**, 86, 1652.
- [70] S. J. Berners-Price, P. Sadler, *J. Coord. Chem. Rev.* **1996**, 151, 1.
- [71] J. Kašparková, F. S. Mackay, V. Brabec, P. J. Sadler, *J. Biol. Inorg. Chem.* **2003**, 8, 741.
- [72] A. Habtemariam, M. Melchart, R. Fernandez, S. Parsons, I. D. H. Oswald, A. Parkin, F. P. A. Fabbiani, J. E. Davidson, A. Dawson, R. E. Aird, D. I. Jodrell, P. J. Sadler, *J. Med. Chem.* **2006**, 49, 6858.
- [73] F. Y. Wang, A. Habtemariam, E. P. L. van der Geer, R. Fernandez, M. Melchart, R. J. Deeth, R. Aird, S. Guichard, F. P. A. Fabbiani, P. Lozano-Casal, I. D. H. Oswald, D. I. Jodrell, S. Parsons, P. J. Sadler, *Proc. Natl. Acad. Sci. USA* **2005**, 102, 18269.
- [74] A. E. Egger, C. G. Hartinger, A. K. Renfrew, P. J. Dyson, *J. Biol. Inorg. Chem.* **2010**, online.
- [75] F. Barragán, P. López-Senín, L. Salassa, S. Betanzos-Lara, A. Habtemariam, V. Moreno, P. J. Sadler, V. Marchán, *J. Am. Chem. Soc.* **2011**, 133, 14098.
- [76] H. Chen, J. A. Parkinson, R. E. Morris, P. J. Sadler, *J. Am. Chem. Soc.* **2003**, 125, 173.
- [77] J. Kljun, A. K. Bytze, W. Kandjoller, C. Bartel, M. A. Jakupec, C. G. Hartinger, B. K. Keppler, I. Turel, *Organometallics* **2011**, 30, 2506.
- [78] I. Turel, J. Kljun, F. Perdih, E. Morozova, V. Bakulev, N. Kasyanenko, J. A. W. Byl, N. Osheroff, *Inorg. Chem.* **2010**, 49, 10750.
- [79] Burke, K.; Perdew, J. P.; Wang, Y.; Impey, R. W. In *Electronic Density Functional Theory*; J. F. Dobson, G. Vignale, M. P. Das, Eds.; Plenum: New York, **1998**.
- [80] D. Andrae, U. Haussermann, M. Dolg, H. Stoll, H. Preuss, *Theor. Chim. Acta* **1990**, 77, 123.
- [81] A. Bergner, M. Dolg, W. Kuechle, H. Stoll, H. Preuss, *Mol. Phys.* **1993**, 80, 1431.
- [82] A. D. Becke, *J. Phys. Chem.* **1993**, 98, 5648.
- [83] J. V. Burda, M. Zeizinger, J. Sponer, J. Leszczynski, *J. Chem. Phys.* **2000**, 113, 2224.

- [84] P. Politzer, P. R. Laurence, K. Jayasuriya, *Environ. Health Perspect.* **1985**, 61, 191.
- [85] P. Sjöberg, J. S. Murray, T. Brinck, P. Politzer, *Can. J. Chem.* **1990**, 68, 1440.
- [86] J. V. Burda, Z. Futera, Z. Chval, *J. Mol. Model.* **2013**, 19, 5245.
- [87] J. P. Foster, F. Weinhold, *J. Am. Chem. Soc.* **1980**, 102, 7211.
- [88] A. E. Reed, F. Weinhold, *J. Chem. Phys.* **1983**, 78, 4066.
- [89] Weinhold F, University of Wisconsin, Madison, Wisconsin 53706: Wisconsin, **2001**.
- [90] Bader, R. W. F. *Atoms in Molecules: A Quantum Theory*; Clarendon Press: Oxford, U.K., **1990**.
- [91] Keith, T. A. Available at: <http://aim.tkgristmill.com>, **2009**.
- [92] M. Mitoraj, A. Michalak, T. Ziegler, *Organometallics* **2009**, 28, 3727.
- [93] R. F. Nalewajski, J. Mrozek, *Int. J. Quantum Chem.* **1994**, 51, 187.
- [94] M. Cossi, N. Rega, G. Scalmani, V. Barone, *J. Comput. Chem.* **2003**, 24, 669.
- [95] J. Tomasi, R. Cammi, B. Mennucci, *Int. J. Quantum Chem.* **1999**, 775, 7783.
- [96] M. Cossi, G. Scalmani, N. Rega, V. Barone, *J. Chem. Phys.* **2002**, 117, 43.
- [97] V. Barone, M. Cossi, J. Tomasi, *J. Chem. Phys.* **1997**, 107, 3210.
- [98] T. Zimmermann, J. V. Burda, *J. Chem. Phys.* **2009**, 131, 135101.
- [99] T. Zimmermann, Z. Chval, J. V. Burda, *J. Phys. Chem. B* **2009**, 113, 3139.
- [100] J. Berges, I. Fourré, J. Pilmé, J. Kozelka, *Inorg. Chem.* **2013**, 52, 1217.
- [101] Z. Chval, Z. Futera, J. V. Burda, *J. Chem. Phys.* **2011**, 134, 024520.
- [102] Z. Futera, J. Klenko, J. E. Sponer, J. Sponer, J. V. Burda, *J. Comput. Chem.* **2009**, 30, 1758.

Received: 28 October 2015
Revised: 23 February 2016
Accepted: 24 February 2016
Published online on 17 May 2016